Long-period orbital climate forcing

Hemmo Anne Abels

GEOLOGICA ULTRAIECTINA

Mededelingen van de
Faculteit Geowetenschappen
departement Aardwetenschappen
Universiteit Utrecht

No. 297

Members of the dissertation committee:

Prof. dr. José Pedro Calvo Sorando
Instituto Geológico y Minero de España (IGME)
Madrid, Spain

Prof. dr. Isabelle Cojan
Ecole Nationale Supérieure des Mines des Paris
Fontainebleau Cedex, France

Prof. dr. Poppe L. de Boer
Department of Earth Sciences, Utrecht University
Utrecht, the Netherlands

Prof. dr. Cornelis G. Langereis
Department of Earth Sciences, Utrecht University
Utrecht, the Netherlands

Prof. dr. Noël Vandenberghe
Afdeling Geologie, Katholieke Universiteit Leuven
Heverlee, Belgium

This study was supported by the Netherlands Council for Earth and Life Sciences (ALW) with financial aid from the Netherlands Organisation for Scientific Research (NWO).

The research for this thesis was carried out at the Stratigraphy/Paleontology Group, Department of Earth Sciences, Utrecht University, Budapestlaan 4, 3584 CD, Utrecht, the Netherlands. (http://www.geo.uu.nl/Research/Strat_Paleontology)

The author can be reached through e-mail; abels@geo.uu.nl

ISBN/EAN: 978-90-5744-161-5

Graphic design: Geomedia (7362), Faculteit Geowetenschappen, Universiteit Utrecht

Long-period orbital climate forcing

Cyclostratigraphic studies of Cenozoic continental and marine successions in Europe

Lang-periodieke orbitaal forcering van het klimaat

Cyclostratigrafische studies van Cenozoïsche continentale en mariene successies in Europa

(met een samenvatting in het Nederlands)

PROEFSCHRIFT

ter verkrijging van de graad van doctor aan de Universiteit Utrecht
op gezag van de rector magnificus, prof.dr. J.C. Stoof,
ingevolge het besluit van het college voor promoties
in het openbaar te verdedigen
op dinsdag 9 december 2008 des middags te 2.30 uur

door

Hemmo Anne Abels

geboren op 26 juli 1980
te Stadskanaal

Promotor
Prof. dr. G.J. van der Zwaan

Co-promotores
Dr. F.J. Hilgen
Dr. H. Abdul Aziz

Contents

To Whom It May Concern

"The human mind may not have evolved enough to be able to comprehend deep time. It may only be able to measure it"

J. McPhee, 1980

CHAPTER 1

Introduction and hypothesis

1.1 Introduction

"Geology is the science which investigates the successive changes that have taken place in the organic and inorganic kingdoms of nature; it enquires into the causes of these changes, and the influence which they have exerted in modifying the surface and external structure of our planet." (Lyell, 1830)

These are the first words in the famous book 'The Principles of Geology' by which Sir Charles Lyell gave his definition of geology already in the year 1830. Except for adding 'and internal' at the end of the last sentence, his definition still sounds up-to-date. In the following, he continued with the rationale of the, at that time, relatively new branch of science.

"By these researches into the state of the earth and its inhabitants at former periods, we acquire a more perfect knowledge of its *present* conditions, and more comprehensive views concerning the laws *now* governing its animate and inanimate productions. When we study history, we obtain a more profound insight into human nature, by instituting a comparison between the present and former states of society. We trace the long series of events that have gradually led to the actual posture of affairs, and by connecting effects with their causes, we are enabled to classify and retain in the memory a multitude of complicated relations; (…). As the present condition of nations is the result of many antecedent changes, some extremely remote and others recent, some gradual, others sudden and violent, so the state of the natural world is the result of a long succession of events, and if we would enlarge our experience of the present economy of nature, we must investigate the effects of her operations in former epochs." (Lyell, 1830)

Since the advance of classical geology in the early nineteenth century scientific tools have increased and geologic sub-disciplines grown, but the prime goals never changed; How does our physical world work? How did Earth's history look like? And how did it come to where we are now?

1.1.1 Cyclostratigraphy

Stratigraphy is the subdiscipline of geology that comprises the study of rock layers and layering and their content. Reconstruction of paleoenvironments by using for example sedimentary properties, biological content, and chemical proxies allows geologic processes to be resolved, especially when the data are being placed in accurate time frames. Cyclostratigraphy specifically aims at studying cyclic variations in the stratigraphic record and focuses on the impact of variations in solar radiation at the top of the atmosphere on climate and subsequently on continental and marine palaeoenvironments. Changes in solar radiation are caused by quasi-periodic variations of Earth's orbit and axis with respect to the sun through time that occur due to the gravitational interaction with other masses in the solar system. These gradual motions lead to changes in seasonality and solar radiation received at the top of the atmosphere, depending on latitude, hemisphere, and

season (Hinnov, 2000; Milankovitch, 1941). These orbital variations thus change climate through time that in its turn leads to changing paleoenvironments, as for example to (part of) the large late Pleistocene glacial/interglacial cyclicity (Hays *et al.*, 1976; Huybers and Wunsch, 2005; Milankovitch, 1941; Ruddiman, 2006). The dominant 'Milankovitch' cycles have periodicities of around 19 and 23 kyr for precession, 41 kyr for obliquity, 95 and 124 kyr for short eccentricity, and 405 kyr for long eccentricity (Laskar *et al.*, 2004), although in reality these consists of more than thousand components (Hinnov, 2000).

Confirmation of the presence of orbital climate variability in a sediment or proxy record should come from detailed sedimentological or geochemical analysis, ideally combined with accurate age control and statistical analysis (Hinnov, 2000; Schwarzacher, 2000; Weedon, 2003). If available for the time interval studied, computed astronomical target curves can be used for detailed comparison of characteristic patterns in both records, occasionally leading to absolute astronomical age control and a fixed astronomical tuning (Hilgen, 1991; Shackleton *et al.*, 1990). When this correlation is not or can not be made the tuning is called to be "floating" (Hinnov, 2000), by which still internal time control is gained. The reasons for a floating tuning are the lack of sufficient age control or a computed target curve, that are now calculated back reliably to 40 to 50 million years ago for all orbital components (Laskar *et al.*, 2004; Pälike *et al.*, 2004; Varadi *et al.*, 2003), and back to at least the Cretaceous – Paleogene boundary for the most regular and stable components that do not include the Earth-Moon system, such as the 405-kyr eccentricity cycle (Laskar *et al.*, 2004).

1.1.2 History

Since Lyell, reconstruction of Earth's geologic and climatic histories remain the prime goals of geologists studying sedimentary rock records from land and sea. Cyclostratigraphy has a considerable added value to the package of stratigraphic sub-disciplines that exist, but also to elementary sedimentology. When orbital cyclicity is proven, part or whole of the variation in a sediment record can be explained, leaving behind trends or events that have to be explained differently (Chapters 2 and 3). Furthermore, if the orbital climatic circumstance is known that forced the data to certain end-members, this can be added to the general model developed for the generation of these end-members (Chapter 2 and 7). And finally, a major deliverable is the chronostratigraphic potential (Hilgen *et al.*, 1999; Lourens *et al.*, 2004; Schwarzacher, 2000).

Astronomical forcing of climate variability has been hypothesised since the early 19th century by Adhémar (1842). James Croll formulated in 1864 a theory that predicted that when the northern hemisphere was in the grips of an ice age, the southern would be in an interglacial and as the Earth's orbital elements varied, this situation would eventually be reversed (Croll, 1864; Fleming, 1998). He assumed only the well established variations in orbital eccentricity and obliquity of the ecliptic. Charles Lyell, who was in favour of climate change due to changing geographical position of the continents, hesitated adopting this theory (Fleming, 1998). After numerable discussion with other scientists like Charles Darwin, he finally added a chapter on the astronomical theory of climate change starting from the tenth edition of his 'Principles'. Milutin Milankovitch was able to further develop these early ideas by publishing the first insolation curves and formulating a new theory of the ice ages (Milankovitch, 1941). Cyclostratigraphic studies on much older strata were already being done at that time (Bradley, 1929; Gilbert, 1894). After Milankovitch' publication, resistance came especially from meteorologists, who claimed that insolation differences were too small to change climate, and from geologists who argued that a lack of sufficient dating hampered

proof of the orbital duration of sedimentary cyclicity (Duff 1966). Few geologic studies however clearly found evidence of pre-Pleistocene orbital forcing (Schwarzacher, 1947; Van Houten, 1964). Final confirmation for orbital pacing of late Pleistocene glacial/interglacial cyclicity came in late sixties to early seventies due to the study of deep sea cores, the development of new proxies for climate and ice volume, as $\delta^{18}O$ (Emiliani, 1955; Shackleton and Opdijke, 1973), and dating tools, as magnetostratigraphy and radiometric dating (Hays *et al.*, 1976; Imbrie *et al.*, 1984; Shackleton and Opdijke, 1973). This finding and the newly developed tools led to renewed interest to astronomical forcing of paleoenvironments resulting in a wealth of studies reporting the presence of orbital climate variability in various marine and continental sedimentary systems (De Boer and Smith, 1994; Einsele *et al.*, 1991; Olsen, 1986). At present, cyclostratigraphy is being applied widely and is rather popular among scientists.

1.1.3 Long-period astronomical cycles

Low frequencies cycles modulate the amplitude of precession and obliquity. In the last 40 Myr, eccentricity exhibits a 0.97-Myr and a *ca* 2.4-Myr cycle (Fig. 1.1), which respectively are the 7th and 6th resolved eccentricity related terms in the orbital solution of Laskar *et al.* (2004). Further back in time, the relatively stable 2.4-Myr cycle is estimated to shift from a 2.4-Myr period to a 1.2-Myr period related to the chaotic behaviour of the inner planets (Laskar, 1999; Laskar *et al.*, 2004; Pälike *et al.*, 2004). This chaotic behaviour is related to a combination of angles in the precession motion of the orbits of Earth and Mars, which currently is in resonance (Pälike *et al.*, 2004). The timing of this shift is now estimated to be between 53 and 57 Ma (Lourens *et al.*, 2005), although it might even be stable until at least the Cretaceous – Paleogene boundary at 66 Ma (L.J. Lourens, personal communication, 2008). Olsen and Kent (1999) claim to provide geological evidence for the chaotic behaviour of the solar system by recognition of a 1.72-Myr cyclicity in the Late Triassic, which reveals that the original 2.4-Myr eccentricity cycle was much shorter at that time. Over the last 40 Myr, obliquity amplitude variation is modulated by low frequency components of 172 kyr and 1.2 Myr (Fig. 1.1).

1.1.4 Imprint in the geological record

The long-period astronomical cycles are now shown to have a major impact on earth's climate system based on geological archives. In the marine realm, Neogene long-term climate variations, Mi-isotope events, and 3rd order sea level fluctuations have been tentatively related to long-period orbital control by Beaufort (1994) and Lourens and Hilgen (1997). Following these studies, major ice volume increases, that occurred as excursions and transitions, are indeed shown to coincide with long-period nodes in obliquity amplitude related to the 1.2-Myr cycle in close harmony with low eccentricity values related to the 405-kyr cycle. These are the Eocene – Oligocene boundary climate transition (Oi-1; Coxall *et al.*, 2005), the Oligocene – Miocene boundary climate excursion (Mi-1; Fig. 1.1; Billups *et al.*, 2004; Pälike *et al.*, 2006a; Zachos *et al.*, 2001b), the middle Miocene climate transition (Mi-3b; Fig. 1.1; Abels *et al.*, 2005; Holbourn *et al.*, 2005; Holbourn *et al.*, 2007), and furthermore recurrent "glacial" episodes in the Oligocene (6 episodes – Pälike *et al.*, 2006b; Wade and Pälike, 2004) and Miocene (Mi-5 and Mi-6; Fig. 1.1; Turco *et al.*, 2001). The Paleocene Eocene Thermal Maximum (PETM/ETM1) and the subsequent ETM2 warm excursion are reported to occur during maxima in the 405-kyr and 100-kyr eccentricity cycles that post-date prolonged minima in the, in the Early Eocene already shortened, 2.25-Myr eccentricity cycle. This would imply that these thermal maxima are orbitally forced, although this has recently been challenged (Lourens *et al.*, 2005; Westerhold *et al.*, 2007).

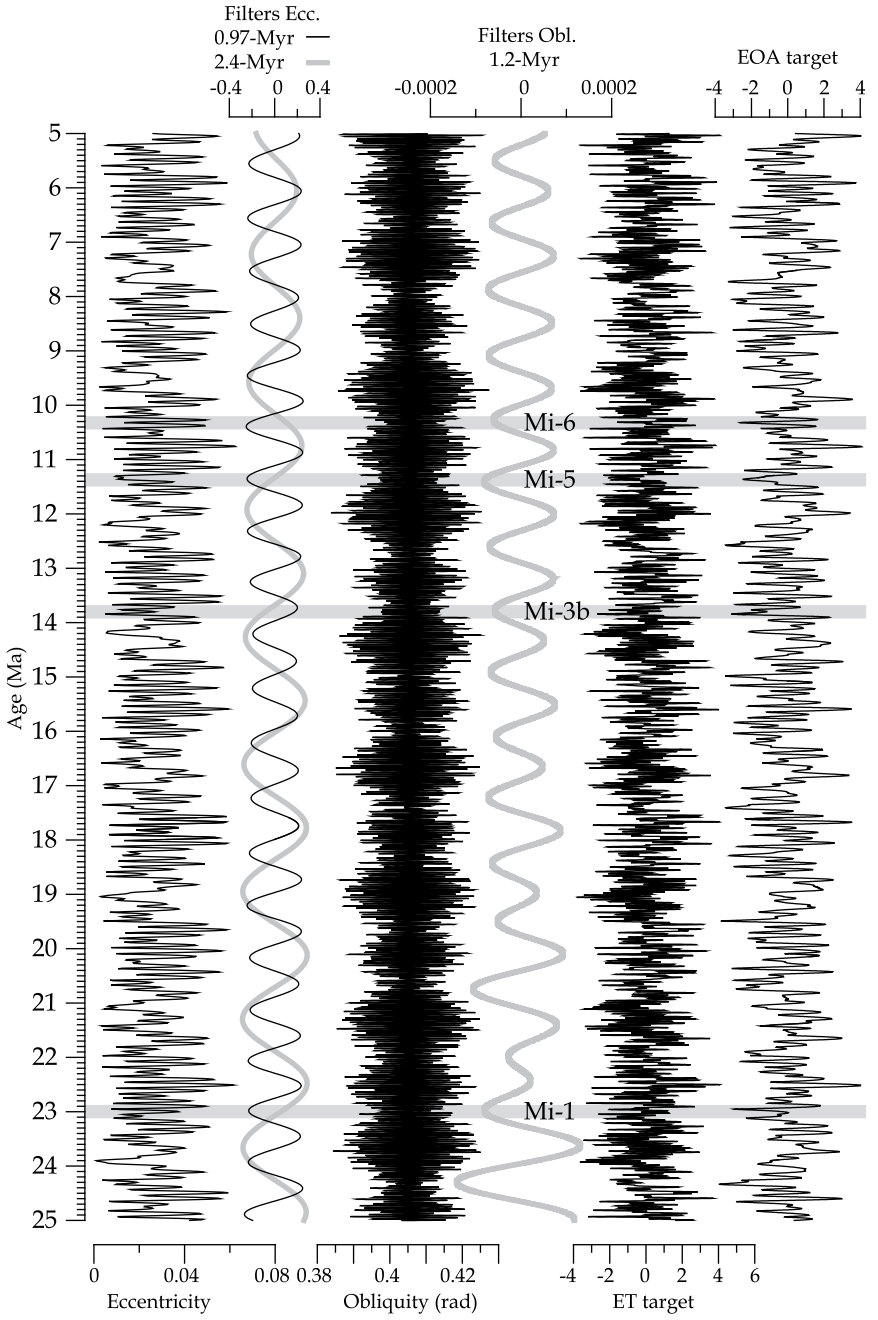

Figure 1.1 Eccentricity and its 0.97-Myr (0.8-1.2 Myr) and 2.4-Myr (1.8-3.0 Myr) bandpass filters, obliquity and its 1.2-Myr (0.85-1.55 Myr) bandpass filter, the Eccentricity-Tilt (ET) and the EOA target curve (see Chapter 6 for explanation) for the whole Miocene epoch from Laskar *et al.* (2004). Indicated are the well-dated Mi-isotope events that mark glacial transitions (Mi-1 and Mi-3b) and episodes (Mi-5 and Mi-6) supposedly on Antarctica, see text for references.

In the continental realm, the study of Olsen and Kent (1996; 1999) is one of the most convincing examples of long-period variations within orbitally forced sediment records. The very long Late Triassic sediment record of the Newark rift basin displays episodes of lake expansion and contraction caused by the astronomical forcing of tropical climate (Olsen, 1986). Low-frequency modulation of basic lithofacies sequences occurs at a period close to 1.72 Myr, related to long-period eccentricity, as discussed above. The impact of the long-period orbital forcing appears as a relatively linear response, despite the fact that sub-aerially deposited, dry sediments can not record even drier periods or vice versa with deep lacustrine deposits (Olsen and Kent, 1999). Van Dam *et al.* (2006) provide a record of small-mammal turnover in Spain over Early Miocene to Late Pliocene times. Statistical analysis indicates increased turnover rates at 0.97 and 2.4-Myr eccentricity minima as well as 1.2-Myr obliquity minima. Long-period eccentricity minima would have caused prolonged periods of cooler and more humid climate, while long-period obliquity minima resulted in dry climates.

In Mesozoic marine records, long period orbital forcing also has been recognized or hypothesized. A few are mentioned here. De Boer (1983) showed a 2 Myr eccentricity forcing of Albian to Cenomanian deep sea carbonate-marl alternations in the Apennines (Italy). Hemipelagic sedimentation Coniacian age (L. Cretaceous) in the Niobrara Formation (Western Cordillera, U.S.A.), reveal a vague long-period variability (Fischer, 1991). Sprovieri *et al.* (2006) report a consistent recording of the 2.4-Myr eccentricity cycle in the middle Berrasian to lower Aptian (L. Cretaceous) pelagic Maiolica Formation (Italy). These marine studies as well as the continental example from the Newark Basin report rather different durations for the low frequency signal in the sediment or proxy records varying from 1.3 Myr in the Western Cordillera to 2.4 Myr in the Maiolica Formation. This indicates that claim of proof for the chaotic behaviour of the solar system is to be corroborated (Olsen and Kent, 1999). A major step forward with these records will be possible when orbital target curves are reliably calculated for this time period (Laskar, 1999; Laskar *et al.*, 2004; Varadi *et al.*, 2003), but unfortunately this is unlike in the near future. The solution by Laskar and co-workers that is in progress is expected to be valid until 50 to 60 Ma and adding another 10 Myr again requires an accuracy increase of numerical models of an order of magnitude (L.J. Lourens, personal communication, 2008; Laskar *et al.*, 2004). Improvement of the Mesozoic geologic time scale will also help to solve the cyclostratigraphic questions. The latter is however intimately related to astronomical tuning itself (Gradstein *et al.*, 2004; Hilgen *et al.*, 1999), to the availability of suitable long stratigraphic records (Dinarès-Turell *et al.*, 2003; Lourens *et al.*, 2005; Westerhold *et al.*, 2007; Westerhold *et al.*, 2008), and to the advancements made in radiometric dating (Kuiper *et al.*, 2008; Kuiper *et al.*, 2004).

1.2 Hypothesis

The reason behind this PhD-research project was the evaluation of the influence of long-period astronomical cycles in controlling lake level in Spanish Neogene continental basins. Despite the general acceptance of orbital forcing on shorter time scales, it remains controversial in controlling continental basin infill on million year, tectonic time scales. Large-scale or formation-scale genetic, sedimentary sequences in continental basins are commonly being referred to as tectono-sedimentary units (*cf* Pardo *et al.*, 1988), implying they are of tectonic origin. Impressive examples are present in many Spanish basins, as large-scale alternations of lake and red bed sequences. An

integrated stratigraphic approach showed that Neogene sedimentary records in the Teruel and Calatayud Basins could be dated very accurately and orbital forcing of small-scale cyclicity proven (Abdul Aziz, 2001; Abdul Aziz *et al.*, 2000; Abdul Aziz *et al.*, 2004). Therefore, the imprint of long eccentricity on lake level in the Triassic Newark Basin (see above – Olsen and Kent, 1999), the recognition of small-scale orbital cycles in Spanish continental sediments, and the suggestion of a connection between glacial episodes and low frequency orbital modulations thus inevitably asked for the evaluation of long-period astronomical forcing in the Spanish Neogene Basins.

Six studies are presented. Four studies in the continental realm, in two different basins, and two studies in the marine realm. The studies range in age from Early Oligocene to Late Miocene. The marine realm was added to the project because of the promising anticipated results regarding long-period orbital forcing. Hereafter, the studies will be further introduced in detail.

1.2.1 Continental realm – Teruel Basin

In the Teruel Basin, the integrated stratigraphic study of Abdul Aziz (2001) indicated precession forcing on basic, meter-scale lithofacies cycles in the Cascante section (see also Abdul Aziz *et al.*, 2004). The study used colour records as proxy for lithology, that however did not reveal prominent cyclicity other than the precession-related variation. Here, we further analyse the Cascante section, because it is part of a large-scale genetic sedimentary sequence. At the top of the dominantly siliciclastic Cascante section studied by Abdul Aziz (2001), a thick lacustrine limestone unit is present. The lack of for example short and long eccentricity related paleoenvironmental signal in the section hampered an astronomical calibration to orbital target curves and it indicated that the paleoenvironment was not sufficiently understood. Moreover, lack of eccentricity forcing on high frequencies would make eccentricity forcing on low frequencies rather remarkable. Therefore, successive limestone beds in the siliciclastic Cascante section have been sampled in order to perform microfacies analysis of which the results are being presented in **Chapter 2**. Short and long eccentricity forcing of lake-level variation through successive limestone beds is indeed shown, an astronomical tuning constructed, and a suggestion made on the long-period orbital control on the gradual change to full lacustrine conditions in the top part of the section.

To further analyse the significance of the lacustrine limestone unit at Cascante, the lateral equivalents of the unit had to be found within other parts of the basin. The Prado area revealed to display excellent outcrops of roughly similar age. Sediments display a rather different type of lithofacies associations that indicate deposition in a less regular and stable environment than in the Cascante area. Complex basic, meter-scale cycle are recognised that change rapidly through time and are variable laterally as well. The lower part of the section is laterally connected to distal portions of an alluvial fan system, indicating the relative proximity of the area to the basin margin. Integrated stratigraphic methods have been applied to place the Prado section in an accurate timeframe. These are the construction of a high resolution magnetostratigraphy and repeated accurate logging of the section in different lateral transects. Also, paleontological sampling has taken place of which preliminary data corroborate the time-equivalence of the section. The results are shown in **Chapter 3**. These demonstrate the precession forcing of meter-scale cyclicity together with the additional imprint of obliquity and long eccentricity, while the imprint of short eccentricity has not been found. Also, the relatively rapid vertical changes of the character of the basic cycle are not explained by orbital climate forcing, and it is suggested that orbital forcing acted in harmony with other processes such as autogenic variability and possibly tectonics.

Finally, the Prado section has been tied to astronomical target curves resulting in a high resolution astrochronology for the succession.

These results paved way for integration of the Cascante and Prado magneto-astrochronologies in order to analyse the lateral behaviour of the large-scale genetic sedimentary sequence. Therefore, the Cascante section had to be extended upwards to cover the limestone unit and document its transition into overlying siliciclastic sediments. Also, near the Cascante section, the limestone unit revealed to split with siliciclastic sediments in between and become thinner as well, which had to be investigated. In this split, red mudstones allowed paleomagnetic sampling in order to extend the Cascante magnetostratigraphy into the limestone interval. In **Chapter 4**, the results of the comparison of both sections using the high resolution chronologies in different parts of the Teruel Basin are presented. It indicates that the shift to the limestone interval at Cascante is time-equivalent to a shift to dominantly siliciclastic sediments at Prado. Inversely changing relative, local groundwater and lake levels occurred, supposedly due to a common origin. The origin remained enigmatic, although at present a tectonically or geomorphically caused drainage area increase seems the most tentative explanation.

1.2.2 Continental realm – Madrid Basin

In the Madrid Basin, excellent outcrops are preserved of the so-called Intermediate tectono-stratigraphic unit of middle Miocene age. Here, the work aimed at accurate dating of this succession in the north-eastern part of the basin, where much sedimentological work had been done by Spanish geologists. In this sector, the Intermediate unit displays two genetic sedimentary sequences consisting of red beds at their base and pedogenic calcrete and pond limestones at their top. Mainly, a tectonic origin has been given to these sequences, although rarely arguments were given. We thus hypothesized that long-period orbital forcing could play a dominant role as well. High-frequency lithofacies alternations could then possibly relate to orbital forcing on smaller scales. In **Chapter 5**, the results of the integrated stratigraphic study of the Valdearenas – Muduex (VDA-MX) composite section is presented. A high resolution magnetostratigraphy provides an accurate age model for comparison of lithofacies shifts in the section as well as statistical analysis of colour records as proxy for lithology. The results are in line with long-period eccentricity forcing of the genetic sedimentary sequences and other scales of eccentricity forcing seemed to have influenced sediment supply and palaeosol development in the floodplain setting.

1.2.3 Marine realm

The two marine studies, that were added because of their high potential in proving long-period forcing, are of rather different character. The middle Miocene climate transition was already suggested to be related to a 1.2-Myr obliquity amplitude node by Lourens and Hilgen (1997). On Malta, the climate transition interval was supposedly present in a well-exposed sediment record estimated to cover the middle Miocene time interval. Mediterranean integrated stratigraphic frameworks of bio-, cyclo-, and magnetostratigraphies had been extended down to the middle Miocene in the Tremiti and Monte dei Corvi sections, that however exactly lacked the climate transition interval. These frameworks on the other hand were excellent starting points for integrated stratigraphic analysis of the Blue Clay Formation on Malta and Gozo, as this succession does not reveal prominent small-scale cyclicity or sapropel patterns. Detailed sampling for in first instance magnetostratigraphy, biostratigraphy, and chemostratigraphy were taken across the boundary between the Globigerina Limestone Formation and upwards into the Blue Clay Formation. In **Chapter 6**, the results of this study are presented. The high resolution biostratigraphy and

magnetostratigraphy allow first order age control. Orbital control of the cyclicity is proven and an accurate age model could be established. The middle Miocene global cooling is being recognised in bulk carbonate isotope records and dated by the astronomical calibration of the section. Long-period orbital control is suggested by a peculiar configuration of minima of the 1.2-Myr obliquity cycle and the 405-kyr eccentricity cycle at 13.82 Ma, as in the mean time also found for other climate steps (Fig. 1.1).

The other marine study regards the cyclostratigraphic analysis of well-log data of the Boom Clay Formation in Belgium. In this early Oligocene succession, a long record of eustatic sea level variations was shown to be present as winnowing on the extremely flat seafloor is the only mechanisms that can explain the lateral very continuous silt and clay layering (Vandenberghe *et al.*, 1997). The drilling of the Boom Clay successions, for reasons of storage of nuclear waste, revealed much longer records than previously known from outcrop areas (Van Simaeys *et al.*, 2004). These new records enquired re-evaluation of the orbital cyclicity in the succession that was done already on the basis of outcrop data (Echelpoel, 1994; Echelpoel and Weedon, 1990; Vandenberghe *et al.*, 1997). Firstly, the prime goal was to look for the expression of long-period orbital forcing of major ice sheet expansions, as known from deep-sea oxygen isotope records. Secondly, the decomposition into temperature and ice volume components in benthic oxygen isotope records is rather difficult and in the Boom Clay a direct measurement of sea level variability could be gained (Bintanja *et al.*, 2005; Pälike *et al.*, 2006b; Wade and Pälike, 2004). In **Chapter 7**, this cyclostratigraphic analysis is shown. Dominant obliquity control of silt-clay couplets is suggested together with additional imprint of the short and long eccentricity cycles. To unravel long-periodicities the studied part of succession finally showed to be too short, as lack of absolute age control hampered direct comparison with orbital target curves.

CHAPTER 2

Shallow lacustrine carbonate microfacies document orbitally paced lake-level history in the Miocene Teruel Basin (NE Spain)

Hemmo A. Abels, Hayfaa Abdul Aziz, José Pedro Calvo, and Erik Tuenter

Based on:
H.A. Abels, H. Abdul Aziz, J.P. Calvo, and E. Tuenter, 2008. Shallow lacustrine carbonate microfacies document orbitally paced lake-level history in the Miocene Teruel Basin (NE Spain). *Sedimentology,* Online Early, in the press.

2.1 Abstract

Results are presented of a detailed carbonate petrographic study of an Upper Miocene lacustrine mixed carbonate-siliciclastic succession in the Teruel Basin (Spain) with the aim of constraining lake-level variability at different stratigraphic scales. Regular alternations of red to green mudstone and lacustrine limestone, termed the 'basic cycle', reflect lake-level variations at the metre-scale. In an earlier study, the basic cycle was shown to be controlled by the climatic precession cycle. Petrographic analysis made it possible to distinguish two main carbonate microfacies groups characteristic of very shallow transient and shallow permanent lake environments, respectively. In addition to the basic cyclicity, the microfacies analysis reveals lake-level variations on a larger scale. As a consequence, the astronomical forcing hypothesis of the cyclicity in the Cascante section is explored further. A climate modelling study of orbital extremes indicates that high lake levels could relate to enhanced net winter precipitation and runoff during precession minima, consistent with Mediterranean geological data. Using this phase relationship, an astronomical tuning of the cycles is established starting from astronomical ages of magnetic reversal boundaries. Subsequently, successive basic cycles are correlated to precession minima. The tuning reveals an identical number of basic cycles in the Cascante section as precession-related sapropel cycles in the deep marine succession at Monte dei Corvi (Italy), corroborating the precessional control of the basic cycles at Cascante. Lake-level highstands in the large-scale cycle identified by the microfacies analysis relate to maxima in both the *ca* 100 and 405 kyr eccentricity cycles, again consistent with Mediterranean geological data. Subtraction of the identified astronomically related (lake-level) variations from the palaeoenvironmental record at Cascante indicates a shift to deeper and more permanent lacustrine environments in the upper half of the section. The cause of this shift remains unclear, but it may be linked to tectonics, non-astronomical climate, long period astronomical cycles or autogenic processes.

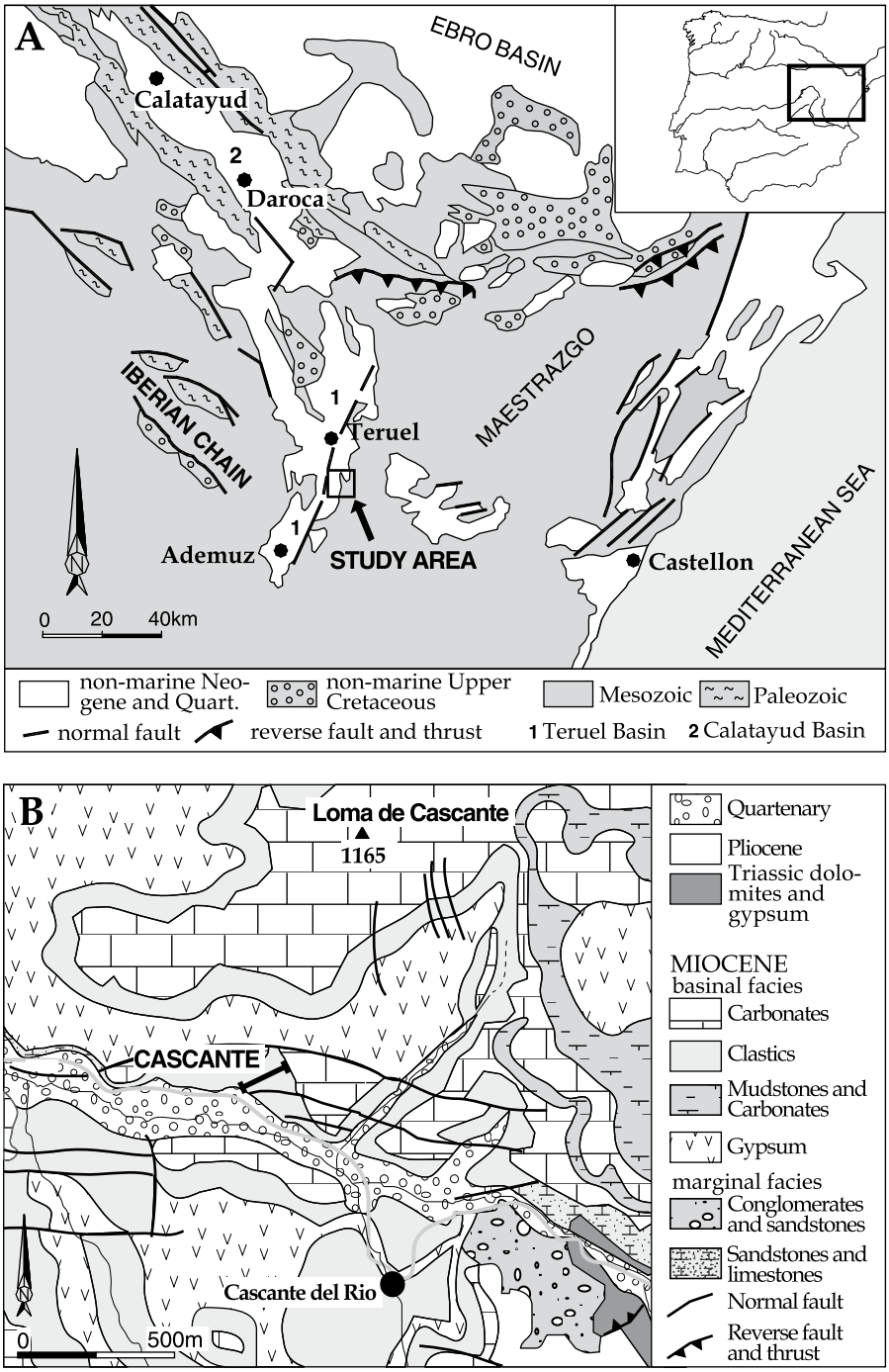

Figure 2.1 (A) Geological and location map of the region of the NNE-SSW trending Teruel Basin. (B) Detailed geological map and location map of the Cascante section (after Abdul Aziz, 2001). Miocene basinal facies are depicted in the legend from bottom to top according to their stratigraphic order.

2.2 Introduction

Reconstruction of the evolution of sedimentary environments requires distinction among tectonic, climatic and autogenic processes, which is often difficult to achieve because they may result in similar palaeoenvironmental shifts and act simultaneously as well. However, high-resolution (*ca* 10^4 yr) age control may provide critical information about the forcing mechanisms of the palaeoenvironmental changes. Recent improvements of the Cenozoic, and especially the Neogene, magnetic polarity timescale (Gradstein *et al.*, 2004; Lourens *et al.*, 2004) offer an excellent opportunity to correlate lithological and biological changes in sedimentary successions with well dated tectonic and (global) climatic events (Dupont-Nivet *et al.*, 2007). The improvements further allow the presence of astronomical climate forcing to be examined, which potentially yields valuable information on the response of palaeoenvironmental and sedimentological processes to known climate variations in terms of relative humidity and seasonality (Weedon, 2003). In addition, the identification and subsequent removal of orbitally induced climate variations from the sedimentary record reveal other variations that may be related to autocyclicity, tectonics or non-astronomical climate-forcing mechanisms.

Neogene continental successions in Spain offer long sedimentary records of low-gradient endorheic basins in which climate and tectonics theoretically have a great impact on the depositional environment (Sanz *et al.*, 1995; Abdul Aziz *et al.*, 2003b). In the present paper, a continued cyclostratigraphic study of the Cascante section in the southern Teruel Basin (NE Spain; Fig. 2.1) is presented, elaborating on a previous study by Abdul Aziz *et al.* (2004). The section is characterized by a distinct alternation of red to green mudstone, interpreted to be deposited in a distal alluvial floodplain environment, and shallow lacustrine to palustrine limestone (Fig. 2.2). Magnetostratigraphy and small-mammal biostratigraphy revealed that deposition took place between 9.4 and 10.2 Ma (Abdul Aziz *et al.*, 2004). Abdul Aziz *et al.* (2004) applied spectral analysis on high-resolution colour records. Results revealed a cyclicity at a 1:2:5 ratio, resembling the ratio of the climatic precession, obliquity and short eccentricity cycles. Combining the statistical and magnetostratigraphic results, those authors showed that the basic, metre-scale mudstone-limestone cycles are related to the precession cycle (Abdul Aziz *et al.*, 2004). However, no palaeoenvironmental significance could be assigned to the other scales of cyclicity that were tentatively attributed to obliquity and short-eccentricity. consequently, no astronomical tuning of the Cascante section was established. In this study, a detailed sediment petrographic study of all 34 lacustrine and palustrine limestone beds was therefore performed. In addition, simulations with a global climate model were carried out as an independent check on the phase relationship between lake-level highstands and precession as derived from published geological data. Finally, an astronomical tuning of the Cascante succession is presented, allowing a quantification of the influence of climate and tectonic variability on this continental sedimentary environment.

2.2.1 Geological Setting

In the Teruel Basin (Fig. 2.1A), a 100 km long and 15 km wide NNE-SSW trending half-graben, sediment deposition started in the Early Miocene and lasted until the Late Pliocene (Anadón & Moissenet, 1996). Sedimentation took place in an internally drained continental setting dominated by red alluvial terrigenous beds, lacustrine and palustrine limestones, and gypsum. The sedimentary succession is characterized by large-scale (40 to 200 m) alternations of red siliciclastic sediments

Figure 2.2 View to the east of the siliciclastic Cascante section with the limestone unit on top of cycle number 34. Red/green mudstone-white limestone cycles are indicated by numbers in black (except for cycle 25, shown in grey because it is not well visible in the picture). The scale bar is approximately valid for the middle of the photograph (for actual thicknesses, see Fig. 4).

and lacustrine carbonate or evaporitic sediments (Anadón *et al.*, 1997; Alonso Zarza & Calvo, 2000).

The studied Cascante section is located in the southern part of the basin (Fig. 2.1B), along the Villel-Cascante del Rio road, in the Teruel-Ademuz sub-basin. The sub-basin is flanked by Mesozoic rocks, predominantly composed of Triassic mudstone and evaporite rocks and Jurassic limestone. The presence of gypsum deposits in the basin has been related to leaching of Triassic sediments cropping out along the basin margin (Broekman, 1983; Anadón *et al.*, 1992). The Neogene infill starts at the basin margin with alluvial fan conglomerates and breccias that grade laterally, within a few kilometres, into fine-grained distal alluvial fan sediments and shallow lacustrine deposits towards the centre of the basin.

2.2.2 The Cascante section

The studied Upper Miocene section comprises the siliciclastic interval of the Loma de Cascante Formation, one of the formation-scale siliciclastic-limestone alternations in the Teruel Basin (Fig. 2.2). The lithology is characterized by a distinct regular sedimentary cyclicity of red and green,

orange mottled, distal alluvial fan mudstone and white, shallow lacustrine limestone (Abdul Aziz *et al.*, 2004). This basic mudstone-limestone cycle has an average thickness of 2.2 m (Abdul Aziz *et al.*, 2004) (Fig. 2.3). Thirty-four basic cycles were observed in the Cascante section. A 30 m thick lacustrine limestone unit characterized by metre-scale bedding overlies the mixed carbonate-siliciclastic succession (Fig. 2.2).

2.3 Sedimentology – Outcrop scale

The outcrop data presented in this paper are a compilation of new and published observations and interpretations (Broekman, 1983; Broekman *et al.*, 1983; Kiefer, 1988; Abdul Aziz, 2001; Abdul Aziz *et al.*, 2004). The specific outcrop characteristics of all 34 basic cycles are consistent laterally over a distance of 300 m to the west of the studied section. Some unique mudstone colour patterns in outcrops between 1 and 2 km to the east were proven to be time-equivalent using detailed magnetostratigraphy (Abdul Aziz *et al.*, 2004).

2.3.1 Red and green mudstone

Description
The average thickness of the mudstone part of a basic cycle is 1.8 m (ranging from 1.4 to 3.3 m). The mudstone commonly starts with a dark red colour at the base, gradually changing to orange with upward increasing greyish-green mottling, followed by an often sharp transition to greenish mudstone showing abundant yellow mottling (Fig. 2.3). The mudstone usually is massive and commonly contains some randomly distributed gypsum aggregates with arbitrarily oriented well-developed crystal structure and few millimeter- grained spherical gypsum nodules. Sparse, millimetre-sized to centimetre-sized carbonate lithoclasts are found locally floating in the mudstone. Illite and smectite are the dominant clay minerals in these mudstones (Abdul Aziz *et al.*, 2004). Freshwater gastropods, bivalves and small-mammal fossil remains are scarce and are specifically concentrated in dark grey, organic rich centimetre-thick beds (Broekman, 1983; Abdul Aziz *et al.*, 2004). The organic matter is millimetre-grained and originates from plant remains. The organic-rich layers are unconsolidated and occasionally show millimetre-scale lamination. These layers occur beneath, on top of, and locally within the limestone beds; they also contain fragmented charophyte remains and millimetre-scale to centimetre-scale spherical gypsum nodules.

Interpretation
The mudstone deposits are interpreted to have accumulated out of suspension following flood events in distal mudflat areas of alluvial fans on an usually dry and exposed basin floor, in accordance with the interpretation given by Kiefer (1988). Lack of evidence for stream action in the mudstone strata suggests that the supply of mud occurred through flood events that rapidly washed the mud into the basin without causing any apparent erosion. However, the massive internal structure of these deposits only displays indications of root bioturbation by mottling obscuring any sedimentary clues of a transport mechanism. The massive structure could have been caused by extensive mud-cracking and bioturbation because of root activity after deposition. Wright & Marriott (2007) report that these two mechanisms can, together with compaction, easily remove sedimentary structures after deposition. In addition to the removal of all primary sedimentary structures, prolonged sub-aerial exposure caused pervasive oxidation within the

Figure 2.3 Basic mudstone-carbonate cycle recognized in the Cascante section with an indication of the main lithofacies features and their sedimentological interpretation.

mudstone. The green mudstone on top of the red mudstone might be indicative of initially red sediments that were subjected to reduction and leaching after deposition (Eardley *et al.*, 1973; Broekman, 1983; Abdul Aziz *et al.*, 2004). Similar reduction features have also been reported from the Upper Kizilirmak Basin in Turkey (Türkmen & Kerey, 2000) and from the Calatayud Basin in Spain (Abdul Aziz *et al.*, 2003b).

As mentioned above, gypsum is present in the mudstone as aggregates and millimetre-sized spherical nodules, which occur especially in the organic-rich layers just above and below the limestone beds. The aggregates are interpreted as secondary deposits because of their well-developed crystal structures, random orientation and occurrence. The millimetre-sized spherical nodules, that are found mainly in the organic-rich layers, are interpreted as transported and re-deposited gypsum. An alternative origin is interstitial nodular gypsum growth. The absence of (other) clearly primary deposited subaqeous gypsum is remarkable. Warren (1999) reports that deposition of gypsum in continental settings mainly depends on three critical factors: (i) abundant water to evaporate and introduce solutes; (ii) sufficient solutes to precipitate; and (iii) time. Taking into account the ample time for mudstone deposition and the abundance of gypsum sources, *i.e.* Triassic formations, at the basin margin (Broekman, 1983), the limiting factor for gypsum deposition in the Cascante region is water. Thus, the lack of well-developed gypsum beds could indicate that during mudstone deposition phreatic groundwater levels in the basin were not high enough to reach the solute concentration necessary to precipitate gypsum (Rosen, 1994). This observation suggests that the mudstone deposits accumulated throughout prolonged dry periods during which the basin was flooded only occasionally. The rare small carbonate pebbles are interpreted as relicts of sheet floods that transported larger clasts than average, derived from the Jurassic rocks in the basin margin.

2.3.2 Limestone

Description

The average thickness of limestone beds in the basic cycle is 0.5 m (0.2 to 0.9 m). The limestone beds are poorly laminated or massive, whereas their top parts commonly show vertical tubes and horizontal cracks (Fig. 2.3). Vertical tubes are a few millimetres in width and usually up to several centimetres in length, but they can reach up to 20 cm in massive limestones. Individual tubes show upward and downward divergent patterns, so that many tubes appear to be interconnected. Millimetre-thick horizontal cracks can be present ubiquitously, especially towards the top of the limestone beds. The cracks and vertical tubes locally produce a fragmented limestone, a feature that is especially visible in the top part of pronounced massive limestones. Fossil remains of complete charophyte stems and gyrogonites, broken and complete gastropods, ostracods and some undifferentiated green algae are found. Rare, very fine sand-sized quartz grains are present. Gypsum is present usually as nodules or as fillings of horizontal cracks and vertical structures (Abdul Aziz, 2001). Fine-grained, organic rich laminae (see description in the Red and Green Mudstone section) are present locally within the limestone beds. The degree of consolidation of the limestone beds depends on the amount of clay, gypsum and organic matter, with high gypsum contents resulting in very consolidated limestones. In the upper part of the section, some limestone beds show undulating structures, with locally centimetre-scale cross-stratification, which are present mainly at the base and in the lower half of the limestone beds.

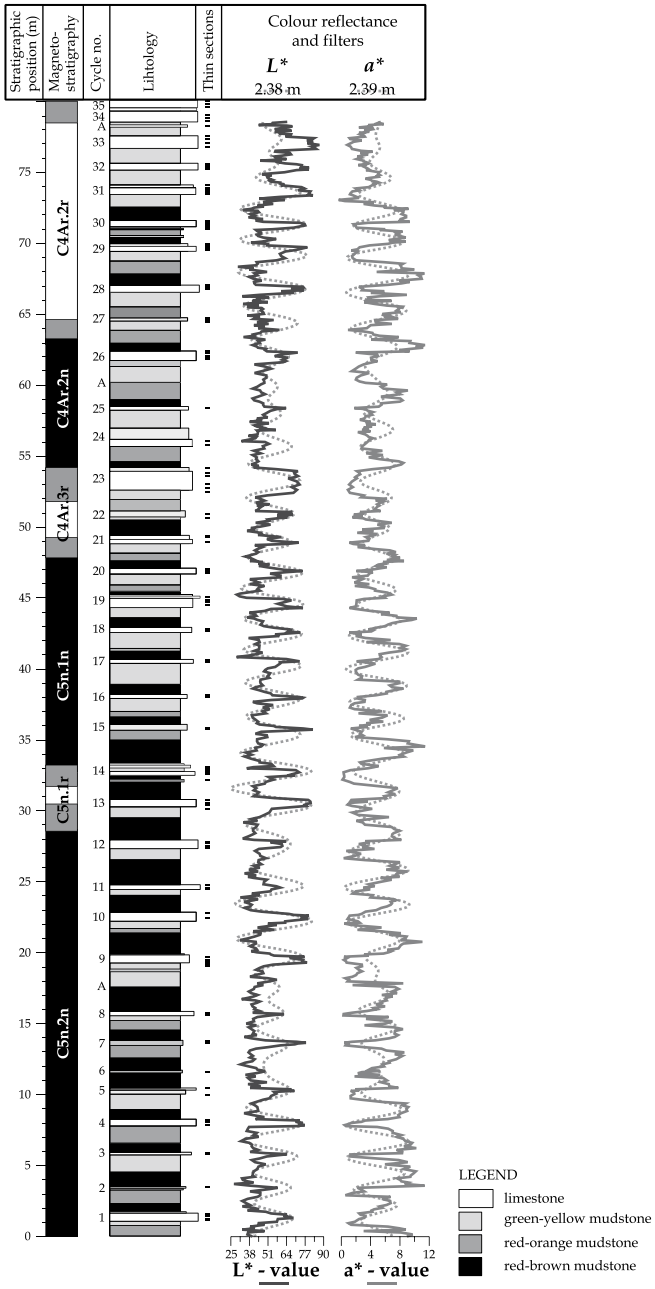

Figure 2.4 Lithologic column and magnetostratigraphy of the Cascante section. Grey shading in the polarity record represents uncertainty intervals between samples with certain polarity. Grey shades in the lithological column represent colour differences, see legend. Basic mudstone-carbonate cycles are numbered to the left of the column. Location of limestone samples collected for thin sections is also indicated. The graph is completed by a* (red) and L* (blue) colour reflectance records and their 2·38 and 2·39 m filters (dotted lines) (modified from Abdul Aziz *et al.*, 2004).

Interpretation

The limestone beds are interpreted as lacustrine carbonate deposits that accumulated in a shallow lake. The vertical tubes are interpreted as root bioturbation from a plant cover that developed on top of the limestone mainly after deposition. The horizontal cracks are interpreted as desiccation cracks that developed during short and/or repetitive periods of subaerial exposure and finally the desiccation of the lake. The root bioturbation and desiccation cracks lead to the formation of palustrine limestone. The cross-stratification and undulating character, mainly in the lower part of the limestone beds, are indicative of flowing water. In contrast, the abundant presence of complete charophyte stems is indicative of a low-energy environment and shallow water depth (Cohen & Thouin, 1987; Platt & Wright, 1991; García, 1994). The establishment of a shallow lake on the distal alluvial plain of a fan system could account for the reduced conditions leading to green-coloured clayey sediment in the top part of the mudstone in a basic cycle (Eardley *et al.*, 1973; Broekman, 1983; Abdul Aziz *et al.*, 2004). Alternatively, the green colour could be the result of reducing conditions during the deposition of the mudstone (Sagri *et al.*, 1989). According to Broekman (1983), the fine-grained organic matter is of allochtonous origin and was deposited on the lake shoreline during the transition from floodplain to lake depositional environment and vice versa. This interpretation is followed here, because the occasionally found horizontal laminations might indicate transportation of plant material into the basin. The organic material possibly was derived from the vegetation cover along the lake margin, which was washed into the basin during transgressive and regressive periods. Wetter climate conditions may have caused higher lake levels during limestone deposition and this may have enhanced vegetation growth that, in turn, reduced the inflow of clastic material further into the basin (Broekman, 1983; Platt & Wright, 1991).

2.4 Sedimentology – Microfacies Analysis

A detailed petrographic analysis of the limestone beds was performed to reconstruct duration and stability of lake expansions and water depth. Outcrop-scale description of the carbonate facies provides a rough estimate of these lake variables and the subsequent use of microfacies permits analysis of larger scale variations within these dynamic lake features. Carbonate petrography was carried out on a total of 145 thin sections from all 34 limestone beds in the Cascante section (Fig. 2.4). The limestone beds were sampled at a resolution of at least one thin section per 10 cm. To increase the visibility of carbonate particles, especially bioclast remains, the thin sections were partly stained using the red staining method of Lindholm & Finkelman (1972).

The microfacies analysis resulted in a grouping based on petrographic features and textures. Two main microfacies groups and eight sub-groups were differentiated (Table 2.1). The first group includes limestone beds showing microfacies typical of a shallow permanent lake environment, whereas the second group includes carbonate deposits showing features characteristic of a very shallow, transient (sensu Currey, 1990) lake environment. Currey (1990) defines transient lakes as having an inundation to desiccation time ratio of around 1:1, whereas permanent lakes have a ratio of over 1000:1. Letter labels for microfacies sub-groups were arbitrarily chosen. Thin sections that show characteristics in between two sub-groups were labelled as intermediate between the two sub-groups. Limestone beds consequently were labelled according to the microfacies code indicative of the deepest and most permanent lake environment recorded within the bed.

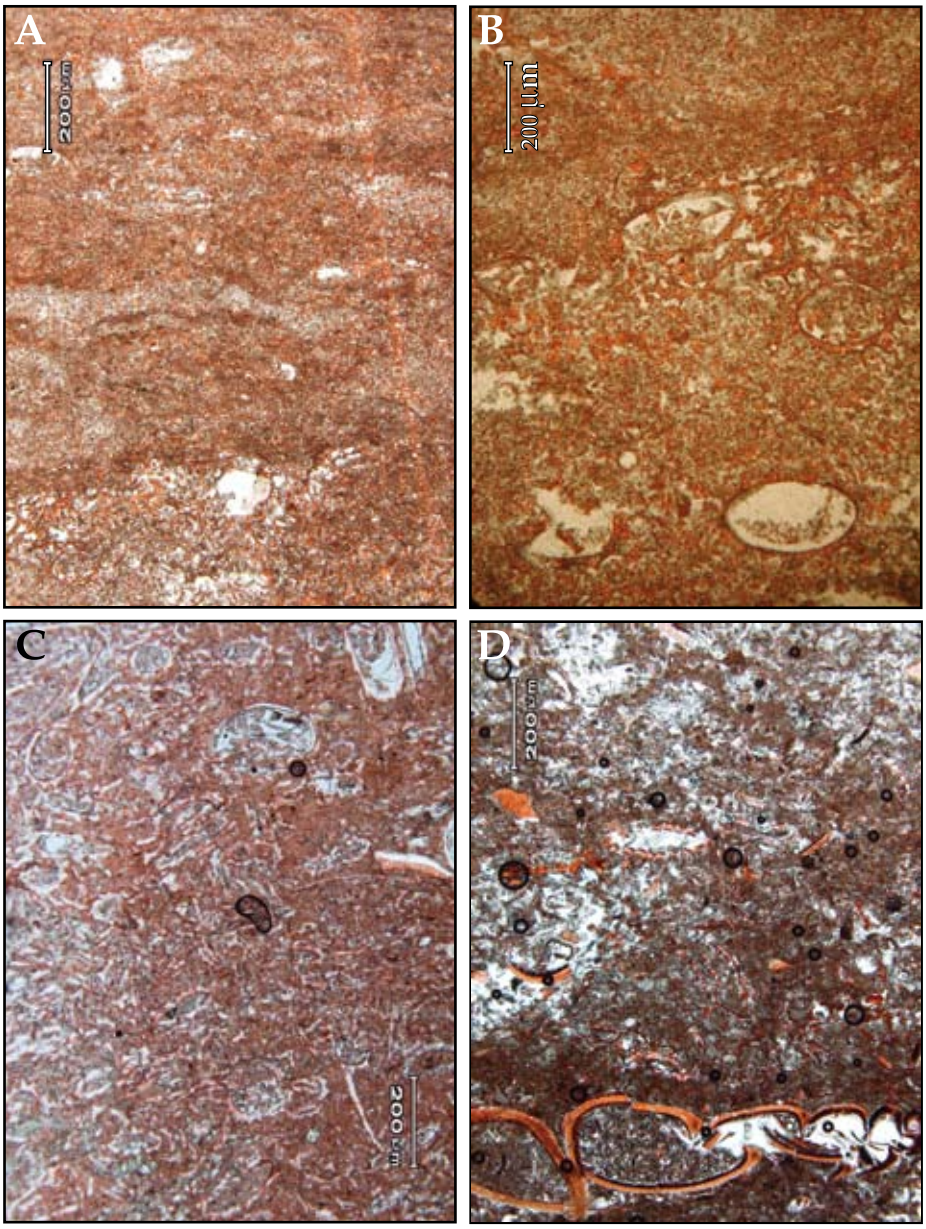

2.4.1 Shallow permanent lake microfacies

Description

The carbonate microfacies representative of shallow, permanent lake conditions include sub-groups Q, R and S (Figs. 2.5A, B and 6A). These sub-groups show a dense packing of carbonate micrite and bioclast fragments and, from sub-group Q to R to S, an increase in submillimetre-

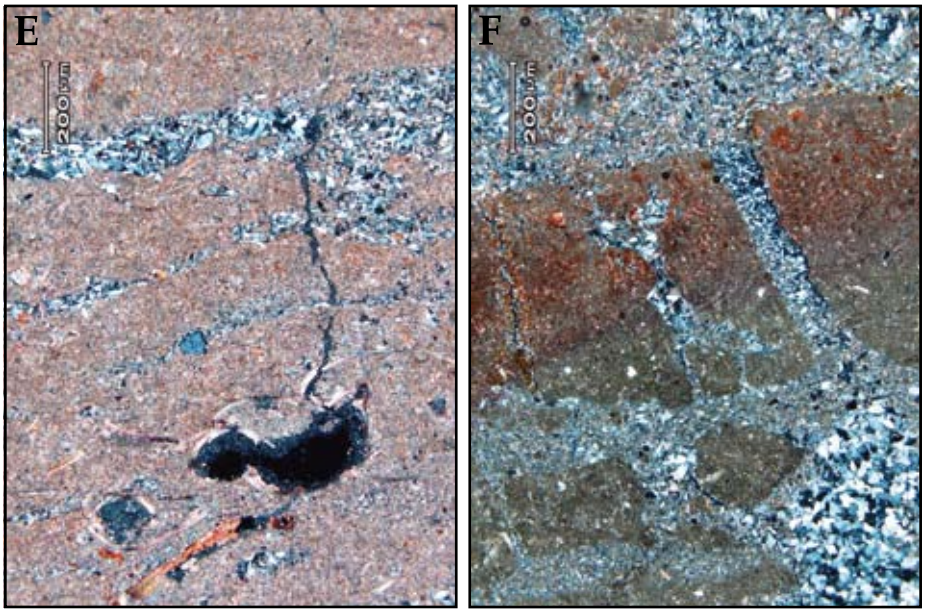

Figure 2.5 (A) Example of permanent lake microfacies sub-group R showing lamination of micrite and broken remains of charophyte stems and gyrogonites that were transported to (slightly) deeper lake environments, normal polarized light. (B) Example of permanent lake microfacies sub-group Q showing lamination of dense micrite and both broken and complete charophyte remains indicative for only short transportation, red stained section, normal polarized light, scale as on other photomicrographs. (C) Example of transient lake microfacies sub-group A displaying a high concentration of charophyte stems that show a slight orientation, some gastropod remnants are present, the completeness of delicate charophyte remains indicative for low-energy environments without much transportation before deposition, section red stained, normal polarized light. (D) Example of transient lake microfacies sub-group C showing a relatively high concentration of broken and complete bioclast remains of mainly gastropods, red stained section, normal polarized light. (E) Example of transient lake microfacies sub-group D showing broken gastropod and ostracod shell remains, (primary) lenticular gypsum occurs as filling of horizontal desiccation cracks, red stained section, cross-polarized light. (F) Example of transient lake microfacies sub-group E showing microbreccia with host rock and filling of cracks with micrite and gypsum, palustrine limestone, upper half red-stained, cross-polarized light.

scale lamination of micrite and bioclast fragments. Bioclast diversity and fragmentation, as well as packing of the bioclast fragments, increase from sub-group Q to S ('concentration' in Table 2.1). Bioclasts consist mainly of fragmented charophyte stems and gyrogonites and minor ostracod and gastropod shells, which are present chiefly in sub-group Q (Fig. 2.5B). None of the three sub-groups contains siliciclastic material coarser than the mud fraction, whereas clay material is present in minor amounts. No cracks and burrows have been observed, nor gypsum crystals. On outcrop scale, the limestone beds of this microfacies are indurated and have a well defined base and top. Beds are internally laminated to massive; small-scale cross-stratification and undulating structures are common, especially in the basal part of the beds. Bed thickness ranges from 0.4 to 0.9 m.

Interpretation

The dense packing of micrite and bioclast fragments and the sub-millimetre-scale laminations are interpreted as the result of deposition in relatively low-energy water environments. Lenticular gypsum, that is interpreted as primary gypsum by Anadón *et al.* (1992), is present abundantly

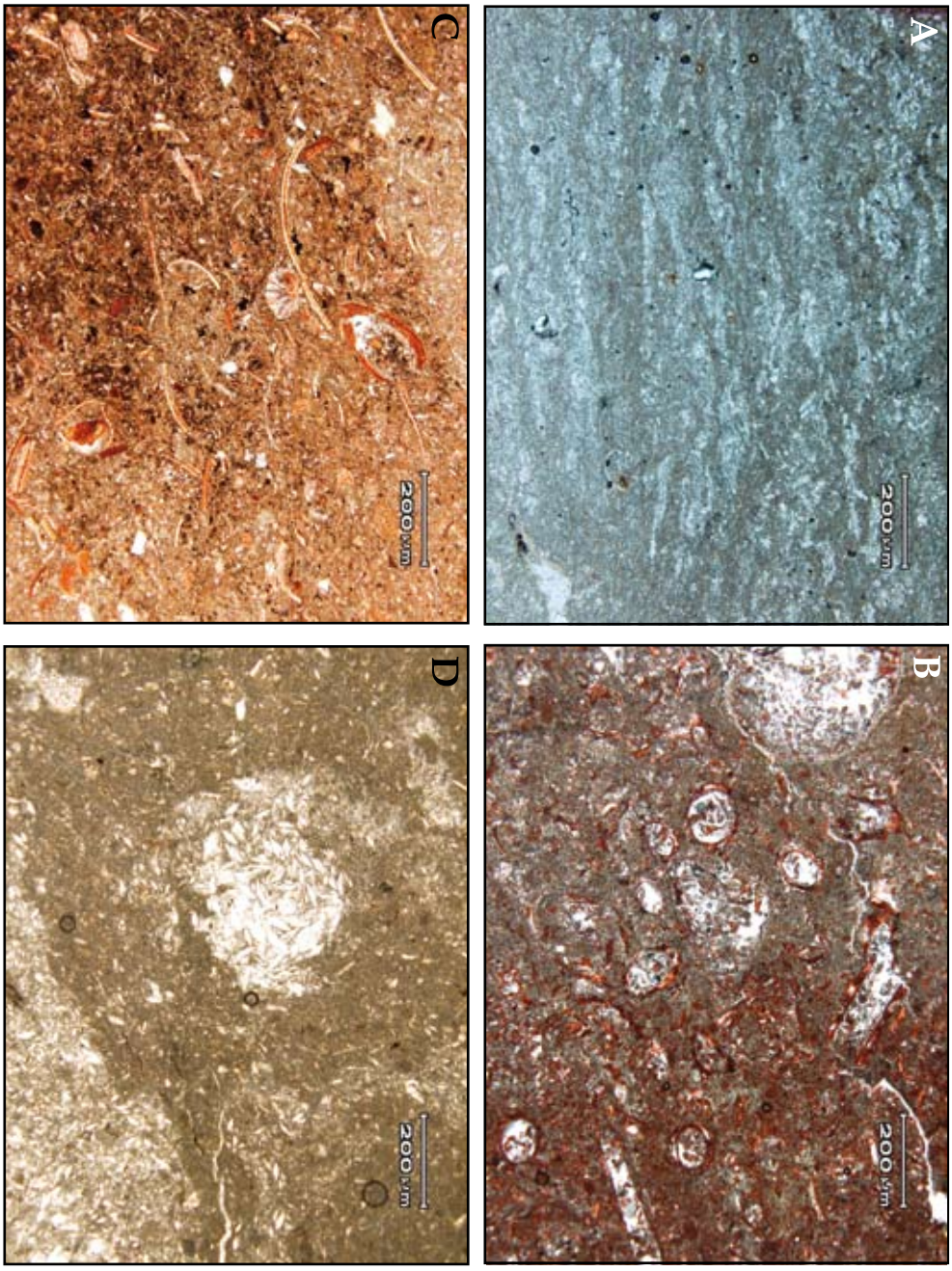

in the very shallow transient microfacies. The absence of cracks, burrows and lenticular gypsum in the shallow permanent lake microfacies indicates stable lacustrine conditions that prevailed for relatively long time periods (Currey, 1990). The abundance of fragmented charophyte stems and gyrogonites suggests that they were transported over a short distance from very shallow lake areas, where charophytes flourished, towards slightly deeper waters (Platt, 1989; Pérez *et al.*, 2002). Platt (1989) and Pérez *et al.* (2002) state that water depth in these environments probably does not exceed a few metres. Stable lacustrine conditions prevail when evaporation and groundwater discharge from the lake system are lower than precipitation and groundwater influx. These circumstances may be related to relatively continuous water inflow, together with low evaporation, and/or lack of extremely dry climatic conditions for a certain period of time. The increase in horizontally oriented bioclasts, clast fragmentation, and micrite and bioclast lamination from sub-group Q to S is interpreted as slightly higher energy and deeper conditions towards sub-group S. No microfacies are observed that indicate the deeper and less energetic settings that are expected when lake levels rise even more; this means that in the case of Cascante the 'deepest' observed lake is also the relatively highest energy environment probably indicating a shallow lake environment with a flat bottom.

2.4.2 Very shallow transient lake microfacies

Description

Limestones of this microfacies consist of massive, uniform carbonate micrite lacking lamination (microfacies A to E) and scarcely containing very fine sand-sized quartz grains (see also Freytet & Verrecchia, 2002). The distinction between subgroup Q (a microfacies typical of deposition in shallow permanent lake conditions; Fig. 2.5B) and sub-group A (Fig. 2.5C) is based primarily on the absence of lamination and reduced packing of micrite in sub-group A. From sub-group A to E, a decrease in diversity and packing of bioclasts is observed (Figs. 2.5C to F and 6B, C; Table 1). Charophyte stems and gyrogonites prevail in subgroups A and B (Figs. 2.5C and 6B), while many complete and some broken ostracod and gastropod shells are more common in sub-groups D and E (Figs. 2.5E and F). In sub-group C (Fig. 2.5D), all four types of, dominantly broken, bioclasts are present, although they are often not well-mixed. An increase in the amount of sub-millimetre-sized particles of organic matter, most probably derived from plant material, can be observed from sub-group C to D (Figs. 2.5D, E and 6C). Sub-millimetre-sized lenticular gypsum crystals occur often floating in the carbonate micrite, with their presence increasing from sub-group B to E. Limestone beds showing this microfacies group usually display mainly horizontal and some vertical cracks (Figs. 2.5E and F), and vertical burrow (striotubules) structures (Fig. 2.6D). The burrows become significantly more abundant from sub-group A to E. Horizontal cracking and

← *Figure 2.6* (A) Example of permanent lake microfacies sub-group S lamination of micrite and broken remains of charophyte stems and gyrogonites transported to (slightly) deeper lake environments, normal polarized light. (B) Example of transient lake microfacies sub-group B showing abundant and mostly complete charophyte remains indicative of low energy conditions, no preferred orientation of micrite or bioclasts, some signs of sub-aerial exposure and/or root action in upper part of photograph, section red stained, normal polarized light. (C) Example of transient lake microfacies sub-group C/D showing gastropod and unidentified shell remains at intermediate densities without clear orientation and organic matter, section red stained, normal polarized light. (D) Root burrow or striotubule filled with lenticular gypsum, host rock around burrow shows primary lenticular gypsum as well, not red stained, normal polarized light.

bioturbation features are virtually absent in subgroup A, while in sub-group E brecciation is intense (Fig. 2.5F). Cracks commonly are filled with a mosaic of lens-shaped sub-millimetre-scale gypsum crystals but, in some cases, they are filled partially with silt-sized to clay-sized siliciclastic material or fragmented host carbonate rock, the latter especially in desiccation breccia (sensu Normati &

Table 2.1 Specification of petrographic description, matrix, and bioclast characteristics of the eight carbonate microfacies sub-groups recognized in the Cascante section.

Group	Shallow *permanent lake* microfacies			Very Shallow *transient lake* microfacies				
Sub-group	S	R	Q	A	B	C	D	E
General characteristics (classification according to Dunham, 1962, and Folk, 1959)	Packstone and biomicrite. Charophyte stems, gyrogonites, ostracods and bivalves.	Wackestone and biomicrite. Ostracods, gastropods, charophyte stems, gyrogonites and bivalves. Some clotted micrite + fenestral features.	Wackestone and biomicrudite. Ostracods and charophytes. Clotted micrite and fenestral fabrics.	Packstone, biomicrite or biomicrudite Charophytes and gyrogonites, few gastropods, bivalves and thin ostracods	Wackestone and biomicrite Bioclasts same as in A.	Wackestone and biomicrite Gastropods, some charophyte stems gyrogonites and some ostracods	Wackestone and biomicrite to biomicrudite. Some quartz grains and organic matter	Mud to wackestone and biomicrite. Ostracods and some gastropods and bivalves. Organic matter and peloids. Intraclast character. Some quartz grains.
Micrite Concentration	-	+	++	- -	+/-	+/-	+/-	++
Lamination	++	+	+/-	- -	- -			- -
Prim. gypsum	- -	-	+/-	- -	-	+/-	+	++
Burrows/roots	- -	- -	- -	-	+/-		+	++
Sorting	++	+	+		+	+/-	+/-	- -
Diversity	+	+/-		++	+	+/-	-	- -
Orientation	++	+	+/-	+/-	+	+/-	-	- -
Fragmentation	++	+	+/-	+	+/-			++
Concentration	++	+	-	++	+	-	- -	- -
Net water budget during deposition (interpretation) low high								

Salomon, 1989) of sub-group E. The sub-groups B, C and D show gradational microfacies features between the two end-member sub-groups A and E.

In outcrop, the carbonate beds displaying very shallow transient lake microfacies usually are massive and/or poorly laminated and frequently intercalate with thin green clay and dark grey organic-rich mudstone beds that have a thickness between 1 and 10 cm.

Interpretation

The lack of lamination in all sub-groups, minor amounts of gypsum and abundant well- preserved charophyte cysts and stems, and gyrogonites in this microfacies indicates a very shallow, low energy freshwater lake environment. The delicate charophyte stems grow in shallow lake margins and usually break apart when agitated and transported, as observed in modern lake environments, where meadows of charophytes flourish at depths of less than 5 m (Platt, 1989; García, 1994; Pérez *et al.*, 2002).

The decrease in abundance and diversity of bioclasts and the increased organic matter and amount of root burrows in the limestone, as observed from sub-group A to E, indicate a gradual change from a low energy, shallow lake environment (sub-group A; Fig. 2.5C) towards a shallow lake environment that is more swampy. This interpretation is supported by the increase in lenticular gypsum floating in the carbonate micrite from sub-group A to E. Anadón *et al.* (1992) relate similar lenticular gypsum crystals to a primary evaporate phase in extremely shallow lake environments, even though Albesa *et al.* (1997) report that the salinity is not necessarily high. The higher amount of horizontal cracks, that are interpreted as desiccation cracks, and root burrows (striotubules) observed from sub-group A to E, suggests an increase in frequency and duration of sub-aerial exposure (sub-group E in Fig. 2.5F). Alonso Zarza (2003) states that the absolute exposure time and frequency needed to form palustrine features in freshwater lake carbonate deposits are not known and may be relatively short, even a season. The primary exposure features can form under fluctuating lake water level, which is accompanied by deposition of organic plant material and clay laminae intercalated in the limestone bed. In terms of inundation versus exposure time, carbonate microfacies sub-groups A and B characterize a 'persistent' lake environment, suggesting an inundation versus desiccation ratio of 10 to 1000:1 (Currey, 1990), while microfacies sub-groups C to E represent a 'transient' lake environment, with a ratio of 1 to 10:1. Limestone beds of the very shallow transient lake microfacies sub-groups generally show their relatively deepest lake phase just above the middle of the bed.

2.5 Palaeoenvironmental Cycles

2.5.1 Sedimentary model for the basic cycle

The remarkable lateral continuity of lithologic features of both mudstone and limestone beds in the Cascante succession suggests that they were deposited in a low-energy, endorheic ramp-type basin. In this setting, small-scale lake-level fluctuations resulted in the submergence or desiccation of large areas of the basin (Platt & Wright, 1991). The description and interpretation of the basic mudstone-limestone sedimentary cycle are schematically depicted in Figure 2.3. It should be noted that the mudstone part of the cycle is on average three to four times thicker than the limestone interval. Within the basic cycle, red mudstone is interpreted as a low-energy sheet flow deposit that underwent sub-aerial exposure after deposition in a distal alluvial plain setting. The transition from a red to a greenish colour towards the top of the mudstone deposit most probably is caused

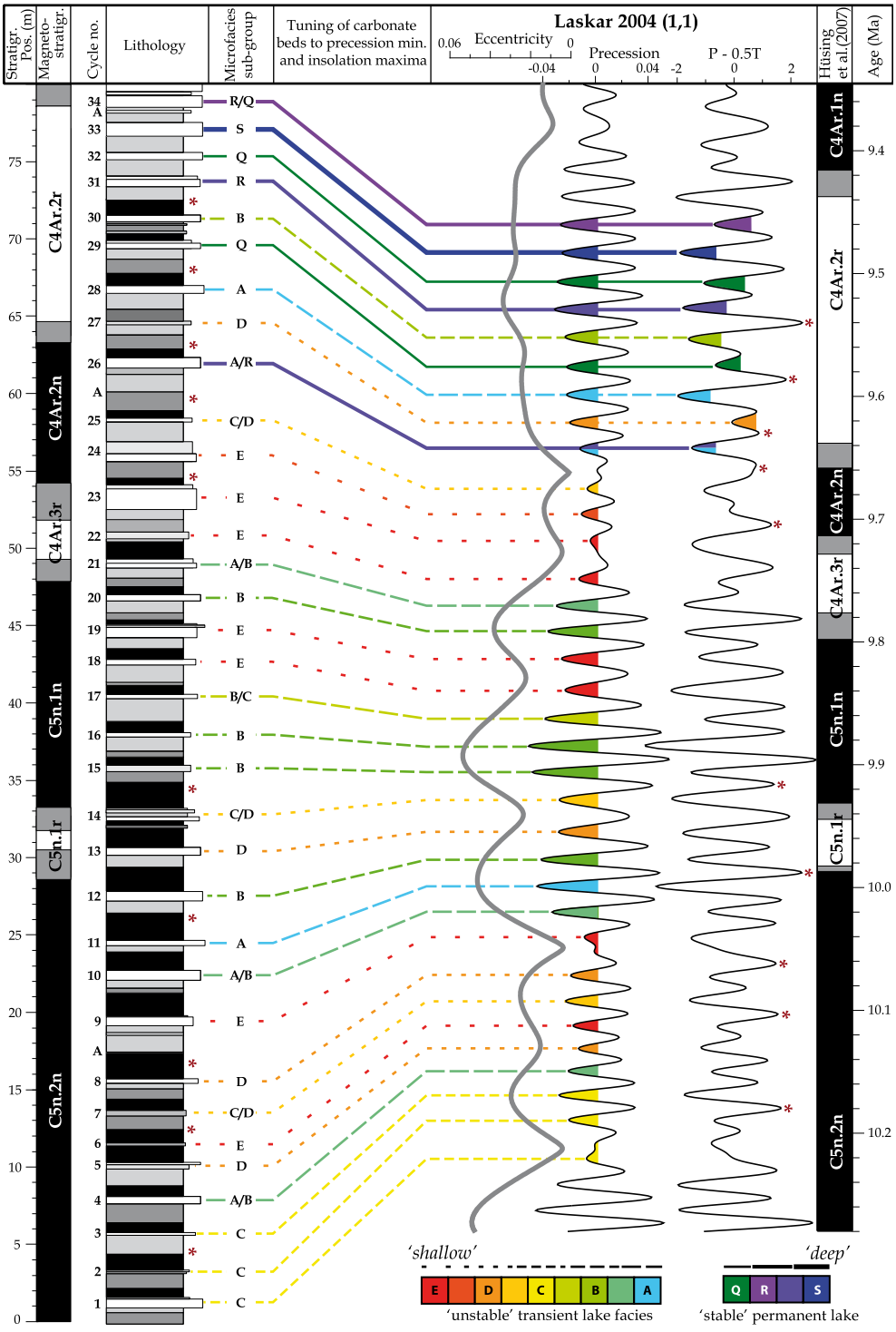
Stratigr. Pos. (m)
Magneto-stratigr.
Cycle no.
Lithology
Microfacies sub-group
Tuning of carbonate beds to precession min. and insolation maxima
Laskar 2004 (1,1)
Eccentricity
Precession
P - 0.5T
Hüsing et al.(2007)
Age (Ma)
C4Ar.2r
C4Ar.2n
C4Ar.3r
C5n.1n
C5n.1r
C5n.2n
'shallow'
'deep'
'unstable' transient lake facies
'stable' permanent lake

← *Figure 2.7* Microfacies analysis results of all limestone beds in the Cascante section and their correlation to successive precession minima and insolation maxima according to the magnetostratigraphy of Hüsing *et al.* (2007). Grey in the polarity record indicates age uncertainty intervals as given by these authors. Colours and different line characteristics indicate microfacies sub-groups (see legend). Asterisks indicate thick mudstone intervals. For details on the lithological column see Figure 4.

by reduction and leaching of the underlying muddy sediment when lake levels rose following mudstone deposition. Organic-rich layers below and on top of the lacustrine limestones are interpreted as deposited during the lake transgression and regression. The freshwater limestone is associated with lake-level highstands resulting in a shallow lake undergoing varying scales of fluctuating lake levels. In some cases, low lake levels resulted in episodic exposure of the carbonate mud and the formation of palustrine features. Lack of significant siliciclastic input into the carbonate lake can be related to high lake levels, resulting in a rise of the base level of erosion trapping the sediment in higher areas (Picard & High, 1981), and/or to the development of a dense vegetation cover along the lake margin that kept sediments in place and promoted chemical instead of physical weathering (Platt & Wright, 1991).

2.5.2 Larger-scale environmental variations

The codes of the different microfacies sub-groups for the 34 limestone beds in the Cascante section have been plotted in Figure 2.7. Carbonate microfacies characteristics of very shallow transient lake environments prevail in the lower part of the section below cycle 26. Two intervals with three basic cycles (10 to 12 and 15 to 17) and one interval with two cycles (20 and 21) contain limestones representative of more 'persistent' (see above) lake environments (sub-groups A and B). Except for cycle 4, all other limestones in the lower part of the section show more 'transient' lake environments (*i.e.* palustrine limestones of sub-groups C, D and E) representing shallower and more variable lake conditions. Below cycle 26, no limestone bed with microfacies indicative of shallow permanent lake conditions is present. Above that cycle, the limestone beds comprise microfacies sub-groups that indicate the more persistent environments of the very shallow transient lake microfacies (sub-groups A and B) and the permanent environments of the shallow permanent lake microfacies (sub-groups Q, R and S), except for cycle 27. Thus, lake levels increase and lake environments become more stable from cycle 26 onwards, probably indicating the transition to the thick lacustrine limestone unit that overlies the studied section. This uppermost interval is characterized by alternation of relatively deeper and shallower lakes in every other bed. This pattern shifts one cycle from 28 to 29. Somewhat deeper lakes are found in cycles 26, 28, 29, 31 and 33, whereas shallower lakes are found in cycles 27, 30, 32 and 34.

2.6 Cyclostratigraphy

2.6.1 Astronomical forcing

The stratigraphic regularity of the basic cycle in the Cascante section strongly suggests an allocyclic forcing mechanism. Abdul Aziz *et al.* (2004) therefore applied Blackman-Tukey (BT) and maximum entropy (ME) spectral analysis on colour reflectance records (Fig. 2.4) in the depth domain. The dominant peak in the resulting power spectra could be related to the basic, 2.2 m cycle. Additional power was found at lower frequencies, with a thickness ratio of about 1:2:5. This ratio closely corresponds to the astronomical period ratio of climatic precession, obliquity and

short (*ca* 100 kyr) eccentricity (Abdul Aziz *et al.*, 2004). Detailed age control in the section was derived from the magnetostratigraphy (Fig. 2.4) calibrated to the geomagnetic polarity timescale CK95 using mammal biostratigraphic data (Abdul Aziz *et al.*, 2004). Application of this age model revealed a period of 20 to 26 kyr for the basic cycle. This period is well within the range of the duration of the climatic precession cycle. The other peaks identified by the spectral analysis indicate a period of *ca* 41 kyr for the cycle with a thickness twice that of the basic cycle and around 100 to 150 kyr for the cycle with a thickness of five times the basic cycles. These cycles are tentatively related to obliquity and the *ca* 100 kyr period of the short eccentricity cycle. Abdul Aziz *et al.* (2004) concluded that these results strongly indicate that the sedimentary cyclicity in the Cascante section is related to astronomical forcing. The use of the recently improved astronomical tuned timescale (Lourens *et al.*, 2004) and the astronomical ages resulting from the tuning of the deep marine Monte dei Corvi section (Hüsing *et al.*, 2007) does not change the outcome of the statistical analysis.

The potential astronomical control requires further exploration. In order to elaborate on this, the sedimentary cycles need to be interpreted in terms of astronomical climate forcing. Once the phase relationships have been established, an astronomical tuning of the sedimentary cycles by correlation of individual cycles to calculated astronomical target curves can be constructed starting from the magnetostratigraphic age calibration. Finally, the environmental interpretations derived from the carbonate microfacies analysis can be compared with the target curves and the working hypothesis can be examined. This cyclostratigraphic exploration does not imply that alternative interpretations of the cyclicity are excluded. However, the data strongly suggest orbital forcing and this option has been elaborated to (finally) prove astronomical forcing using an integrated approach.

2.6.2 Climatic interpretation of the sedimentary cycles

The alternation of shallow lake and distal alluvial plain facies indicates constant shifts at 10^4 year timescales between an annual or seasonal net positive and negative water budget, when the basic cycles are interpreted as forced by climate variations. From the sedimentological data alone, it is impossible to deduce whether these variations were caused by changes in precipitation, evaporation, seasonality, rain season and/or possibly other climatic factors. Horizontal desiccation cracks and root traces, which increase towards the top of the carbonate beds, indicate that lake levels often were variable and high lake levels only prevailed for a short period of time. Lake-level fluctuations resulted in rapid drowning or desiccation of the depositional site. The weak development of palustrine features indicates that sedimentation resumed not long after the ending of lake conditions, as palustrine features can form rapidly in *ca* 10^1 to 10^3 years (Alonso Zarza, 2003). The amount of time represented by the limestone versus mudstone part of the basic cycle is difficult to specify. The lack of well-developed pedogenic features in the mudstones suggests that sedimentation kept pace with soil formation processes within the mudstones (Buurman, 1980). Sedimentation was apparently relatively continuous during both the deposition of the mudstone and limestone part of the basic cycle. However, major differences in the sedimentation rate between the two end-member lithologies may exist. In conclusion, the observed regular and repetitive development of full lacustrine conditions in a prevailing subaerially exposed distal floodplain requires a cyclic forcing mechanism to yield a positive water budget during specific and relatively short time periods.

2.6.3 Phase relationships – geological data

Correlation of individual mudstone and carbonate cycles with calculated astronomical target curves requires a knowledge of the phase relationship of the two basic cycle end-member lithologies with the orbital parameters. Consequently, the climatic influence in terms of net water budget of orbital extremes and, additionally, the climatic conditions required for development of the depositional environments of mudstone and limestone have to be unravelled. This rationale is termed phase relationship between lithology and orbital parameters.

In the northern hemisphere, climatic precession minima (summers in perihelion) cause high summer and low winter insolation at the top of the atmosphere resulting in enhanced seasonality. Numerous studies have demonstrated the influence of precession on circum-Mediterranean climate as recorded by Neogene marine (Rossignol-Strick, 1983; Hilgen *et al.*, 1999; Foucault & Mélières, 2000) and continental sediments (Steenbrink *et al.*, 1999; Abdul Aziz *et al.*, 2000; Magri & Tzedakis, 2000). Increased clay contents in cyclic Pliocene marl sequences deposited offshore Gulf of Cadiz suggest higher annual runoff from a southern Spanish drainage area at times of precession minima (Sierro *et al.*, 2000). Similarly, indications for humid conditions during precession minima have been implied for marl sequences of the Abad Formation in the Sorbas Basin in southern Spain (Sierro *et al.*, 1999; Vázquez *et al.*, 2000). Sapropel formation in the eastern and western Mediterranean basins has been related to increased winter precipitation from southern, and possibly northern, Mediterranean borderlands during precession minima (Lourens, 2004). Magri & Tzedakis (2000) reported temperate-stage forest expansions during boreal summer insolation maxima (during precession minima) for the last 200 kyr in central Italy, which they relate to higher annual net precipitation. Maximum forest coverage occurs during autumn insolation maxima, which Magri & Tzedakis linked to the absence of extreme summer evaporation and, consequently, to maximum net water budget. On the other hand, a significant contraction of the forest coverage is found during winter insolation maxima (*i.e.* summer insolation minima during precession maxima) and March insolation maxima.

Reduced clastic supply that resulted in marl-rich intervals in the Pliocene Gulf of Cadiz is observed during short and long eccentricity minima (Sierro *et al.*, 2000). Moreover, intervals devoid of sapropels in the Mediterranean occur during eccentricity minima and are related to lower precipitation in the southern, and possibly northern, borderlands (Lourens, 2004). Short (*ca* 100 kyr) and long (405 kyr) eccentricity minima most probably result in prolonged periods of relatively dry climate conditions that can lead to lake-level lowstands in the Spanish mainland.

2.6.4 Phase relationships – climate modelling

In order to determine the impact of climatic precession extremes on climate in Spain, model simulations were performed by using an atmospheric global climate model of intermediate complexity, SPEEDY, coupled to a slab ocean and a simple land model. SPEEDY is a primitive equation model with simplified physics parameterizations (Molteni, 2003) that has a horizontal resolution of about 3.75x3.75 (T30) and seven vertical levels (Hazeleger *et al.*, 2003). The land model consists of a simple bucket model, which implies that the soil moisture cannot exceed 15 cm per grid box. Redundant soil moisture is defined as runoff. Three 100 year simulations using the SPEEDY climate model were carried out: (i) a control run with present-day orbital parameters; (ii) a minimum precession run (eccentricity = 0.056, precession = 0.055); and (iii) a maximum precession run (eccentricity = 0.058, precession = 0.058). A precession maximum (minimum) means winter (summer) solstice in perihelion. Precession is defined as $e \sin(p + x)$ with e the eccentricity of the orbit of the Earth and x the angle between the vernal equinox and perihelion

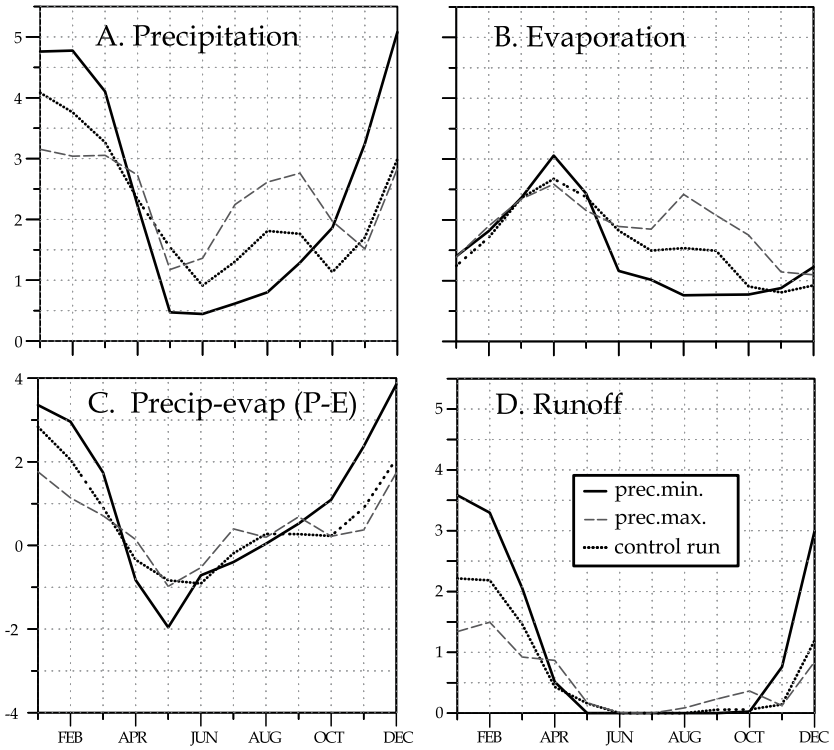

Figure 2.8 Monthly area averaged values for 'Spain' (10.5 to 2° W; 37 to 44.5° N, four gridboxes) of: (A) precipitation; (B) evaporation; (C) precipitation minus evaporation; and (D) runoff for the control run (dotted black line), minimum (climatic) precession run (solid line) and the maximum precession run (dashed line). All values are in mm day^{-1} and averages of the last 10 years of 100 year simulations (see text for details).

(measured counter-clockwise). The used values for precession are the extreme values occurring in the last one million years (Berger, 1978). For the precession simulations, obliquity was kept fixed at 22.08, *i.e.* the minimum value for the last one million years. A fixed obliquity was used to focus on the precession signal without the possible interference of obliquity. For all three runs, boundary conditions such as orography, concentration of trace gases, vegetation and ice sheets were kept to present-day values. A more extensive description of the experimental set-up can be found in Tuenter *et al.* (2003). The model results are shown as averages over the last 10 years of 100 year simulations. Ten years are used to average out annual variability, while a longer averaging period is not used to ensure that the model is in equilibrium after 90 years.

The model shows that during winter, net precipitation (precipitation minus evaporation) in precession minimum is higher than in precession maximum (Fig. 2.8C) while, for summer, there is not much difference between the precession extremes. The large difference in net winter precipitation is caused by stronger precipitation during minimum precession, whereas winter evaporation is equal for both minimum and maximum precession (Fig. 2.8B). In the model, the reason for enhanced winter precipitation during precession minima is higher Mediterranean sea surface temperatures both in summer and in winter. These higher temperatures are due to increased summer insolation which, in the winter, results in higher evaporation and formation of clouds

Table 2.2 Annually averaged values for 'Spain' (10.5 to 2° W; 37 to 44.5° N, four gridboxes) of precipitation, evaporation, precipitation minus evaporation (net precipitation), and runoff for the control run, minimum precession, and maximum precession. All values are averages of the last 10 years of 100 year simulations.

Simulated annual values	Precipitation (mm day^{-1})	Evaporation (mm day^{-1})	Precip.-Evap. (mm day^{-1})	Runoff (mm day^{-1})
Control run	2.22	1.61	0.61	0.66
Precession min.	2.47	1.47	1.00	1.10
Precession max.	2.37	1.88	0.49	0.54

over the Mediterranean. In summer, higher precipitation occurs during maximum precession (Fig. 2.8A), although summer net precipitation is similar for both precession extremes (Fig. 2.8C) because of an increase in evaporation (Fig. 2.8B). Annually, higher net precipitation occurs during minimum precession (Table 2.2).

In the model, the annual net precipitation is dominated by winter precipitation for both minimum and maximum precession, suggesting that winter precipitation plays an important role in runoff and groundwater supply that together determine lake levels. Runoff acts accordingly with higher winter and annual runoff during precession minima (Fig. 2.8D; Table 2.2). Therefore, it is probable that high lake levels and carbonate deposition in the Cascante section occurred during precession minima.

The phase relationship of high lake levels during precession minima derived from the SPEEDY model are in line with the sedimentological findings in the Gulf of Cadiz (Sierro *et al.*, 2000) and the Sorbas Basin (Vázquez *et al.*, 2000) as well as those from sapropelic layers in the Mediterranean (Lourens, 2004). Moreover, the results agree with forest expansions during precession minima (Magri & Tzedakis, 2000). Considering the geological and modelling data, the phase relationship between high lake level (and limestone formation) and enhanced net winter precipitation during precession minima is favoured.

2.6.5 Astronomical Tuning

An astronomical tuning is constructed for the Cascante section using the astronomical ages for the reversal boundaries of Hüsing *et al.* (2007) and the inferred phase relationships between the carbonate beds to minimum precession and mudstone beds to maximum precession, as discussed above. The astronomical tuning is established by correlating the basic cycles to the precession target curve of Laskar *et al.* (2004) starting from all the reversal boundaries upwards and downwards (Fig. 2.7). Except for the base of chron C5n.1r, which is *ca* 10 kyr younger in Cascante, the tuning produces similar astronomical ages for chron boundaries as calculated by Hüsing *et al.* (2007). This observation implies that exactly the same number of precession-related cycles is present in the Cascante section as in the time-equivalent interval in the Monte dei Corvi section. This outcome confirms the astronomical forcing and dominant precession control of the basic cyclicity at Cascante.

As described above, the microfacies analysis revealed larger scale lake-level variations comprising several basic cycles. Lowstands therein, with beds showing features indicative of the shallowest transient lake environment (microfacies sub-groups C, D and E; cycles 1 to 3, 5 to 6, 7 to 9, 13 to 14, 18 to 19 and 22 to 25), correlate to minimum eccentricity related to the *ca* 100 kyr cycle

(Fig. 2.7). Highstands with beds that formed in the relatively deeper transient lake environment (microfacies sub-groups A and B; cycles 4, 10 to 12, 15 to 17 and 20 to 21) were deposited during maxima of the short eccentricity cycle. The prolonged lowstands (cycles 1 to 9 and 22 to 25) correspond to long (405 kyr) eccentricity minima and prolonged highstands (cycles 10 to 21 and 26 to 34) to long eccentricity maxima (Fig. 2.7). This link between lake level, as derived from microfacies analysis, and eccentricity indicates that the eccentricity modulation of the precession amplitude played an important role in determining longer-term variations in lake level. The observed lake-level lowstands during short and long eccentricity minima are in line with the modulating effect of eccentricity and with Mediterranean marine geological data (Sierro *et al.*, 2000; Lourens, 2004).

In the interval above cycle 25, successive limestone beds display an alternation of deeper and shallower lake carbonate deposits (Fig. 2.7). Moreover, the mudstone beds reveal a regular alternation in this interval; successive mudstones show a thick and thin alternation while red colouring is present in the thicker beds (shown with an 'asterisk' in Fig. 2.7) and absent in the thinner beds (cycles 27 to 31 in Fig. 2.7). These kinds of alternations in basic precession controlled cycles are found in the marine realm as well, where thick pronounced and thin, vague sapropels alternate (Hüsing *et al.*, 2007). Such alternating patterns that occur superimposed on a basic precession-forced cyclicity are called precession-obliquity interference patterns. These patterns originate from interference of these two orbital parameters, which typically are found during times of low eccentricity when the precession amplitude is reduced. In particular, these patterns occur at times of minimum eccentricity related to the long-period 2.4 Myr eccentricity cycle (Abdul Aziz *et al.*, 2003a; Laskar *et al.*, 2004; Hüsing *et al.*, 2007). Precession-obliquity interference patterns have also been recognized in continental sediments (Abdul Aziz *et al.*, 2003a). The interference pattern in the Cascante section (cycles 26 to 34) indeed occurs during a minimum of the 2.4-Myr eccentricity cycle. This cycle reaches its absolute minimum at 9.52 Ma, which is the minimum in the 2.4-Myr bandpass filter of the eccentricity time series (Laskar *et al.*, 2004).

In the marine realm, the interference patterns in sapropel successions fit with those in the insolation target curves (Hüsing *et al.*, 2007). Such a fit can be used to confirm the astronomical tuning in these sensitive deep marine settings. In the Cascante section, the details in the interference pattern also fit with the combined precession-obliquity target curve (P-0.5T in Fig. 2.7). Deeper, more permanent lakes occur during extreme summer insolation maxima (P-0.5T minima) and thicker, more intense red mudstones during extreme summer insolation minima, which results from the additional influence of obliquity maxima and minima, respectively. This fit is consistent with the astronomical tuning of the Cascante section. In the lower part of the section, interference patterns also are present, especially below cycle 9 (see Fig. 2.7). However, this is not further discussed in detail because the patterns are much less pronounced in this interval and an independent quantitative record is needed to prove the correlation. Nevertheless, there is a good fit with the interference patterns in P-0.5T in this interval as well.

In conclusion, the astronomical tuning of the Cascante cycles to the precession time series does not reveal any significant difference in the astronomical age of the magnetic reversal boundaries as compared with the astronomically tuned sapropel succession at Monte dei Corvi (Hüsing *et al.*, 2007). The larger scale lake-level variations, revealed by microfacies analysis, fit well with the eccentricity target curve as expected from Mediterranean marine geological data. Additionally, precession-obliquity interference patterns in the upper part of the section reveal a good fit with the insolation target curve. These results confirm the astronomical forcing working hypothesis of the sedimentary cycles in the continental Cascante section.

2.7 Discussion

The integrated cyclostratigraphic study was carried out to explore further the astronomical forcing of sedimentary cyclicity in the Cascante section, as previously suggested by the results of spectral analysis of colour records (Abdul Aziz *et al.*, 2004). All data are now consistent with the astronomical forcing hypothesis, indicating that astronomical forcing is indeed the most probable mechanism. Outcrop sedimentology, microfacies analysis, magnetostratigraphy and modelling results show that (all) palaeoenvironmental variations at 10^4 to 10^5 year time scales could be related to astronomically forced climate variations. The basic cycle is forced by the climatic precession cycle, whereas longer-term lake-level variations are related to the short and long eccentricity cycles. Obliquity influence is observed during periods of low eccentricity.

The dominance of astronomically forced environmental variations throughout the Cascante section implies that orbitally induced changes in insolation had a prominent imprint on climate in Spain during the Late Miocene. These variations are recorded, especially in low-gradient closed basin settings such as Cascante. Lake-level fluctuations could have been forced by various mechanisms, mainly tectonics, climate and autogenic processes. Based on the combined cyclostratigraphy and microfacies study of the Cascante section it is argued that tectonic, autogenic and local climate processes had no significant effect on the Cascante palaeoenvironment on 10^4 to 10^5 year time scales. From a tectonic point of view, basin subsidence and/or margin uplift apparently occurred at constant rates or at least the difference between the two factors remained similar on the 10^4 to 10^5 year time scales, such that recorded palaeoenvironmental changes at these timescales are exclusively related to orbital climate variations.

2.7.1 Gradual change

Different scales of lithological cyclicity in the Cascante section are ascribed to astronomical forcing. In theory, these astronomical signals can be subtracted from the record in order to examine whether other unexplained palaeoenvironmental variations exist in the Cascante section; however, this can strictly be done only by using quantitative records. The present proxies are not indicative of any variations on timescales of 10^4 to 10^5 years, that are not related to astronomical forcing. On longer timescales, a gradual shift from dominant transient to mixed transient-permanent lake environments is observed after cycle 25 (Fig. 2.7) culminating in the fully lacustrine limestone unit on top of cycle 34 (Fig. 2.2). Clearly, this shift cannot be explained by the astronomical cycles discussed before. The causes for this major shift can be tectonics, non-astronomical climate, astronomical climate forcing because of cycles with a longer period, or autogenic processes.

Million-year timescale changes, such as the shift to deeper and more permanent lake environments after cycle 25 in the Cascante section, commonly are related to tectonic processes. In the lacustrine record of the Triassic Newark Basin, large-scale lithological variations are interpreted to reflect long-period astronomical climate variations (Olsen & Kent, 1996). However, a decisive conclusion about the potential long-period orbital climate forcing in the succession studied by Olsen & Kent (1996) cannot be made because of insufficient absolute age control and lack of an astronomical target curve for the Triassic. In the Neogene, eccentricity and obliquity comprise long-period cycles of *ca* 2.4 Myr and *ca* 1.2 Myr, respectively (Laskar *et al.*, 2004). Recently, the influence of these quasi-cycles on temperature and precipitation of climate of the Iberian Peninsula has been suggested by their impact on mammal turnover rates (Van Dam *et al.*, 2006). In particular, long-period eccentricity minima, that are successively 2.0 and 2.8 Myr apart, resulted in prolonged absence of extreme summer conditions leading to an increase in both wet-adapted

small mammal lineages and total diversity (Van Dam *et al.*, 2006). In Cascante, the shift above cycle 25 from transient lake environments in the wettest phase of the basic cycle to a mix of transient and permanent lake environments occurs at an eccentricity minimum of *ca* 2.4 Myr (Fig. 2.7), whereas the environmental effect is consistent with the results of Van Dam *et al.* (2006). This coincidence is tempting, although proof for such a link should come from the accurate dating of a number of such large-scale transitions, ideally in different basins. Note that the phase relationship with eccentricity would then be different for the *ca* 2.4-Myr cycle than for the much better known short and long eccentricity cycles.

2.8 Conclusions

In the Cascante section, high-resolution magnetostratigraphic age control, together with carbonate petrography and outcrop sedimentology, as environmental proxies, reveals that all palaeoenvironmental signals at 10^4 and 10^5 year time scales are related to astronomical climate forcing. Modelling results show, consistent with geological data, that lake-level highstands are related to higher net winter precipitation during precession minima. The robust astronomical tuning reveals that the longer-term lake-level highstands, as revealed by the microfacies analysis, occur during *ca* 100-kyr and 405-kyr eccentricity maxima, as a consequence of the modulation of the precession amplitude. Subtracting the astronomical signals from the palaeoenvironmental variation in the Cascante section revealed a shift towards deeper and more permanent lake environments at times of precession minima in the upper part of the section. This shift, which culminates in a thick lacustrine limestone unit on top of the studied section, remains unexplained, but may be triggered by tectonics, non-astronomical climate change, astronomical climate forcing because of very long period cycles, and autogenic processes.

In summary, the results illustrate that cyclostratigraphy is a powerful tool to study palaeoenvironmental variations in continental successions at timescales greater than 10^3 years. Astronomical climate forced variability can be constrained very well, if sufficient age control and palaeoenvironmental proxies are present. Such a detailed study can be especially useful in Late Neogene successions, for which the geomagnetic timescale has been improved considerably by the incorporation of astronomically tuned reversal ages (Lourens *et al.*, 2004; Hüsing *et al.*, 2007).

2.9 Acknowledgements

Jesus Sanchez-Corral from the Universidad Complutense de Madrid and Otto Stiekema from Utrecht University are thanked for thin section preparation, the Instituto Aragone´s de Gestión Ambiental (INAGA) for sampling licenses, and Dr Anne van der Weerd for field assistance. HA acknowledges the financial support of the Dutch Science Foundation (NWO-ALW). Dr Frits Hilgen is thanked for useful discussions and improvements on earlier versions of the manuscript. Prof. Ildefonso Armenteros, Dr Miguel Garcés and Dr Wan Yang are acknowledged for their constructive reviews.

CHAPTER 3

Orbital climate forcing in mudflat to marginal lacustrine deposits in the Miocene Teruel Basin (NE Spain)

Hemmo A. Abels, Hayfaa Abdul Aziz, Dario Ventra, Frederik J. Hilgen

Based on:
H.A. Abels, H. Abdul Aziz, D. Ventra, F.J. Hilgen, in review. Orbital climate forcing in mudflat to marginal lacustrine deposits in the Miocene Teruel Basin (NE Spain). *Journal of Sedimentary Research*.

3.1 Abstract

Upper Miocene, mudflat to marginal lacustrine sediments were deposited on the fringes of an alluvial fan system in the low gradient, endorheic southern Teruel Basin, North-East Spain. The 147 m thick Prado succession consists of fifty-five meter-scale lithofacies cycles, displaying a clastic-rich and a carbonate-rich interval. The clastic-rich parts are weakly pedogenized, red to yellow-orange mudstones and are interpreted as well-drained mudflat deposits. The carbonate-rich sediments present more varied facies, consisting of calcretes, marls, and muddy limestones. The calcretes are of pedogenic origin related to the development of a calcic soil profile. The marls and muddy limestones are light- to dark-grey and rich in organic matter, shell fragments, and gastropods. They are interpreted as ephemeral pond to marginal lacustrine deposits. The studied section is subdivided into six stratigraphic intervals based on lithofacies and meter-scale cycle character. A composite sedimentary cycle is presented summarizing the different facies and their vertical distribution throughout the Prado area. On 10-m scale, distinct stratigraphic intervals show lithologic trends representing alternating wetter and drier paleoenvironments. Cycle characteristics are laterally consistent, whereby limestone beds pinch out towards the basin margin and thicken towards the central parts of the 10 km wide and 20 km long sub-basin. The high-resolution magnetostratigraphy allows to resolve four normal and four reversed polarity intervals that are straightforwardly correlated to chron interval C5n.2n to C5Ar.1r in the ATNTS04 time scale. The resulting age control indicates a duration of 19 to 23 kyr for the metre-scale facies cycles, suggesting control by precession-driven climate change. An astronomical tuning is established by correlating the individual sedimentary cycles to successive precession cycles using recently recalibrated ages for the polarity reversals. The resulting astronomical ages for the reversals in the Prado section are consistent with the astronomically calibrated magnetostratigraphy and cyclostratigraphy of the marine Monte dei Corvi section in Italy. At Prado, three intervals with twice the average cycle thickness reflect obliquity modulation of the precession cycle during long eccentricity minima (405 kyr). The presence of this obliquity and long eccentricity imprint corroborates the orbital forcing hypothesis of the sedimentary cycles and the astronomical tuning

of the Prado succession. The cyclostratigraphy method applied in this study shows to be of high potential for detecting orbital climate forcing in continental successions.

3.2 Introduction

The recognition of astronomically forced sedimentary cyclicity in continental basin fills can considerably enhance both relative and absolute age control (Kent and Olsen 1999; Hinnov 2000), understanding of the sedimentology (Meyers *et al.* 2001; Weedon 2003), quantification of rates and duration of sedimentary, climatic, and paleontological processes (Fischer and Roberts 1991; Meyers *et al.* 2001), and possibilities for correlation within and beyond the basin (Van Vugt *et al.* 1998). The influence of astronomical climate forcing has now been demonstrated and suggested for various types of lacustrine successions with different geological ages (Bradley 1929; Eardley *et al.* 1973; Olsen 1986; Astin 1990; Fischer and Roberts 1991; Abdul Aziz *et al.* 2000; Reinhardt and Ricken 2000; Luzón *et al.* 2002). The detection of astronomical cyclicity requires sufficiently long sediment records (Olsen 1986; Abdul Aziz *et al.* 2003) or a first-order reliable age control, than can be magnetostratigraphic (Van Vugt *et al.* 2001; Kruiver *et al.* 2002; Abdul Aziz *et al.* 2004) or radiometric dating of ash layers intercalated within the sediment record (Pietras and Carroll 2006; Meyers and Sageman 2007; Machlus *et al.* 2008). The Neogene, and recently the Paleogene, geomagnetic polarity time scales have been considerably improved by (new) astronomically calibrated ages for polarity reversals (Lourens *et al.* 2004; Pälike *et al.* 2006; Westerhold *et al.* 2008). These improved ages allow the detection of orbital climate forcing in continental sediment records and the construction of astrochronologies in, even relatively short, sedimentary successions (Van Vugt *et al.* 1998; Steenbrink *et al.* 1999; Abdul Aziz *et al.* 2004; Abels *et al.* 2008) while avoiding statistical analyses that are reported to often contain a certain degree of subjectivity (Wilkinson *et al.* 2003; Meyers and Sageman 2007; Bailey and Smith 2008).

The Upper Miocene Cascante section in the southern Teruel Basin (NE Spain) displays very regular, meter-scale cyclicity of alternating red-brown, distal alluvial fan mudstones and palustrine to shallow lacustrine limestones. High-resolution magnetostratigraphic age control, substantiated by mammal biostratigraphy, revealed that this meter-scale cyclicity is related to the climatic precession cycle (Abdul Aziz *et al.* 2004). Carbonate microfacies analysis of limestone beds of successive basic cycles revealed the additional presence of larger scale lake-level variations that are related to the short and long eccentricity cycles. These results allowed the construction of an astrochronology for this part of the basin (Abels *et al.* 2008). Roughly time-equivalent deposits are present in the Prado area, 6.5 km NNW of the Cascante section and located in the same structural segment of the Teruel Basin, but at the opposite basin margin.

The succession at Prado shows different lithological characteristics than the succession in the Cascante area, being dominated by yellow-orange to red-brown mudstones and pedogenic calcretes from well-drained mudflats and marginal lacustrine marls and muddy limestones. In analogy with the Cascante section, the Prado section is characterized by meter-scale, mudstone – limestone cycles over its whole stratigraphic extent, but with a higher variability in sedimentological characteristics, both laterally and vertically. On a larger scale, stratigraphic intervals dominated by limestones or marls alternate with intervals characterized by prevalent mudstone deposits. A direct, bed-to-bed, lithological correlation to the Cascante section cannot be achieved, either physically or by matching lithological characters. Therefore, detailed magnetostratigraphic sampling has been carried out to obtain a first-order age control that allows detecting orbital forcing within the Prado

section, and, subsequently, constructing an independent astrochronological framework for this part of the Teruel Basin. The vertically and laterally more complex meter-scale cyclicity and dominant long-term changes in the sedimentary successions of the Prado area, on the other hand, might reflect processes other than orbital forcing.

Controls on the short- and long-term trends of sedimentation in low-energy, endorheic continental environments are often difficult to evaluate, because of the range of responses to environmental forcing in such settings. The Prado section offers the opportunity to examine the signature of astronomically-forced climate variations and their interplay with other processes within a high-resolution chronological framework.

3.3 Geological Setting

The Teruel Basin (Comunidad de Aragón, Teruel Province, NE Spain; Fig. 3.1) is a complex of axially linked, NNE-SSW oriented half grabens developed on top of the Central Iberian Range. After the main Paleogene constructive phases of the Iberian Range, the Teruel basin formed as a result of reactivation of Mesozoic tectonic lineaments during E-W extension from the Early Miocene onwards (Anadón and Moissenet 1996). The Teruel Basin is approximately 100 km long and 15 km wide and the main phase of deposition took place between Early Miocene and Late Pliocene (Anadón and Moissenet 1996). Sedimentation occurred in an internally drained, semi-arid, continental setting dominated by marginal to axial alluvial systems as well as lacustrine-palustrine domains of variable depth and extent (Broekman 1983; Kiefer 1988; Anadón *et al.* 1997). The basin fill is characterized by large-scale (>40 m) alternations of red, alluvial siliciclastics and lacustrine carbonates or evaporites (Broekman *et al.* 1983; Kiefer 1988; Anadón *et al.* 1997; Alonso Zarza and Calvo 2000). The Cascante and Prado areas are both located in the southern part of the Teruel Basin in the Teruel-Ademuz Sub-Basin (Fig. 3.1). This sub-basin is approximately 35 km long and 15 km wide. The Prado area is accessible from the N-330 from Teruel to Ademuz, via a dirt road east of Villastar (040°12'18" N, 001°07'22" W). The sub-basin is flanked by a Mesozoic basement, predominantly composed of Triassic fine-grained siliciclastic and evaporitic rocks and Jurassic limestones. Miocene alluvial-fan conglomerates and breccias dominate along the basin margin and grade laterally, within a few kilometres, into fine-grained distal fan to mudflat and shallow lacustrine deposits in the more central part of this relatively small sub-basin (Kiefer 1988).

In the Prado area (~5 km^2), a dominantly siliciclastic succession is situated stratigraphically between the top of the Libros Gypsum Unit exposed in the southern part of the area (Anadón *et al.* 1997; Ortí *et al.* 2003), with an approximate age of 11 Ma (Abdul Aziz *et al.* 2004), and a red mudstone unit with intercalated fluvial conglomerates in the northeast (Fig. 3.1). The sediments of the succession consist of red to yellow orange mudstones and pedogenic calcretes to shallow lacustrine to palustrine limestones. The lateral continuity of exposures allows to trace individual carbonate beds and mudstone colour patterns over hundreds of meters from the northwest to the southeast across the area, while lateral trends from northeast to southwest can only be studied over tens of meters (Fig. 3.1). To the west, conglomerates and sandstones, that were sourced by an adjacent alluvial fan along the western basin margin, interfinger with the lower part of the stratigraphic succession in Prado. Paleocurrent directions indeed indicate a western to northwestern source. The stratigraphic relationships between distal lobes of the alluvial fan and lithofacies cyclicity in the lowermost interval of the Prado section are sorted out and discussed in

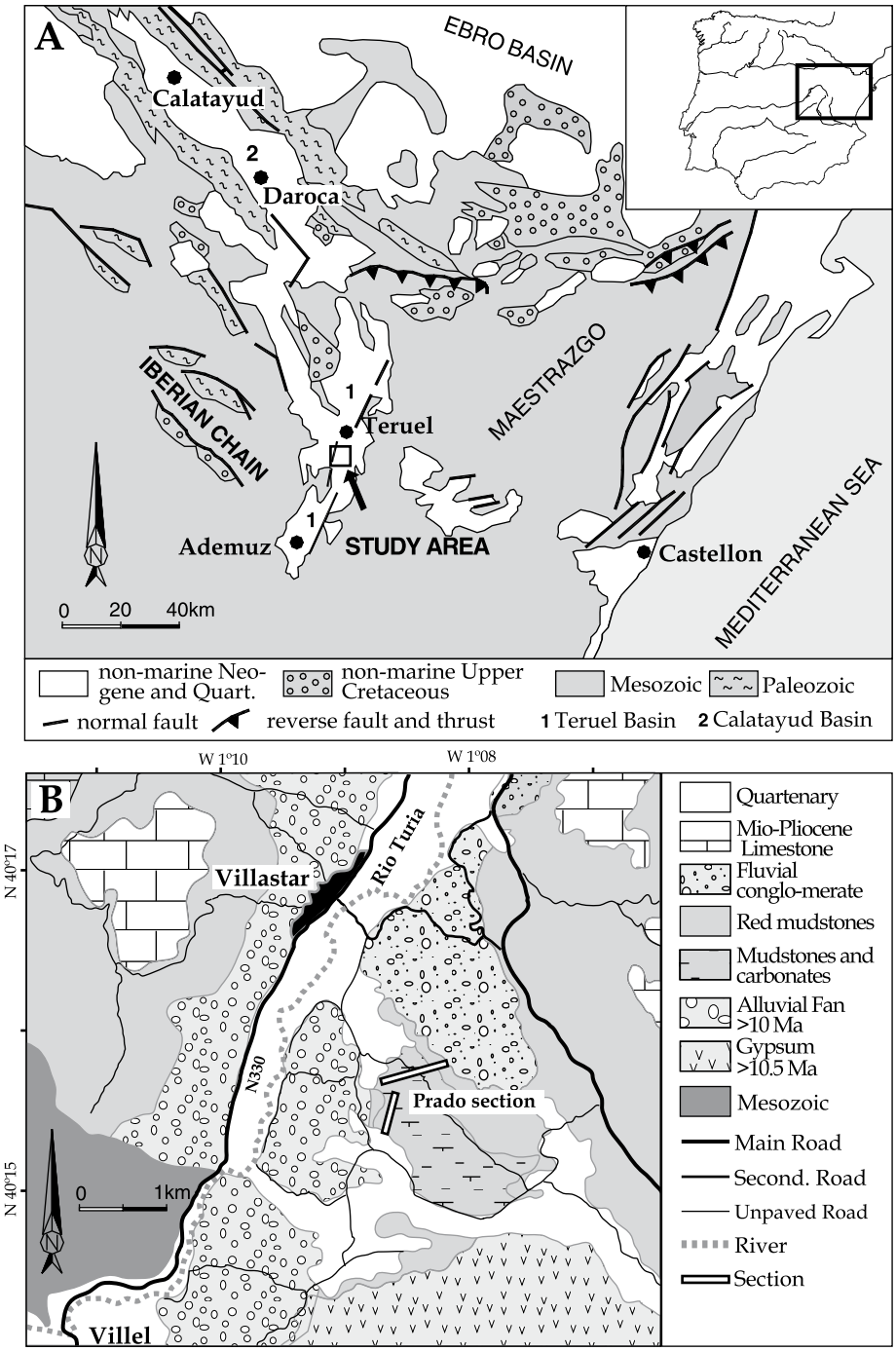

Figure 3.1 Geographic locations of the Prado area within (A) Spain and (B) the southern part of the Teruel Basin. In (C) a schematic geological map of the Prado area is shown. The position and extent are indicated of the two transects that make up the sedimentary log of the Prado section.

Ventra *et al.* (in prep). The fluvial conglomerates delimiting the top of the Prado section instead indicate a source in the north.

3.4 Sedimentology

3.4.1 The Prado section

A continuous sedimentary log of the Prado section (PS; Fig. 3.1; Fig. 3.2) was recorded. Due to the structural dip towards the NNE, the section is a composite of two transects; the 'lower' sub-log trends laterally towards the ENE, and the 'upper' sub-log to the north (Fig. 3.1). The overall section is 155 m thick, and its base (040°15'17" N 001°08'45" W) is located about 730 m SW from its top (040°15'47" N 001°08'12" W).

Based on distinct facies associations, the section has been subdivided into six intervals labelled I to VI (Fig. 3.2). In total, fifty-five lithofacies cycles have been counted and numbered from bottom to top (Fig. 3.2). Ten additional cycles have been counted, with less distinct lithological characteristics; these are coded with an additional "a" following the number of the cycle they are in. The sedimentological characteristics of each interval (I to VI) are reported below. The recognized lithological colours comprise brownish black (7.5YR 3/1), dark red (10R 3/4-6), red (10R 4-5/6-8), orange (2.5YR 6-7/6-8), pale orange (5YR 8/4), yellow orange (10YR 7-8/8), light-yellow orange (10YR 8/3-4), pale yellow (2.5Y 8/3-4), grey (5Y 4-6/1), and light grey (2.5Y 7-8/1) (Munsell 1999). The qualifier *centimetre-scale* refers to a size between 1 and 3 cm, *millimetre-scale* to less than 1 cm, and *sub-millimetre-scale* to less than 1 mm. The pedogenic calcrete classification follows Machette (1985), as also applied by Wright and Tucker (1991).

Interval I (cycles 1 to 12)

This interval is mainly characterized by weakly pedogenized, red, clayey siltstones with meter-scale intercalations of carbonate-enriched beds, with a few orange sandy and dark-red clayey mudstone horizons. The dark-red clayey mudstone horizons occur every 2.5 to 3 m and contain (<2 mm) thin-walled shell fragments. In most cases, the mudstones display sparse millimetre-scale, and occasionally centimetre-scale, grey and infrequently yellow-orange mottles and contain few, dispersed carbonate nodules. The carbonate-enriched beds (in cycles 1, 3, 4a, 6, and 8 to 12; Fig. 3.2) are between 20 and 60 cm thick and are interpreted as pedogenic calcretes reaching Stages II to III (Machette 1985). These calcretes are mainly pale-orange to orange with few light-grey mottles and have a dominantly silty matrix. To the top of this interval, the calcretes are light-yellow-orange and have more frequently a very-fine sand matrix. Slightly enriched carbonate levels occur also between calcretes, with caliche nodules ranging from 5 to 20 mm in size, located just below or above the calcretes, but also as individual levels within the clayey siltstones. The carbonate-enriched beds, and to a lesser extent the calcretes, present a high lateral variability, changing in thickness over tens of metres or disappearing completely. In the logged transect, two pale-orange, limey, fine-grained sandstones occur. These have a clearly defined bottom and top and internally a thinner bedded, centimetre-scale planar structure (cycles 5 and 7; Fig. 3.2). These beds are enriched in carbonate and appear as indurated levels. Here, the complete stratigraphic framework of this interval has not been worked out, because that is beyond the purpose of this study. Also because their occasional occurrence does not seemed to have a consistent relation to the cyclic sedimentary dynamics observed.

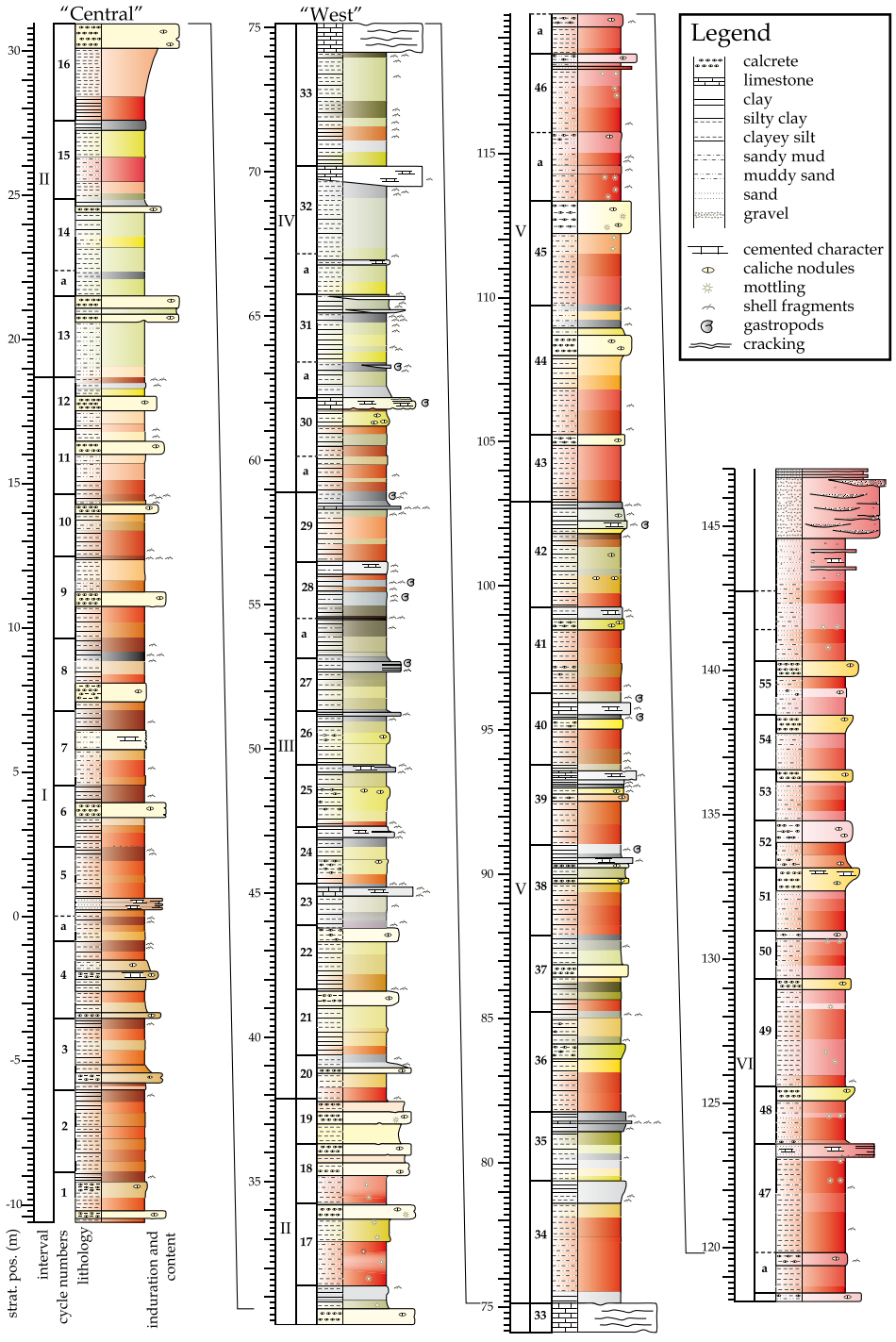

Figure 3.2 Detailed lithological log of the Prado section along the 'West' and 'Central' transects. Stratigraphic positions, interval numbering, and cycle numbering are indicated.

Dark-red and, in cycle 8, grey mudstones with shell-fragments occur regularly at an average stratigraphic distance of 2.5 m. In the lower part of interval I, these cycles are around 3 m thick, while in the upper part their thickness is less than 2.5 m. Calcretes and carbonate-enriched beds in the lower part of this interval do not show any consistent stratigraphic relation with these cycles. Higher up, above cycle 9, pedogenic calcretes occur directly below the dark-red or grey clay layers. Lithofacies cycles in interval I have been counted on the basis of the occurrence of dark-red mudstones.

Interval II (cycles 13 – 19)

This interval comprises the overlap between the 'lower' and 'upper' sub-logs and includes cycles 13 to 16 (Fig. 3.3 A; Fig. 3.2). Cycles in interval II contain 20 to 80 cm thick pedogenic calcretes intercalated in red, orange and light-yellow-orange, occasionally sandy, siltstones. The siltstones display sparse millimetre-scale orange-yellow and light-grey mottling. Except in cycle 15, the calcretes generally reach Stage III to IV, with a light-yellow-orange colour, displaying yellow-orange mottling and a silty to fine-sandy matrix. In cycles 18 and 19, the thick calcretes appear as couplets with a slightly undulating base. Within the calcrete of cycle 13, a thin pebble layer occurs that grades laterally to a thick conglomerate bed (Ventra *et al.*, in preparation). Below and on top of the calcretes, light-grey, limey, clayey siltstones of variable thickness occur. Especially close to the calcretes, these siltstones present an intense yellow-orange mottling. Above the calcretes, fining-upward trends from siltstone to silty claystone are found, accompanied by more grey colours and an increase in organic matter content and shell fragments (*e.g.* base cycle 13 and 17; Fig. 3.2).

This interval comprises 10 or 11 sedimentary cycles, consisting of a mudstone and a limestone or limey part. Cycle thickness varies from 0.9 m (cycle 13a) to 4.2 m (cycle 16), with an average of 2.5 m.

Interval III – Cycles 20 – 29

This interval is characterized by metre-scale intercalations of pedogenic calcrete beds and light-grey silty carbonates within light-grey to light-yellow-orange mudstone with sparse yellow-orange mottling (Fig. 3.3 C). Pedogenic calcretes are 20 to 50 cm thick and light-yellow-orange in colour, with yellow-orange mottles in a silty matrix. They reach Stage I to III (cycles 20 to 22 and 24 to 26; Fig. 3.2). Calcretes in the lower part of this interval (cycles 19 to 22; Fig. 3.2) are directly overlain by brownish-black limey mudstones that contain millimetre-scale to centimetre-scale shell fragments. These mudstones are in turn overlain by light-yellow-orange mudstone. Higher up in this interval (cycles 23 to 26), grey limey siltstones and light-grey silty carbonates occur 50 to 75 cm above the calcrete. Above cycle 26, calcretes are absent, and thicker, grey limey mudstones or light-grey muddy carbonates occur (cycles 26 to 29), rich in shell fragments and often complete gastropods. Carbonates are generally soft, dusty, poorly lithified, and display sparse millimetre-scale yellow-orange mottling, ranging in thickness between 10 and 40 cm. The thicker beds (*e.g.*, cycles 23 and 27) also show vertically oriented, centimetre-scale root traces and, especially at their top, horizontal cracks. Tens of metres eastwards from the logged transect, the limestone beds of cycles 23, 26, 27, 29 and 30 are much thicker, reaching up to 60 cm. Limestones occur stratigraphically associated with intervals of shell-bearing (light-)grey limey siltstones. Pale-yellow siltstones occur between the carbonate-rich levels of the lithofacies cycles in interval III, with red mudstones within cm's above the carbonate interval in cycles 20, 24, 25, 28, 29.

Ten or eleven regular lithological repetitions occur within Interval III, on average every 2.0 m (range 1.6 to 2.5 m). As described above, the position of the calcretes within the mudstone –

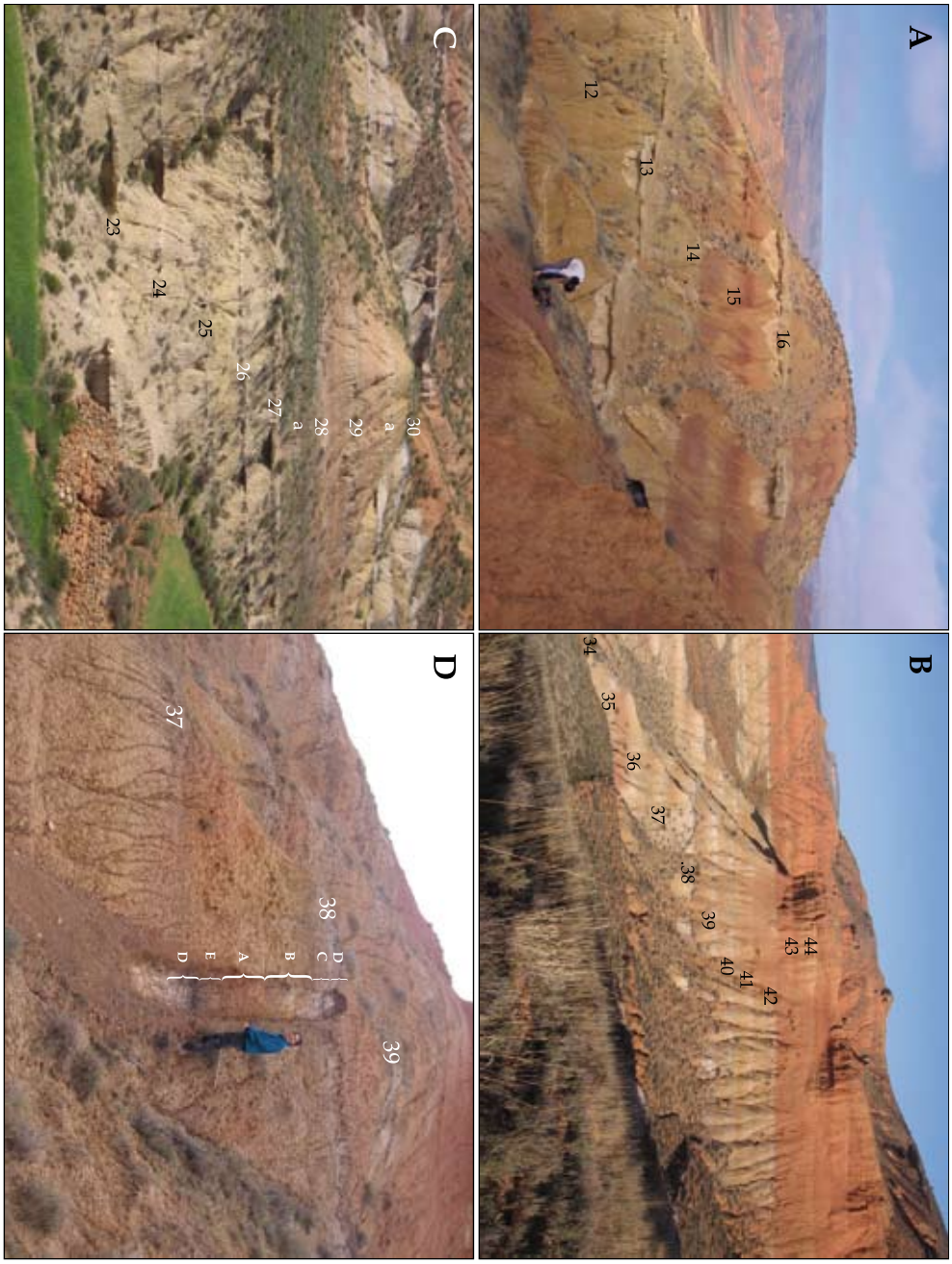

Figure 3.3 Photographs of the Prado section along the logged transects. See Figure 3.2 for scales. A. Cycles 12 to 16 in the top of the 'Central' transect. B. Cycles 34 to 44 (with cycles 45 and 46 vaguely visible to the right) of the 'West' transect. Above cycle 42, the second shift to well-drained floodplain sediments is visible. On top, an angular unconformity with Pleistocene conglomerates is present. C. Cycles 23 to 30 in the 'West' transect. D. Cleaned surface across cycle 38 in the 'West' transect as part of Figure 3.3B. Lithologies A to E are indicated (Fig. 3.4).

limestone cycles changes trough the interval. Cycle boundaries are defined at the top of the grey, shell-fragment rich siltstones or carbonates.

Interval IV – Cycles 29a – 33

In interval IV, light-grey mudstones prevail, with varying amounts of yellow-orange mottling and metre-scale intercalations of gastropod-rich, light-grey, muddy limestones and (dark-)grey mudstones. The limestones range from 10 cm up to 1 m in thickness, and pinch out over a distance of a few metres mainly towards the basin margin in the west and locally in the other directions as well. Towards the basin centre in the east, most limestone and stratigraphically associated grey mudstone intervals become thick and prominent limestone beds. In the logged transect, the basal and top transitions of the beds are rather sharp. Mostly, they show gentle centimetre-scale undulations both at the base and within the bed, and, locally, centimetre-scale bedding. Bed tops commonly feature horizontal cracks. The beds are soft, porous, with relatively much organic matter, and often full of complete or fragmented gastropod remains. Sparse millimetre-scale yellow-orange mottling and locally centimetre-scale root traces are present. The limestone beds are stratigraphically associated with (dark-) grey mudstones that are rich in very fine-grained organic matter, most probably plant debris, and fragmented and complete gastropod shells. The organic-rich levels in interval IV are occasionally rich in small mammal remains and sparse large mammal remains have been found. Light grey mudstones display millimetre-scale yellow-orange mottling that increases in intensity and size (up to centimetre-scale) just above the grey mudstones and limestones (cycles 28a, 28, 26a, 26).

In this interval, cycle boundaries are defined at the top of the grey mud- or limestone beds. Cycle thickness varies between 3.3 to 5.0 m for the 4 well-defined cycles (cycles 30, 31, 32, 33). In between these cycles, three less clear cycles are present (cycles 29a, 30a, and 31a; Fig. 3.2).

Interval V – Cycles 34 – 42

Interval V is dominantly characterized by red mudstones with intercalations of light-grey limestones, light-yellow-orange calcretes, and (dark-)grey mudstones on metre scale (Fig. 3.3 B and D). The intercalations vary in thickness between 75 and 150 cm and generally start with pedogenic calcretes. The calcretes reach Stage II to III (cycles 36 to 41; Fig. 3.2), with thicknesses between 20 and 50 cm. They are followed by a limey (light-)grey mudstone with sparse shell fragments. In some cycles, a (dark-)grey marl rich in shell fragments occurs, with local intercalations of a light-grey limestone (cycles 34, 35, 38 to 40, and 42). The thickness of the grey limey mudstone ranges between 20 and 125 cm. The limestone beds range between 10 and 40 cm, are light-grey, have an undulating base, and contain shell fragments and infrequently complete gastropod shells. The limestone beds in this interval have sedimentological characteristics similar to the limestones of cycles 30 to 33 in interval IV, although the latter are thicker. Locally, the limestone pinches out or increases in thickness laterally over a few metres towards the east as well as west. The dominant mudstone between the intercalations has a red colour, with sparse millimetre-scale yellow-orange and light-grey mottling and occasionally millimetre-scale caliche nodules. The basal part of this mudstone is often dark-red changing upwards to red, while more intense yellow-orange mottling is usually found towards the top, resulting in orange colours.

Interval V comprises nine lithofacies cycles with an average thickness of 3.3 m, and ranging between 2.4 and 4.3 m in thickness. The repetitive pattern of sediments is very regular in this interval and cycle boundaries are easily defined at the base of the red mudstones or at the top of the grey limey mudstone.

Interval VI – Cycles 43 – 55

A distinct change occurs above interval V (cycle 42; Fig. 3.2; Fig. 3.3 B), from dominant (light-yellow-)orange and red mudstones with intercalated grey mud- and limestones, to dominant orange silty and sandy mudstones (Fig. 3.3 B). This transition can be traced laterally from east to west over a distance of 0.5 km, which is the limit of the outcrop exposures, thus excluding that it only may represent a local depositional signature. The interval above this shift is characterized by the dominance of orange (2.5YR 6/8), fine-sandy silt and light-orange (2.5YR 7/6-8), silty, fine sandstone. Sparse, millimetre-scale light-grey mottling occurs, with occasional levels of centimetre-scale, light-grey mottling and sparse millimetre- to centimetre-scale carbonate nodules. On metre scale, intercalations of pedogenic calcretes and fine to pebbly sandstones occur. Calcretes generally reach Stage II and in one case Stage III (cycle 44; Fig. 3.2) and are developed in a silty matrix. They display millimetre-scale (light-)yellow-orange mottling. In cycle 44, the calcrete is covered by a grey, organic-rich, fine-sandy mudstone, while in other cycles (cycles 43, 45, 46, and 48) calcretes are followed by red sandy siltstones with shell fragments. The fine-sandy to pebbly intercalations are cemented by carbonates and fine slightly upward. At the base of the sandstone bed in cycle 47, a 50-cm thick conglomeratic lobe pinches out within 10 m both to the east and west. This conglomerate is characterized by a clast-supported fabric of sub-rounded pebbles and rare cobbles, a poorly sorted muddy to coarse sandy matrix, and a relatively high matrix to clast ratio. The associated sandstone beds consists of poorly sorted, fine to very coarse sand with plane-parallel lamination and sparse, floating pebbles. On top of cycle 55, two dark-red mudstone beds likely indicates two additional cycles. Above interval VI, a coarsening-upward towards a 2 to 5 m thick conglomerate is present. Locally, the base of the conglomerate incises up to 3 m in the sandy interval below. The conglomerate consists of several *ca* 30 cm thick, distinct fining-upward beds. The pebble clasts vary in size from 1 to 30 cm, with an average of 4 cm. The sub-rounded clasts are densely packed in a fine to very coarse sand matrix.

Cycles in interval VI have an average thickness of 2.9 m, but show a wide range from 1.6 to 5.2 m. Depending on two less well defined cycles (45a and 46a), 13 to 15 cycles are present. The lower part of this interval consists of relatively thick cycles thicker than 3 m (cycles 44 to 47, and 49), while towards the top the average cycle thickness is only 1.8 m (cycles 50, and 52 to 55).

3.4.2 Composite sedimentary cycle

The persistent, metre-scale lithofacies cycles in the Prado section generally consist of a red and/or (light-)yellow-orange mudstone part, mainly encompassing the lower, thicker fraction of the cycle, and a carbonate-rich unit (Fig. 3.4; Fig. 3.3 D) represented by light-yellow-orange pedogenic calcretes, grey organic-matter-rich muddy limestones or marls. Cycle boundaries have consistently been placed at the transition from dominantly limey to dominantly siliciclastic intervals (see above for details). In total, 55 cycles show a well-defined lithofacies transitions at their top (solid lines in Fig. 3.2), while 8 additional cycles show more diffuse transitions (dotted lines in Fig. 3.2). The average thickness of a sedimentary cycle in the Prado section is 2.6 m, with a standard deviation of 0.9 m and extremes ranging from 1.2 to 5.2 m. Three intervals with thick cycles (> 3.5 m) occur in the section: cycles 16 and 17 in interval II, cycles 30 to 33 in interval IV, and cycles 46, 47, and 49 in interval VI (Fig. 3.2). In order to facilitate interpretation and discussion of facies and the variable sedimentological expressions of stratigraphic intervals an idealized, composite sedimentary cycle has been constructed (facies A to E; Fig. 3.4; Fig. 3.3 D). This cycle consists of five distinct facies, superposed according to their recurrent vertical transitions in the different types of cycles discussed above. This composite cycle is thus not found as a real stratigraphic unit

Figure 3.4 Sedimentological description, lithological column, and sedimentological interpretation of the composite sedimentary cycle in the Prado section. Lithologies A to E are distinguished (see text). To the right, interpretation in terms of net water budget and the precession-induced insolation cycle are given. Scale is in metres.

at outcrop, but it reliably represents the overall facies variability, and especially facies transitions, which are consistently recognized throughout the section.

Sedimentology

Facies A – *description*

The composite cycle starts with a red, occasionally orange or dark-red, massive and homogeneous silty mudstone (Fig. 3.4), displaying different amounts of sparse, light-grey, millimetre- to centimetre-scale mottling and rhizocretions. Rare, millimetre-scale carbonate nodules are found and locally slightly carbonate-rich levels occur, especially in interval I. Infrequent, millimetre-scale shell fragments are found, especially toward the base of beds. Overall, mudstones lack primary depositional structures and pedological horizons and structures. Beds do not present internal discontinuities, and their bases and tops lack erosional features. Transitions to overlying lithologies, even when sharp, reflect continuous deposition.

Facies A – *interpretation*

The massive and homogenous red mudstones display the characteristics of a well drained mudflat deposit with very weak pedogenic overprint. Pedoturbation, desiccation and compaction likely removed any original structures (*cf.* Wright and Marriott 2007). The fine-grained sediments were probably deposited by distal sheetwash during waning-flow stages of major flood events from the adjacent basin margin where these lost capacity over the flat, sparsely vegetated distal surfaces (Abels *et al.* 2008). The sparse, light-grey mottling indicates weakly reducing conditions due to short periods of seasonal wetting (Kraus 2002) or localized biological activity. The scarce presence of rhizocretions and the absence of bioturbation point to very poor colonization by vegetation or other organisms. The rare carbonate nodules, interpreted as incipient caliche, indicate precipitation of calcium carbonate in the Bk-horizon of a calcic soil profile (Retallack 2001). Lack of well-developed soil profiles and structures indicate only minor pedogenesis within the deposit. A semi-arid climate could have been a significant cause of poor pedogenesis, but the overall homogeneity of facies vertically through the beds also suggests that time was a significant factor. The slow development of a mature soil profile was probably hindered by continuous, relatively high aggradation rates (Buurman 1980).

Facies B – *description*

The transition from facies A to B is usually gradual. Facies B consists of orange to light-yellow-orange, massive, silty to sandy mudstones. These mudstones display abundant centimetre-scale, yellow-orange mottling, minor millimetre-scale, light-grey mottling, and a generally higher content in carbonate nodules and rhizocretions than in facies A. In some cycles, the sediment presents a rather uniform colour, whereas in others it has a multi-coloured, patchy appearance with red, yellow-orange, light-yellow-orange, and light-grey mottling. The abundance of millimetre- to centimetre-scale carbonate nodules and intense yellow-orange mottling tend to increase towards the top of facies B. Similarly as facies A, facies B is also characterized by internal homogeneity and the absence of primary sedimentary at outcrop scale. The boundary between facies A and B is defined arbitrarily within the composite cycle, whereas in the field, it is usually diffuse over a interval with intermediate characteristics between A and B.

Facies B – *interpretation*

The sedimentary processes by which facies B was formed must have been fairly similar to those for A. The most significant difference is a slightly coarser grain size and slightly higher carbonate and rhizocretion content in facies B, accompanied by a greater size and colour intensity

of mottled domains. The upward increase of yellow-orange mottles from the red mudstones of facies A to the orange mudstones of facies B is interpreted as an increase of (seasonal) soil forming processes (Kraus 2002). The slightly coarser grain size, increased carbonate content, and increasing pedogenesis might be indicative of a more frequent or persistent availability of water. The prevalence of Jurassic and Cretaceous carbonate formations in the Mesozoic catchment areas granted high availability of dissolved carbonates in both surface runoff and groundwater. The increase in overall carbonate content from facies A to B might be thus related to rising availability of water via groundwater and/or runoff. Towards the top of the facies B interval, these (seasonally regulated) soil forming processes were further enhanced.

Facies C – *description*
A Stage II to IV, light-yellow-orange to yellow-orange pedogenic calcrete is developed above facies B, with a gradual transition in between. Locally, calcretes only reach Stage I. Their matrix is silty to (very-)fine sandy, and rare to abundant yellow-orange mottling occurs. Some vague (sub-) millimetre-scale red and millimetre-scale light-grey mottling is locally present. Calcrete tops are generally sharp. In interval III, the pedogenic calcrete occurs lower in the composite sedimentary cycle relative to facies D than sketched in Figure 3.4 (see description of interval III; Fig. 3.2 and 5).
Facies C – *interpretation*
Stage II to IV pedogenic calcretes are interpreted as the Bk-horizons of calcic soil profiles (Retallack 2001). The calcrete precipitated from a saturated calcium-carbonate solution due to high evaporation rates and higher water tables compared to facies A and B. Increased amounts of yellow-orange mottling upwards within mudstones underlying the calcrete horizons could represent part of the soil profile that developed during calcrete formation, overprinting the original colour of the sediment. This interpretation is supported by the upward increase in carbonate content and the sharp top of the calcretes (Wright and Tucker 1991). Alternatively, a gradual increase in pedogenic mobilization and re-deposition of carbonates might have occurred through time, starting from facies B onwards. It thus is not possible to quantify the rate of paleoenvironmental change represented by transitions from facies B to C. By analogy with facies B, given the abundant sources of dissolved carbonates from basement rocks, local variations through time in water availability could have been the main factor regulating ion circulation and secondary remineralisation within top soil profiles.

Climate in central Spain around 8-10 Ma is inferred to have been semi-arid, seasonally dry, with annual precipitation of about 500 mm to 550 mm (Van Dam 2006). Under these conditions, the depth of calcrete formation within recent soil profiles is estimated to be between 10 cm and 1 m (Royer 1999; Retallack 2005). The lack of extensive pedogenesis within the grey marls and muddy limestones of facies D indicates that the top of the soil profile that relates to the calcrete precipitation must have been below this level. The thickness of the light-yellow-orange mudstone between the top of the calcrete level below and the grey limey mudstone above could define the depth of calcrete formation within the calcic soil profile, although (slight) erosion can not be discarded. In the Prado section, the depth of calcrete precipitation would then range between 0 and 60 cm, or more if erosion of the top of the profile occurred. Increasing depths of calcrete formation have been related to increasing mean annual precipitation (McFadden and Tinsley 1985; Retallack 2005), although this relationship has been disputed as well (Royer 1999). It is remarkable that the largest apparent depths of calcrete formation are present in interval III (Fig. 3.5), that contains sediments that relate to the highest groundwater levels recorded within the Prado section.

Facies D – *description*
The lower portion of facies D, over a variable thickness between 0 and 60 cm, represents transitional characteristics from facies C. This transitional interval constitutes grey limey mudstones with light-orange-yellow mottling. This interval is covered by dominantly light- to dark-grey limey mudstones and marls, locally intercalated by 20 cm thick, light-grey limestone beds that have a maximum thickness of 1 m. Mudstones and marls contain abundant millimetre- to centimetre-scale shell fragments and complete gastropod remains. Thin (<10 cm) organic-rich layers are present, usually containing coarse plant debris, small mammal and occasionally large mammal remains. The intercalated light-grey limestone beds have a sharp undulating base, are weakly indurated, and contain a relatively high amount of fine siliciclastic components. In many cycles, the limestones are rich in dispersed organic matter and intact or fragmented gastropod remains. Besides the undulating base, slightly undulating internal surfaces are locally evident within the limestone beds, especially in the thicker ones. Certain beds pinch out laterally over distances of a few metres, but they usually extend over 50 metres at outcrop, and some are traceable over hundreds of metres towards the more central parts of the basin, farther east from Prado. The top of the Limestone beds usually feature horizontal cracks, while sparse rhizoturbation is present throughout the bed, and more frequently within its upper part.
Facies D – *interpretation*
Deposition of grey, gastropod-rich, limey mudstones and marls indicates rising groundwater levels and occasional ponding of the surface. These conditions rapidly halted calcrete development, and caused fine clastic sedimentation to alternate with (biochemical) carbonate precipitation. Temporary reduced oxygenation is indicated by preservation of abundant organic matter, including gastropod and mammal remains. Intercalated, undulating, light-grey limestones are interpreted as the result of carbonate deposition in very shallow and relatively wide, elongated depressions through which sluggish surface waters were slowly directed towards the basin centre, or to local small ponds on the mudflat. Thicker limestone beds, laterally continuous over long (> 500 m) distances, are interpreted as pond and marginal lacustrine deposits. The absence of extensive palustrine features within and on top of limestones beds suggests that their deposition rates were relatively fast, leaving no significant time for reworking at the sediment/water interface in shallow water conditions. Palustrine features are reported to develop rapidly in freshwater limestones (Alonso Zarza 2003), while desiccation is particularly expected in very shallow water environments in a semi-arid, seasonal climate (Van Dam 2006).

Facies E – *description*.
The topmost facies within the composite sedimentary cycle is represented by a dark-red to brownish-black, massive silty clay containing dispersed millimetre-scale shell fragments. No primary sedimentary structures are evident at outcrop. Millimetre-scale, yellow-orange and red mottling is present.
Facies E – *interpretation*
The dark mudstones are interpreted as mudflat deposits, analogue to those of facies A and B. Environmental conditions did not consent more than a weak pedogenesis keeping pace with aggradation of the surface. Mild pedoturbation disrupted any primary sedimentary structures, but did not reach a full stage of soil formation. The vague reddish and occasionally yellow-orange mottles characterizing facies E probably indicate a return to more oxygenated conditions of the floodplain, related to a gradual shift from a poorly drained (facies D) to a well-drained (facies A)

mudflat environment. Within the interpretive framework of our representative sedimentary cycle, facies E is regarded as a transitional facies between D and A.

3.4.3 Depositional model

The representative facies succession A to E in the basic, metre-scale sedimentary cycles in Prado are interpreted as deepening-upwards sedimentary sequences due to variations in groundwater level at the site of deposition. Groundwater level was low on a well-drained mudflat during deposition of facies A. The subsequent rise of the water table resulted in more effective pedogenic processes, produced facies B, and eventually lead to the development of calcic soil profiles and the formation of a pedogenic calcrete (facies C). The further rise of groundwater levels resulted in more persistent saturation up to the ground surface, with temporary development of poorly oxygenated wet mudflat environment of facies D, in which sluggish elongated, low-energy channel bodies and small ponds developed. Occasionally, this lead to the development of marginal lacustrine environments, especially towards the centre of the basin. Finally, a lowering of groundwater level resulted in a stratigraphically rapid return to the well-drained, dry mudflat environment represented by facies A, with facies E as a transitional stage. In the composite sedimentary cycle, the facies A and B, related to groundwater level low-stands, are referred to as the 'dry' part of the cycle. Conversely, the facies C, D and E that are related to groundwater level high-stands are referred to as the 'wet' part of the cycle.

Preservation of this rhythmic sedimentary signature appears to have been substantially complete throughout the timespan comprised by the Prado section. No distinct surfaces of discontinuity are recognizable at outcrop, not within single facies and not between them. No major erosional features are present in the area both on small or large scales, except for very shallowly scoured erosive bases of rare coarse clastic units, that reached the mudflat in the lower part of the section from the adjacent alluvial fan to north-west. The reasons for this excellent preservation potential of the sedimentary column are related to both local, low-energy, paleogeographic setting and the endorheic character of the basin, inhibiting base level changes larger than the ground surface in the centre of the basin.

3.4.4 Large-scale changes

Throughout the Prado section, the intervals I to VI all show different facies characteristics that are variations of the composite cycle. Four characteristic intervals (part of intervals I, III, V and VI) are compared (Fig. 3.5), in order to illustrate these major sedimentary signatures and paleoenvironmental changes. The sediments of the other two intervals, II and IV, are not elaborated here because they represent transitional intervals with double cycle thicknesses. Grey lines in Figure 3.5 indicate cycle boundaries and thus the transition of the 'wet' part to the 'dry' part of the cycles. In the basal part of interval I, the stratigraphic log is mainly composed of facies A, B, E, and occasionally C. In interval III, cycles are dominantly composed of facies C, D and only rarely E, while A and B are absent. Higher up, in interval V, facies A and B reappear and basic cycles closely resemble the composite sedimentary model, displaying the whole facies spectrum from A to E. With a sharp transition above cycle 42, cycles in interval VI are again dominated only by facies A and B, with thin intercalations of facies C. Main differences between intervals I and VI are the absence of facies E and the higher lateral continuity of carbonate-rich beds in VI. Interpretations in terms of hydrological balance suggest a progressively rising groundwater table from interval I to III, followed by a subsequent lowering in two main steps: at the transition from interval IV to V (above cycle 33), and at the transition from interval V to VI (above cycle 42).

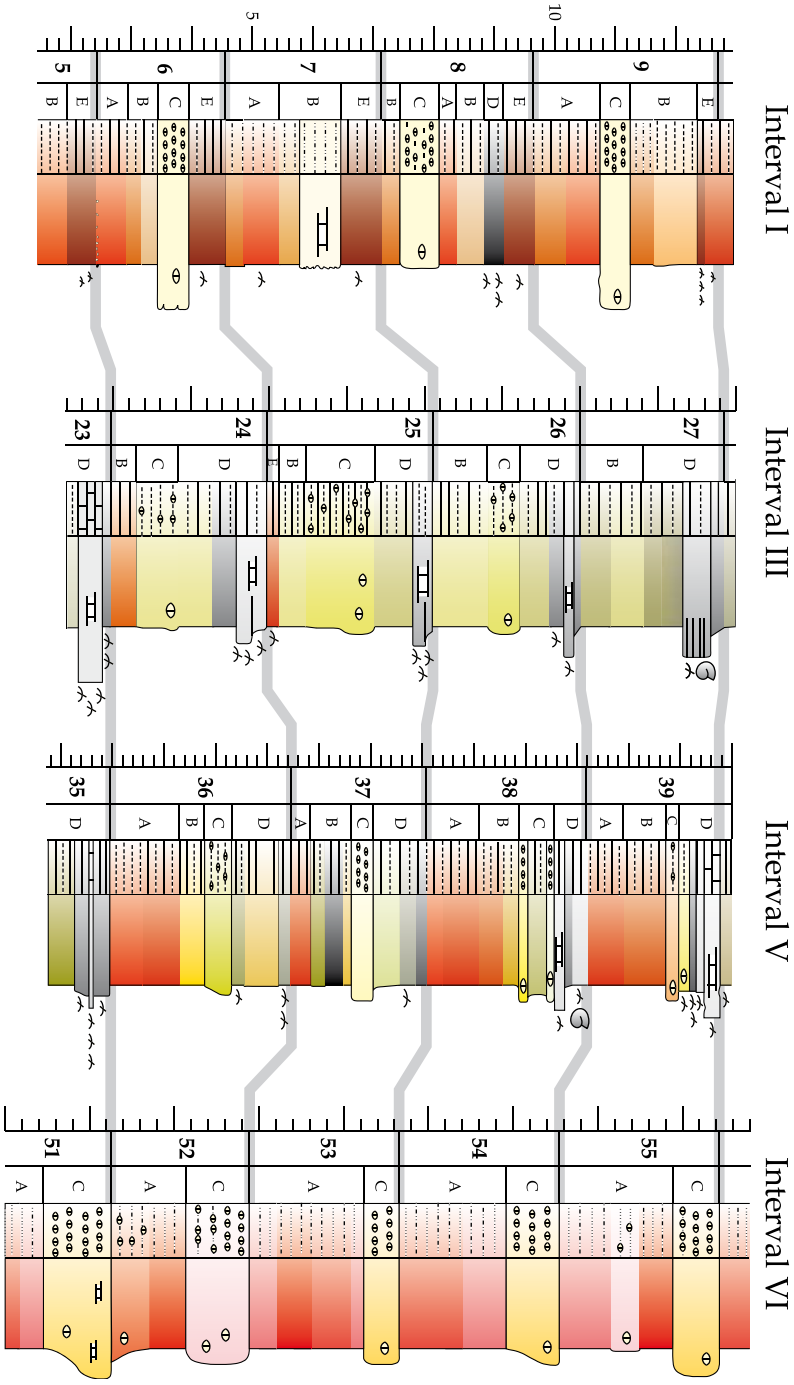

Figure 3.5 Detailed comparison of four distinct stratigraphic intervals in the Prado section. Disappearance of well-drained, red mudstone facies occurs from interval I to III. Reappearance occurs in two-steps from III to V and from V to VI (see text for explanation).

Above interval VI, the Prado section is topped by tens of metres of red, weakly pedogenized mud deposits with minor sandstone sheets and conglomeratic channel fills in single and multiple storey's. On a decimetre to metre scale, the mudstones present rhythmic facies transitions similar to facies A and B. The lateral continuity of these deposits is occasionally interrupted by the erosional bases of coarse-clastic channel bodies and associated sandstone splays. This overlying succession is interpreted as being deposited in a poorly confined, ephemeral fluvial system sourced from the north, which is along strike of the basin. The greatest volume of sediments is represented by overbank fines grading laterally to shallow, isolated channels that are locally filled by much coarser and poorly organized sediment, in correspondence of major floods. The presence of these erosive channels suggests higher gradient within the basin, that is related to increased accumulation rates. The end of the endorheic configuration of the basin is discarded here, as clearly endorheic lacustrine sediments are present up to the Pliocene in the basin.

3.5 Magnetostratigraphy

A detailed magnetostratigraphic age model has been established to test whether the regular occurrence of metre-scale facies cycles is related to orbital climate forcing. First-order age control is derived from lithostratigraphic correlation to the well-dated time-equivalent Cascante section (Abels *et al.* 2008), where the magnetostratigraphy was tied to the geomagnetic time scales using biostratigraphy of small mammal faunas (Abdul Aziz *et al.* 2004). The presence of the top of the Libros Gypsum Unit (Anadón *et al.* 1997; Ortí *et al.* 2003) below both the Cascante and the Prado sections indicates that they are roughly time-equivalent, which is confirmed by preliminary mammal biostratigraphic results (J. Van Dam, pers. comm., 2008).

3.5.1 Methods

The Prado section was sampled at average stratigraphic intervals of 35 cm (range 10 cm to 1 m). Samples were drilled using an electric, water-cooled drill powered by a portable generator. The characteristic remanent magnetization (ChRM) was determined by thermal demagnetization, using incremental heating steps of 20 and 30°C, carried out in a laboratory-built shielded furnace. The natural remanent magnetization (NRM) of 170 samples was measured on a vertically oriented 2G Enterprises DC SQUID cryogenic magnetometer (noise level 10^{-7} A/m) in a magnetically shielded room at the Niederlippach paleomagnetic laboratory of Ludwig-Maximilians-University Munich, Germany. The NRM of the other 204 samples were measured on a horizontal 2G Enterprises DC SQUID cryogenic magnetometer (noise level 3×10^{-12} A/m) at the Paleomagnetic Laboratory Fort Hoofddijk, Utrecht University, the Netherlands, following the same analytical procedure. Demagnetization results are plotted on orthogonal vector diagrams (Zijderveld 1967) and ChRM directions are calculated using principal component analysis (Kirschvink 1980).

3.5.2 Results

The results of the thermal demagnetization for the Prado samples are of good quality (Fig 6 A-D). Initial NRM intensities vary according to facies (Fig. 3.7), with highest NRM intensities (7.8 to 95.4 mA/m) in the red mudstones and siltstones of facies A and E that typically dominate in intervals I, II, and VI. The lowest intensities (0.04 to 7.8 mA/m) are found in facies B and D that contain more carbonate, and dominate intervals III and IV. The calcretes of facies C show a wider range of NRM intensities varying between 0.07 and 87.3 mA/m, with highest values corresponding to

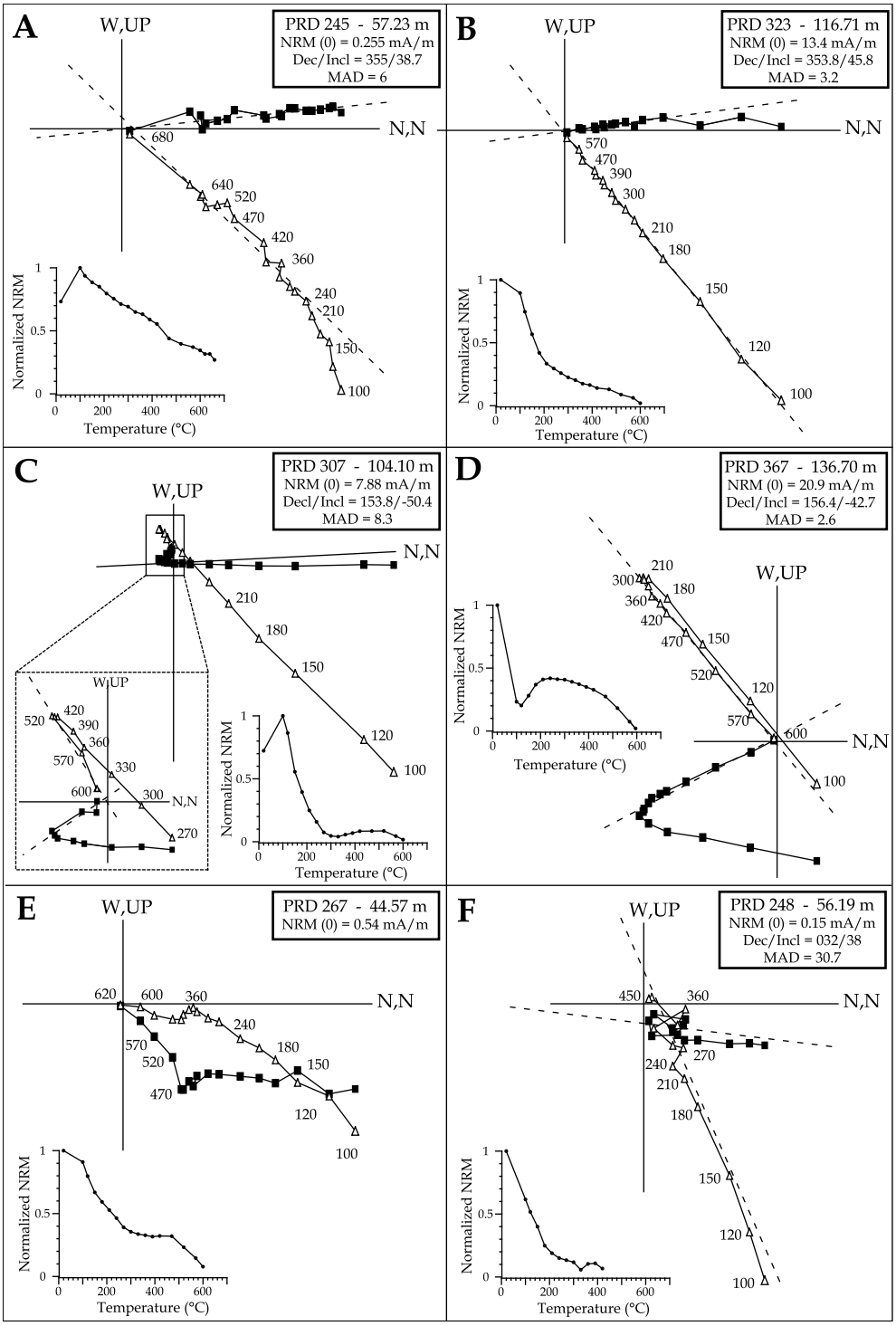
A
W,UP
N,N
PRD 245 - 57.23 m
NRM (0) = 0.255 mA/m
Dec/Incl = 355/38.7
MAD = 6
680
640
520
470
420
360
240
210
150
100
Normalized NRM
Temperature (°C)
B
W,UP
N,N
PRD 323 - 116.71 m
NRM (0) = 13.4 mA/m
Dec/Incl = 353.8/45.8
MAD = 3.2
570
470
390
300
210
180
150
120
100
Normalized NRM
Temperature (°C)
C
W,UP
N,N
PRD 307 - 104.10 m
NRM (0) = 7.88 mA/m
Decl/Incl = 153.8/-50.4
MAD = 8.3
210
180
150
120
100
520
420
390
360
570
330
600
300
270
Normalized NRM
Temperature (°C)
D
W,UP
N,N
PRD 367 - 136.70 m
NRM (0) = 20.9 mA/m
Decl/Incl = 156.4/-42.7
MAD = 2.6
210
300
180
360
420
470
150
520
120
570
600
100
Normalized NRM
Temperature (°C)
E
W,UP
N,N
PRD 267 - 44.57 m
NRM (0) = 0.54 mA/m
620
600
360
240
570
180
520
150
470
120
100
Normalized NRM
Temperature (°C)
F
W,UP
N,N
PRD 248 - 56.19 m
NRM (0) = 0.15 mA/m
Dec/Incl = 032/38
MAD = 30.7
450
360
270
240
210
180
150
120
100
Normalized NRM
Temperature (°C)

← *Figure 3.6* Thermal demagnetization diagrams and decay curves (inset) of selected samples from the Prado section. Open (closed) symbols denote projection on the vertical (horizontal) scale. Numbers along demagnetization trajectories indicate temperature steps in °C. Dashed lines are the interpreted declination and inclination direction of the characteristic remanent demagnetization (ChRM). MAD denotes the maximum average deviation of the interpreted ChRM direction. See text for details on A-E.

the lithologies from interval VI (cycles 43-55) (see Fig. 3.7). The Zijderveld diagrams and thermal decay curves show that the total remanent magnetic signal consists of three components. The first is a randomly oriented component that is removed between temperatures of 100°C and 120°C, and represents a laboratory-induced magnetization related to storage. The second component is removed between 210°C and 270°C; however, in a few samples this component is removed up to temperatures of 390°C (especially in cycles 49 to 51; see Fig. 3.6 C). This component has a normal polarity and is interpreted to represent a viscous overprint by the present-day Earth's magnetic field. The third component displays dual polarities and is interpreted as the characteristic remanent magnetization (ChRM) of the sediment. Three unblocking temperatures of the ChRM can be distinguished in the Prado section. The ChRM of *ca* 60% of the samples is fully demagnetized at temperatures from 600°C up to 700°C, indicating unblocking temperatures for (fine-grained) hematite (Fig. 3.6 A, C, and E). Samples with these unblocking temperatures are mostly from lithologies A and B (and E), *i.e.*, from the well-drained mudflat deposits. The ChRM of *ca* 35% of the samples is removed between 520°C and 600°C, which is a typical unblocking temperature range for magnetite (Fig. 3.6 B and D). Samples with this temperature range include all facies A to E. The remaining 5% of the samples have unblocking temperatures between 390°C and 480°C, suggesting iron sulphides as the main carrier of the ChRM (Fig. 3.6 F). Most of these samples belong to carbonate-rich mudstones of facies D. Susceptibility measurements indicate stable values for the samples with high unblocking temperatures (570°C and higher) with no significant change in mineral composition during the thermal demagnetization. The samples from the limey grey mudstones of facies D show a distinct increase of susceptibility values from temperatures around 360°C and higher, probably due to the oxidation of the iron sulphides.

The ChRM directions were calculated for more than five temperature steps in the range 270 to 700°C. The quality of the measurements and the line fitting were evaluated by visual inspection of Zijderveld diagrams and by calculating the maximum angular deviation (MAD). The magnetic polarity record of the Prado section was interpreted using MAD values smaller than 20° as cut-off. Values larger than 20° and non-interpretable samples are indicated in Figure 3.7 by open circles and crosses, respectively.

3.5.3 Correlation to the ATNTS2004

Declination and inclination data are plotted in stratigraphic order and reveal seven polarity reversals, with grey colours indicating the uncertainty intervals of the reversal level (Fig. 3.7). The established lithostratigraphic and time-equivalent relationships between the Prado and Cascante sections consent a straightforward correlation of the Prado polarity record to the ATNTS04 (Lourens *et al.* 2004). Starting from the base of the Prado section, the long normal polarity interval N1 is correlated to chron C5n.2n. The subsequent three normal polarity intervals N2, N3, and N4 are correlated to chrons C5n.1n, C4Ar.2n and C4Ar.1n, respectively. The correlation of the Prado magnetostratigraphy to the ATNTS04 of Lourens et al. (2004) reveals a complete polarity record ranging from chron C5n.2n to C4Ar.1r and covering a timespan of more than 1 million years, *i.e.*,

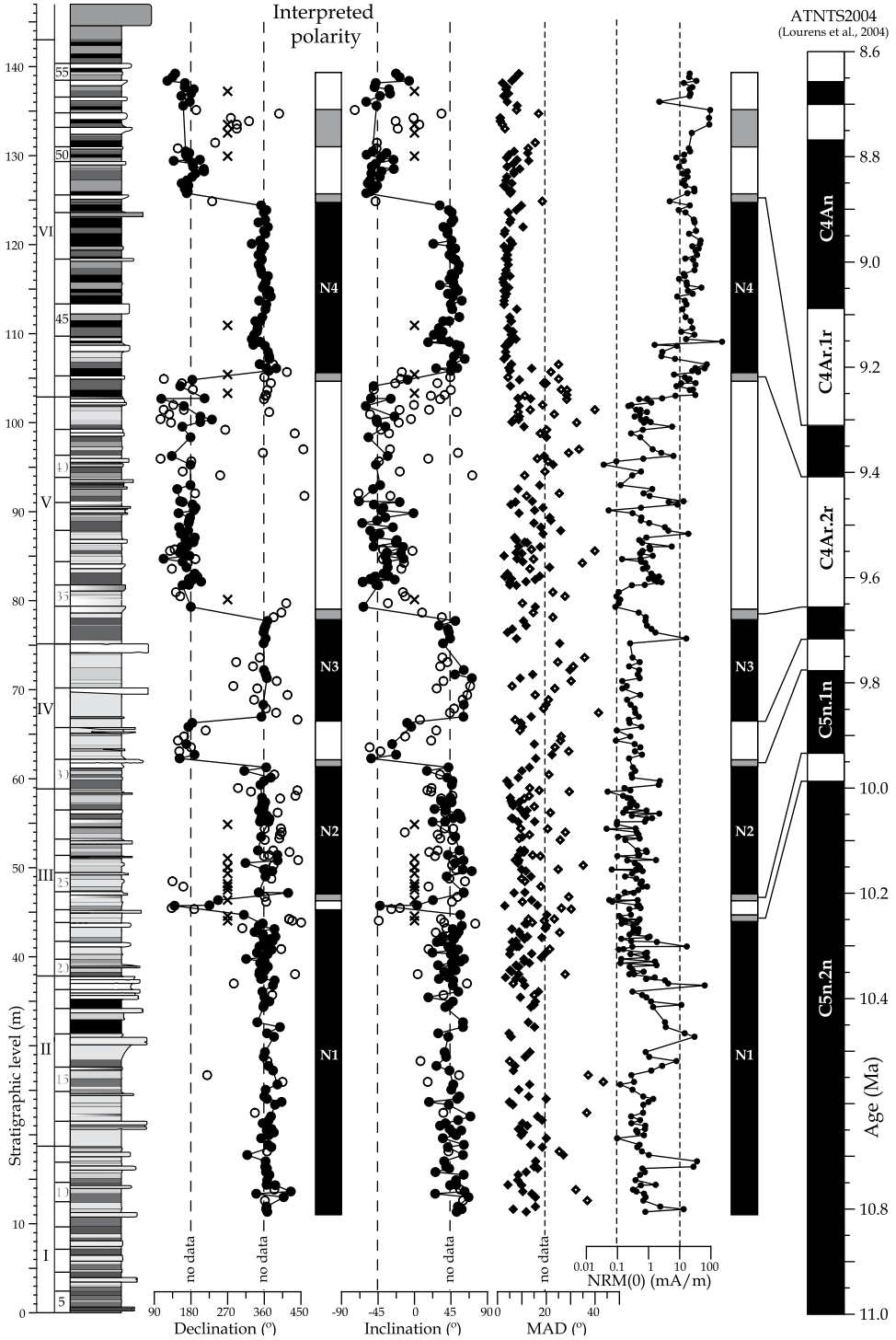
Interpreted polarity
ATNTS2004
(Lourens et al., 2004)
Stratigraphic level (m)
Age (Ma)
N1
N2
N3
N4
C4An
C4Ar.1r
C4Ar.2r
C5n.1n
C5n.2n
no data
Declination (°)
Inclination (°)
MAD (°)
NRM(0) (mA/m)

← *Figure 3.7* Declination, inclination, and interpreted polarity for the Prado magnetostratigraphy. To the left, a schematic column of the section is given, including stratigraphic position, and interval and cycles numbers. The graphs to the right show the maximum average deviation (MAD), initial natural remanent magnetization (NRM) and the correlation of the interpreted polarity record at Prado to the ATNTS04 of Lourens *et al.* (2004).

from *ca* 10.3 to 9.2 Ma. An alternative correlation would be possible if cycles 51 and 52 indeed were of normal polarity, as suggested by paleomagnetic results of poor quality (open circles in Fig. 3.7). Subsequently, this presumed normal polarity could be correlated to chron C4r.2r-1 and the long normal N4 to C4An. However, this correlation is rejected here, because it suggests the presence of a hiatus in interval V which is not plausible because no indications of unconformities have been found. In addition, the sedimentation rates in the upper part would be lower, where it is expected to be similar to or higher than the weakly pedogenised siliciclastic sediments below.

3.6 Cyclostratigraphy

3.6.1 Orbital forcing

Correlation of magnetostratigraphy to the ATNTS2004 time scale (Lourens *et al.* 2004) provides a detailed age model for the Prado section. In the time interval considered, the astronomical ages for polarity reversals in the ATNTS2004 were derived from astronomically tuned sapropel patterns in the deep marine Monte dei Corvi section in northern Italy (Hüsing *et al.* 2007). In Figure 3.8, the magnetostratigraphy of the Prado section is compared to the recently improved astronomically dated ages of polarity reversals in this deep marine section. Grey bars represent ranges of uncertainty in depth at Prado and time at Monte dei Corvi.

There are 24 well-defined facies cycles in the Prado section between the top of chron C5n.1r and the top of C4Ar.1n, with an uncertainty of half a cycle in both directions. Additionally, there are 5 less well-defined "a"-cycles in this interval, making a total of 29 ± 0.5 cycles. In the Monte dei Corvi section, the time comprised between these two reversals ranges between 626 ± 9 kyr (Hüsing *et al.* 2007). This results in a period between 25.1 to 27.0 kyr for a well-defined lithofacies cycle, and 20.9 to 22.3 kyr when the "a"-cycles are included. The latter period is suggestively close to the duration of a *climatic* precession cycle with main periods of 18.9, 22.2 and 23.5 kyr (Laskar *et al.* 2004). The suggestion by the age control that the metre-scale facies cyclicity may be driven by precession is further elucidated.

3.6.2 Precession phase-relation

In the depositional model presented in Figure 3.4, the paleoenvironmental interpretation of the facies cycles was formulated in terms of hydrological balance. As precession forcing is suggested by the age control, metre-scale sedimentary rhythms controlled by groundwater levels must be related to precession. The phase relation between changes in the regional water table and precession remains, however, unknown. The phase relation relates to two elements: the relationship between groundwater level (and, consequently, sedimentology) with local climate and the link between local climate and precession.

The relation between groundwater level (and sedimentological processes) and local climate can be straightforward. Lower groundwater levels inferred from the development of well-drained floodplains in facies A and B ('dry' part of the cycle) might indeed relate to decreased precipitation rates, and vice versa. However, increased sedimentation rates caused by increased precipitation

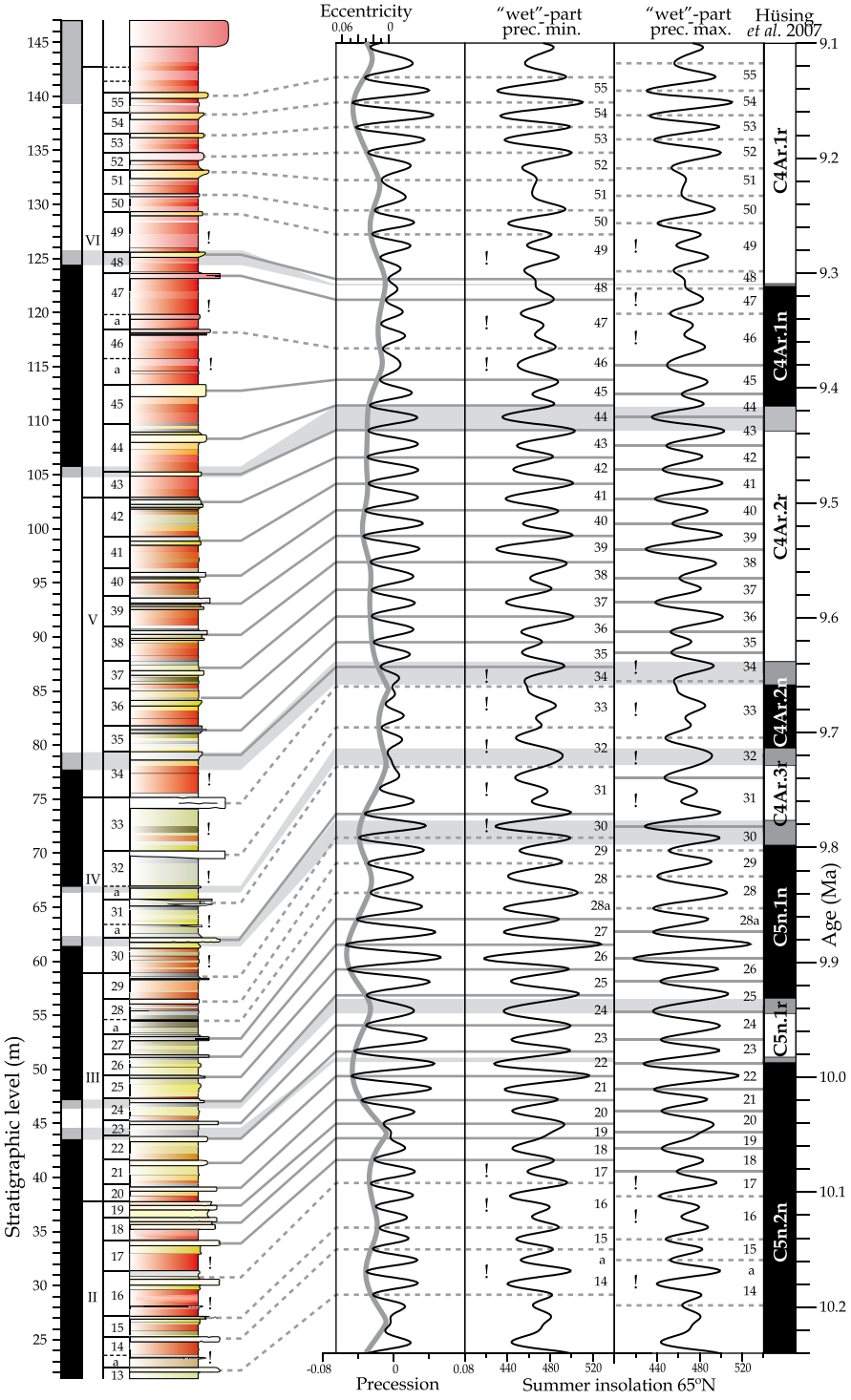
Eccentricity
0.06
0
"wet"-part prec. min.
"wet"-part prec. max.
Hüsing et al. 2007
Stratigraphic level (m)
Age (Ma)
Precession
Summer insolation 65°N
-0.08
0
0.08
440
480
520
C4Ar.1r
C4Ar.1n
C4Ar.2r
C4Ar.2n
C4Ar.3r
C5n.1n
C5n.1r
C5n.2n
II
III
IV
V
VI

← *Figure 3.8* Astronomical calibration of the sedimentary cycles in Prado to precession and insolation target curves of Laskar *et al.* (2004), according to the two phase-relations discussed in the text. To the left, a schematic log of the Prado section is shown, including the interpreted polarity results, and interval and cycle numbers. Cycle numbers are also indicated along the insolation curves. Thick cycles are indicated by "!" and occur during long, 405-kyr eccentricity minima. Grey-shaded bands indicate the correlation of polarity reversals and their respective uncertainty intervals in the Prado section to the astronomically calibrated reversals of the Monte dei Corvi in Italy (Hüsing *et al.* 2007).

could have a similar effect. According to the latter hypothesis, water-logged environments could then occur during times of sediment starvation due to decreased precipitation. These processes might have a different effect on different parts of the basin (Picard and High 1981).

Abels et al. (2008) elaborated on the second aspect when trying to solve the same problem for the sedimentary cycles in the nearby, time-equivalent Cascante section in the Teruel Basin. Geological data as well as climate modelling of precession extremes pointed out that winter precipitation increased significantly during precession minima (and related boreal summer insolation maxima), while increased summer precipitation is cancelled by high summertime evaporation rates during these times (Abels *et al.* 2008). In their climate model, increased winter precipitation is due to elevated Mediterranean Sea temperatures and resulting cloud formation. Consequently, precession minima most likely resulted in a significant increase in the net water budget for the Teruel Basin. Following this reasoning, precession minima should be correlated with increased winter precipitation and lake-level high-stands, and vice versa, in agreement with previous studies (Sierro *et al.* 2000; Kruiver *et al.* 2002; Abdul Aziz *et al.* 2003; Abels *et al.* 2008). Most probably 'wet' part (facies C, D, and E; see above 'Depositional Model') of the lithofacies cycles and related groundwater level high-stands in Prado related to precession minima and association summer insolation maxima. The remaining uncertainties however lead to the consideration of both phase-relations in the established astronomical tuning (Fig. 3.8).

3.6.3 Astronomical tuning

Starting from the polarity reversals, the astronomical tuning of the Prado section is based on the correlation of successive sedimentary cycles to consecutive precession cycles (Fig. 3.8). The tuning of the 'wet' part (see above) of the cycles to precession minima and 65°N summer insolation maxima is shown, as well as the alternative tuning following the opposite phase relation (Fig. 3.8). Solid lines in the Figure 3.8 are used when only one possible correlation exists, primarily due to the location and age of polarity reversals. Dotted lines instead indicate that the suggested correlation is the most probable, but an alternative correlation is possible with one precession cycle up- or downwards. The resulting astronomical ages for the polarity reversals in the Prado section fall within the uncertainty intervals of the ages in the Monte dei Corvi section (Fig. 3.8). This implies that similar amounts of sedimentary cycles are present in the same intervals in both sections constrained by their independent, high-resolution magnetostratigraphies.

The variable thicknesses of cycles 18, 17, 16 and 14 hamper a direct calibration to the precession curve due to the low eccentricity values in this interval. As a consequence, an uncertainty of one cycle exists in the tuning of this interval, which increases downwards to an uncertainty of two cycles. Therefore, the tuning is only presented for the 'West' transect of the Prado section and not extended to the 'Central' transect. Additional (magneto-)stratigraphic constraints, that have to come from locating two cryptochrons of the long chron C5n.2n (Evans *et al.* 2007), are necessary to solve the tuning of the cycles in this lowermost part of the Prado section. The astronomical tuning

from cycles 13 to 30 is straightforward. The tuning in this interval depends on counting cycle 30 as a single or double cycle. If considered as a double cycle, the tuning would shift one precession cycle downwards. In this case, the reversed chron found in cycles 23 and 24 still matches the ages for chron C5n.1r (Fig. 3.8; Hüsing *et al.* 2007). In addition, the match of the closely spaced cycles 18 and 19 with two closely spaced precession cycles at 10.05 Ma makes the presented tuning even more likely. From cycle 30 to 34 and from cycle 45 to 49, the precise tuning of individual facies cycles to precession is also uncertain, due to low eccentricity and to the interplay between precession and obliquity. In between, however, cycles 34 to 45 are well constrained by the polarity reversals and the tuning seems to be correct.

The tuning reveals that the three intervals with thicker than average sedimentary cycles (cycles 13 to 17, 29 to 34, and 45 to 49) correspond to 405-kyr eccentricity minima (Fig. 3.8). Such minima display reduced amplitudes of precession due to low eccentricity values, thus allowing the 41-kyr obliquity cycle to interfere with precession. Consequently, the thickest cycles (14, 16, 17, 30 to 34, 46, 47, and 49; most including an "a"-cycle; indicated by "!" in Fig. 3.8) may represent obliquity cycles, each comprising two precession cycles. This suggests that the "a"-cycles should indeed be regarded as full precession cycles. Also, some of them may represent the longest or most extreme precession minima (or, oppositely, maxima).

The magnetostratigraphic age model for the Prado section thus strongly suggests that the metre-scale sedimentary cycles are forced by climate variations dominantly driven by the *climatic* precession cycle. Additionally, the astronomical tuning reveals the imprint of low long (405-kyr) eccentricity values by reducing the amplitude of precession. In these periods, obliquity interferes with precession or even might dominate the climate forcing (Abdul Aziz *et al.* 2003; Hüsing *et al.* 2007). Astronomical forcing of sedimentation processes recorded in the Prado section is therefore regarded to be proven, or at least to be the most likely hypothesis underlying the three superimposed scales of lithofacies cyclicity.

3.6.4 Precession – obliquity interference patterns

In Mediterranean deep-marine successions, distinct sedimentary patterns often show a close match with patterns in the summer insolation curve for 65°N (Lourens *et al.* 2001; Hüsing *et al.* 2007). The 65°N summer insolation curve is used here, because this target curves best reflects the Mediterranean marine sedimentary cycle patterns in the Neogene (Hilgen *et al.* 2003; Hüsing *et al.* 2007). In times of low eccentricity values, the relative influence of obliquity on insolation becomes more prominent, and consequently obliquity can interfere with precession. The resulting distinct patterns in insolation curves are used to evaluate the match with sedimentary cycle patterns (Lourens *et al.* 2001). In the interval between 9.65 and 9.45 Ma in the Cascante section, the sedimentary record shows a distinct precession – obliquity interference pattern that approximately matches the P-0.5T (precession minus half obliquity) target curve (Abels *et al.* 2008), which is similar to the 65°N summer insolation curve. A different target curve might be needed for the sediments in the Iberian peninsula. In the Prado section, alternating thick and thin 'dry' parts of the cycle (*i.e.*, facies A and B corresponding to groundwater table low-stands) occur in the same time interval as in Cascante, confirming the presence of an obliquity – precession interference pattern in the stratigraphic column at Prado. The thick 'dry' parts (cycles 34, 36, 38, 39, 41; Fig. 3.8) do not specifically match with extreme insolation minima and, conversely, thin 'dry' parts do not match with relatively high insolation minima. On the contrary, a good pattern match is achieved when the opposite phase relation is regarded (Fig. 3.8), *i.e.*, the 'dry' part corresponding to precession minimum. At present, it is not possible to use this thickness mismatch with insolation

as proof for the opposite phase relation. This is because of the remaining uncertainties in the relation between local groundwater fluctuations and local climate and in the relation between local climate and precession, as discussed above. Moreover, it can be argued whether tuning should be performed towards the 65°N summer insolation or a different target curve. The 65°N summer insolation is similar to the P-0.5T curve (precession minus half times obliquity). Here, the 65°N summer insolation is used as a target because of the good to perfect resemblance of facies patterns in marine Mediterranean sediment records with this curve (Hilgen *et al.* 2000; Sierro *et al.* 2000; Lourens *et al.* 2001; Hilgen *et al.* 2003; Hüsing *et al.* 2007).

3.6.5 Large-scale trends

Most large-scale paleoenvironmental shifts in the Prado section occur in intervals where eccentricity values are low, due to the influence of the 405-kyr cycle. The first shift is the change from well-drained mudflat environments in intervals I and II to more persistently water-logged environments of intervals III and IV, at *ca* 10.05 Ma. The reverse change occurs in two steps. The first occurs at 9.65 Ma, from interval IV to V, in which well-drained environments re-enter the stratigraphy. This drying trend culminates with a second one occurring at 9.44 Ma, from interval V to VI, after which well-drained mudflat to floodplain environments dominate. The relation between large-scale trends and 405-kyr eccentricity is suggestive, but the timespan comprised by the sedimentary record in Prado is regarded to be too short to directly relate such paleoenvironmental shifts to eccentricity. Furthermore, while the 405-kyr minima at 9.35 Ma and 10.15 Ma are related to thick well-drained mudstones, the 405-kyr minimum at 9.7 Ma is related to thick water-logged mudstones. This suggests that throughout the Prado section the sedimentary paleoenvironments would have reacted differently to long period eccentricity minima. It is then more plausible that other forcing mechanisms played a role as well on these time scales. These may include tectonics, non-orbital climate variations, climate variations related orbital cycles of longer periodicity, or a geomorphic shift of the lacustrine environment.

3.7 Discussion

Orbital climate forcing is demonstrated as a primary driver of paleoenvironmental change, and therefore of local patterns in sedimentation, by applying an integrated stratigraphic and sedimentologic methodology to the deposits in the Prado area. In addition, the cyclostratigraphic approach enables to establish a high-resolution magneto-astro-chronological framework and analyze the meaning and architecture of facies variability at a temporal scale of 10^3 to 10^5 yr, which is usually hard to attain in ancient continental successions.

The Miocene facies organization on a metric scale in Prado is dominantly controlled by the climatic precession cycle, with a recognizable imprint by long, 405-kyr eccentricity and by obliquity on stratigraphic scales variable from metres to tens of metres. The influence of the precession cycle on the climate of the Iberian Peninsula and its signature in the geologic record has been previously identified in the Late Cenozoic Spanish sedimentary record (Abdul Aziz *et al.* 2000; Sierro *et al.* 2000; Krijgsman *et al.* 2001; Sierro *et al.* 2001; Kruiver *et al.* 2002; Luzón *et al.* 2002; Abdul Aziz *et al.* 2004). Some of these studies also confirmed the concomitant role of obliquity and short and long eccentricity in coupling longer-term climate change to sedimentation (Krijgsman *et al.* 1994; Barberà *et al.* 1996; Sierro *et al.* 2000; Abdul Aziz *et al.* 2003; Abels *et al.* 2008).

Orbital forcing in the Prado section is demonstrated with the use of polarity reversal ages that have been calculated by astronomical tuning of sapropel patterns in the Miocene Monte dei Corvi section, in northern Italy (Hüsing *et al.* 2007). Our reasoning thus highly depends on the integrated stratigraphic work in Monte dei Corvi. The astronomical control of sedimentary cyclicity at Monte dei Corvi in its turn was confirmed by the astronomically tuned sapropels at Monte Gibliscemi (Hilgen *et al.* 2000; Hilgen *et al.* 2003). Further corroboration comes from the $^{40}Ar/^{39}Ar$ dating of biotites from two intercalated ash layers that indicate an average periodicity close to 20 kyr for basic cycles, of *ca* 40 kyr for intermediate cycles, and of *ca* 100 and *ca* 400 kyr for the larger-scale cycles in the interval bracketed by the ash layers (Cleaveland *et al.* 2002; Hilgen *et al.* 2003). It must be noted that importing astronomically calibrated ages for polarity reversals to construct an age model in an independent section is not equivalent to importing orbital cycle frequencies recognized in the section where these ages were derived from. This is because reversals of the Earth's magnetic field occur independently from orbital climate forcing. This means on the contrary that the results from the Prado section can rather be regarded as a corroboration of the constructed time scale and astronomical forcing hypothesis for the Monte dei Corvi section, similar to the corroboration based on comparing sapropel patterns of Monte dei Corvi and Monte Gibliscemi. The three cyclostratigraphic studies were carried out independently, even though Monte dei Corvi reversal ages were imported into Prado as first order age control. The three sedimentary systems of these sections developed totally independently in separate marine environments and in the continental realm.

The cyclostratigraphy method applied in this study has a high potential for detecting orbital climate forcing in continental successions. Importing astronomically calibrated ages of reversal boundaries does not imply that the age model of the studied succession is biased towards astronomical forcing. Instead, if the astronomical time scale is correctly calibrated, then potentially the best possible detailed age model is used (Van Vugt *et al.* 1998; Kruiver *et al.* 2002; Abels *et al.* 2008). Also, the method avoids demonstration of astronomical forcing by comparing the lithofacies cyclicity with orbital cycle ratios derived from statistical analysis (Wilkinson *et al.* 2003; Meyers and Sageman 2007; Bailey and Smith 2008).

3.8 Conclusions

Astronomical climate forcing of facies organization is demonstrated in the continental Prado section as part of the Upper Miocene fill of the endorheic, low gradient southern Teruel Basin (North-East Spain). Detailed sedimentological logging coupled to stratigraphic analysis allowed the recognition of a metre-scale, composite facies cycle. This basic sedimentary cycle consists in an alternation of predominantly fine clastic and carbonate or carbonate-rich facies, and is interpreted in terms of relative variations through time of groundwater levels. The detailed magnetostratigraphic age model provided for the Prado section suggests that the basic, metre-scale cyclicity is regulated by the climatic precession cycle. An astrochronology is established by correlating the individual metre-scale cycles to successive precession cycles. The resulting astronomical ages for polarity reversals at Prado are within the uncertainties of the used time scale. The age framework shows the superposed imprint of long eccentricity and obliquity in modulating precession-scale cyclicity in three stratigraphic intervals. Uncertainties remain regarding the exact phase relation of groundwater to local climate and local climate to precession. Nevertheless, the astronomical tuning clearly reveals that orbital forcing was the prevailing forcing mechanism in

the Prado mudflat to marginal lacustrine paleoenvironments at 10^3 yr to 10^5 yr time scales. This study shows that importing astronomically calibrated ages for reversal boundaries is an useful method for demonstrating orbital forcing in non-marine successions.

3.9 Acknowledgements

Jan van Dam, Liesbeth Jasperse, Karel Steensma, and Anne van der Weerd are thanked for field assistance. Uwe Kircher (LMU Munich, Germany) is thanked for assistance with palaeomagnetic measurements. José Pedro Calvo (IGME, Spain) is thanked for fruitful sedimentological discussions in the field. Poppe de Boer (Utrecht University, Netherlands) is thanked for constructive remarks on earlier version the text. Fieldwork permits in this protected area are kindly supplied by the Instituto Aragonés de Gestión Ambiental (INAGA).

CHAPTER 4

Synchrony of opposite lithofacies transitions in the Miocene continental Teruel Basin, NE Spain, as revealed by magneto-astrochronology

Hemmo A. Abels, Hayfaa Abdul Aziz, Frederik J. Hilgen

4.1 Abstract

The continuous Upper Miocene fill of the low-gradient, ramp-type, endorheic southern Teruel Basin is studied in the Prado and Cascante areas located seven kilometres apart near opposite basin margins. Basinal sediments comprise well-drained distal floodplain mudstones with regular intercalations of palustrine to shallow lacustrine limestone beds. In both the Prado and Cascante section, previous studies revealed the imprint of precession, and short and long eccentricity climate forcing on meter-scale lithofacies cycle patterns and, hence, lake and groundwater level. Here, we use and extend the established astrochronologies to construct a high-resolution astronomical time framework and bed-to-bed correlations between the sections, with the aim to unravel forcing mechanisms behind formation-scale lithofacies changes between limestone dominated and floodplain-mudstone dominated stratigraphic intervals.

The integrated stratigraphy reveals the synchrony of the termination of water-logged mudflat to marginal lacustrine environments in Prado with the onset of shallow lacustrine conditions in Cascante, in both sections occurring in two distinct steps at 9.65 Ma and 9.45 Ma. The synchrony of the inverse facies shifts argues for a common origin, that might be climatic, tectonic, or autogenic. At present, no mechanisms can be exclusively appointed, although a tectonic or geomorphic induced drainage area increase seems the most plausible explanation. The correlation of opposite paleoenvironmental shifts would not have been considered on the basis of lithostratigraphic or sedimentologic data alone. This result highlights the chronologic potential of the working method, and more importantly indicates the necessity of high resolution age control, preferably down to Milankovitch time scales, in terrestrial sediment records, that are commonly used as paleoclimate archives and for reconstruction of geologic history.

4.2 Introduction

Untangling tectonic, climatic, and autogenic or geomorphic processes is one of the challenges of geological studies in continental basins (Caroll and Bohacs, 1999; Gawthorpe and Leeder, 2000). To reach such a goal, it is essential to place stratigraphic and paleoenvironmental records in high-resolution time-frameworks (DeCelles *et al.*, 2007; Horton *et al.*, 2004), preferably down to resolutions that allow to resolve the dominant orbital cycle frequencies (Meyers, 2008). In addition, determination of astronomically forced climate variability in continental records is valuable for understanding the impact of climate on terrestrial environments and for the subsequent potential

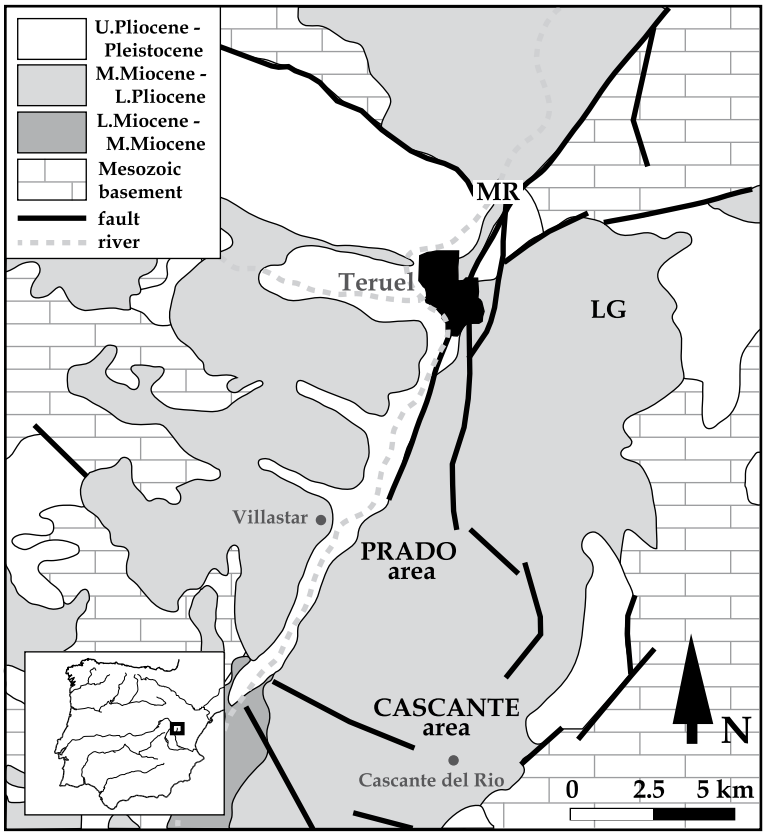

Figure 4.1 Geological map of the northern part of the southern Teruel Basin, Spain (modified after Arlegui *et al.*, 2005). The location of the study area in Spain is shown in the inset. The locations of the Prado area, Cascante area, as well as the La Gloria (LG) and Masada Ruea sections (MR) are shown.

to gain high-resolution age control (Abdul Aziz *et al.*, 2008; Ashley, 2007; Kemp and Coe, 2007; Meyers, 2008). Often, however, the key-problem is the poor age control itself preventing paleoenvironmental records to be accurately placed within tectonic, paleoenvironmental, and regional or global climate histories (Cojan *et al.*, 2000; Dupont-Nivet *et al.*, 2007), and to calibrate observed sedimentary rhythms in order to demonstrate orbital climate forcing (Machlus *et al.*, 2008; Meyers, 2008; Pietras and Carroll, 2006).

A continuous record of Middle to Upper Miocene continental sediments is present in the southern Teruel Basin, NE Spain. The succession includes several 10^1-10^2 m scale lithofacies alternations of dominantly siliciclastic and dominantly evaporite or carbonate sediments (Broekman, 1983; Ortí *et al.*, 2003). These alternations can be of multiple origin and solving the forcing mechanism requires basin-wide sedimentologic and stratigraphic control as well as high-resolution age control. Small-scale rhythmic lithofacies alternations in two distinct basinal successions have been related to orbital climate forcing using high-resolution magnetostratigraphic age control (Abdul Aziz *et al.*, 2004; Chapter 2; Chapter 3). These results lead to exceptional understanding of the two paleoenvironmental settings and allowed to establish astrochronologies for parts of the stratigraphic infill in this relatively small basin. Here, these astrochronologies are

used and extended in order to correlate the two successions, which is a major step forward to a 3-D basin fill reconstruction with unprecedented age resolution down to Milankovitch time scales.

4.2.1 Geological Setting

The Teruel Basin is a 15 km wide and 100 km long, E-W extensional basin with a half-graben architecture that developed in the Iberian Chain and is bounded by en échelon NNE-SSW normal faults (Fig. 4.1; Anadón and Moissenet, 1996). The basin is bordered by Triassic siliciclastics and evaporites and Jurassic carbonates. The segment of the basin studied here is located directly south of Teruel city and contains Middle Miocene to Pliocene sediments deposited in a low gradient, endorheic setting (Broekman, 1983; Ortí *et al.*, 2003). The distal portions of two alluvial fan systems as well as a younger, along-axis ephemeral fluvial system, are present along the western basin margin (Chapter 3). Along the eastern margin, no coarse clastic sediments have been found except for some thin and small ephemeral fluvial and debris-flow conglomerates suggesting that the half-graben depocentre was situated along the western margin. The studied Cascante and Prado areas are close to the opposite basin margins and located 7 km apart (Fig. 4.1).

4.3 Results

4.3.1 Cascante composite section

The sections that make up the Cascante composite section are located relatively close to the eastern basin margin and include the Cascante, Cañizar, Molatilla and Camarena sub-sections (Figs. 4.1 and 4.SN1). The lower part of the Cascante Composite comprises the Cascante and the Cañizar sub-sections that have been extensively studied (Abdul Aziz *et al.*, 2004; Chapter 2). They consist of mudstones with thin limestone intercalations on meter scale (Fig. 4.2B). Magnetostratigraphic dating confirms the bed-to-bed correlation between Cascante and Cañizar on the basis of mudstone colour patterns (Supplementary Notes; Abdul Aziz *et al.*, 2004). The homogeneous, weakly pedogenized, red and green mudstone are interpreted as a well-drained distal alluvial plain deposit (Abdul Aziz *et al.*, 2004). The limestones in the lower half of the subsection were deposited in very shallow, unstable lake environments, while the limestones in the upper half the sub-section were deposited in shallow, more stable lake environments (Chapter 2). A time-equivalent shift occurs in the Cañizar sub-section (Supplementary Notes; Fig. 4.SN5) where intercalated limestones change from poorly-developed pedogenic calcrete beds to marginal lacustrine limestone beds. Both changes are interpreted to reflect higher groundwater and lake levels during deposition of the limestone part of the meter-scale cycle.

A thick limestone interval is found above cycle 33 in the Cascante sub-section (Fig. 4.1A). A similar transitions occurs two and three lithofacies cycles later in the Molatilla and Cañizar sub-sections, respectively. In the Molatilla sub-section, 21 to 23 meter-scale marl-limestone cycles are present in the limestone interval (Supplementary Notes). The cycles comprise a 0.1 to 0.5 m thick green marl layer with slight reddish mottling and a 0.5 to 2.0 m limestone bed that is often rich in gastropod remains. Root bioturbation increases towards the top of the limestone beds. The limestone is interpreted as a deposit of permanent, shallow lake environments that occasionally desiccated resulting in scarce palustrine features. Lowered lake levels are indicated by more common root penetration at the top of the beds. The marl is interpreted as a water-logged mudflat deposit. Reddish mottling could indicate occasional draining of the environment. Alternatively, the


A
55
50
45
40
35

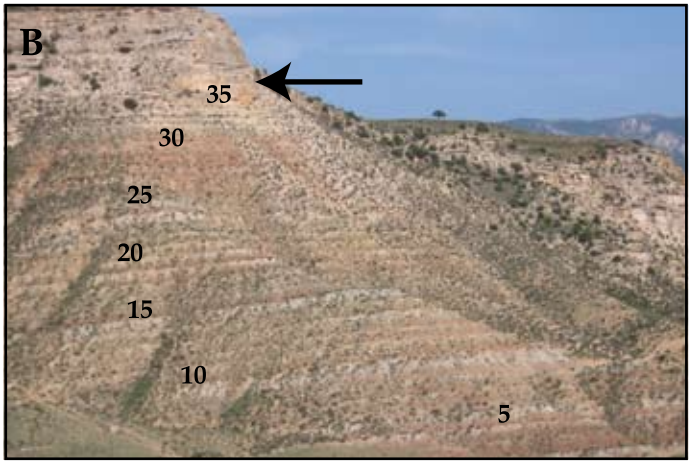
B
35
30
25
20
15
10
5

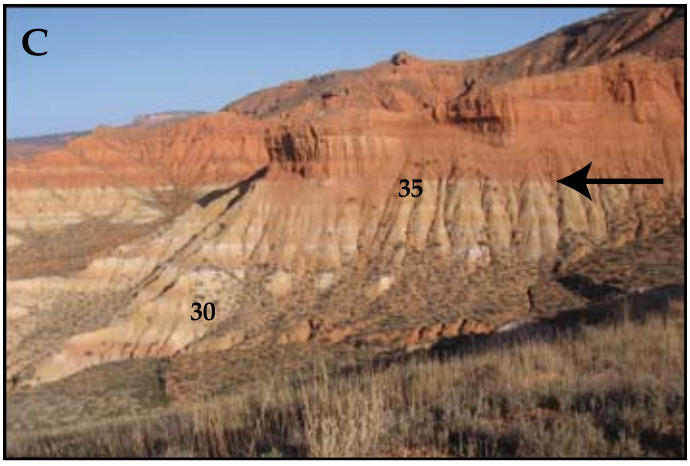
C
35
30

← *Figure 4.2* Photos of the (A) Cascante limestone interval in the Molatilla section, (B) Cascante section below the limestone interval, and (C) the upper part of the Prado section. Indicated are the cycle numbers from the two sections, as used in Chapters 2 and 3. The arrows indicate the second lithofacies shift at 9.45 to 9.40 that occurs synchronous at the Cascante and Prado sections but has opposite character.

marl could be interpreted as deposited during deeper lacustrine conditions or during periods with higher siliciclastic input to the lake environment.

The lacustrine limestone unit at Molatilla is conformably overlain by siliciclastic sediments. The first two cycles above the limestone unit are identical in the continuous outcrops towards the Camarena sub-section (Fig. 4.SN2) indicating a conformable and most probably continuous nature of the transition from the lacustrine limestone unit to the siliciclastic dominated unit (Supplementary Notes). The latter interval is similar to the siliciclastic interval below the limestone unit with red-brown well-drained floodplain mudstones in which thin lacustrine limestone beds intercalate on meter scale.

4.3.2 Prado section

The Prado section is located about 7 km to the NNW relatively close to the western basin margin (Fig. 4.1; Supplementary Notes; Chapter 3). The section consists of meter-scale mudstone – limestone cycles. The homogeneous mudstones are red at the base and yellow-orange at the top and are weakly to moderately pedogenized. The red mudstones are interpreted as well-drained floodplain deposits and the yellow-orange mudstone as water-logged mudflat deposits that increasingly were affected by seasonal pedogenesis. The limestone part of the cycle consists of pedogenic calcrete, grey marls and muddy limestones. The calcrete is related to the development of a calcic soil profile. The marl and muddy limestone are interpreted as deposits of water-logged mudflat, pond, and marginal lacustrine environments (Chapter 3).

The lower part of the Prado section dominantly consists of well-drained floodplain mudstones. A transition to dominant water-logged mudflat and marginal lacustrine sediments occurs at around cycle 18 indicating a rise of the water table. Towards the east, which is in direction of the basin centre, the limestones in the interval of cycles 18 to 33 are much thicker and deposited in deeper, more stable lacustrine environments with less clastic material. Above cycle 33, this limestone-rich interval ends with the return of well-drained, red floodplain mudstones in part of the basic, lithofacies cycle (Fig. 4.3). Higher up above cycle 42, a sharp change occurs towards a succession dominated by well-drained floodplain mudstone with thin intercalations of pedogenic calcrete beds (Fig. 4.2C; Fig. 4.3). This change is recognized in a transect of 500 m, which is as far as outcrops permit. Above the logged interval in the Prado section, tens of meters of red, weakly pedogenized, mud deposits are present. The first 20 to 30 meter of this succession display intercalation of minor sandstone sheets and shallowly incising conglomeratic channel fills (Chapter 3). These facies are interpreted to be the result of the progradation of a poorly confined, ephemeral fluvial system sourced from the north, which is along strike of the basin.

4.3.3 Astrochronology

Precession control on meter-scale lithofacies cycles and the influence of short, *ca* 100-kyr, and long, 405-kyr, eccentricity forcing on larger-scale lake level and groundwater table variations in both the Cascante and Prado section has been demonstrated by magnetostratigraphic age control and sedimentological analyses (Abdul Aziz *et al.*, 2004; Chapter 2; Chapter 3). Subsequently, astrochronologic frameworks for the Cascante and Prado sections have been established.

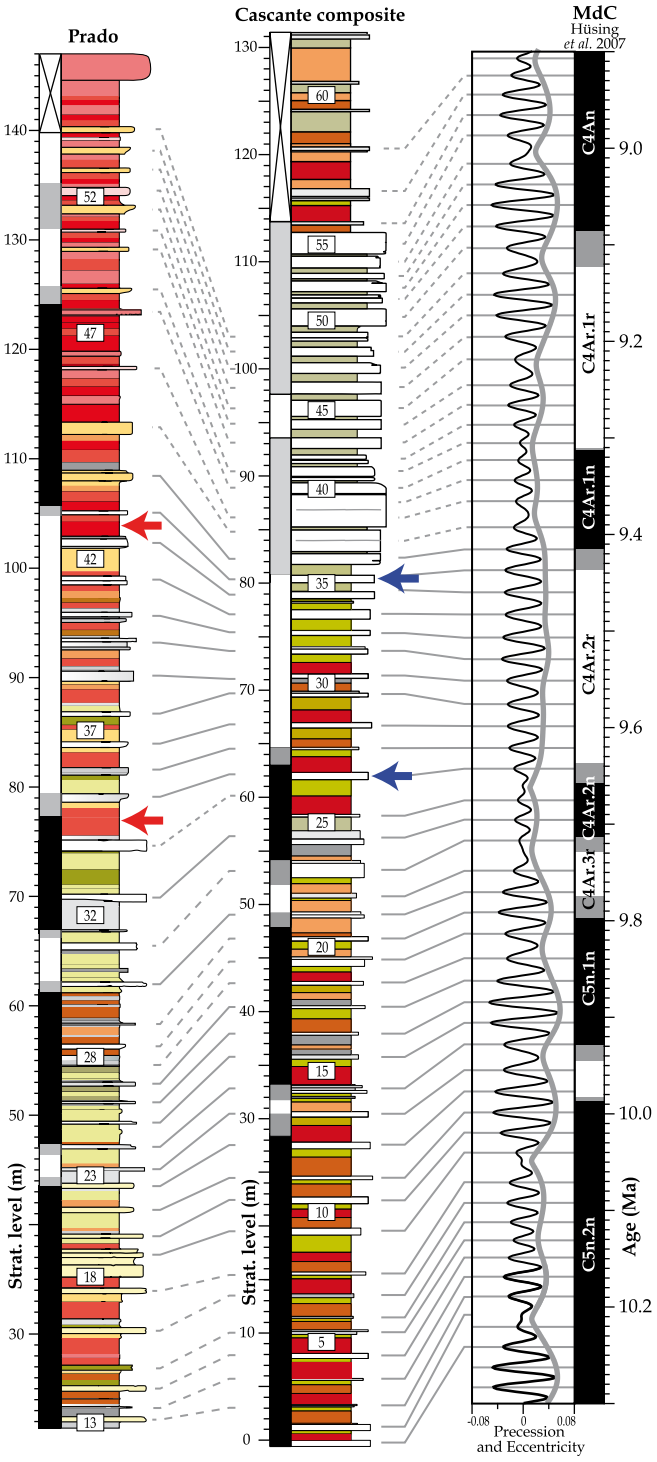
Prado
Cascante composite
MdC
Hüsing
et al. 2007
Strat. level (m)
Strat. level (m)
Age (Ma)
C4An
C4Ar.1r
C4Ar.1n
C4Ar.2r
C4Ar.2n
C4Ar.3r
C5n.1n
C5n.2n
Precession
and Eccentricity

← *Figure 4.3* The lithological logs of the Prado and Cascante sections, their magnetostratigraphies, basic cycle numbering following Chapter 3 and 2, respectively and to the right the precession and eccentricity target curves of the La04 (1,1) solution of Laskar *et al.* (2004) and the astronomically calibrated magnetostratigraphy of the Monte dei Corvi section in Italy of Hüsing *et al.* (2007). The astronomical calibrations of both section used to correlate both sections in high detail to each other and the precession curve. Solid lines indicate relatively certain correlations, while dotted lines indicate uncertain correlations of approximately 1 basic or precession cycle, except sediment younger than 9.4 where uncertainties increase (see text).

Here, the astrochronology of the Cascante composite section (Chapter 2) is extended upwards by correlating successive marl-limestone cycles in the Molatilla sub-section to precession (Supplementary Notes). In the Camarena sub-section, paleomagnetic analyzed samples from the red mudstone interval within the limestone unit all indicate reversed polarity. Following detailed lithostratigraphic correlations, this reversed interval is exported to the Molatilla sub-section (Fig. 4.3; Supplementary Notes) and corresponds to chron C4Ar.1r dated between 9.311 and 9.105 Ma (Hüsing *et al.*, 2007). The phase relation of the small-scale cyclicity to precession is uncertain and leads to 10 kyr age uncertainty (Chapter 2). In addition, a tuning uncertainty of maximal one precession cycle exists in both sections. This uncertainty increases higher in the Cascante Composite section to maximal 5 cycles at the top of the limestone interval (Supplementary Notes).

4.3.4 Correlation between Cascante and Prado

The established magneto-astrochronologies allow bed-to-bed correlations between the Cascante composite and the Prado section with a maximum of one cycle uncertainty up to cycle 44 in Prado and 36 in Cascante (Fig. 4.3). The time-equivalence of the main two-step lithological changes in both sections is unambiguous. The first step at *ca* 9.65 is a shift towards higher lake and groundwater levels during the wet part of the basic, meter-scale cycles in the Cascante Composite and Cañizar sections (Chapter 2), which coincides with the end of dominantly lacustrine conditions and the reappearance of well-drained floodplain environments in the Prado section. The second step, at *ca* 9.45 to 9.40 Ma, marks the onset of full lacustrine conditions in the Cascante Composite section and coincides with the sharp transition to dominantly well-drained floodplain conditions in the Prado section (Fig. 4.2; Fig. 4.3). The detailed correlation around the sedimentary shifts in the two sections is constrained by the polarity reversals that correspond to the top of chron C4Ar.2n at 9.647 Ma and the base of chron C4Ar.1n at 9.426 Ma. Additionally, the number of small-scale precession cycles that are bounded by these reversals is in good agreement.

4.4 Discussion

The synchrony of the flooding of the Cascante area with the drying up of the Prado area suggests a common origin. Outcrops do not indicate any structural obstacle between the two sites that are 7 km apart, which implies that the paleoenvironments were environmentally connected and their hydrologic states in the low gradient basin interrelated. Inversely changing lake and groundwater levels then would indicate that the gradient between the two sites reversed across the two-step shift, which can be of multiple origin.

4.4.1 Global or regional climate

The inverse character of the shifts demands for an asymmetric response if global or regional climate change would have been the cause. This can be due to basin configuration or to differences in the geology of the source area at the basin margins, which presently consists of indurated Jurassic limestones and non-indurated Triassic mudstones and evaporites. No major changes are evident around 9.7 to 9.4 Ma in deep sea benthic oxygen isotope records thought to record global ice volume and temperature variations (Shackleton and Hall, 1997; Westerhold *et al.*, 2005; Zachos *et al.*, 2008). Increased sedimentation rates occur at Monte dei Corvi (central Italy) at 9.65 Ma and at Metochia (Crete) at 9.5 Ma suggesting enhanced runoff or changing physical to chemical weathering ratios (Hüsing *et al.*, 2007; Krijgsman *et al.*, 1995). However, at Monte Gibliscemi (Sicily) no change is present at this time (Hilgen *et al.*, 2000). In Spain, the "Mid Vallesian Crisis" is a major faunal change at the Early to Late Vallesian boundary dated at 9.7 Ma, in chron C4Ar.3r (Agustí, 2001; Garcés *et al.*, 1996). The exact timing of the associated cooler and drier conditions and enhanced wet-dry seasonality is however unsure and varies between 9.7 Ma, just before the lithofacies shifts, and 9.1 Ma, at the base of the fluvial conglomerates at Prado (Casanovas-Vilar and Agustí, 2007; Garcés *et al.*, 1997; Van Dam and Weltje, 1999). Increased wet-dry seasonality and aridity could indeed have reduced chemical weathering and vegetation such that coarse clastics penetrated farther into the basin. However, the entrance of a stable lacustrine water body at Cascante that does not reveal large lake-level fluctuations argues against this. Detailed Mediterranean climate records can solve this question, when available, to check for coincident regional climate change.

4.4.2 Long-period orbital forcing

Van Dam *et al.* (2006) observed higher small mammal turnover rates at times of 2.4-Myr eccentricity minimum, suggested to relate to cooler and more humid conditions due to the absence of highly evaporative conditions during extreme precession minima. Such conditions could cause the observed enhanced runoff and lake filling in the Teruel Basin. In Chapter 2 (Abels *et al.*, 2008), it is suggested that the long-period minimum at 9.52 Ma might be the driver behind the Cascante limestone interval, now being extended with the Prado transition. After around 450 kyr, the Cascante limestone interval gave way to alluvial fan deposits similar to those found below the limestone unit. Long-period eccentricity forcing could thus be the mechanism behind the Cascante limestones, despite the lack of a clear 405-kyr eccentricity forcing that would then also be expected. A strong non-linear response of the paleoenvironment to long-period eccentricity and a memory effect leading to continuous limestone deposition until long after the long-period minimum are then required. The latter effect has been suggested to relate to the gradual filling up and emptying of groundwater reservoirs in the basin and basin margins (Chapter 2). The Prado succession however shows a shift from the two-step transition to renewed floodplain deposition upwards to the ephemeral fluvial conglomerate on top of the section. It seems unrealistic that this major change resulted by a cyclic process related to the 2.4-Myr eccentricity cycle, although it can not be excluded, as also the axial fluvial system is estimated to cease after approximately 250 kyr. To extend on this, the activity of the fluvial system within the stratigraphy on top of the Prado section has to be dated as well as independent climate records over the Iberian peninsula should confirm the expected imprint of the long-period eccentricity cycle.

4.4.3 Tectonics

In tectonic models for foreland basins, enhanced subsidence results in coarse clastic sedimentation only immediately next to the active basin margin (Blair and Bilodeau, 1988; Heller *et al.*, 1988). Further away rapid onset of lacustrine deposition or the entrance of axial fluvial systems occurs in the depocentre during active subsidence. Ceasing of subsidence allows the alluvial fan sediments to prograde into the basin or even to rework proximal coarse sediments and deposition of sheet conglomerates into distal parts of the basin (Blair and Bilodeau, 1988; Heller *et al.*, 1988). Using these models for forelands basin for the supposed half-graben of Teruel would suggest an enhanced subsidence pulse at the time of the paleoenvironmental shifts. However, to be able to really compare the Teruel Basin example with theoretical tectonic models, the basin has to be studied in much more detail with respect to its tectonic character and activity, basin margin faults, and stress fields during the Late Miocene.

4.4.4 Drainage Area

A considerable increase or major change in drainage area to the north of Prado would also fit with the observed enhanced runoff and clastic supply. The northern border of the studied segment of the Teruel Basin shows a complicated structure due to the presence of Neogene NNE-SSW fault lineations, reactivation of pre-Neogene NW-SE oriented faults, and Triassic evaporite diapir activity (Fig. 4.1; Garcés *et al.*, 1997). In this area, sedimentation started at around 11 Ma unconformably on the Triassic basement (Garcés *et al.*, 1997). In the Masada Ruea section (MR in Fig. 4.1; Garcés *et al.*, 1997; Van Dam *et al.*, 2006), a change from alluvial red bed to palustrine sedimentation occurs at 9.7 Ma, while higher up at around 9.4 Ma, a lacustrine limestone started to develop. In the La Gloria section (LG in Fig. 4.1), a hydromorphic clay interval abruptly ends a continuous regular alternation of red siltstone and caliche beds around 9.4 Ma (Kruiver *et al.*, 2003; Van Dam *et al.*, 2006). These changes thus coincide with the lithofacies steps at Prado and Cascante. Higher up in the La Gloria section around 9.1 to 9.0 Ma, a hiatus corroborated by small mammal biostratigraphy is present on top of a thick limestone unit (Van Dam *et al.* 2001). Both the hiatus at La Gloria and the activity of the fluvial system at Prado start around 9.1 to 9.0 Ma (Fig. 4.3) and are estimated to last around 250 kyr, suggesting a common origin. Paleoenvironmental changes in the area just north of our study area thus seem to be coincident with the two steps found at Prado and Cascante, and with the fluvial conglomerate, possibly suggesting that tectonic or diapiric activity in this region could have affected the southern segment of the basin. This explanation has to be further investigated by placing the fluvial conglomerate at Prado in the chronology is well, by studying its provenance, by checking for cannibalism of Late Miocene sediments, and by further investigation of the hiatuses at La Gloria and Masada Ruea.

4.4.5 Autogenic origin

The possibility of an autogenic or autocyclic origin of the shifts should not be discarded, despite the tentative explanations so far. Low accumulation rates during lacustrine limestone precipitation could have created topographic lows that ultimately led to a shift of the clastic depositional systems from Cascante to Prado. To study this possibility, first intermediate sections are needed to trace lateral equivalents of the two lacustrine limestone units and document their interfingering, and second additional outcrops in other parts of this segment of the basin will help to determine if continuously shifting lacustrine limestone units existed or if these occurred during phases of dominantly lacustrine limestone deposition and phases of dominantly floodplain mudstone sedimentation.

4.5 Conclusions

The achieved orbital time control on two successions in the Teruel Basin clearly reveals unexpected lithostratigraphic correlations, that would not have been considered without the gathered age control. This emphasises the importance of high-resolution age models preferably down to Milankovitch time scales in continental sediment records that are being used as paleoclimate archives, as data background of geologic theoretical models, or for reconstruction of geologic history. The origin of the inverse groundwater and lake level shifts remains enigmatic, although climate forcing seems less likely than a tectonic or autogenic mechanism. An increase in northern drainage area of tectonic or geomorphic origin is proposed as the most tentative working hypotheses. Additional intermediate successions between Prado and Cascante areas are needed to fulfil the magneto-astrochronological stratigraphic framework at precession scale time resolution in order to detect the transition between the two inversely changing paleoenvironments. Furthermore, detailed sedimentological analysis of the fluvial conglomerate unit that occurs above the present Prado section will help to detect the source area of this unit, and possible cannibalism of late Miocene rocks. Finally, Late Miocene sections in the northern area are to be further studied from an integrated stratigraphic and sedimentologic point of view to place changes in the highly detailed stratigraphic framework now achieved in the southern segment of the basin and analyse the hiatuses.

4.6 Ackowledgements

The Instituto Aragonés de Gestión Ambiental (INAGA) is thanked for supplying fieldwork permits. José Pedro Calvo and Dario Ventra are thanked for fruitful discussions on the subject.

Chapter 4 Supplementary Notes

4.7 Cascante Composite

The Cascante composite is composed of the Cascante section, that covers the siliciclastic lower part, and the Molatilla section, that covers the carbonatic upper part as well as the siliciclastic interval on top. The Camarena and Cañizar sections are nearby and supply additional stratigraphic and sedimentologic constraints. A location map of the four sections is supplied (Fig. 4.SN1). The Cascante, Molatilla, and Camarena section are close to the paved road from Villel to Cascante del Rio, Valacloche and Cubla. The Cañizar section can be reached by taking the unpaved road opposite to the second turn to Cascante del Rio village (when coming from Villel).

4.7.1 Camarena section

In the Camarena section (Fig. 4.SN1), 41 magnetostratigraphic samples have been obtained that could be placed stratigraphically in the Cascante composite section by lateral tracing of beds via the Tovadizas section (Fig. 4.SN2 and 4.SN3). Samples were thermally demagnetized in a shielded over using steps of 30°C up to 400°C at the paleomagnetic laboratory 'Fort Hoofddijk' at Utrecht

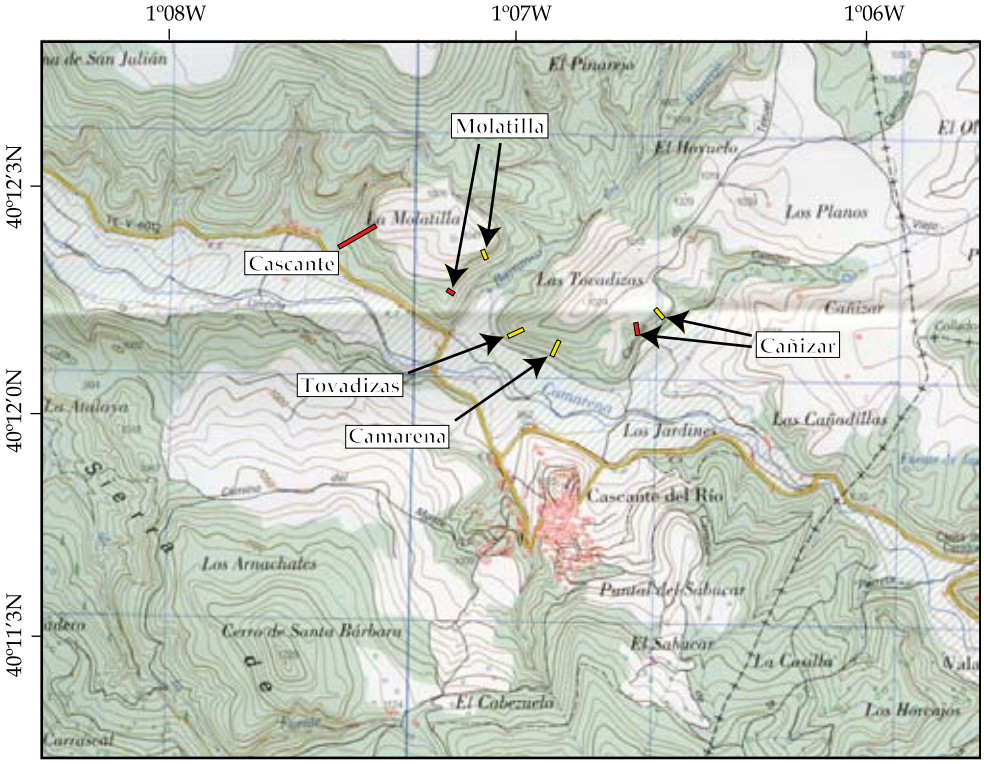

Figure 4.SN1 - Topographic map of the Cascante composite section area. Indicated are the Cascante, Molatilla, Tovadizas, Camarena, and Cañizar sections. Red (yellow) bars refer to mudstone (limestone) intervals. Map after from the Mapa Topográfico Nacional de España 590-IV 1:25.000, Ministerio de Fomento, Instituto Geográfico Nacional, Madrid, Spain.

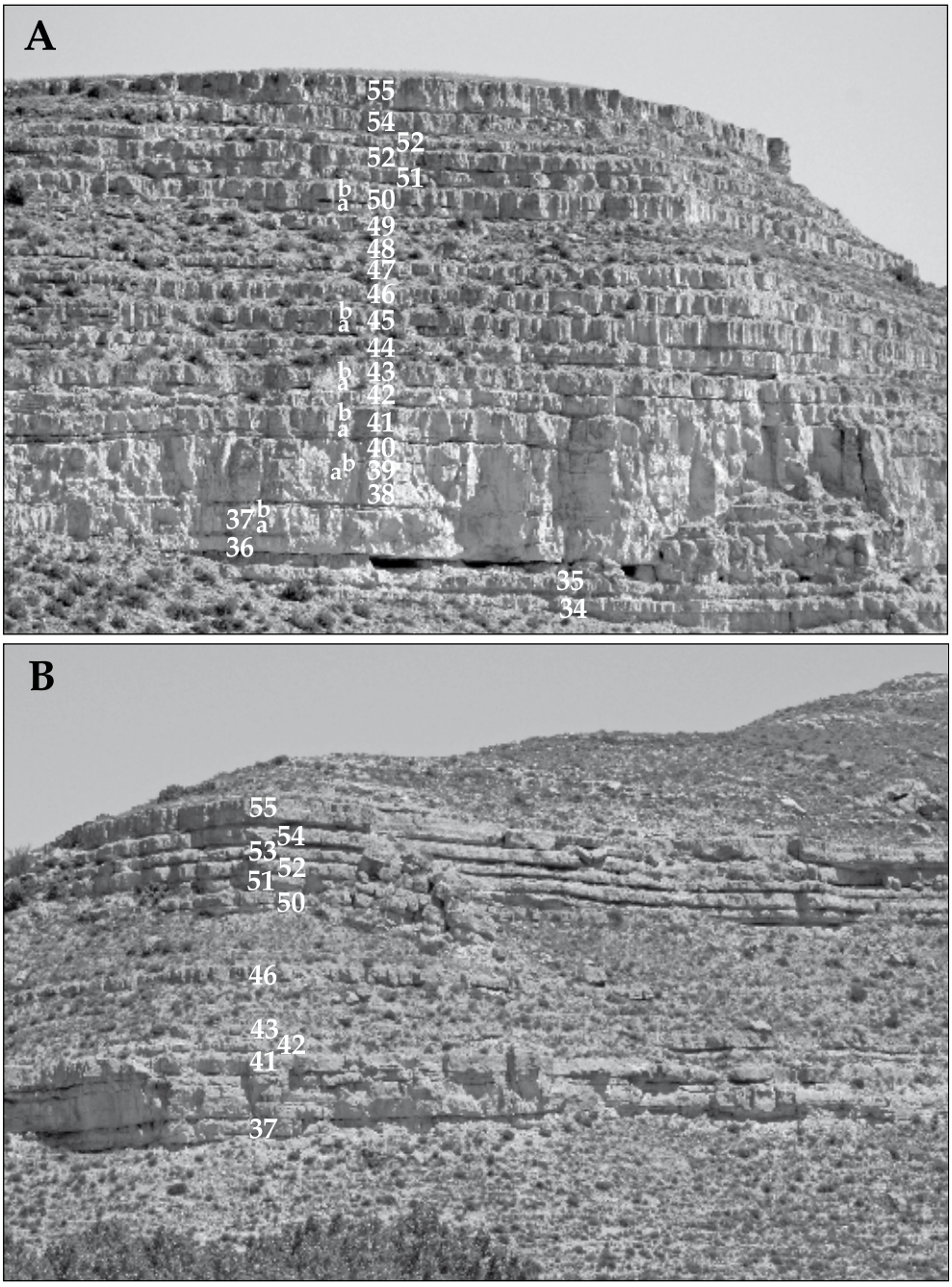

Figure 4.SN2 - Photo of limestone unit in the Molatilla section (A) and the same stratigraphic interval in the Tovadizas section (B) that is situated only 150 meters to the east. The limestone unit splits into two major units (lower consisting of cycles 37 to 41 and upper unit of cycles 50 to 55) and a laterally persistent limestone bed (cycle 46) in the middle.

University. Initial natural remanent magnetization (NRM) intensities are very low between 0.5 and 0.2 mA/m in these samples, but few samples from the middle siliciclastic interval show a reversed component in the temperature range above 280° C, which is regarded as the unblocking temperature for the recent overprint in the similar sediments of the Cascante section (Abdul Aziz *et al.* 2004).

Pilot samples from the marls and limestones in the limestone unit itself showed insufficient NRM-intensity to reveal a reliable polarity, therefore no extensive sampling has been carried out in the carbonate interval.

4.7.2 Molatilla section

The age model for the Molatilla section is primarily based on recognition of mudstone color patterns that are similar to mudstone patterns in the top of the Cascante section. Especially the conspicuous last red mudstone that occurs within the same precession cycle in the Cascante as well as the Cañizar sections (Abdul Aziz *et al.* 2004) is well-visible in the intermediate Molatilla section. This suggests that there is no uncertainty on the age model at the base of the limestone unit in the Molatilla section. Paleomagnetic sampling has not been done in this part of the section, because outcrop quality is very low.

In the Molatilla section, the limestone unit crops out in three sections that are separated by more recent north-south extensional normal faults. The sedimentary log of the unit is derived from the biggest most northern section. Starting at the base of the limestone unit, the astronomical age model is extended upwards by correlation of marl-limestone couplets to successive precession cycles. It is assumed that one lithological cycle is driven by precession, because this has been proved for the lower interval of the section and cycle thicknesses do not essentially differ. Also, in the time-equivalent Prado section, it has been shown that in the southern Teruel Basin the precession cycle was very dominantly controlling depositional environments. Cycle counting in the limestone unit is straightforward, except for the lower interval, where between cycles 37 and 40 a thick laminated limestone bed occurs that occasionally shows two to three vague subdivisions. Finally, two cycles have been counted here and used in the age model, because then cycles have roughly similar thickness than in the rest of the unit. Alternatively, it can not be excluded that three cycles are present. Also, the lamination might indicate transport at the lake floor and with that during some time deposition can have been low to absent. If considerable erosion might have existed, this was of regional character, because the total thickness of the limestone unit is only slightly less towards the marginal sections of Camarena and Cañizar. In the upper part, no uncertainties in amount of cycles exist.

The top of the limestone unit is estimated to be at 8.93 Ma. Uncertainties are due to cycle counting, especially in just discussed interval from cycles 37 to 41. The reversed polarities measured up to cycle 46 indicate that at maximum cycle 45 could be correlated 5 precession cycles younger than in the presented tuning. On the other hand, the reversed polarities measured down to cycle 43, means that this cycle could be correlated 2 cycles older at maximum. This results in a total error at the top of the limestone unit of plus 0.105 Myr and minus 0.42. Adding the half a precession cycle uncertainty, due to uncertain phase-relationship to precession, increases these uncertainties with 0.011 Myr to both sides.

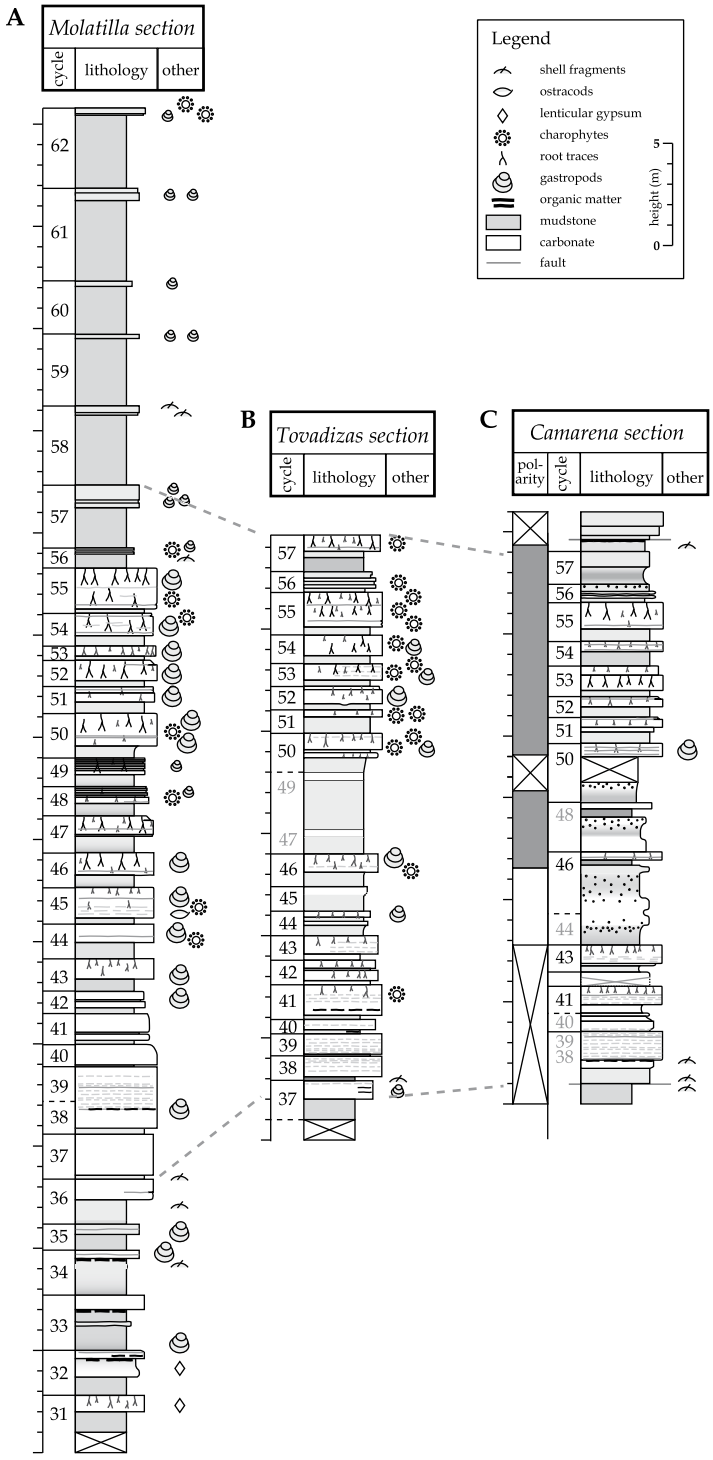
A
Molatilla section
cycle
lithology
other
62
61
60
59
58
57
56
55
54
53
52
51
50
49
48
47
46
45
44
43
42
41
40
39
38
37
36
35
34
33
32
31
B
Tovadizas section
cycle
lithology
other
57
56
55
54
53
52
51
50
49
47
46
45
44
43
42
41
40
39
38
37
C
Camarena section
pol-
arity
cycle
lithology
other
57
56
55
54
53
52
51
50
48
46
44
43
41
40
39
38
Legend
shell fragments
ostracods
lenticular gypsum
charophytes
root traces
gastropods
organic matter
mudstone
carbonate
fault
height (m)
5
0

← *Figure 4.SN3* - Lithological columns of the limestone unit in the Cascante Composite section at three sites (Fig. 4.SN1). Indicated are the small-scale cycle numbers, lithology and induration, content (see other). (A) The Molatilla section (Fig. 4.SN2A), B. the Tovadizas section (Fig. 4.SN2B), and C. the Camarena section. To the left of the Camarena column the interpreted reversed polarity interval is indicated in white, uncertain polarity intervals are indicated in grey, and not sampled intervals with a cross. Cycle numbers in grey indicate inferred but uncertain position of these cycles in that section.

The siliciclastics on top of the limestone unit, crop out best in a sliced part in between the middle and southern most section. Paleomagnetic sampling was impossible in the siliciclastic sediments above the limestone unit (cycles 57 to 61; Fig. 4.SN4), because of the poor quality of the outcrop.

4.7.3 Cañizar section

The correlation of the Cañizar section to the Cascante section, and subsequently to the Prado section, is shown in Figure 4.SN5. The correlation of Cañizar follows the correlation established by Abdul Aziz *et al.* (2004). The limestone below cycle 27 are poorly developed pedogenic calcretes interpreted to be related to the period development of calcic soil profiles. The limestones from cycle 27 onwards are mud-rich, grayish, soft limestone beds with relatively high content of organic matter and broken shell fragments and complete gastropod remains. To the top these show horizontal cracks. These beds are interpreted as being deposited marginal lacustrine to pond environments. Grey cycle numbers refer to uncertain labeling. Lithostratigraphic characteristics as well as stratigraphic thickness justify the presented numbering.

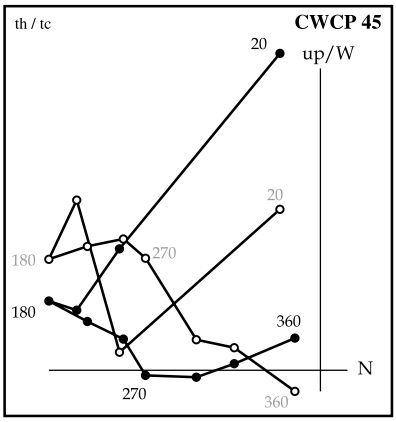

Figure 4.SN4 - An example of a Zijderveld diagram of one of the magnetostratigraphic samples of the Camarena section that are interpreted as carrying reversed original polarity. Declination (inclination) is indicated with closed (open) dots. Temperature steps are indicated in degrees Celsius.

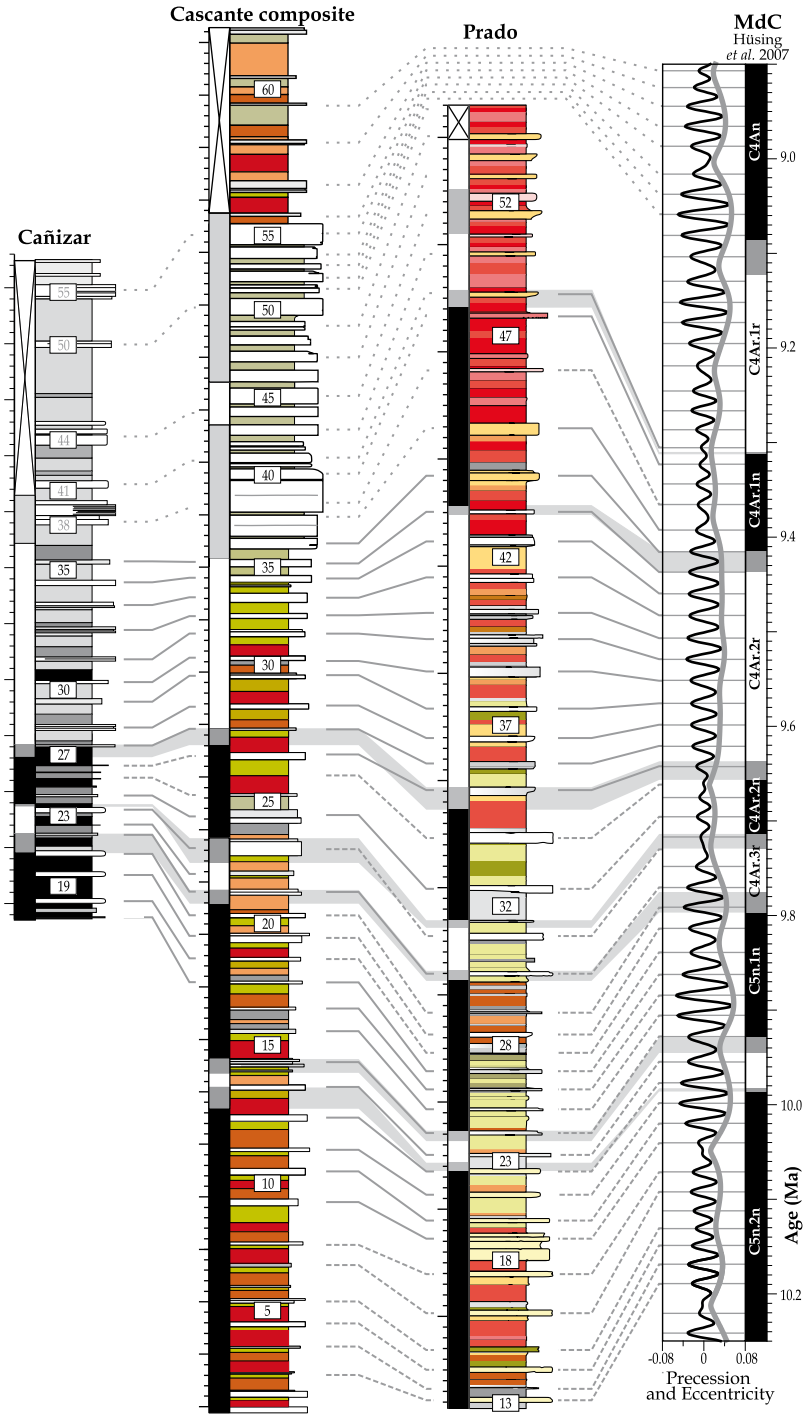

Figure 4.SN5 Correlation panel showing the magneto-astrochronological correlation of the Cañizar, Cascante, and Prado sections. The correlations are explained in the text.

CHAPTER 5

Testing the hypothesis of long-period orbital forcing on formation-scale genetic sequences in the Miocene infill of the Madrid Basin (central Spain)

H.A. Abels, H. Abdul Aziz, W. Krijgsman, S.J.B. Smeets, and F.J. Hilgen

5.1 Abstract

The Valdearenas-Muduex (VDA-MX) section in the north-eastern part of the Madrid Basin covers two genetic sedimentary sequences in the middle Miocene Intermediate unit, which reveal a progressively upward increase in thickness and abundance of carbonate beds topped by a sharp return to red bed sedimentation. The origin of these sequences remains enigmatic. Here, we try to substantiate the long-period orbital forcing hypothesis by accurate magnetostratigraphic dating and statistical analysis of colour records as proxy for lithology.

The magnetostratigraphy is correlated to the ATNTS04 time scale, indicating sedimentation between 15.5 and 11.5 Ma, in line with scarce biostratigraphic constraints. Both limestone intervals in the upper parts of the genetic sequences start during minimum values of the 2.4-Myr eccentricity cycle, identical to the configuration found for a similar Late Miocene transition in the Teruel Basin, suggesting an orbital origin. Spectral analysis of the L* colour time series reveals the presence of 405-kyr eccentricity cyclicity and additional imprint of the 0.97-Myr eccentricity cycle. The response to both the 2.4-Myr and 0.97-Myr cycles was out of phase, while the response to the 405-kyr cycle was in phase. Lithological variation lags all three eccentricity cycles. Cross spectral analysis indicate a lag of 100° for 405-kyr eccentricity. The lags may originate from gradual changes in the system, like in groundwater reservoirs, vegetation, and weathering. A lack of short or long-term obliquity forcing suggests a local instead of global forcing of the paleoenvironment. The genetic sequences should be roughly synchronous within segments of the basin that were connected during deposition, in order to corroborate the long-period eccentricity control. Also, other sequences in the Madrid as well as other Spanish Cenozoic basin have to be dated, among others to check for phase relation consistency. The dating of the VDA-MX section further indicates that tectono-stratigraphic units traditionally recognised among the whole Madrid Basin do not represent time-equivalent stratigraphic intervals and their boundaries are not synchronous, possibly indicating no common development between different segments of the basin.

5.2 Introduction

The mechanisms that control sedimentary infill of continental basins are divided into climatic, tectonic, and geomorphic processes (Leeder and Gawthorpe, 1987; Nichols and Watchorn, 1998). Distinguishing between such processes is rather difficult, because they can theoretically result in similar imprints on the rock record (Caroll and Bohacs, 1999). Sufficient outcrop can allow distinction between processes (Nijman, 1998), but is rarely present. Gaining high-resolution age control is another way to discriminate between forcing processes (Caroll and Bohacs, 1999; Gawthorpe and Leeder, 2000). Time frameworks allow comparison of sedimentary sequences with climatic and tectonic histories, and orbital target curves. In addition, different successions within the same basin can be compared in time to check for iso- or diachrony of major lithological changes (Chapter 4).

One of the mechanisms that is proposed and occasionally indicated as an important player on long, million-year time scales in continental and marine settings are low-frequency modulations of orbital oscillations (Abels *et al.*, 2005; Beaufort, 1994; Lourens and Hilgen, 1997; Olsen and Kent, 1999; Pälike *et al.*, 2006; Shackleton *et al.*, 1999; Wade and Pälike, 2004). Eccentricity of the earth's orbit has long-periodicities of 0.97 Myr and 2.37 Myr, of which the latter periodicity is stable at least over the last 40 Myr (Laskar *et al.*, 2004; Varadi *et al.*, 2003). Obliquity has a long periodicity of 1.2 Myr that modulates its amplitude. In the Triassic Newark Basin, the low frequency modulation of lithological cyclicity was related to long-period eccentricity forcing (Olsen, 1986; Olsen and Kent, 1999). Lack of reliable astronomical target curve before approximately 40 Ma (Laskar *et al.*, 2004; Varadi *et al.*, 2003), prevents corroboration of the Newark results by calibration with calculated eccentricity curves. Increased turnover rates of Neogene small mammal fauna in Spain occur during 0.97 and 2.37-Myr eccentricity minima, possibly due to cooler and more humid conditions that are suggested to simultaneously force lake expansions (Van Dam *et al.*, 2006). Renewed turnover acceleration and possible ending of lake phases are suggested to occur due to cooler and drier conditions during 1.2-Myr obliquity nodes.

The Miocene infill in the endorheic, continental Madrid Basin, is characterised by three large-scale sequential units recognised in different parts of the basin and bounded by sedimentary disconformities; the Lower, Intermediate, and Upper units (Alonso Zarza and Calvo, 2002; Alonso Zarza *et al.*, 1990; Alonso Zarza *et al.*, 1992; Calvo, 1989; Calvo *et al.*, 1989; Cañaveras *et al.*, 1996). The origin of these genetic sedimentary sequences, that are progressively enriched in carbonate towards their top within a dominantly floodplain mudstone succession, remains enigmatic, although mainly a tectonic origin has been suggested (Alonso Zarza *et al.*, 1990; Alonso Zarza *et al.*, 1992; Calvo *et al.*, 1996; Calvo *et al.*, 1989). Poor to low-resolution biostratigraphic age control hampers to unravel the origin of the sequential units, because intra-basinal correlations depend on lithostratigraphic patterns (Montes *et al.*, 2006; Pelaez-Campomanes *et al.*, 2000; Sesé *et al.*, 1990). Also, comparison of sedimentary sequences with tectonic and climatic records, or orbital target curves is not possible without good age control. Recently, the first paleomagnetic data confirmed the Middle to Late Miocene age of the Lower and Intermediate Units in west-central and southern parts of the basin (Montes *et al.*, 2006).

Here, a composite section in the north-eastern part of the basin is studied that covers most of the Intermediate Unit. The site was at a position where clastic alluvial fan and fluvial floodplain from the north and west interacted with carbonate sedimentation resulting from palaeosol formation during low clastic input and lacustrine environments spreading over the area from the east. This resulted in a clear representation of two conformable sequential units within the Intermediate

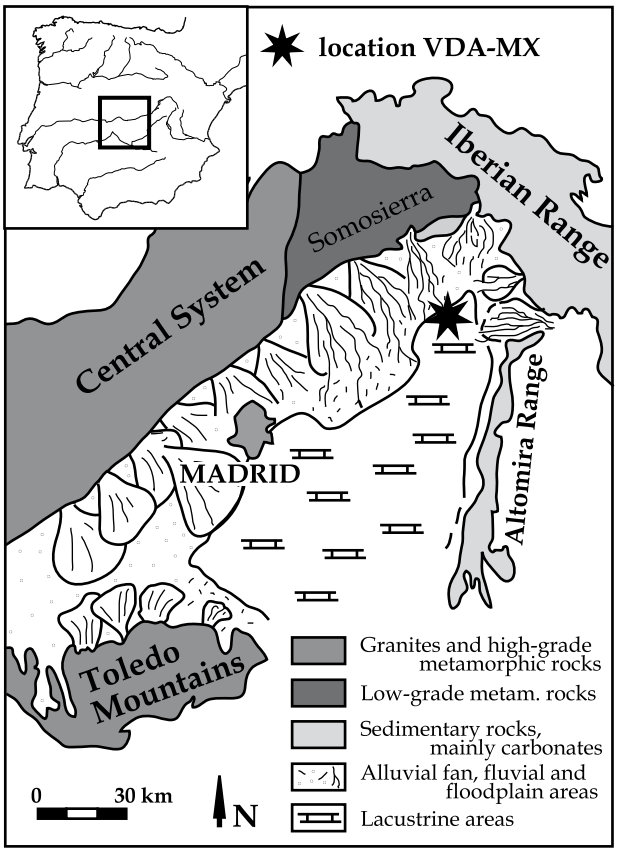

Figure 5.1 Geological and paleoenvironmental map of the Madrid Basin during the deposition of the Intermediate unit, modified after Alonso-Zarza *et al.* (1992). The location of the VDA and MX sections are indicated.

unit. A detailed magnetostratigraphy is established to gain accurate age control. High-resolution colour reflectance time series are statistically analysed to detect sedimentary cyclicity that could be related to orbital climate variations using the age model. In addition, the sequential units are compared with long-period orbital target curves to discover a possible relation and with ages for similar transitions in other parts of the basin to analyse the basin-wide significance of the genetic sequences.

5.2.1 Geological Setting

The Madrid Basin forms the major part of the Tajo Basin in central Spain. The over 10.000 km^2 large basin is locked between the Central System in the northwest, the Iberian Range in the northeast, the Altomira Range in the east, and the Toledo Mountains in the south (Fig. 5.1; Calvo, 1989). Granites and high-grade metamorphic rocks dominate the Toledo Mountains in the south and the Central System in the north and west. Low-grade metamorphic rocks and sedimentary rocks formed lower relief in the easternmost part of the Central System, more specifically the Somosierra area (Fig. 5.1), and the Iberian Range. Sedimentary rocks, mainly Jurassic and Cretaceous carbonates, were exposed in the eastern part of the basin, the Iberian

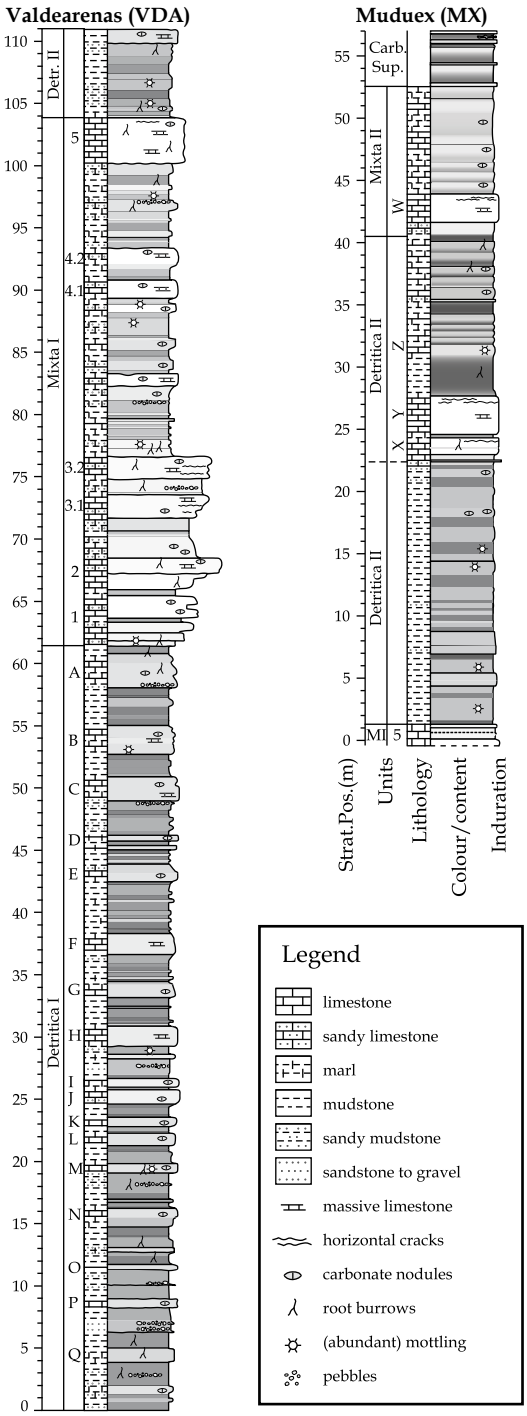

Figure 5.2 Lithological columns of the Valdearenas and Muduex sections. Indicated are the labelling of sequence intervals and arbitrary labelling of typical carbonate beds.

and the Altomira Range (Alonso Zarza *et al.*, 1992). The basin originates from compressional Alpine movements. The main tectonic phase started compressional and ended shortly extensional in ENE-WSW direction, due to the Altomira Range activity, and is of Late Oligocene to Late Miocene age (Alvaro, 1975; De Vicente, 1988). In the basin, Miocene sediments unconformably overlie Paleogene and older rocks (Alonso Zarza *et al.*, 1990). The total thickness of Miocene sediments varies between 300 to 800 m from the margin to the centre of the basin.

In the north-eastern part of the Madrid basin, biostratigraphic age constraints indicate Miocene deposition from Ramblian to Turolian times (*ca* 19 Ma to *ca* 5 Ma; Alonso Zarza *et al.*, 1990; Sesé *et al.*, 1990). In this area, especially the Intermediate Unit is well represented in outcrop. In the distal parts of the area, the Intermediate unit is divided into two sedimentary sequences with a conformable contact (Alonso Zarza *et al.*, 1990; Alonso Zarza *et al.*, 1992; Calvo, 1989). Each sequence starts with fine siliciclastic sediments that are interpreted as floodplain deposits of terminal fluvial systems (Alonso Zarza *et al.*, 1990; Sanz *et al.*, 1995). Intercalated pedogenic calcretes and palustrine limestones reflect calcic palaeosol and carbonate pond environments developed during times of low clastic supply and lateral to active fluvial systems (Alonso Zarza *et al.*, 1990; Sanz *et al.*, 1995). These calcareous intercalations progressively increase in number and thickness towards the top of the each sequence. In the upper parts of the sequences, marginal lacustrine environments occasionally reached the area (Alonso Zarza *et al.*, 1990; Calvo, 1989; Sanz *et al.*, 1995). The top of the first sequence is characterised by a relatively sharp transition to the clastic sediments at the base of the second sequence, related to rapid increase in clastic supply (Sanz *et al.*, 1995). In the top of the second sequence widespread freshwater conditions occur, which have been related to a coincident tectonic quiescence (Calvo *et al.*, 1989). The transition to the Upper unit is characterised by a paleokarst surface that represents a hiatus (Alonso Zarza, 1992; Cañaveras *et al.*, 1996).

5.3 Sections and Lithology

The Valdearenas-Muduex composite section (VDA-MX) is composed of the Valdearenas section (VDA) that covers the lower sequence (also referred to as Lower Stage and Intermediate Sequence I) of the Intermediate unit and the Muduex section that covers the lower and middle part of the upper sequence (or Upper Stage and Intermediate Sequence II). Both sections are located *ca* 2.2 km apart along the western flank of the Badiel river valley, close to the two villages after which the sections have been named. The sections have been part of earlier studies (Alonso Zarza, 1990; Alonso Zarza *et al.*, 1990; Sanz *et al.*, 1995).

5.3.1 Valdearenas section

The base of the Intermediate Unit is not present in the Valdearenas section or outcrop area. The basal 61 m of the Valdearenas section are dominantly siliciclastic sediments with limestone intercalations on meter scale (Fig. 5.2; Fig. 5.3). This interval is also referred to as the Detritica I (Fig. 5.2; Alonso Zarza *et al.*, 1990). Red and red-brown sandy mudstones display light-grey mottling and mm-size to cm-size carbonate nodules. The dominant clay mineral is illite, with minor amounts of smectite and levels of chlorite and kaolinite (Alonso Zarza *et al.*, 1990). Darker clay-rich and lighter sand-rich intervals occur. Few sandstone and gravel beds are present as sheet-like tabular beds, especially in the lower part of this interval, and a few with a shallow channel-like

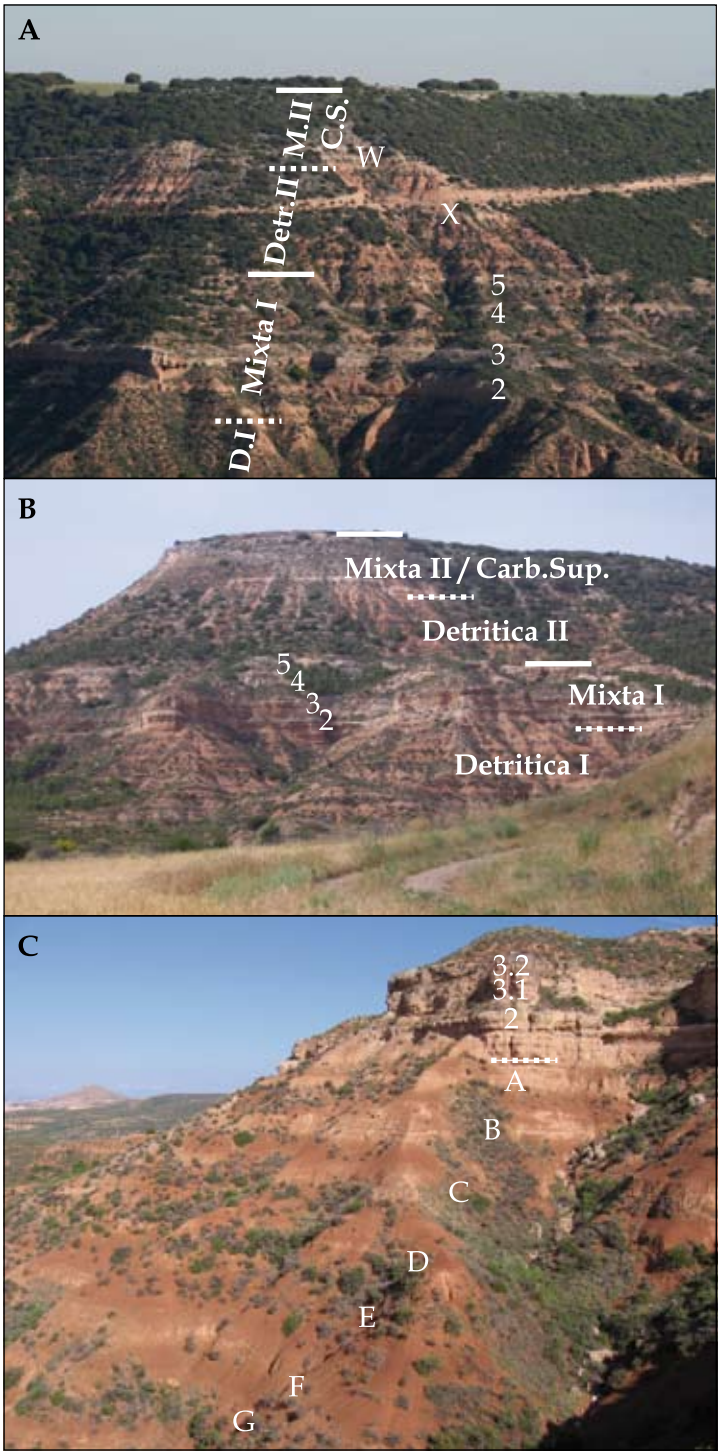
A
C.S.
M.II
Detr.II
Mixta I
D.I
W
X
5
4
3
2
B
Mixta II / Carb.Sup.
Detritica II
Mixta I
Detritica I
5
4
3
2
C
3.2
3.1
2
A
B
C
D
E
F
G

← *Figure 5.3* (A-C) Photographs of the Muduex (A) and Valdearenas sections (B and C). Indicated are the stratigraphic intervals Detritica I and Mixta I belonging to the lower sequence, and Detritica II, Mixta II, and Carbonatica Superior belonging to the upper sequence in the Intermediate Unit. Also, arbitrary labels of particular limestone beds are indicated, see Figure 5.2 for corresponding lithologies.

geometry. Paleocurrent directions point to a S to SW transport direction (Alonso Zarza *et al.*, 1990). These siliciclastic sediments have been interpreted as floodplain deposits of terminal fluvial systems (Alonso Zarza *et al.*, 1990; Sanz *et al.*, 1995). Sandstones relate to occasional enhanced fluvial activity and carbonate nodules are interpreted as pedogenic caliche nodules. Nodular and few prismatic, mottled, light-red calcareous beds intercalate on a meter scale in the dominantly siliciclastic Detritica I. In the top half of this lower siliciclastic part, these intercalations occur more regularly approximately every 3 to 5 m (limestone beds H to A; Fig. 5.3C; Fig. 5.2). Intercalating calcareous levels have been interpreted to be related to carbonate precipitation in calcic palaeosols, that developed during times of low clastic input and further away from fluvial systems (Alonso Zarza *et al.*, 1990; Sanz *et al.*, 1995).

The siliciclastic interval is followed by a 43 m thick interval that is characterised by thick carbonate beds with intercalations of marls and red mudstones (Fig. 5.2). This interval is the top part of the lower sequence and referred to as the Mixta I (Fig. 5.2; Alonso Zarza *et al.*, 1990). Limestone beds are up to 4 m in thickness, and have a progressive nodular to prismatic and massive, mottled character. Few carbonate levels occur as tabular beds, with a rather sharp, undulating base. These occur in the lower part of Mixta I. The upper part of Mixta I is more characterised by smooth, often softer, well mottled limestones. The red to light-red mudstones that occur in between calcareous levels are rich in cm-scale carbonate nodules, display intense light-grey, and yellow mottling. The carbonates as well as the mudstone may be rich in sand to gravel-sized material. This sequence has been interpreted as increased palaeosol development during times of low clastic input (Sanz *et al.*, 1995). Coarse clastic levels indicate occasional fluvial activity. High carbonate content of the intercalating mudstones are interpreted as indication of continuous palaeosol activity. The smooth, mottled limestones have been interpreted as typical palustrine limestones that relate to carbonate deposition in a pond environment with subsequent sub-aerial exposure (Alonso Zarza *et al.*, 1990; Sanz *et al.*, 1995). In the Valdearenas section, from the base of the top of the Detritica I, increased carbonate precipitation and decreased clastic input thus occur, with the topmost carbonates related to occasional pond development.

5.3.2 Muduex section

Poor outcrops above the first sedimentary sequence in the Valdearenas section necessitate a 2.2 km lateral shift to the Muduex section towards the north-east (Fig. 5.1). The correlation can not be done physically over the whole transect, and partly depends on limestone bed characteristics as induration and stratigraphic pattern (Fig. 5.3). The Muduex section covers 38 m red siliciclastic sediments that are part of the lower, siliciclastic interval of the second sedimentary sequence and referred to as the Detritica II (Alonso Zarza *et al.*, 1990). This is followed by 12 m limestones, marls, and mudstones that are part of the upper, carbonatic interval at the top of the second, large-scale sequence and referred to as the Mixta II (Alonso Zarza *et al.*, 1990). The position of the base of the Mixta II is arguable, because a calcareous interval 'W' is present further down, at meter 125, after which a thin clastic interval is present before carbonates dominate (Fig. 5.3A; Fig. 5.2). The top of the section is at the base of full lacustrine limestone beds that are part of a thin, third

sequence in the Intermediate unit and referred to as the Carbonática Superior (Alonso Zarza *et al.*, 1990; Alonso Zarza, 1992).

The siliciclastic lower part of the Muduex section is sedimentologically fairly similar to the lower part of the Valdearenas section. The interval is dominated by red to red-brown and brown mudstones. Most mudstones display light-grey and yellow mottling and dispersed carbonate nodules. Locally, levels rich in carbonate nodules occur and few smooth, mottled carbonate levels intercalate. With respect to the Detritica I, the Detritica II is less coarse, and more often displays darker, clay-rich mudstones as well as more carbonate beds. Calcareous levels that intercalate in the Detritica II and that are part of the Mixta II are most smooth, massive limestone beds with a progressively increasing carbonate content at the base and top. The limestones are well mottled and display rhizotubules and desiccation cracks (Alonso Zarza *et al.*, 1990). This sequence is similarly interpreted as distal floodplain environments with occasional palaeosol and pond development (Alonso Zarza *et al.*, 1990; Sanz *et al.*, 1995). The higher clay and carbonate content with respect to the Detritica I indicates more water available in the system for palaeosol or pond development. The Mixta II is characterised by a dominance of carbonate levels with occasional intercalation of brown clayey mudstones. Locally, these alternations are on meter scale, much thinner than in the section below. Limestones are typical palustrine, with heavy mottling and interpreted as pond deposits (Alonso Zarza *et al.*, 1990; Sanz *et al.*, 1995).

The uppermost part of the Muduex section is composed of a meter-scale alternation of clayey mudstones and limestone beds, which is part of the so-called Carbonatica Superior (Alonso Zarza *et al.*, 1990; Alonso Zarza, 1992). The mudstones are red and green, with smectite as dominant clay mineral and minor amounts of illite (Alonso Zarza *et al.*, 1990). The limestone beds are very tabular and consist of micritic carbonate beds, in which gastropods and ostracods have been found (Alonso Zarza *et al.*, 1990). These characteristics are prevalent for 20 m above the Muduex section showing a progressively increase in number and thickness of the carbonate beds. In this sequence, silicified concretions are present starting in the very top of the studied part of the section. This sequence is being recognised over large parts of the basin, at least in the north-eastern segment, and interpreted as widespread development of more stable and deeper lacustrine conditions (Alonso Zarza *et al.*, 1990; Calvo *et al.*, 1989).

5.4 Magnetostratigraphy

5.4.1 Methods

The VDA-MX section was sampled at average stratigraphic intervals of 23 cm. Samples were drilled using an electric, water-cooled drill powered by a portable generator. The characteristic remanent magnetization (ChRM) was determined by thermal demagnetization, using incremental heating steps of *ca* 50° below and 30° above 240°C, carried out in a laboratory-built shielded furnace. First, every other sample was selected for paleomagnetic analysis. Later, in intervals across chron boundaries sample resolution was increased. Finally, the natural remanent magnetization (NRM) of 433 samples (on a total of 669) was measured on a horizontal 2G Enterprises DC SQUID cryogenic magnetometer (noise level 3 x 10^{-12} A/m) at the Paleomagnetic Laboratory "Fort Hoofddijk", Utrecht University, the Netherlands. Demagnetization results are plotted on orthogonal vector diagrams (Zijderveld, 1967) and ChRM directions are calculated using principal component analysis (Kirschvink, 1980).

5.4.2 Results

Most samples display good quality results for the thermal demagnetization. Initial NRM intensities vary, depending on lithology, with high intensities (3 to 20 mA/m) in red mudstones and low intensities (0.1 to 4 mA/m) in calcareous beds. The Zijderveld diagrams display a separation of the thermal decay curves into three components (Fig. 5.4). The first component is a randomly oriented component that is removed below 120°C. This represents a present-day induced magnetization. The second component is present in 99.4% of the samples and is removed between 200°C and 270°C (Fig. 5.4). This component has in all cases a normal polarity and is interpreted to represent a viscous overprint by the present-day Earth's magnetic field. The third component displays dual

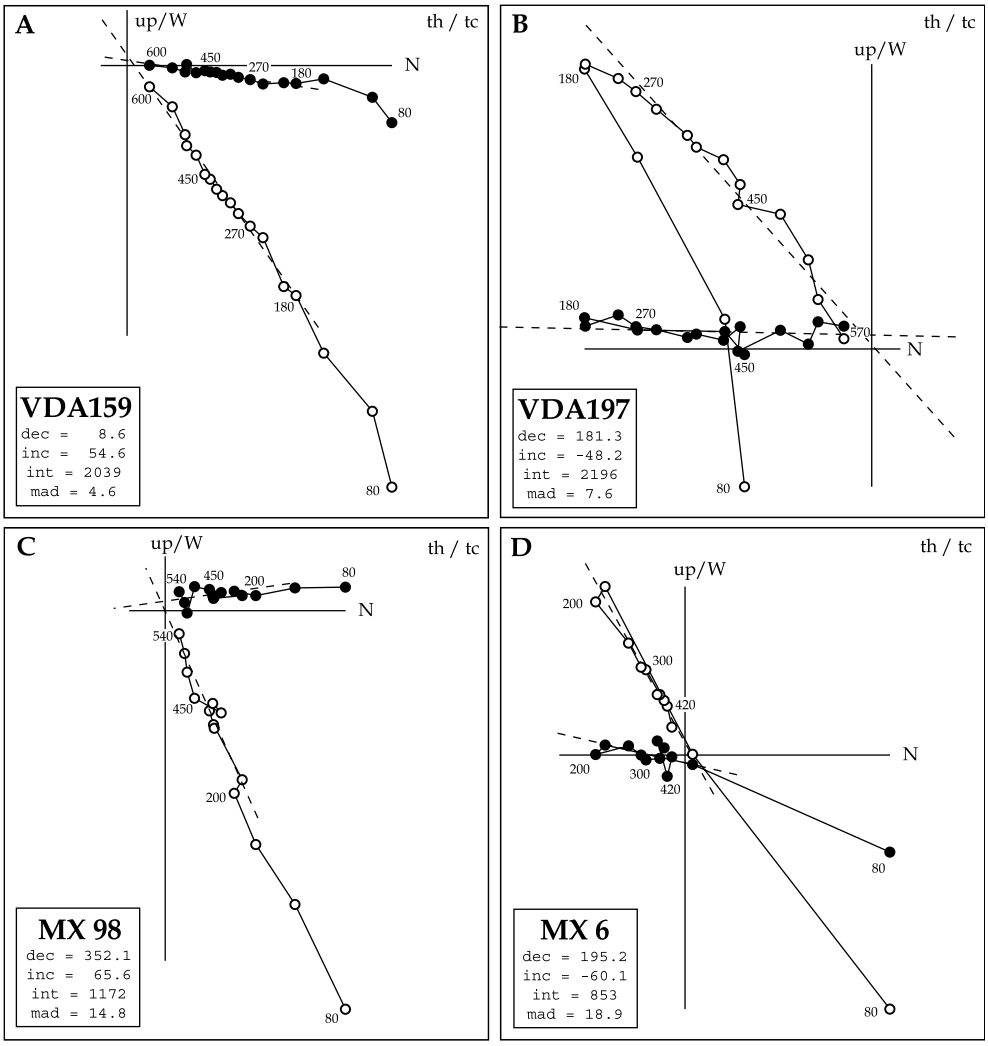

Figure 5.4 A-D Zijderveld thermal demagnetization diagrams of two paleomagnetic samples of the Valdearenas (A and B) and two of the Muduex section (C and D). Interpreted declination and inclination lines and values of the ChRM, and thermal steps are shown.

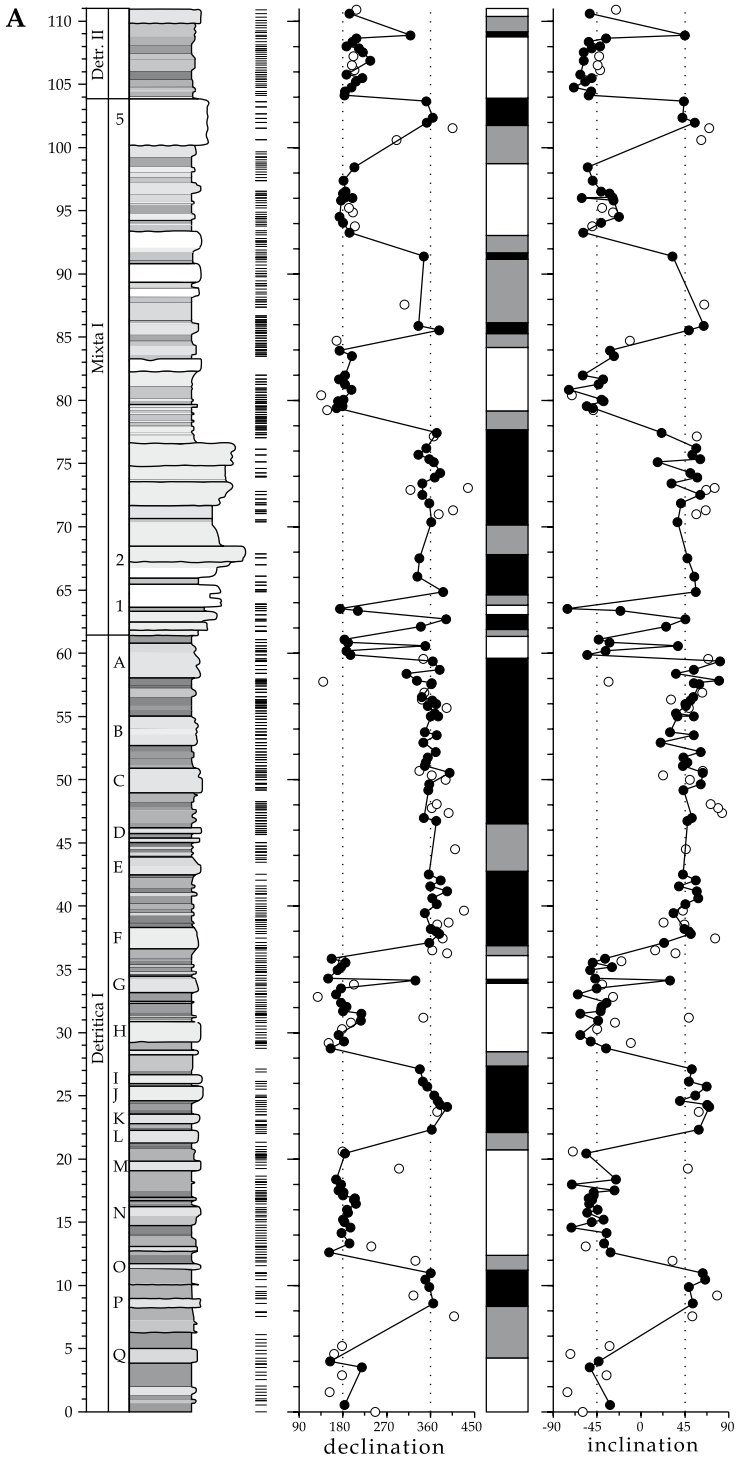
A
Detr. II
Mixta I
Detritica I
5
2
1
A
B
C
D
E
F
G
H
I
J
K
L
M
N
O
P
Q
110
105
100
95
90
85
80
75
70
65
60
55
50
45
40
35
30
25
20
15
10
5
0
90
180
270
360
450
declination
-90
-45
0
45
90
inclination

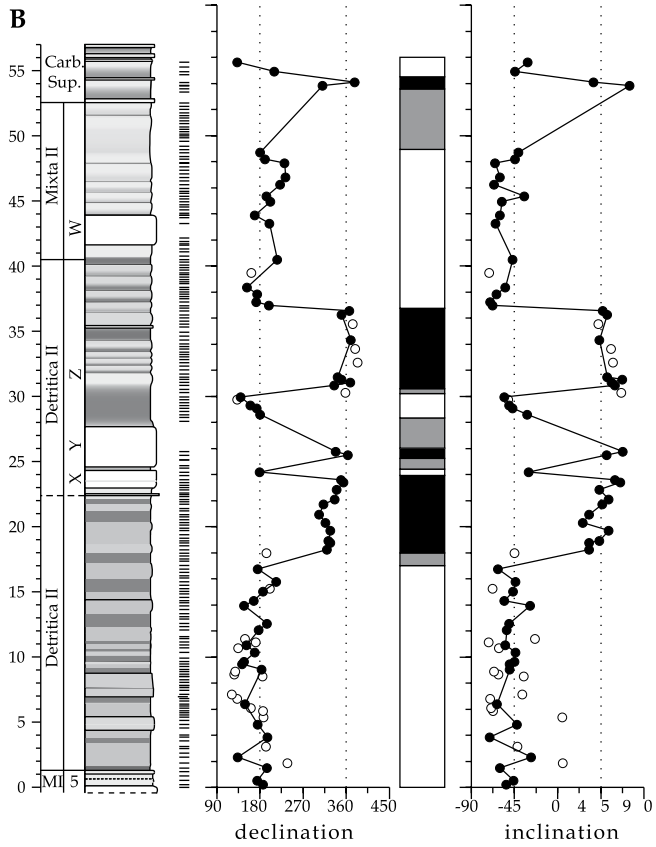

Figure 5.5 Lithological logs, position of paleomagnetic samples, declination and inclination results of good quality (closed) and poor quality (open) interpreted ChRM, and interpreted magnetostratigraphies for the (A) VDA and (B) MX sections.

polarities and is interpreted to represent the characteristic remanent magnetization (ChRM) of the sediment at times of deposition. The ChRM of 60% of the samples shows a stable linear decay curve from 240˚ to 420˚C with varying intensities and clear normal or reversed polarity (Fig. 5.4). These samples have been used for the construction of the magnetostratigraphy and are represented by solid dots in Figure 5.5.

From the samples displaying a linear decay between 240˚C and 420˚C, approximately 18% have unblocking temperatures between 390˚C and 480˚C, suggesting iron sulfides as the main carrier of the ChRM (Fig. 5.4). These samples mostly occur in the calcareous levels, mainly in the Mixta I and II intervals. The ChRM of 43% of the samples is removed between 500˚C and 600˚C, which is the typical unblocking temperature range for magnetite (Fig. 5.4). Samples with these unblocking temperatures are present in all types of sediments, and most samples used for the magnetostratigraphy at least display a magnetite component. The remaining 38% of the samples is fully demagnetized at temperatures from 600˚C up to 700˚C, indicating unblocking temperatures for (fine-grained) hematite (Fig. 5.4). Samples with these unblocking temperatures are mostly

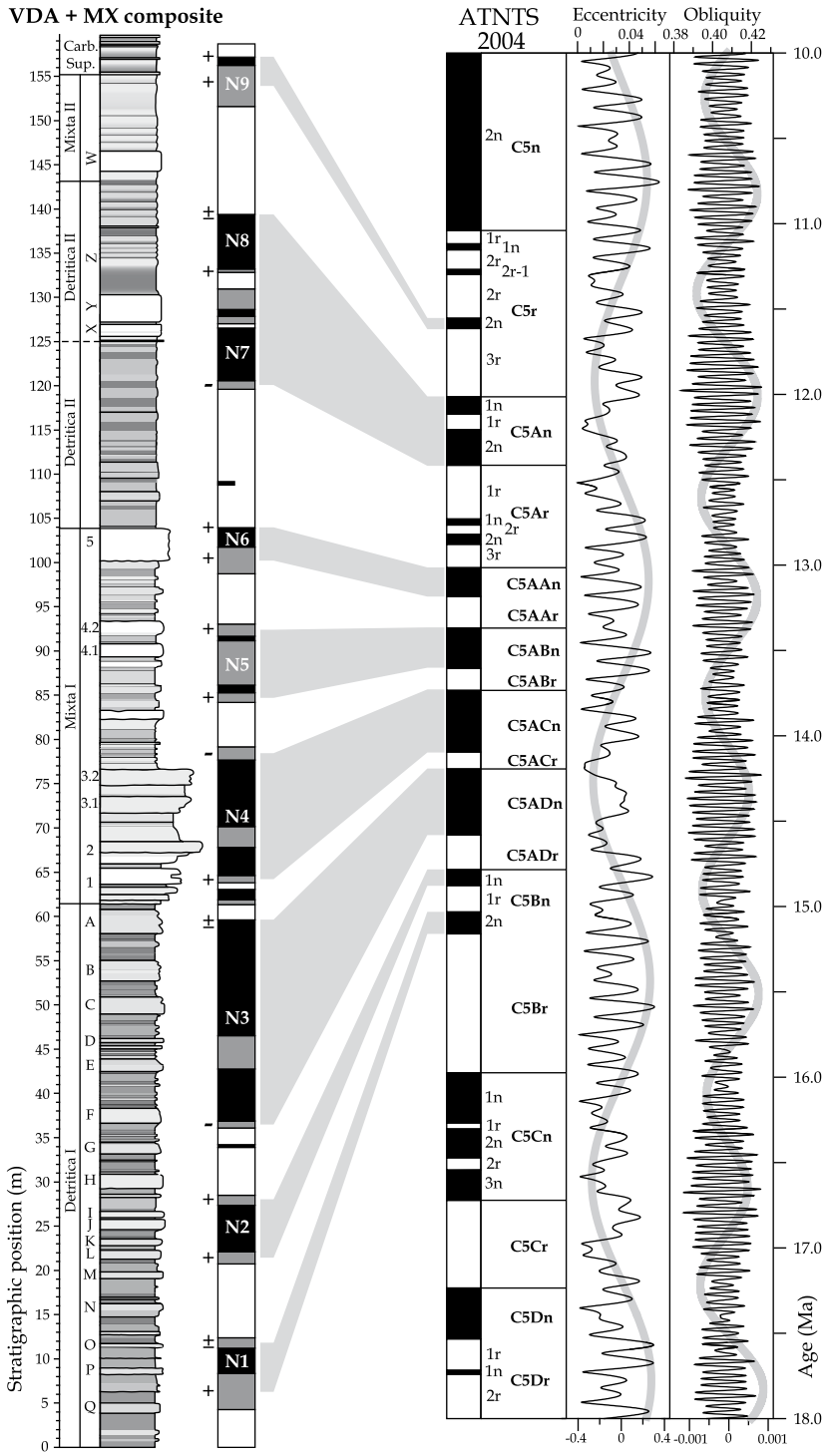
VDA + MX composite
Stratigraphic position (m)
Carb. Sup.
Mixta II
Detritica II
Mixta I
Detritica I
W
Z
Y
X
N9
N8
N7
N6
N5
N4
N3
N2
N1
ATNTS 2004
C5n
C5r
C5An
C5Ar
C5AAn
C5AAr
C5ABn
C5ABr
C5ACn
C5ACr
C5ADn
C5ADr
C5Bn
C5Br
C5Cn
C5Cr
C5Dn
C5Dr
Eccentricity
Obliquity
Age (Ma)

← *Figure 5.6* The lithological log of the composite VDA-MX section with labelling of sequence intervals and limestone beds (see caption Fig. 5.2), the composite magnetostratigraphy of the section, and the proposed correlation to the ATNTS04 of Lourens *et al.* (2004). To the right the eccentricity and obliquity target curves of the La2004 (1,1) solution of Laskar *et al.* (2004) are shown and their low frequency filters of respectively 2.4-Myr and 1.2-Myr. Both the Mixta I and the Mixta II unit start just after a minimum in the 2.4-Myr eccentricity cycle. Left of the magnetostratigraphy tie-points used for the three age models are indicated. For age model 1, with least tie-points, only reversals marked by "-" are used, age model 2, with intermediate amount of tie-points, uses "-" and "±", and age model 3, with most tie-points, uses all marked reversals, i.e. "-", "±", and "+".

from the red mudstones in the Detritica I and II. The ChRM directions were calculated using temperature steps in the range 270 to at least 420°C. A higher upper temperature was used for calculation of the ChRM direction if a linear decay curve is present and no increase in intensity was observed during demagnetization.

5.4.3 Correlation to the ATNTS04

Declination and inclination data are plotted in stratigraphic order in Figures 5.5A and 5.5B. The magnetostratigraphy of the composite section is shown in Figure 5.5A. The resolved magnetostratigraphy reveals 9 substantial normal polarity intervals, labelled N1 to N9, and 3 thin normal intervals below N3, N4, and above N7. A correlation is proposed to the Astronomical Tuned Neogene Time Scale ATNTS04 (Fig. 5.6; Lourens *et al.*, 2004) using the biostratigraphical age constraints as starting point (Alonso Zarza *et al.* 1990; Sésé *et al.* 1990). Typical in the VDA-MX magnetostratigraphy are the dominance of reversed polarity in the lower half of Detritica I, and in the complete upper part of the section starting possibly in the middle of the Mixta I but at least starting at the base of Detritica II. The top of Detritica I and the base of Mixta I are characterised by long normal polarity intervals N3 and N4. The most plausible correlation of these two long normal intervals, N3 and N4, is to the chrons C5ADn and C5ACn in the time scale. Then, the shorter N1 and N2 normal intervals fit with C5Bn.1n and C5Bn.2n in the further reversed interval. The N7 and N8 normal intervals, in the long reversed interval above N6, best fit with the C5An.2n and C5An.1n. Then, the less well resolved N5 and N6 can be correlated to C5ABn and C5AAn. The poor recording of the N5 and N6 intervals is due to the high carbonate content and therefore weak NRM intensity in this part of the VDA section. Of the two short normal polarity chrons C5Ar.1n and 2n, only one is possibly recorded by a single sample indicating normal polarity. The N9 interval is likely correlated with the C5r.2n, but a younger correlation cannot be excluded. In summary, the magnetostratigraphic pattern in the VDA-MX matches the Middle to Late Miocene polarity pattern in the geomagnetic polarity time scale rather well, resulting in one probable correlation.

The biostratigraphic age constraints available from mammal sites in the north-eastern portion of the basin are in line with the suggested correlation. The Ledanca site is closest and located in the upper part of the Intermediate unit most probably just below the paleokarstic surface at the top of the second sequence. The sites yields mammals related to local mammal zone H that has an age between *ca* 11.1 Ma to 10.4 Ma (Daams *et al.*, 1999; Sesé *et al.*, 1990), which perfectly fits the proposed correlation. *Dicerorhinus sausaniensis* is present in the Detritica II in the Tajuña area to the east and indicates Upper Aragonian age between *ca* 13.5 to 11 Ma, also fitting the magnetostratigraphic calibration (Alonso Zarza *et al.*, 1990; Daams *et al.*, 1999).

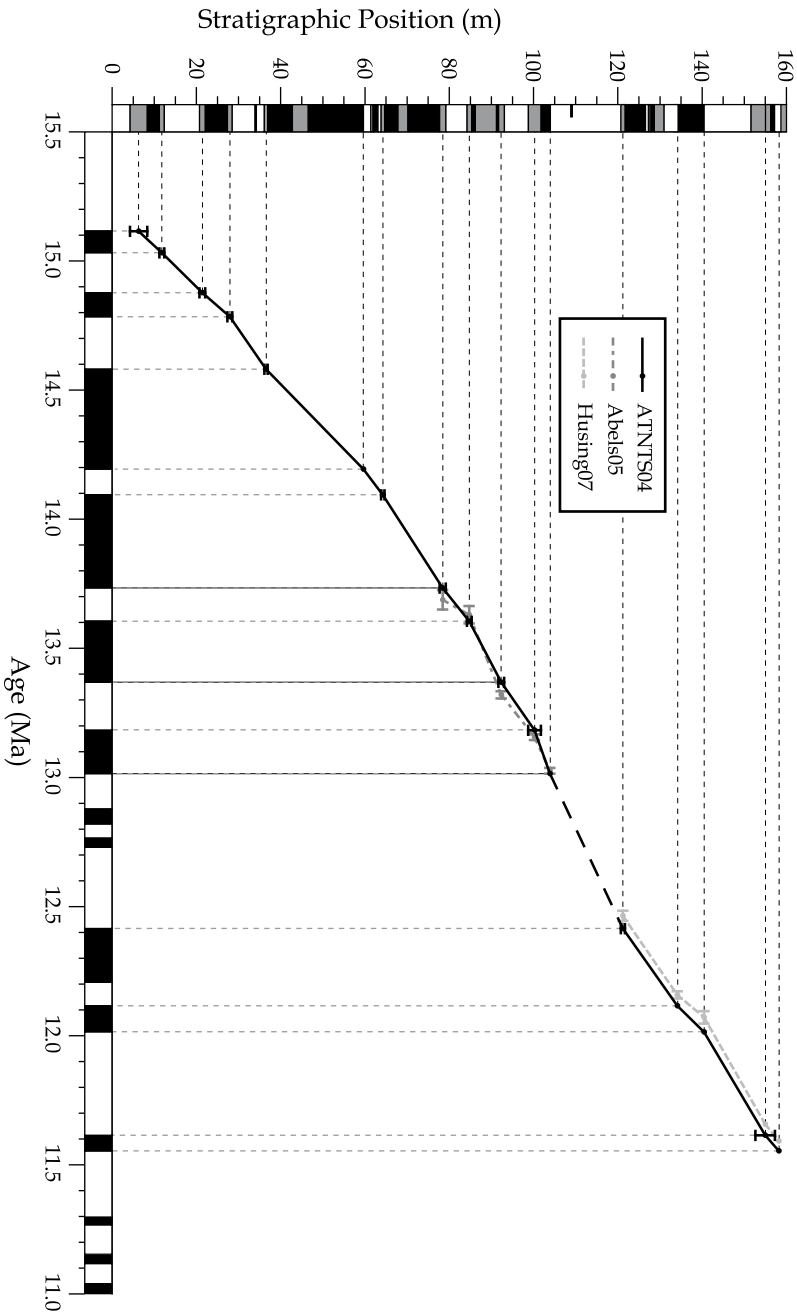

Figure 5.7 Sedimentation rate plot for the VDA-MX section using the correlation of the magnetostratigraphy to the ATNTS04 time scale of Lourens *et al.* (2004). Alternative, newer astronomically calibrated ages of Abels *et al.* (2005) and Hüsing *et al.* (2007) are shown, but do not make much difference. Three intervals can be recognised with different sedimentation rates; the Detritica 1, the Mixta 1, and both the Detritica 2 and Mixta 2. The correlation between the VDA and MX section is shown with a dotted line.

5.4.4 Sedimentation rates

The proposed correlation of the magnetostratigraphy results in an age model for the VDA-MX section that is shown in Figure 5.7. The age-depth plot shows linear accumulation rates within three transects. The first transect covers the clastic Detritica I with aggradation rates of *ca* 6.3 cm/kyr. Sedimentation rate lowers to *ca* 3.6 cm/kyr in the second transect that covers the calcareous Mixta I from 14 to around 13 Ma. The connection between the Muduex and the Valdearenas sections, that are separated 2 km, is indicated by a dashed line. The last transect covers the major part of the clastic Detritica II and the relatively thin calcareous Mixta II with a sedimentation rate of 4.3 cm/kyr. The plots thus shows fairly linear sedimentation rates in distinct sedimentary intervals. The lower sediment rate in the calcareous intervals is expected with respect to the clastic intervals (Alonso Zarza *et al.*, 1990). Also, it could be expected that the sedimentation rate in the Detritica I is higher than in the Detritica II, because of the higher carbonate content in the latter and the less coarse clastic fraction. The low sedimentation rates at the transition from the VDA to the MX section are remarkable however, and require further investigation. The general sedimentation rate can have been lower at the MX section or the correlation between the to sections might contain an error. Downward extension of the MX section is the only way to check the correlation as neither an upward extension of VDA or direct physical correlations are possible. Most likely, the correlation of the magnetostratigraphy to ATNTS04 is correct, in view of the fairly linear sedimentation rates for distinct sedimentary intervals as well as the good agreement with the, albeit scarce, biostratigraphic constraints.

5.4.5 Tectono-sedimentary units (TSU)

The Lower to Intermediate Unit boundary is now estimated to be older than 15.2 Ma. This is the approximate age of the lowermost sample in the VDA section that is clearly above the boundary. Approximately, 20 meters of stratigraphy are expected below the VDA section until the boundary is reached, following thickness estimates of the Detritica I (Alonso Zarza, 1990; Alonso Zarza *et al.*, 1990). This would results in an age of 15.6 Ma for this boundary using extrapolation of the sedimentation rate (Fig. 5.8). The Intermediate I to Intermediate II transition, that is at the Mixta I to Detritica II boundary, is now dated at 13.0 Ma at the top of chron C5AAn. Above the MX section, an additional 20 m is measured until the top of the outcrop, that is regarded as the boundary between the Intermediate and Upper units. Extrapolation of the sedimentation rate for the upper part of the section indicates an age of *ca* 11 Ma for the youngest sediments of the Intermediate Unit that are present below the hiatus between the Intermediate and the Upper units (Fig. 5.8).

5.5 Cyclostratigraphy

5.5.1 Methods

The sedimentary cyclicity is studied using a high resolution colour reflectance record as proxy for, mainly, carbonate content of the succession. The colour reflectance record was obtained by taking measurements at a stratigraphic distance of 5 cm. The measurements were taken using a portable photospectrometer (Minolta CM 508i) and are based on using the automatically calculated average of three measurements that are again automatically converted into the reflectance values L*a*b*. Colour measurements were taken in a straight line oblique to the bedding plane after removing the weathered material. A straight line is used to avoid preferential measurements of

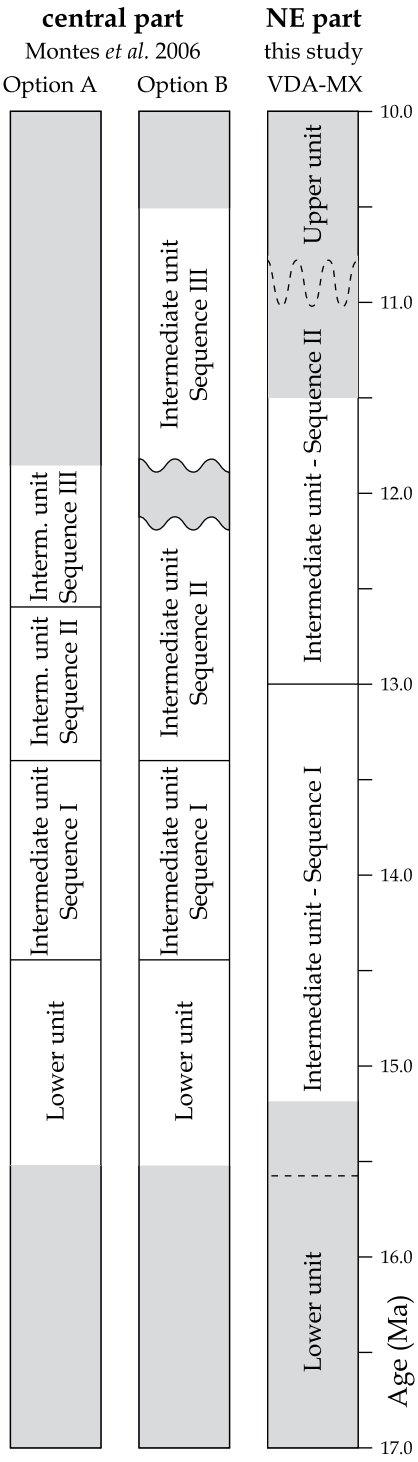
central part
Montes et al. 2006
Option A
Option B
NE part
this study
VDA-MX
Lower unit
Intermediate unit Sequence I
Interm. unit Sequence II
Interm. unit Sequence III
Lower unit
Intermediate unit Sequence I
Intermediate unit Sequence II
Intermediate unit Sequence III
Lower unit
Intermediate unit - Sequence I
Intermediate unit - Sequence II
Upper unit
10.0
11.0
12.0
13.0
14.0
15.0
16.0
17.0
Age (Ma)

← *Figure 5.8* The magnetostratigraphic dating of the genetic sequences in the central and north-eastern parts of the Madrid Basin by Montes *et al.* (2006) and this study, respectively. Gray shades indicate that no sediment is present in the particular studied interval, but dating of boundaries are being extrapolated. Labelling of the stratigraphic intervals according Montes *et al.* (2006).

specific colours with respect to others, as in many parts of the succession the sediments are heavily mottled. L* reflects the whiteness of the sediment and is therefore regarded to approximate the carbonate content. The a* record reflects the redness of the sediment and thought to approximate the inverse carbonate content.

By application of the magnetostratigraphic age model the colour reflectance time series were constructed using the Age Scale option in the Analyseries program (Paillard *et al.*, 1996). Blackman-Tuckey spectral analysis has been applied using the Analyseries 1.1 program (Paillard *et al.*, 1996) with compromise settings. Significant frequency components in the BT spectrum were extracted from the time series using bandpass filters with Bandpass width ranging from the bases of the peak. The CLEAN algorithm was applied using the Pal-Clean program of Heslop and Dekkers (2002) using the red noise simulation type and standard settings. Reconstructed data series are automatically calculated by the Pal-Clean program above the indicated confidence level. Blackman-Tuckey Cross-Spectral analysis was performed with the Analyseries program as well, using 90% confidence limit and compromise settings.

5.5.2 Colour records

The L* and a* records mimic the lithological variations in the VDA-MX succession (Fig. 5.9). Especially, the L* record shows higher values in the major carbonate levels throughout the section. A few prominent patterns in the lithological log are not so well resolved in the colour records like beds 3.1 and X, while more pronounced colour cycles are present in the colour record in parts of the Detritica II and Mixta II than are suggested in the log of those intervals (Fig. 5.9). The a* does indeed reflect the major calcareous beds in the section in an opposite way. These levels are clearly visible in the lower sequence. In the upper sequence, however, the a* record does not display much variability, even the major carbonate-rich beds X, Y, Z, and W can not be easily recognised. Possibly, these limestones display so much red mottling that redness is not a reliable proxy for lithologic variability in this interval. In addition, mudstones display a higher carbonate content in the second sequence, which reduces redness considerably. The statistical analysis therefore focuses on the L* record, as this appears to be a better proxy for lithology in the VDA-MX section. Variable sedimentation rates for different sediment types have been indicated by the magnetostratigraphy (Fig. 5.7). Therefore, the colour records are placed in time domain before proceeding with the spectral analysis.

5.5.3 Time domain

Three age models were constructed using the magnetostratigraphic correlation to the time scale. They have a low (Age model 1), intermediate (Age model 2), and high (Age model 3) amount of age tie-points. The tie-points are shown in Figure 5.6 (see figure caption for explanation). The Age model 1, with only three age tie-points, is thus rather close to the original depth series as was substantiated by spectral analysis in the depth domain, which is not shown here.

The Blackman-Tuckey and CLEAN power spectra of the resulting colour time series are shown in Figure 5.10. The time series based on three different age models reveal rather different spectra, indicating that the number of tie-points for age model construction has considerable impact on

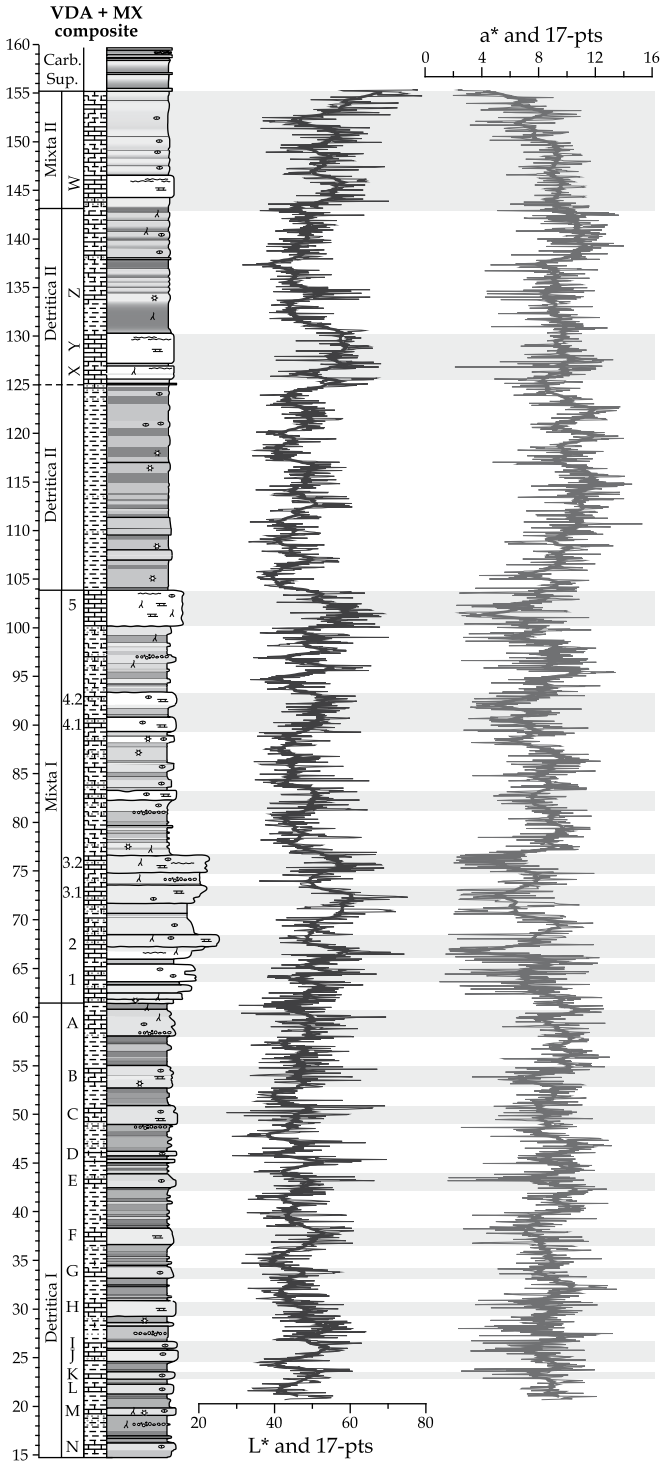
VDA + MX composite
Carb. Sup.
Mixta II
Detritica II
Detritica II
Mixta I
Detritica I
W
Z
Y
X
5
4.2
4.1
3.2
3.1
2
1
A
B
C
D
E
F
G
H
J
K
L
M
N
a* and 17-pts
0
4
8
12
16
L* and 17-pts
20
40
60
80
160
155
150
145
140
135
130
125
120
115
110
105
100
95
90
85
80
75
70
65
60
55
50
45
40
35
30
25
20
15

← *Figure 5.9* Lithological log of the VDA-MX composite sections (see Fig. 5.2) and the L* and a* colour reflectance records and their 17-points moving average in depth domain. Horizontal grey bars indicate limestone beds in the log. Small differences exist between the log and the colour records as the data was obtained during different field campaigns and stratigraphic measurements apparently contain small errors.

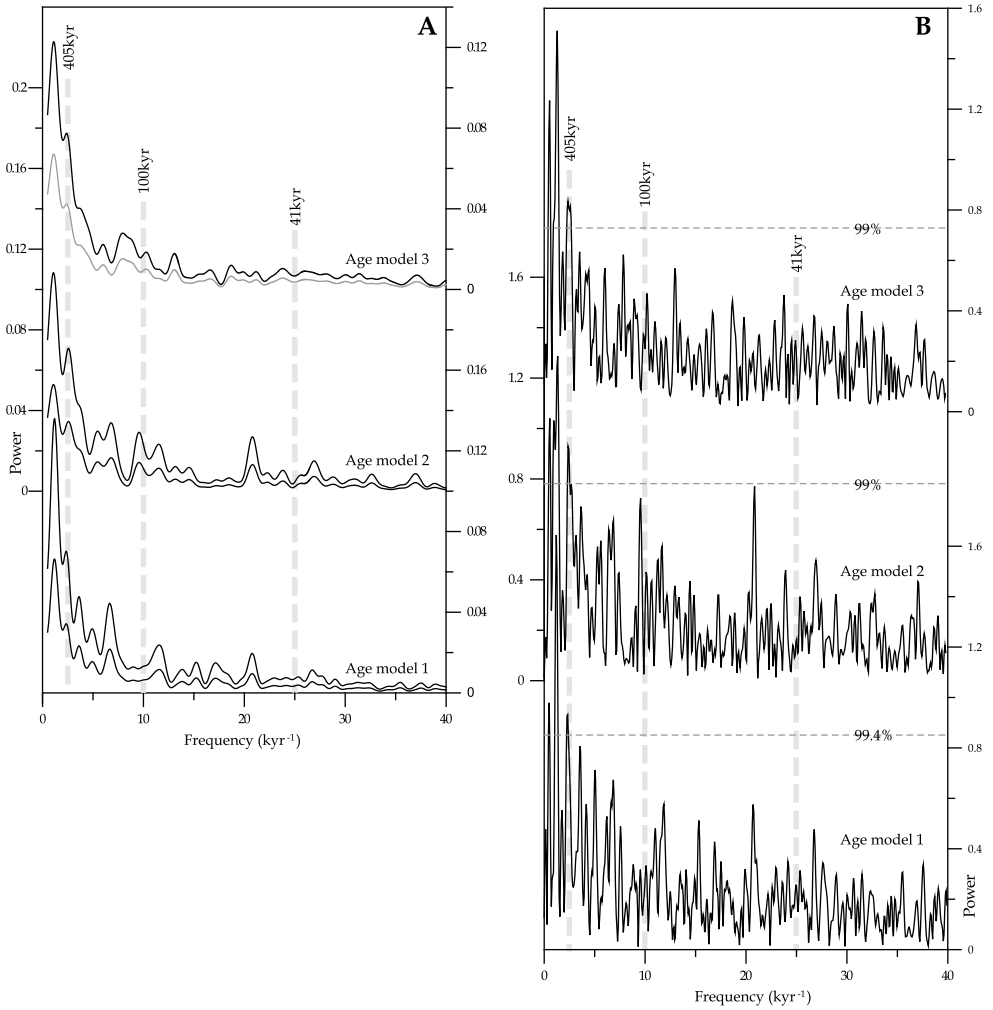

Figure 5.10 The Blackman-Tuckey (A) and CLEAN Red Noise (B) power spectra of the L* time series according to the three age models constructed, see text for explanation. In light grey, the 90% confidence limit is shown for the BT analysis (A). The horizontal dotted line indicates the 99% confidence interval of the CLEAN spectrum. Vertical lines indicate frequencies of obliquity, short and long eccentricity.

the outcome of time series spectral analysis. Age models 2 and 3 result in less noisy spectra than Age model 1, suggesting that the increased time control resulted in a reduction of the disturbance by changes in sedimentation rate. Here, the imprint of the eccentricity forcing is further analysed,

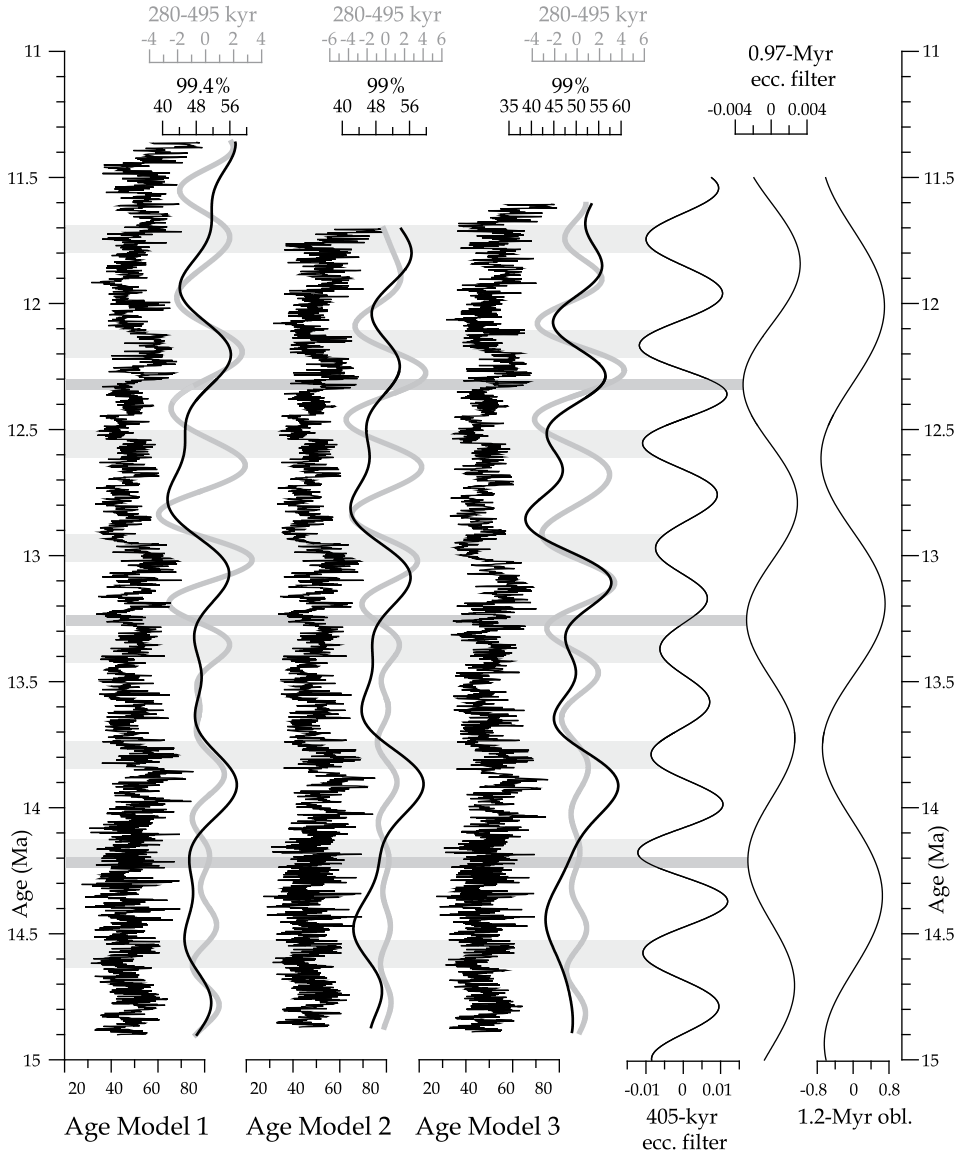

Figure 5.11 The L* time series according to Age Model 1, 2, and 3, their 280-495 kyr Bandpass filters in light-grey, and the 99% and 99.4% reconstructed time series following the CLEAN method. To the right the 405-kyr and 0.97-Myr eccentricity, and 1.2-Myr obliquity cycles are shown, derived from filtering the eccentricity target curve and the amplitude modulator curves obliquity, respectively. Horizontal bars indicate minima in the 405-kyr and 0.97-Myr eccentricity cycles.

firstly, because this is the main objective of the study, and, secondly, because higher frequencies are better studied when the low frequency variability has been reasonably quantified.

5.5.4 Long eccentricity forcing

In all spectra, significant peaks are present that might be related to the long, 405-kyr eccentricity cycle in all three age models with both statistical methods (Fig. 5.10). In Figure 5.11, the reconstructed colour series above 99% confidence limits in the CLEAN spectrum are shown next to the three L* time series and the eccentricity curve. Also, the Bandpass filtered long eccentricity components of the L* series are shown. Light-grey horizontal bars indicate long eccentricity minima (Fig. 5.11). Especially Age model 2 results in a fairly consistent lagged and in phase relation with long eccentricity. This has been further analysed by means of Cross-Spectral analysis between the L* time series, according to Age model 2, and eccentricity (Fig. 5.12). Long eccentricity shows a significant coherence between both records. The phase diagram indicates that long eccentricity leads the L* frequency component by approximately a quarter of a cycle (Fig. 5.12). Note that the short, 100-kyr eccentricity cycle does not show a significant coherence.

5.5.5 Low frequency cyclicity

A lower frequency component that corresponds to a period of approximately 0.8 to 1 Myr is also present in the spectra (Fig. 5.10 and 5.11). In the L* time series and the 99% reconstructed

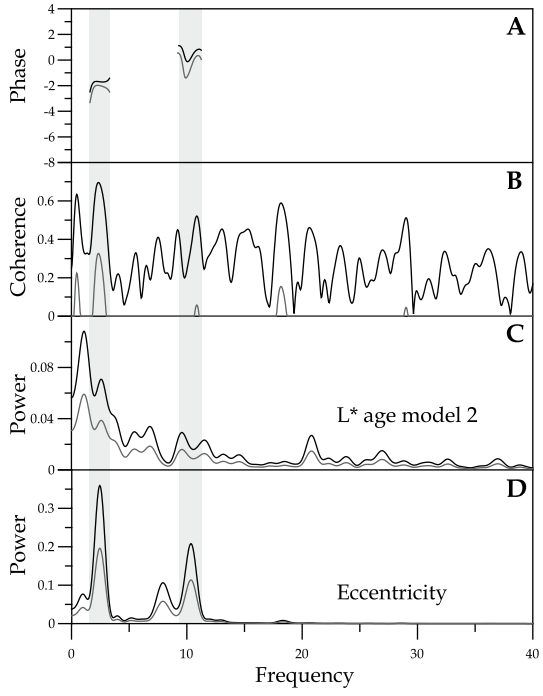

Figure 5.12 Blackman-Tuckey cross-spectral analysis of the eccentricity and L* time series according Age model 2. The BT power spectrum of eccentricity (D) and L* time series (C), and the coherence (B) and phase diagrams (A) are shown. Light-grey lines indicate 90% confidence limit. Grey vertical bars indicate the short and long eccentricity frequency.

L* series of the CLEAN spectra, this component can be recognised by higher values roughly every second supposed long eccentricity cycle. This component might be related to the 0.97-Myr eccentricity cycle or, but less likely regarding its length, the 1.2-Myr obliquity cycle. These cycles have been filtered and plotted next to the time series in Figure 5.11. The dark-grey horizontal bars in the figure indicate minima of the 0.97-Myr cycle. The whitest intervals and maxima in the filtered component reveal to have a slightly lagged, out-of-phase relation with the 0.97-Myr eccentricity cycle. Resolution in the low frequency realm, as a consequence of the limited length of our time series, does not permit comparison of the data with the 2.4-Myr eccentricity cycle. Therefore, this cycle is added to Figure 5.6 for comparison with lithology. Clearly, both limestone intervals, Mixta 1 and Mixta 2, in the upper part of both genetic sequences start during minimum eccentricity values (Fig. 5.6) and continue for a certain time. Lithology thus also has a lagged out-of-phase relation to 2.4-Myr eccentricity. Nodes in obliquity amplitude related to the 1.2-Myr cycle were suggested to have a large impact on terrestrial climate (Van Dam *et al.*, 2006). In the obliquity time series, nodes occur at around 13.8, 12.6, and 11.4 Ma. These are not coincident with lithofacies changes in the VDA-MX section and, thus, a relation with this cycle is not suggested (Fig. 5.6).

In summary, the time series analysis of the L* record suggests the imprint of the 405-kyr and 0.97-Myr eccentricity cycles. Comparison of the VDA-MX lithological log with the 2.4-Myr eccentricity cycle indicates start of limestone deposition during long-period minima. Response to the 405-kyr cycle occurred in phase and lagged with around a quarter of a cycle in phase. The 0.97-Myr and 2.4-Myr cycles also display a lagged response, but out of phase.

5.6 Discussion

The well-calibrated magnetostratigraphy of the VDA-MX section covering the Intermediate unit in the north-eastern part of the Madrid Basin followed by spectral analysis of the colour reflectance data in the time domain have several implications.

5.6.1 Long-period orbital climate forcing

The start of limestone deposition directly after a 2.4-Myr eccentricity minimum is exactly identical to the relation found in Chapter 2 for a similar lithologic transition of Late Miocene age in the Teruel Basin (Abels *et al.*, 2008). A longer period devoid of extreme evaporative conditions due to the absence of precession extremes at times of low eccentricity might have filled groundwater reservoirs (see also Van Dam *et al.*, 2006). After a certain time, threshold conditions for carbonate deposition were crossed due to raised groundwater and/or lake levels, possibly assisted by positive feedback mechanisms like enhanced vegetation cover and increased chemical instead of physical weathering. Van Dam *et al.* (2006) indicate that humidity-adapted rodents migrate from central Europe to Spain during 2.4-Myr eccentricity minima, possibly indicating favourable conditions for lake expansion in the Madrid Basin. In Chapter 2, we further suggested that the delayed response might be related to a memory effect of groundwater reservoirs. Sanz *et al.* (1995) indeed suggest that groundwater might play an important role in feeding the palaeosol and pond environments in the Madrid Basin. Similarly, the lagged response of the paleoenvironment to the 0.97-Myr cycle might be explained. The data clearly reveal an in-phase relation of the 405-kyr cycle versus the out-of-phase relation of the 0.97-Myr and 2.4-Myr cycles, which is remarkable. This is probably connected to a precession amplitude origin of the 405-kyr cycle, against a non-linear response to

the low frequency eccentricity cycles. Anyway, this contradiction requires further investigation by, for example transient runs of climate models depicting orbital climate forcing.

Van Dam et al. (2006) in addition showed that cooler and drier conditions prevailed on the Spanish mainland during long-period obliquity minima, probably due to increased global ice volume. They suggest that lacustrine limestone intervals are replaced by red beds during these obliquity nodes. However, no indication for long-period obliquity forcing is found in the VDA-MX section.

The new data can not reliably prove that the large-scale genetic sedimentary sequences in the Madrid Basin are related to the 2.4-Myr eccentricity cycle. Therefore, additional genetic sequences in the Madrid and other basins have to be studied in the same way. For example, the carbonate-rich top of the Lower unit in the north-eastern part of the basin is should date between 17 and 16 Ma, again just after the 2.4-Myr eccentricity minimum (Fig. 5.6). Also, the limestone intervals need to have roughly the same age in the segment of the Madrid Basin that was hydrologically and physically connected with the VDA-MX area. For the moment, it is promising that exactly the same phase relation has been found for the single transition dated in the Teruel Basin (Chapter 2). As expected for a long-period orbital forcing scenario, other eccentricity related variability is also recorded, although the short eccentricity imprint is not (yet) recognised.

5.6.2 Higher-frequency orbital forcing

The spectral analysis of the colour records revealed the presence of 405-kyr eccentricity forcing. Additionally, the imprint of the 0.97-Myr eccentricity cycle is suggested. No clear indication for short eccentricity has been found. The lack of small scale orbital frequencies in the VDA-MX section can be of several origins.

The colour reflectance data in the VDA-MX is not a perfect proxy for lithology, although it roughly reflects the carbonate content of the sediment. Carbonate precipitation however occurred under different depositional conditions from calcic palaeosols to pond and marginal lacustrine water bodies (Sanz *et al.*, 1995). This means that variable local groundwater conditions may have resulted in similar colour patterns and thus in a similar imprint in the L* colour record. At low frequencies, this effect is not expected to mask the cyclicity, but at higher frequencies it may start to play (a dominant) role. Also, different episodes of pedogenic calcrete development can be masked by vertical stacking of calcrete layers, thereby overprinting part of the original high-frequency cyclic origin.

A small error in the correlation between the VDA and the MX section can have been made. Such an error may have an influence on the outcome of the spectral analysis, although Age models 2 and 3 are based on so many tie-points that the effect can not be large. The correlation between VDA and MX is based on lithostratigraphic patterns and an approximate lithostratigraphic correlation, because the direct physical contact can not be traced (Fig. 5.3). Lower sedimentation rates in the Detritica II and the lack of both C5Ar.1n and 2n chrons in the MX section (whereas one seems to be depicted in the VDA section; Fig. 5.6), despite high resolution sampling, might suggest that the MX section starts higher in stratigraphy (and so time) than the top of the VDA section. To solve this potential problem, the Muduex section should be extended downwards to construct an overlap in the magnetostratigraphy between the sections.

5.6.3 Basin-wide correlations

Montes et al. (2006) have dated the Lower and Intermediate unit in more central and southern parts of the Madrid basin by means of magnetostratigraphy. In their Cerro de los Guardias and

Gurugú sections, the Lower to Intermediate unit boundary is dated at 14.4 Ma using the CK95 time scale (Fig. 5.8; Cande and Kent, 1995). In the Cerro de los Guardias, the magnetostratigraphy does not resolve the middle Miocene pattern in all details, but the correlation is in good accordance with the nearby Paracuellos mammal sites. The Gurugú section shows a more convincing middle Miocene polarity pattern and its correlation to the GPTS is probably correct, also because a similar lithofacies transition as in the Cerro de los Guardias is found in the section. The use of the newer ATNTS04 time scale does not result in very different ages for comparison with the VDA-MX that is tied to the ATNTS04. The comparison leads to the conclusion that the Lower to Intermediate Unit transition are by far synchronous between the central and north-eastern portions of the basin (Fig. 5.8). Montes and co-workers further date the transition from the first to the second sequence in the Intermediate unit in the Cerro de los Guardias section at *ca* 13.4 Ma. The transition from the Intermedia I to II is the traditional location of the lower to upper sequence boundary, which should be coeval with the Mixta I to Detritica II transition in the north-eastern part. An approximate 0.4 Myr age difference between the central and north-eastern parts of the basin is not very large, although the top of chron C5AAn, which marks the transition at VDA-MX, is correlated much higher in the Cerro de los Guardias section (Montes *et al.*, 2006). In addition, they recognise a third sequence within the Intermediate unit, that was not recognised before. Two magnetostratigraphic correlation options, A and B, result in rather different ages for the base of Sequence III in the Intermediate unit and especially also for the possible transition between the Intermediate and Upper units in the central parts of the basin (Fig. 5.8).

The comparison of the magnetostratigraphic dating of the VDA-MX composite section in the north-eastern part of the basin and the middle Miocene stratigraphy in the central part of the basin indicates that tectono-sedimentary unit boundaries are not synchronous trough the entire Madrid Basin. More likely, the distinct areas, that also display distinct lithofacies associations, evolved rather separately from each other. It has been suggested that the abundant evaporites in the Lower unit in the areas west of the Tajuña river probably resulted in a variable landscape over which the Intermediate unit was deposited (Calvo *et al.*, 1989; Megias *et al.*, 1981). Such topographic differentiation between the areas during sedimentation can have led to poor or no physical and/or hydrological contact. Also, the highly different geology of the basin margins sourcing the different areas in the basin can have led to differential response even to similar allogenic forcings (Alonso Zarza *et al.*, 1992; Calvo, 1989).

5.6.4 Middle Miocene climate variability

During the middle Miocene, a major global climate transition occurred presumably due to East Antarctic Ice Sheet increase (Flower and Kennet, 1994; Miller, 1991). In the Mediterranean, this transition has been accurately recorded on Malta (Abels *et al.*, 2005) and by small mammal turnover rates on the Spanish mainland (Van der Meulen *et al.*, 2005). In the small-mammal turnover record, a large step is observed at *ca* 14 Ma, approximately corresponding to the base of the Mixta 1 limestone interval. Holbourn *et al.* (2007) and Raffi *et al.* (2006) provide high-resolution astronomically calibrated benthic oxygen and carbon isotope records from the Pacific and Atlantic over this time interval. These records show a dominance of obliquity variability from 14.5 Ma to the climate transition at 13.85 Ma. Before and after this interval short eccentricity prevails (see also Holbourn *et al.*, 2004). In the VDA-MX section, the obliquity dominated interval should correspond to the top part of the Detritica 1 (Fig. 5.6). This interval is characterised by regular lithofacies cycles of around 4 to 4.5 m thick (Fig. 5.3C; Fig. 5.2) corresponding to *ca* 63 to 72 kyr. This duration is in between the periods of obliquity and short eccentricity, indicating that

the floodplain succession was controlled by local processes, orbital or not, rather than by 'global' climate variations induced by glacial cyclicity at the southern (and northern?) hemisphere. This idea is strengthened by the presence of higher frequency lithological alternations in the interval below 14.5 Ma (Fig. 5.6), which in turn is dominated by major 100-kyr ice volume variability in Pacific and Atlantic records (Holbourn *et al.*, 2007; Raffi *et al.*, 2006). The apparent lack of long-period obliquity control on the floodplain succession, as shown earlier, is in line with this finding as well. Local orbital forcing would imply dominance of precession and eccentricity over obliquity, even during eccentricity minima.

5.7 Conclusions

A detailed magnetostratigraphic age model has been established for the VDA-MX composite section in the north-eastern segment of the Madrid Basin. The age model is in line with biostratigraphic constraints. Direct comparison of the lithological log with orbital target curves indicates the onset of limestone dominated stratigraphy in the large-scale genetic sequences occurred during 2.4-Myr eccentricity minima. This configuration is identical to that found for a similar lithofacies transition of Late Miocene age in the Teruel Basin and might be related to prolonged periods lacking extreme evaporative conditions. Spectral analysis of the L* time series reveals additional imprint of the 405-kyr and 0.97-Myr eccentricity cycles. Response to the 2.4-Myr and 0.97-Myr eccentricity cycles would have occurred out of phase, while the response to the 405-kyr in phase. All three show a consistent phase lag. Cross-spectral analysis indicates a phase lag of 100 degrees relative to long eccentricity. The phase lags possibly relate to memory effects by gradual changes in groundwater reservoirs, vegetation, and weathering. No imprint of 41-kyr and 1.2-Myr obliquity cycles has been found, indicating dominance of local (orbital forcing) processes on the floodplain environment in the Madrid Basin at that time. To corroborate the suggestion of long-period orbital forcing on genetic sequence formation in the Madrid Basin, the synchrony of genetic sequences has to be proven for that part of the basin that was hydrologically and physically in contact during deposition. Subsequently, other genetic sequences in the Madrid Basin as well as in other Cenozoic basins on the Iberian peninsula have to be dated in the same way to test whether a similar orbital configuration existed during limestone formation of the large-scale genetic sequences.

The magnetostratigraphic age model further indicates that the genetic sequences, since long recognised and correlated in the Miocene infill of the basin, do not represent time-equivalent sediment packages, and that their boundaries are diachronous as well. We suggest that these sequences are not of common origin within the complete basin, but that the different segments of the basin evolved separately. Possibly the sectors were not hydrologically and/or physically connected during deposition due to the existence of a palaeotopography within the basin.

5.8 Ackowledgements

Bet Beamud, Mark Dekkers, Miguel Garcés, and Tom Mullender are thanked for paleomagnetic sampling, measuring, and interpretation assistance.

CHAPTER 6

Long-period orbital control on middle Miocene global cooling; Integrated stratigraphy and astronomical tuning of the Blue Clay Formation on Malta

Hemmo A. Abels, Frederik J. Hilgen, Wout Krijgsman, Rink W. Kruk, Isabella Raffi, Elena Turco, and Jan-Willem Zachariasse

Based on:
H. A. Abels, F.J. Hilgen, W. Krijgsman, R.W. Kruk, I. Raffi, E. Turco, and W.J. Zachariasse, 2005. Long-period orbital control on middle Miocene global cooling; Integrated stratigraphy and astronomical tuning of the Blue Clay Formation on Malta. *Paleoceanography*, Vol 20, PA 4012, doi 10.1029/2004PA001129.

and
F.J. Hilgen, H.A. Abels, S. Iaccarino, W. Krijgsman, I. Raffi, R. Sprovieri, E.Turco, and W.J. Zachariasse, in the press, The global stratotype section and point (GSSP) of the Serravallian Stage (middle Miocene). *Episodes*.

6.1 Abstract

Application of an astronomical age model to a bulk carbonate oxygen isotope record in the Ras il Pellegrin section on Malta indicates that the major step in the middle Miocene global cooling (13.82 Ma ± 0.03) coincides with minimum eccentricity values associated with the 400-kyr cycle and minimum obliquity amplitudes associated with the 1.2-Myr cycle. This orbital configuration is very similar to that found for comparable oxygen isotope enrichment events in the late Paleogene and Neogene. The stepwise character of the middle Miocene cooling event appears to be controlled by the combined influence of the 100-kyr eccentricity cycle and the 172-kyr cycle in obliquity amplitude. The integrated stratigraphy further allows extension of the astronomical polarity timescale to the top of chron C5ACn. The boundary between the Globigerina Limestone and the Blue Clay Formation coincides with the major step in middle Miocene global cooling and provides a level suitable for placing the physical reference point for the Langhian/Serravallian boundary.

6.2 INTRODUCTION

Following the Miocene climate optimum between 16 and 14.5 Ma the middle Miocene global cooling at around 14 Ma represents a next important step in the evolution of Cenozoic climate. The

climate change did go along with changes in ocean circulation and floral and faunal distribution, with an increase in the meridional temperature gradient, and with the permanent installation of a larger East Antarctic Ice Sheet (see Flower and Kennett, 1994).

The cause of the middle Miocene cooling has been ascribed to increased weathering of silicate rocks due to uplift in the Himalayan-Tibetan region (*e.g.*, Raymo and Ruddiman, 1992) and to increased burial of organic carbon (*e.g.*, Vincent and Berger, 1985), both leading to the withdrawal of CO2 from the atmosphere and hence a reduction of the greenhouse capacity. However, available pCO2 reconstructions based on different proxies do not show convincing evidence for lower atmospheric CO2 values after or during middle Miocene cooling (Pagani *et al.*, 1999; Pearson and Palmer, 2000; Royer *et al.*, 2001). Further, changes in ocean circulation patterns, for example, due to tectonic closure of basins, may have increased moisture transport or reduced heat transport to the Antarctic region (Shevenell and Kennett, 2004).

The cause of the middle Miocene cooling has been ascribed to increased weathering of silicate rocks due to uplift in the Himalayan-Tibetan region (*e.g.*, Raymo and Ruddiman, 1992) and to increased burial of organic carbon (*e.g.*, Vincent and Berger, 1985), both leading to the withdrawal of CO2 from the atmosphere and hence a reduction of the greenhouse capacity. However, available pCO2 reconstructions based on different proxies do not show convincing evidence for lower atmospheric CO2 values after or during middle Miocene cooling (Pagani *et al.*, 1999; Pearson and Palmer, 2000; Royer *et al.*, 2001). Further, changes in ocean circulation patterns, for example, due to tectonic closure of basins, may have increased moisture transport or reduced heat transport to the Antarctic region (Shevenell and Kennett, 2004).

One of the few places where the middle Miocene climate transition can be studied in continuous marine successions on land is on Malta and Gozo located in the central Mediterranean (Fig. 6.1). Earlier studies on these islands have shown that the major middle Miocene isotopic enrichment event (Mi3b, E3, CM6; *ca* 13.8 Ma) coincides with the transition from the Globigerina Limestone to the Blue Clay Formation (Jacobs *et al.*, 1996; John *et al.*, 2003) and that the cyclically bedded Blue Clay is potentially suitable for astronomical dating (Sprovieri *et al.*, 2002; John *et al.*, 2003). However, the tuned ages of Sprovieri *et al.* (2002) for calcareous plankton events in the middle and upper part of the Blue Clay Formation are significantly younger than tuned ages for the same bioevents in the time-equivalent Monte dei Corvi and Tremiti sections (Hilgen *et al.*, 2003). We therefore decided to independently establish an integrated stratigraphy and astronomical tuning for the uppermost part of the Globigerina Limestone, and the lower and middle part of the Blue Clay Formation on Malta, using high-resolution biostratigraphic correlations to the well-tuned Monte dei Corvi and Tremiti sections as a starting point. In addition, we established a bulk isotope record to locate the position of the major middle Miocene global cooling step and associated events.

6.3 Geological setting, section, and lithology

The sediments of the Globigerina Limestone and Blue Clay Formation on Malta and Gozo were deposited in the Maltese Graben System, a series of Miocene-Quaternary extensional basins that developed on the African foreland of the Sicilian Apennine-Maghrebian fold and thrust belt (De Visser, 1991; Dart *et al.*, 1993). The sedimentary succession exposed on Malta and Gozo consists of five different formations: Lower Coralline Limestone (late Oligocene), Globigerina Limestone (Aquitanian-Langhian), Blue Clay (Serravallian), Greensand (Serravallian-Tortonian),

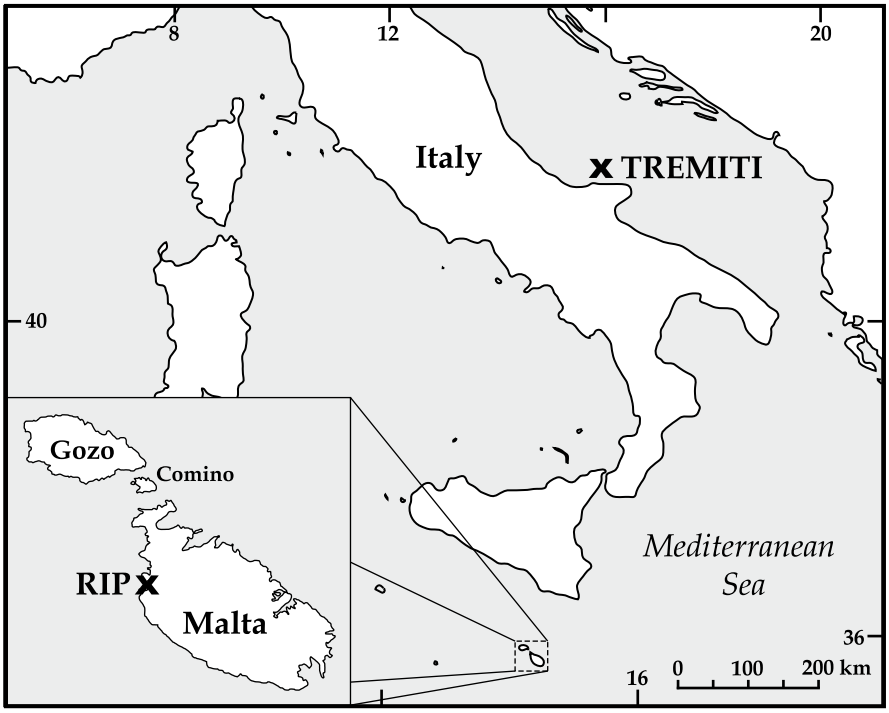

Figure 6.1 Location maps of the Ras il Pellegrin (RIP) section on Malta and the Tremiti section in Italy, both indicated by 'X'.

and Upper Coralline Limestone (Tortonian) (Felix, 1973). All boundaries are conformable except for the contact between the Greensand and the Upper Coralline Limestone Formation. Sediments of the Globigerina Limestone and Blue Clay were deposited in a low-energy, open marine environment. Paleobathymetric estimates point to a depth of around 500-600 m for the Globigerina Limestone and the Blue Clay (Bonaduce and Barra, 2002; Bellanca *et al.*, 2002). Benthic foraminiferal (Bellanca *et al.*, 2002) and clay mineral (De Visser, 1991; John *et al.*, 2003) studies of the Globigerina Limestone and the Blue Clay suggest overall lower bottom water oxygen levels, more humid climate conditions, and more intense continental weathering during the deposition of the Blue Clay.

The Ras il Pellegrin section (RIP), exposed along the Fomm Ir-Rih Bay on the west coast of Malta (Figures 6.1 and 6.2), covers the middle Globigerina Limestone up to the Upper Coralline Limestone Formation and was selected because of its excellent exposures and its distinct sedimentary cycles. A total number of 540 samples were taken from the top part of the Globigerina Limestone up to and including the middle part of the Blue Clay, measuring in total 48.5 m with an average sample distance of 9 cm. A transitional bed separates the yellowish marly limestones of the Globigerina Limestone from the grey clayey marls of the Blue Clay. No indications of erosion or deformation were found at the formation boundary. The measured section ends 20 m below the Greensand Formation and largely overlaps with the nearby Ras il Pellegrin A section studied by an Italian research team (Bellanca *et al.*, 2002; Bonaduce and Barra, 2002; Foresi *et al.*, 2002;

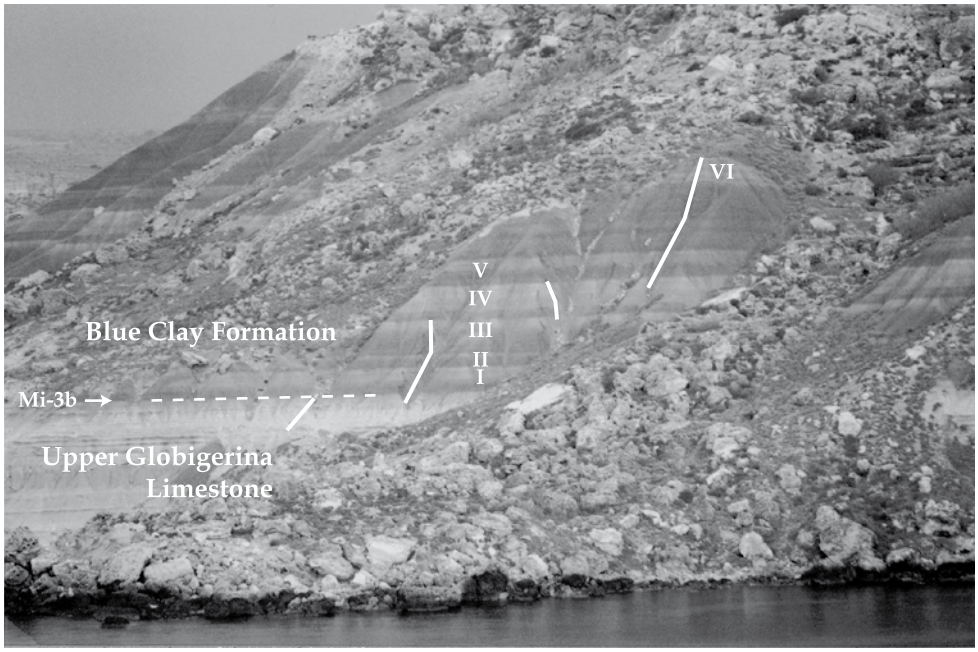

Figure 6.2 Ras il Pellegrin section seen from the southern shore of the Fomm Ir-Rih Bay showing sampling trajectories (solid lines), the boundary between Blue Clay and Upper Globigerina Limestone (dashed line), and large-scale whitish coloured marly intervals (I-VI).

Sprovieri *et al.*, 2002). The Blue Clay at Ras il Pellegrin shows a very distinct and characteristic pattern of homogeneous grey and white coloured marls (Fig. 6.2). The presence of two sapropels and several levels with chondrite trace fossils (Bromley, 1990) point to occasional anoxic or dysoxic bottom water conditions. The sapropels and chondrite trace fossils occur in the grey marl beds. Finally, volcanic minerals found in residues around 40.45 m point to an ash-fall in the younger part of the Blue Clay.

6.4 Cyclostratigraphy

In the lower and middle part of the Blue Clay we distinguished six whitish coloured marly intervals, numbered I to VI in Figure 6.3. These intervals, separated by intervals dominated by grey marls, correspond to the large-scale cyclicity recognized in the Blue Clay by Sprovieri *et al.* (2002) and John *et al.* (2003). The small-scale cyclicity is less easy to distinguish in the field (see also Sprovieri *et al.*, 2002). Rather arbitrarily, we define a small-scale cycle to consist of a greyish marl bed at the base followed by a whitish marl at the top. The Blue Clay part of the studied section contains 44 small-scale cycles that can be recognized in the field and have been labelled I.1 to VI.16 as subdivision of the larger scale intervals (Fig. 6.3).

Discrimination of small-scale cycles is particularly difficult in interval VI. The calcium and potassium content in the samples was measured using ICP-OES to obtain a quantitative measure

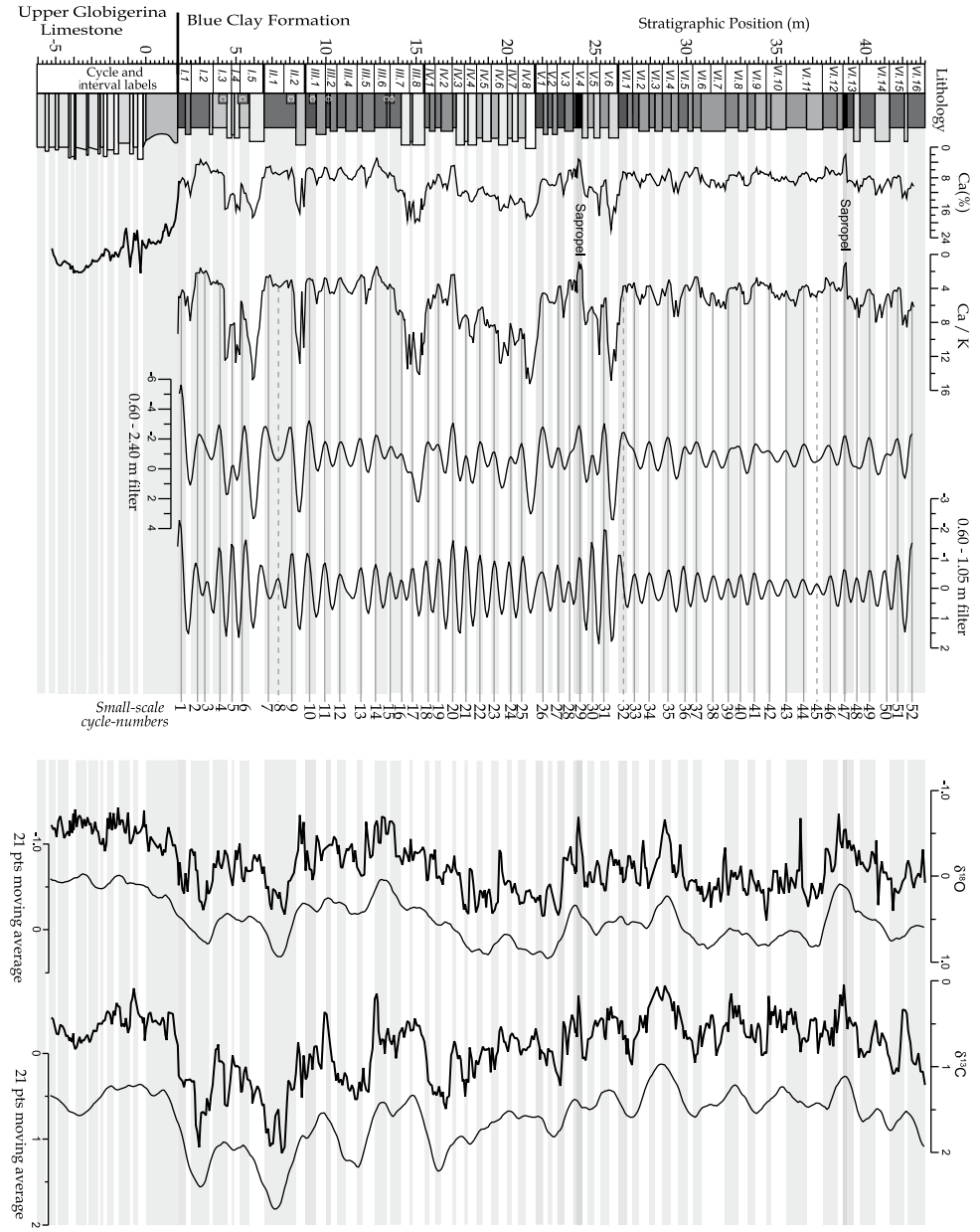

Figure 6.3 Lithological column of the Ras il Pellegrin section showing field-based small-scale cycle and large-scale interval labelling, calcium record, calcium-potassium ratio, 0.6-2.4 and 0.6-1.05 m Ca/K filter, small-scale cycle numbering defined on the basis of chemical records, bulk carbonate isotope records, and 21-point moving averages of the isotope records. "C" indicates levels with chondrite trace fossils.

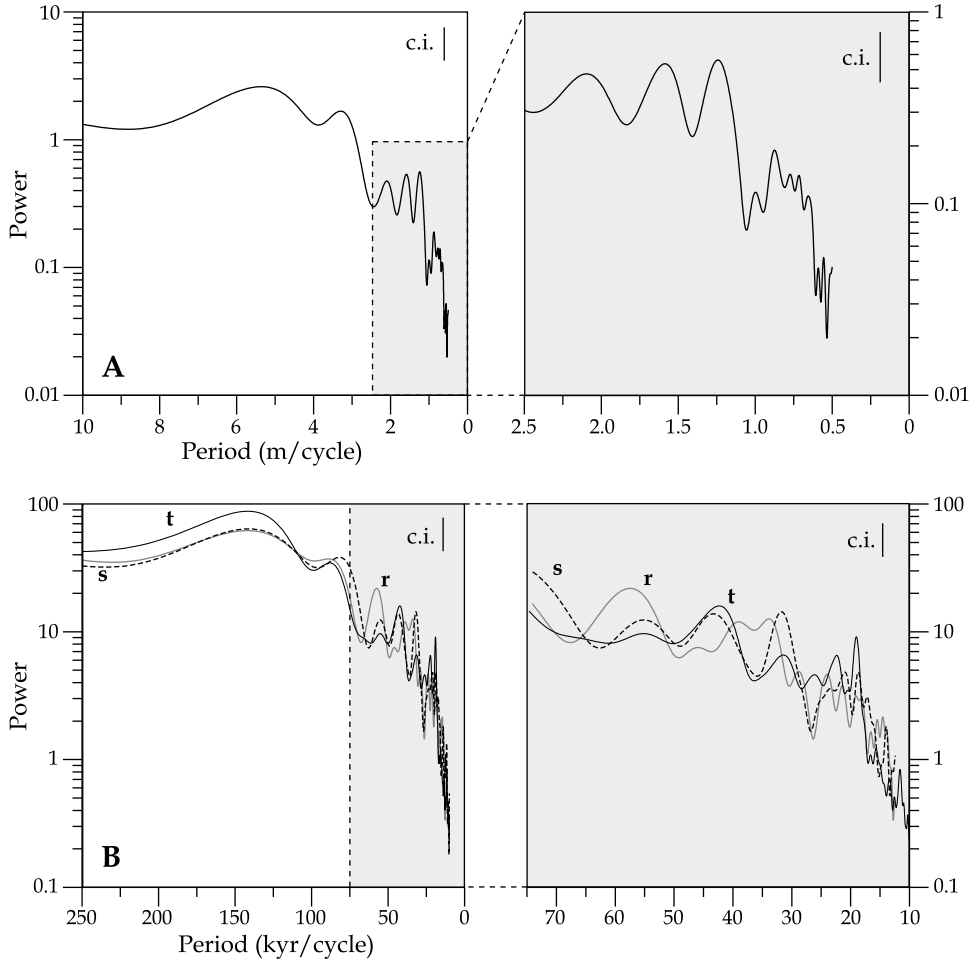

Figure 6.4 Blackman-Tukey power spectra of Ca/K records in the (a) depth domain and in (b) time domain calculated with the AnalySeries program 1.2 (Paillard *et al.*, 1996). All spectra are based on records from bed I.1 upward to avoid disturbance from the Globigerina Limestone in the statistical analysis. The three spectra (r, s, and t) of Ca/K-records in time domain (Fig. 6.4b) result from the application of three age models to the Ca/K record in depth domain. These age models are based on (r) astronomical ages of 10 correlated bioevents, (s) the ages for bioevents 2, 4, 7, and 9, and (t) tuning of the Ca/K record to precession. The 90% confidence intervals are shown in the upper right corner of each spectrum. Plots on the right are enlargements of the left plots.

of the lithology and hence the cyclicity (Fig. 6.3). (The 540 samples were taken at an average distance of 9 cm. A part of each sample was dried, crushed, powdered and homogenized. 125 mg of each sample was subsequently dissolved in 2.5 ml HF (40%) and 2.5 ml mixing acid (HNO_3 (16.25%) and $HClO_4$ (45.5%)) and heated at 90°C in a closed tube for at least 8 hours. Then the sample was dried by evaporating the acids at 160°C and dissolved in 25 ml HNO_3 (4.5%). These solutions were analyzed by a Perkin Elmer Optima 3000 ICP-OES apparatus, at Utrecht University, for the elements Al, Ba, Ca, Ce, Co, Cr, Cu, Fe, K, Li, Mg, Mn, Na, Ni, P, S, Sc, Sr, Ti, V, Y and Zn. The relative errors in duplicate measurements of international standards was for all

elements lower than 3%, except for Ce, Co, P and S, Sr and Y. Results were checked and where needed refined by making use of international standards (ise-921) and Utrecht University in-house standards (SO-1).) Ca mainly reflects the (calcium)carbonate content, because multiplying the Ca value by 2.496, assuming that all Ca is derived from carbonate, yields an average $CaCO_3$-content for the Blue Clay in the RIP section of 23.9%, which is in agreement with $CaCO_3$ values measured by Sprovieri *et al.* (2002) and John *et al.* (2003), who used different methods than ICP-OES. Ca and K showed a strong inverse relation (95%) and the Ca/K ratio was selected to reduce noise in the individual records (Fig. 6.3). The large-scale cycles, observed in the field, are prominently visible in the Ca/K record (Fig. 6.3). The 44 small-scale lithological cycles distinguished in the field are recognizable in this record as well, although small offsets between lithology and chemical records occur especially in interval V and VI. Blackman-Tukey spectral analysis revealed distinct peaks in the depth domain (Fig. 6.4a), which correspond to cycle thicknesses of *ca* 5.5 and 3.5 m. In addition, several peaks are present in the higher-frequency part of the spectrum and correspond to cycle thicknesses between 0.6 and 2.4 m. Band-pass filters were applied to better visualize the smaller-scale cyclicity in the Ca/K record. The 0.6-2.4 m filter includes all peaks in the higher-frequency domain. The 0.6-1.05 m filter extracts cycles with thicknesses similar to that of the small-scale cycles observed in the field. The latter filter indeed shows a strong relation with these small-scale cycles and reveals the presence of 8 additional cycles, most of them in interval VI. Small-scale cycles were subsequently numbered based on successive minima in the (filtered) Ca/K record.

6.5 Oxygen and carbon isotope record

Our oxygen and carbon isotope record (Fig. 6.3) based on bulk sediment for the uppermost Globigerina Limestone and the Blue Clay Formation in the Ras il Pellegrin section reveals a 0.6 ‰ increase in $\delta^{18}O$ and a 1.25‰ increase in $\delta^{13}C$ at the boundary between the Globigerina Limestone and Blue Clay. (Bulk isotope data were generated on dried crushed bulk sediment on a SIRA-24 of VG (vacuum generators), at Utrecht University. Results, in per mil (‰) relative to the Peedee Belemnite standard, were checked by making use of international (Naxos 45-125 um, validated with NBS-18 and 19) and Utrecht University in-house standards (IAEA-CO-1), and by duplicate measurements of the Naxos standard every eight samples. Relative error in duplicate measurements was lower than 2%.) A 21-point moving average was applied to the isotope records to better visualize the long-term variations. In the lower part of the Blue Clay, both $\delta^{18}O$ and $\delta^{13}C$ reach heavier values in the clay-rich intervals. From interval IV upward the smoothed records show less prominent long-term variations in amplitude and are also less consistent with lithology.

6.6 Magnetostratigraphy

A standard paleomagnetic core was drilled at each sample site, with an average sample distance of 9 cm. One of each two cores was stepwise thermally demagnetized with temperature steps of 20° or 30°C, in a laboratory-built shielded furnace. The other core was treated by stepwise alternating field demagnetization with steps of 5 mT at low applied magnetic fields to 50 mT at high magnetic fields. The natural remanent magnetization (NRM) was measured after each step on a 2G Enterprises DC Squid cryogenic magnetometer, at paleomagnetic laboratory "Fort

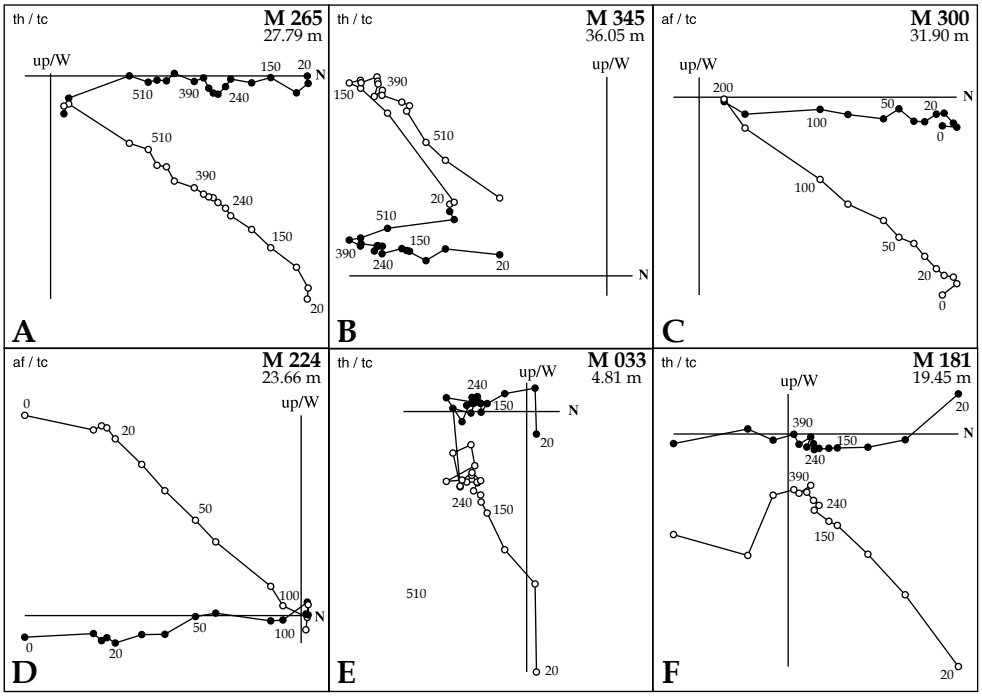

Figure 6.5 Examples of thermal (th) and alternating field (af) demagnetization (Zijderveld) diagrams of specimens in the Ras il Pellegrin section with (a and c) reliable normal and (b and d) reversed polarity and with (e and f) unresolved polarity. Closed (open) circles denote the projection on the horizontal (vertical) scale. Numbers indicate temperature (th) or magnetic field (af) steps in °C or mT. The stratigraphic position and the number of the specimen are shown in the upper right corner.

Hoofddijk," Utrecht University. Intervals that were found to contain a reversal were resampled in more detail to better constrain their stratigraphic position.

The NRM intensity of the samples from the Globigerina Limestone was very weak (0.04 mA/m) and no reliable polarities could be obtained. The Blue Clay showed much higher intensities (up to 125 mA/m). Demagnetization diagrams reveal a clear subdivision into two components, with a break at 260°C and 50 mT. In all samples, the low-temperature, low-field component is of normal polarity. We assume that this component represents viscous magnetite induced by the present-day field, which normally has an unblocking temperature of *ca* 260°C. The high-temperature/high-field component is of dual polarity and we interpreted this as the primary signal, the so-called characteristic remanent magnetization (ChRM). Many samples showed an increase in intensity at temperatures higher than 400°C, indicating a conversion of iron sulphides into iron oxides. Strong samples (>10 mA/m) do not show the intensity increase at 400°C and their Zijderveld diagram can be interpreted up to 600°C.

Samples classified as reliable have an NRM intensity higher than 0.1 mA/m at 270°C (or 50 mT) and a clear normal or reversed component in the interval from 270°C to 400°C (or 50 mT to 100 mT). Examples are shown in Figures 6.5A to 6.5D. Other samples (60%) were considered

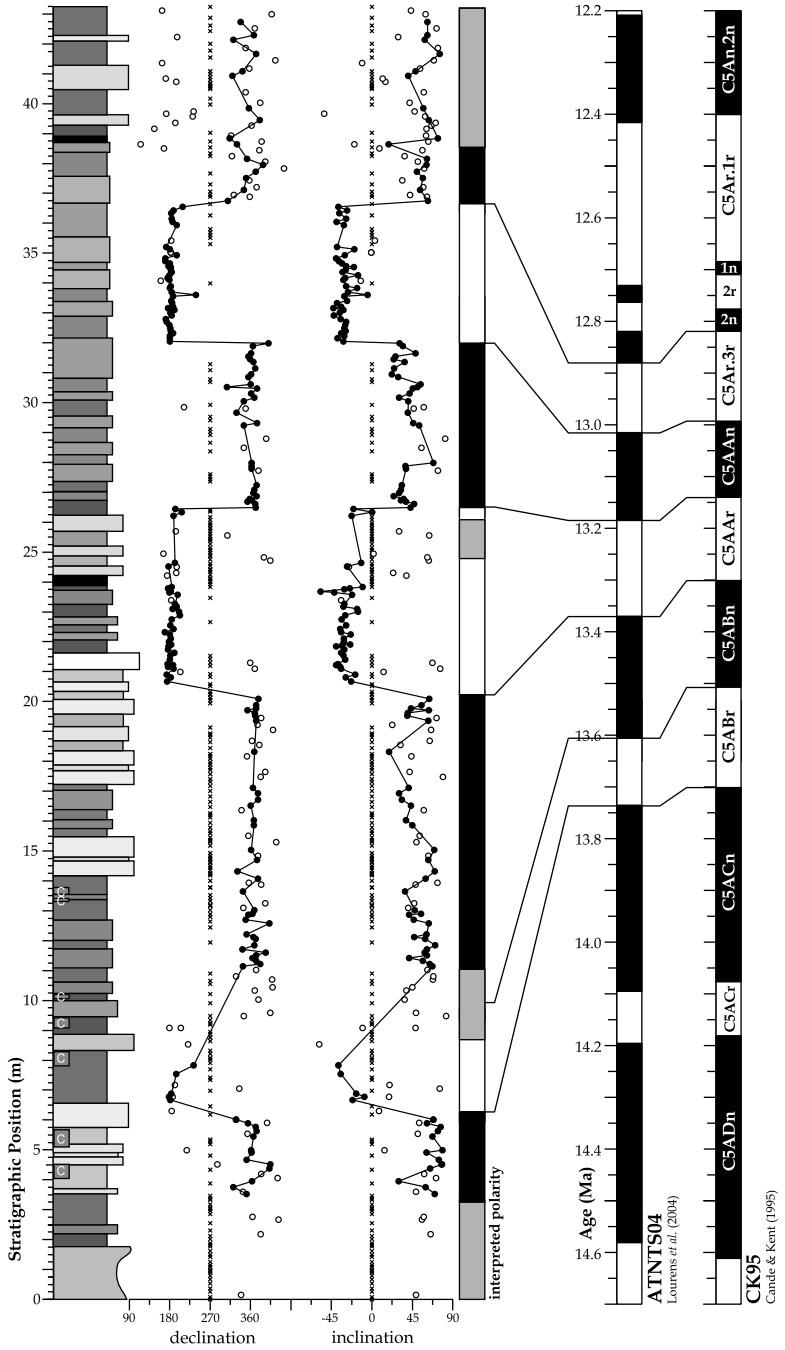

Figure 6.6 Magnetostratigraphic results of the Ras il Pellegrin section. Crosses indicate unresolved signal. In the polarity column, black (white) denotes normal (reversed) polarity, and grey indicates undefined polarity. To the right the correlation to the ATNTS2004 and CK'95 timescales is shown on basis of the age calibration model discussed in the text.

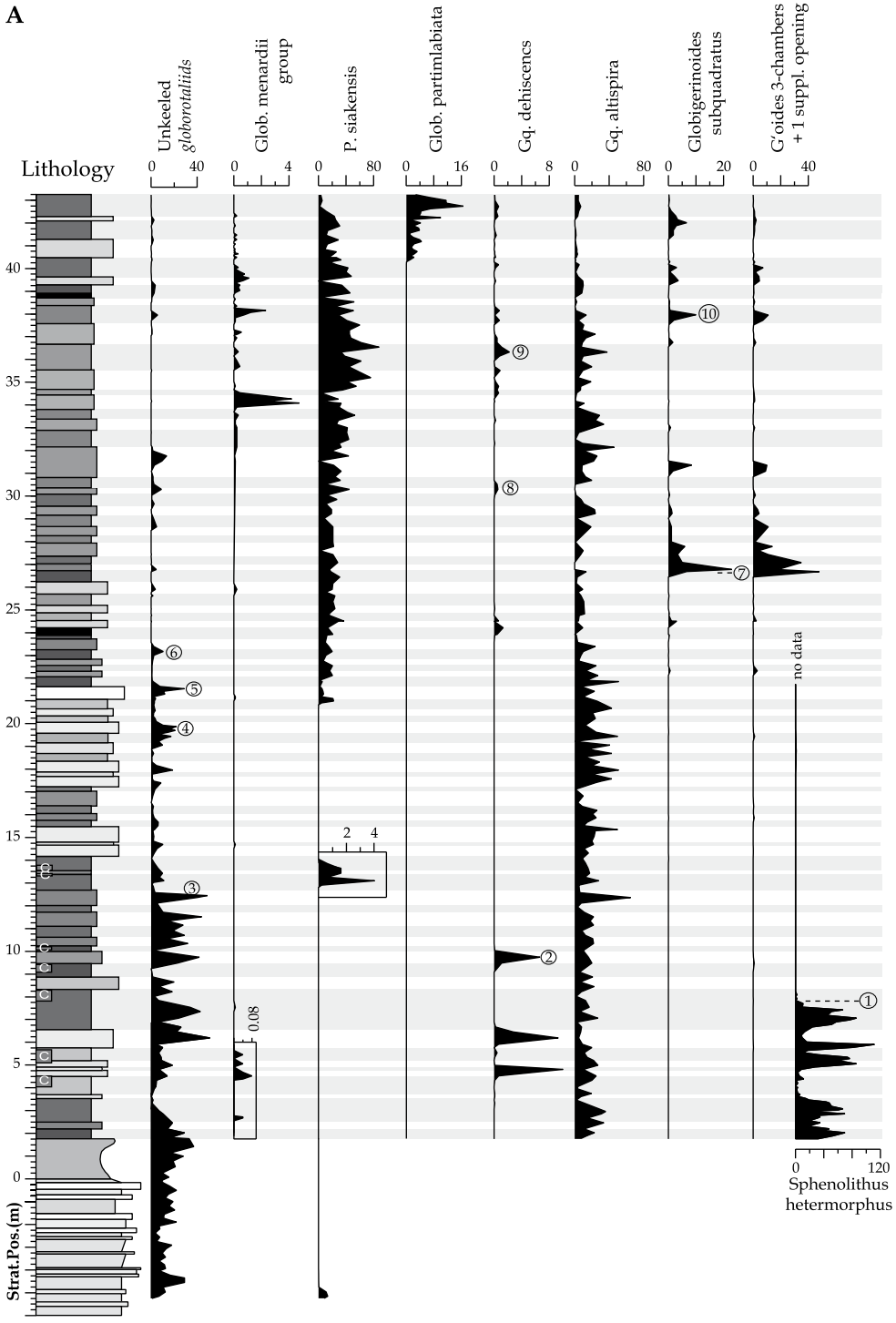
A
Lithology
Unkeeled globorotaliids
Glob. menardii group
P. siakensis
Glob. partimlabiata
Gq. dehiscencs
Gq. altispira
Globigerinoides subquadratus
G'oides 3-chambers + 1 suppl. opening
Strat.Pos.(m)
no data
Sphenolithus hetermorphus

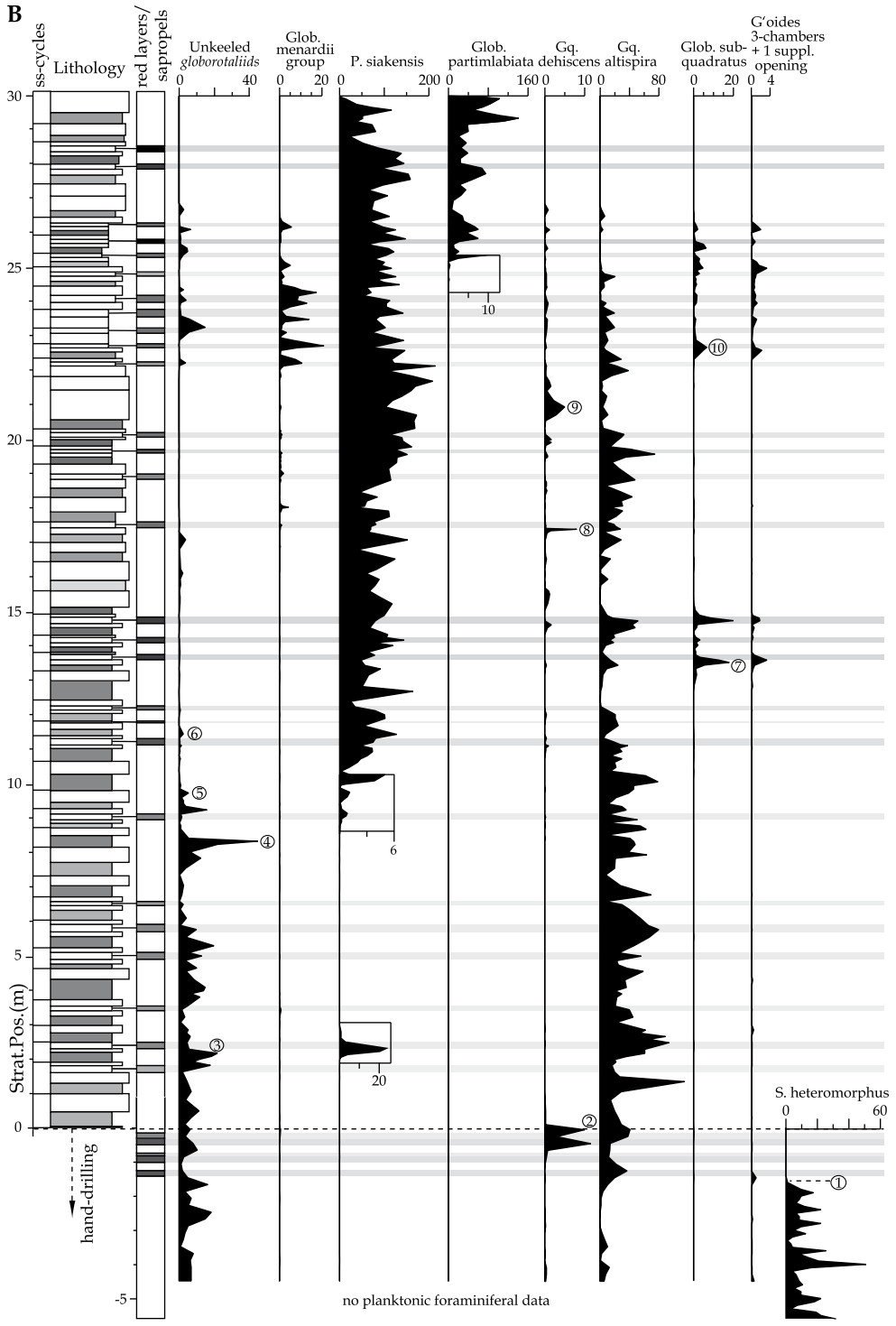
B
ss-cycles
Lithology
red layers/ sapropels
Unkeeled globorotaliids
Glob. menardii group
P. siakensis
Glob. partimlabiata
Gq. dehiscens
Gq. altispira
Glob. sub-quadratus
G'oides 3-chambers + 1 suppl. opening
S. heteromorphus
Strat.Pos.(m)
hand-drilling
no planktonic foraminiferal data

← *Figure 6.7* Semiquantitative abundance patterns for selected planktonic foraminiferal species and of the calcareous nannofossil *Sphenolithus heteromorphus* in the (A) Ras il Pellegrin section and (B) Tremiti section. No data means that the species has not been counted in that particular interval. Numbers (1-10) refer to specific events within the abundance patterns used for correlation between the Tremiti and the Ras il Pellegrin section.

unreliable (examples shown in Figs. 5e and 5f). This procedure resulted in a magnetostratigraphic polarity pattern with four normal and three reversed intervals (Fig. 6.6). The position of four of the six reversals could be very accurately determined. The upper part of the reversed interval at around 25 m contains an interval of uncertain polarity, mainly because of white marls that contain low magnetic intensity. Further, the precise position of the reversal at around 10 m is uncertain. The uppermost part of the section is also considered ambiguous because of an alternation of samples revealing weak reversed polarity with samples revealing normal ChRM. The open dots in the latter interval represent samples showing reversed components in the demagnetization interval between 270° and 400°C. Because of the low intensities (<0.1 mA/m) of these samples they are not included as reversed samples.

6.7 Biostratigraphy

Initially, every other sample was examined for planktonic foraminiferal biostratigraphy. Later, all samples were counted around bioevents. Countings are based on the number of a specific taxon in nine fields with a maximum of 20 specimens using a rectangular picking tray of 45 fields. The counts are shown as number per field in Figure 6.7a.

Comparison of our biostratigraphic data with those from DSDP 372 (Turco *et al.*, 2003; E. Turco *et al.*, unpublished data, 2004) reveals that the formation boundary does not contain a major hiatus and is most likely continuous. This is consistent with our field observations.

The pattern of *Paragloborotalia siakensis* and *Globorotalia partimlabiata* in the RIP section reveals that the section is grossly time-equivalent with the Tremiti section and the lower part of the Monte dei Corvi section in Italy (Hilgen *et al.*, 2003), which is confirmed by the LCO of calcareous nannofossil *Sphenolithus heteromorphus* in the Tremiti and RIP sections. The importance of the time equivalency of these three sections is that it allows us to import astronomical ages from the well-tuned Tremiti and Monte dei Corvi sections to the RIP section using detailed biostratigraphy. Unfortunately, the poor preservation of the planktonic foraminifers in Monte dei Corvi precludes a detailed biostratigraphic comparison with the RIP section, while the excellent preservation in Tremiti makes such a comparison possible. For that reason the same biostratigraphic procedure as used in the RIP section has been carried out on the Tremiti section with the same high resolution (Fig. 6.7b).

Although the semi-quantitative patterns of the selected taxa in both sections are grossly similar, several of the prominent short-term changes are absent in one section or show a different amplitude. This can among others be explained by differences in the relative number of planktonic foraminifers between both sections (*e.g.*, due to differences in P/B ratio between both sections), by hydrographic differences between both locations, or by the fact that the time-equivalent level was not always exactly sampled. Yet we need individual prominent short-term frequency changes to correlate both sections on the small-scale cycle level.

After carefully scrutinizing the patterns we selected 10 of the prominent, short-term abundancy changes to calibrate Tremiti to the RIP section (marked 1 to 10 in Figures 6.7a and 6.7b). These 10 bioevents are co-defined by the position of other (less) well-marked frequency changes. For example, the choice of bioevent 3 is co-defined by the position of the short-term acme of *P. siakensis*, bioevents 4, 5, and 6 are co-defined by the position of the paracme top of *P. siakensis*, and bioevent 8 is co-defined by the prominent bioevent 7 below and the first spike of the *G. menardii* group above.

6.8 Astronomical tuning

Independent orbital tuning of a section can only be established by recognizing characteristic patterns of astronomical forcing in lithology and other proxies. Unfortunately, the various patterns in the Ras il Pellegrin (RIP) section do not provide sufficient characteristic details that would allow an independent tuning. Therefore we used astronomical ages of 10 bioevents (see Biostratigraphy section) in the Tremiti section as a first-order age control on the RIP section.

The Tremiti section contains deep marine sediments that basically show a regular alternation of indurated, whitish coloured, carbonate-rich marls and less-indurated, greyish, carbonate-poor marls. Reddish layers occur regularly within the whitish indurated marls. The pattern of these reddish layers shows a striking resemblance with the sapropel pattern at Monte dei Corvi (Hilgen *et al.*, 2003) indicating that the red layers of Tremiti are the equivalent of sapropels. The cyclostratigraphic correlations between the two sections are consistent with planktonic foraminiferal biostratigraphic data. Hence it is safe to assume that the same phase relationships between the sapropels and orbital parameters, *i.e.*, individual sapropels correspond to precession minima and clusters to eccentricity maxima, are also valid for the reddish layers at Tremiti. Using these phase relationships, the Tremiti section can be tuned to precession (Fig. 6.8). The resulting age model provides astronomical ages for the bioevents in the Tremiti section (Fig. 6.7b). The astronomical tuning of the Tremiti section will be discussed in more detail in a future paper.

The astronomical ages of the 10 selected bioevents (see Biostratigraphy section) were exported from the Tremiti to the RIP section, which seems justified because both sections are located in the central Mediterranean Sea (Fig. 6.1). The correlated bioevents in the RIP section are used as age calibration points for the astronomical tuning of the section.

This first-order age control (Fig. 6.8, solid lines) indicates that the distinct white part of intervals III, IV, and V correspond to eccentricity minima. However, the white part of intervals I and II do not directly correlate with eccentricity minima according to this age model. The age model further indicates that the small-scale cycles in the RIP section are precession controlled, because the number of small-scale cycles based on the combination of lithology and the Ca/K record agrees well with the number of precessional cycles in the astronomical curves between the biostratigraphically controlled age calibration points. Blackman-Tukey spectral analysis was applied on the resulting Ca/K time series. The spectrum reveals power at the astronomical frequencies (Fig. 6.4b), but is less convincing if all 10 calibration points were used to generate the time series. This noisy behaviour of the spectrum is probably due to the close spacing of the bioevents in combination with remaining small uncertainties in the position and, hence, age of the bioevents at Tremiti and RIP. Considerably improved spectra were generated using only 4,

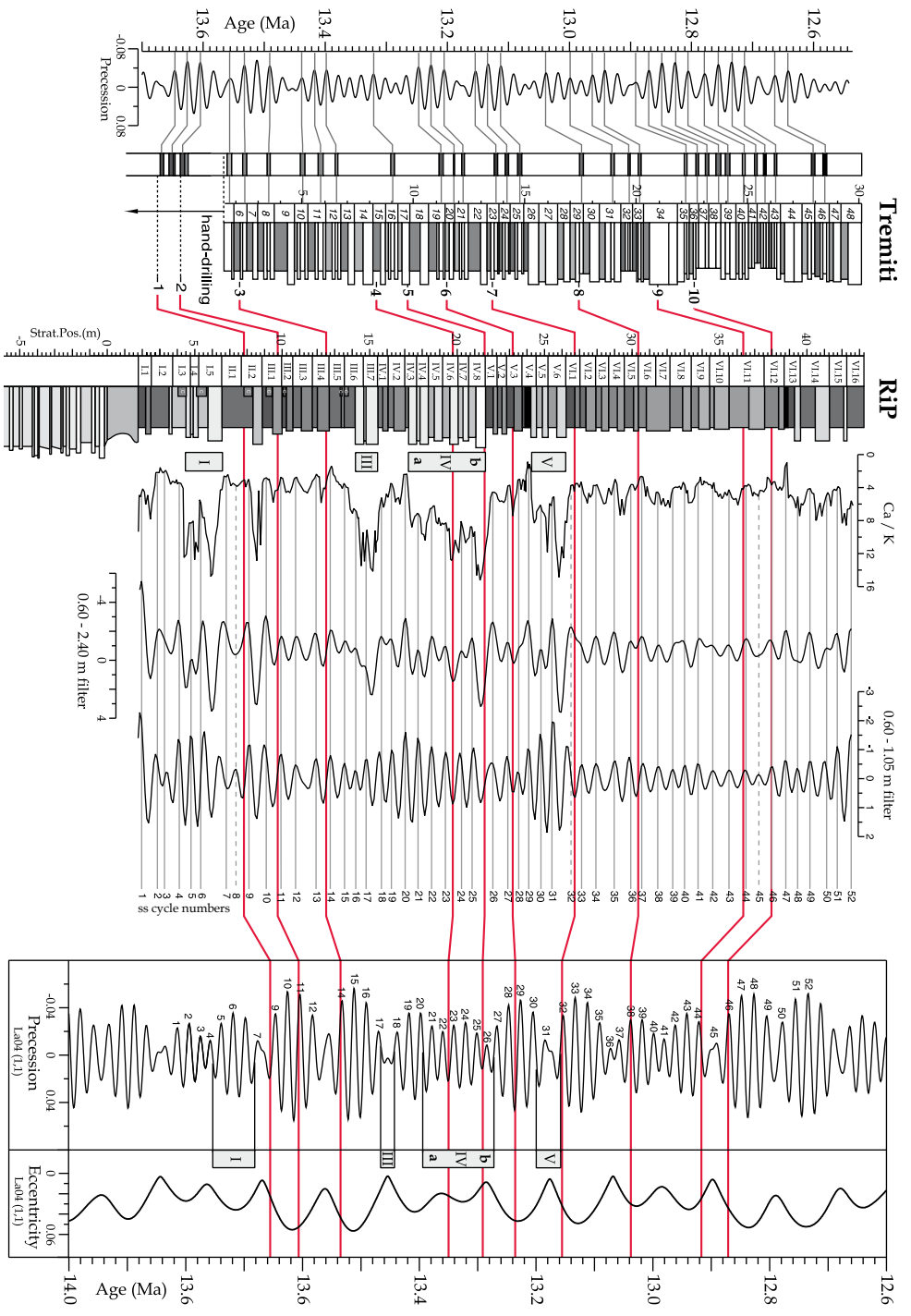
Tremiti
RiP
Age (Ma)
Precession
hand-drilling
Strat.Pos.(m)
Ca / K
0.60 - 1.05 m filter
0.60 - 2.40 m filter
ss cycle numbers
Precession
La04 (1,1)
Eccentricity
La04 (1,1)
I
III
IV
a
b
V

← *Figure 6.8* To the left, tuning of the red layers in the Tremiti section to precession (La04 (1,1) solution; Laskar *et al.*, 2004). In the middle, correlation of 10 bioevents between the Tremiti and the Ras il Pellegrin section (solid lines). To the right, tuning of the small-scale cycles in the Ras il Pellegrin section to precession (La04 (1,1)).

arbitrarily selected, widely spaced bioevents as calibration points. One of these almost identical spectra is shown in Figure 6.4b.

For detailed tuning of the Ras il Pellegrin section to precession we need to know the phase relation between the small-scale cycles and precession. Unfortunately, the detailed biostratigraphic correlations between RIP and Tremiti section do not provide a unique solution.

The two sapropels and the presence of chondrite trace fossils at RIP point to periodically anoxic or sub-oxic conditions during deposition. These sapropels and chondrite beds are almost invariably associated with Ca/K minima and thus with the clayey marl beds (see Fig. 6.3). The basic small-scale cycle in other middle to late Miocene deep marine sections in the Mediterranean consists of an indurated whitish coloured carbonate-rich marl and a softer grey colored carbonate-poor marl. Sapropels, and equivalent reddish layers at Tremiti, develop within the whitish marl when minimum precession forcing is strong enough (see Hilgen *et al.*, 2003). However, occasionally, the part of the whitish marl bed directly underlying or overlying the sapropel lacks sedimentary expression or is not developed (Hilgen *et al.*, 2003). As a consequence, the position of the sapropels/chondrite levels in the RIP section does not provide conclusive arguments for the phase relation of the basic small-scale cycle to precession. Nevertheless, for the moment we assume that the sapropels/chondrite levels correspond to precession minima and hence that also Ca/K minima (and thus grey marl beds) correspond to precession minima and summer insolation maxima. The possibility of an opposite phase relation implies an age uncertainty for the tuned records of at least half a precession cycle.

Furthermore, the relationship between some of the geochemical proxies on the small-scale cycle scale is not always consistent throughout the section. Confirmation about the inferred phase relation may come from future detailed stable isotope measurements on benthic and planktonic foraminifera and quantitative counts of specific planktonic foraminiferal species.

From the lowermost age calibration point, the last common occurrence of *S. heteromorphus*, toward the base of the Blue Clay at RIP the tuning is based on correlating each successive small-scale cycle to successively older precession cycles, apart from the extra thick cycle I.5 that is assumed to contain an extra cycle, as evident from the $\delta^{13}C$ record (Fig. 6.8). This downward extension of the tuning may result in an additional age uncertainty of one precession cycle for the tuning of the lowermost part of the Blue Clay Formation. When combined with the uncertainty in the phase relation with precession this would amount to a total uncertainty of 30 kyr. The entire tuning has not been adjusted to better fit characteristic patterns in the astronomical forcing especially related to precession-obliquity interference, because (1) the phase relation between small-scale cycles and precession needs further confirmation and (2) it is not known which astronomical solution should be used for this time interval in terms of tidal dissipation and dynamical ellipticity values (see Lourens *et al.*, 2001; Hilgen *et al.*, 2003). Nevertheless, applying Blackman Tukey spectral analysis on the tuned Ca/K time series (Fig. 6.4b) resolves the spectral peaks in the precession and obliquity domain much better than in the Blackman Tukey spectra of the age series based on the astronomical ages for bioevents (Fig. 6.4b). However, it should be realized that this improvement is partly a consequence of the tuning itself.

Our tuning of the Blue Clay succession on Malta significantly deviates from the tuning proposed by Sprovieri *et al.* (2002), because they use incorrect astronomical ages for selected bioevents as

starting point for their tuning (Hilgen *et al.*, 2003). Moreover, a poor coherency exists between their $CaCO_3$- and *Globigerinoides* spp. records, while the small-scale cycles are not recorded in a consistent way in the lithology and these proxies. Nevertheless, quantitative counts of the warm water planktonic foraminiferal group of *Globigerinoides* spp. in the Ras il Pellegrin section show lower amplitude variations in the carbonate-rich parts of intervals III and IV, thereby confirming that these intervals correspond to eccentricity minima (see also Sprovieri *et al.*, 2002).

6.9 Discussion

The magnetostratigraphy can now be calibrated to the CK95 or ATNTS04 timescales (Fig. 6.6) confirming the ambiguous nature of the magnetostratigraphy in the uppermost part of Ras il Pellegrin. The tuning provides accurate astronomical ages for five magnetic reversals, thereby extending the astronomical polarity timescale (APTS) based on Mediterranean successions (Table 1). There is an interval of uncertain polarity in the upper part of chron C5AAr, although the reversal (R > N) above this interval is very clear. The stratigraphic position, including uncertainty intervals, of the reversals are given in Table 1. Discrepancies exist in the age and duration of all (sub)chrons between the tuned age model of RIP, the ATNTS2004 and CK95 timescales (Table 1). Confirmation of the newly extended APTS by independently tuned magnetostratigraphies is therefore needed.

The tuning of the RIP confirms that the formation boundary between the Globigerina Limestone and the Blue Clay Formation and the oxygen and carbon isotope shift at this boundary most probably correspond to the second and major step (Mi3b; CM6) in middle Miocene global cooling. This major isotope enrichment event is now astronomically dated at 13.82 ± 0.03 Ma and coincides with a period of minimum amplitudes in obliquity related to the 1.2-Myr cycle and minimum values of eccentricity as part of both the 400- and 100-kyr cycle. This coincidence is very similar to the orbital configuration found for prominent oxygen isotope excursions to heavier values just below the Oligocene-Miocene boundary at 23.13 Ma (Mi-1; Zachos *et al.*, 2001; Billups *et al.*, 2004) and for two excursions at 10.4 and 11.4 Ma (Mi-6 and Mi-5; Turco *et al.*, 2001). A similar orbital configuration during glacial peak excursions has recently been found in the Oligocene (Wade and Pälike, 2004).

The connection between late Cenozoic oxygen isotope excursions and periods of minimum variations in obliquity and precession amplitudes suggests that the 1.2-Myr obliquity cycle and the 100- and 400-kyr eccentricity cycle exerted a prominent control on the factors controlling the size of the Antarctic ice sheet. Most likely, the reduced amplitudes of obliquity and precession (*i.e.*, at times of eccentricity minima) would have prevented significant melting of the ice sheet during the warmer summers at times of obliquity and precession maxima. After the middle Miocene cooling event, the isotope values do not return to values from before that time. This suggests that this peculiar orbital configuration was superimposed on a long-term cooling trend, thereby pushing the climatic system into a colder mode. Vincent and Berger (1985) suggest that atmospheric CO_2 drawdown already started before the middle Miocene, while the cooling step took place at the moment that a threshold was reached. However, several climate proxy records reveal a climate deterioration already from 15 to 14.5 Ma on (*e.g.*, Miller *et al.*, 1991; Shevenell *et al.*, 2004). A climate modelling study of DeConto and Pollard (2003) using a general circulation model, with coupled components for atmosphere, ocean, ice sheet, and sediment, showed that declining Cenozoic atmospheric CO_2 only leads to large ice caps when a threshold is crossed. These ice caps

furthermore show large orbital variations in much the same way as the late Cenozoic ice sheets on the Northern Hemisphere.

To better depict the long-period influence of eccentricity, as amplitude modulator of precession, and the amplitude modulation of obliquity, the bulk isotope records are compared with a target curve (EOA in Fig. 6.9) that combines eccentricity (E) with obliquity amplitude (OA) variations. The EOA curve is the sum of the standardized eccentricity curve and the 100- to 2500-kyr band-pass filter of the positively clipped standardized obliquity curve that describes the envelope of obliquity maxima. We used this envelope because low maxima result in cooler summers at high latitudes that prevent melting and are responsible for substantial ice sheet growth.

The actual major middle Miocene cooling step lags the beginning of the period of minimum amplitude variations in obliquity with approximately 40 kyr and the minimum values in the EOA curve with approximately 20 kyr. The latter difference results from the additional influence of eccentricity in the EOA curve. The age uncertainty of 30 kyr for the tuned ages in the lowermost part of the section is too large to discuss the relationship between the cooling step and the fundamental cycles of precession and obliquity (*i.e.*, 21 and 41 kyr, respectively) in detail. Therefore conclusions can only be drawn concerning the influence of the longer-term modulating cycles of precession and obliquity.

Shevenell *et al.* (2004) investigated the astronomical configuration at times of the middle Miocene climate transition in the South Tasman Rise. Their oxygen isotope record of the benthic foraminifer *Cibicidoides mundulus* reveals a clear picture of the middle Miocene climate transition with the major step toward heavier oxygen isotopes (Mi3b) at around 13.85 Ma, while their Mg/Ca-derived planktonic SST curve shows a gradual stepwise decrease of temperatures starting at around 14.1 Ma. The timing of the major step in middle Miocene global cooling is consistent with our results, although their age model is based on ages of Berggren *et al.* (1995) for bio-, magneto-, and isotope-events (Shevenell and Kennett, 2004). The almost identical ages result from the minor discrepancies between the CK95 and astronomical ages for reversal boundaries in this interval (Table 1). Shevenell *et al.* (2004) were not able to observe a relation between changes in their isotope record and eccentricity due to a lack of cyclostratigraphic control and the absence of an APTS at that time. Moreover, they did not observe a link with the 1.2-Myr obliquity cycle, because their astronomical target curve lacks expression of the distinct 1.2-Myr minimum in obliquity amplitude in this interval. This is rather surprising because they used La2004 to construct their target curve, while a distinct minimum in obliquity amplitudes between 13.85 and 13.6 Ma is clearly present in our La2004-derived target curves and the onset of this minimum coincides with the major step in middle Miocene global cooling (Laskar *et al.*, 2004).

Figure 6.9 shows the bulk carbonate isotope records of Ras il Pellegrin in a global perspective by comparing our records with those of DSDP site 588A (southwest Pacific; Flower and Kennett, 1993) and ODP site 747 (Kerguelen Plateau; Wright and Miller, 1992). The chronology of these open ocean records is rescaled using ATNTS2004 ages (Lourens *et al.*, 2004) for identifiable polarity reversals. The timing and structure of the geographically distant isotope records reveal marked similarities across the middle Miocene climate transition, despite the fact that the isotope signal of the Ras il Pellegrin section is measured on bulk carbonate while the two open ocean isotope records are based on species of the benthic foraminiferal genus *Cibicidoides*. This strongly suggests a global control on isotope records across the middle Miocene climate transition, although the clear stepwise character of the interval before the major transition seems to be recorded differently at various sites in different ocean basins (*e.g.*, Shevenell and Kennett, 2004). At the

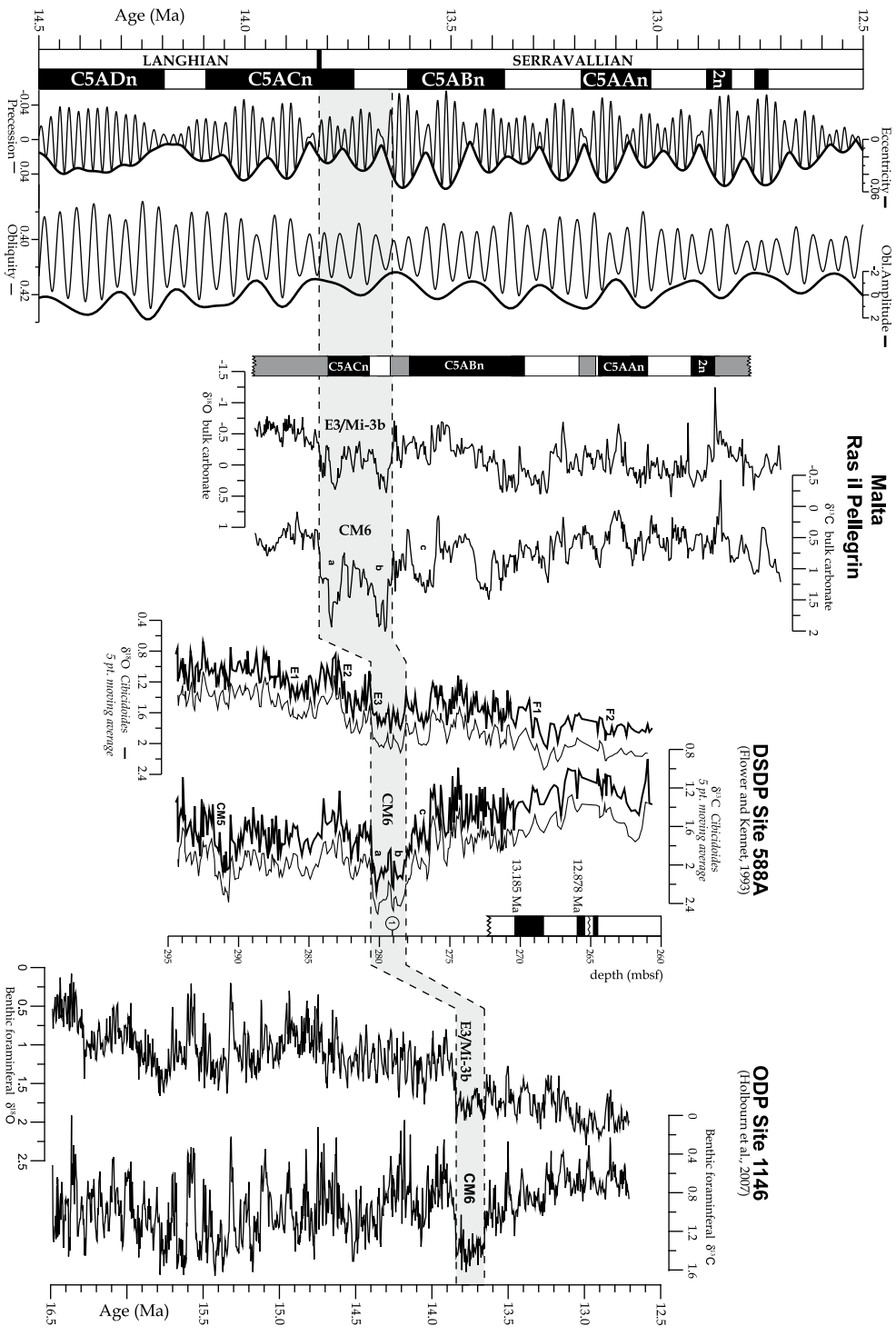
Age (Ma)
LANGHIAN
SERRAVALLIAN
C5ADn
C5ACn
C5ABn
C5AAn
2n
Precession
Eccentricity
Obliquity
Obl.Amplitude
Malta
Ras il Pellegrin
δ13C bulk carbonate
δ18O bulk carbonate
E3/Mi-3b
CM6
DSDP Site 588A
(Flower and Kennet, 1993)
δ13C Cibicidoides
5 pt. moving average
δ18O Cibicidoides
5 pt. moving average
E1
E2
E3
F1
F2
CM5
13.185 Ma
12.878 Ma
depth (mbsf)
ODP Site 1146
(Holbourn et al., 2007)
Benthic foraminiferal δ13C
Benthic foraminiferal δ18O

← *Figure 6.9* Magnetic polarity timescale of the ATNTS2004, precession and its amplitude modulator eccentricity, obliquity, and its amplitude modulator, the EOA target curve (see running text), the magnetostratigraphy of the section, the tuned bulk carbonate isotope time series of Ras il Pellegrin, and the correlation of the bulk isotope stratigraphy to benthos isotope records of Deep Sea Drilling Program (DSDP) Site 588A (Flower and Kennett, 1993) and DSDP Site 747 (Wright and Miller, 1992). The latter two isotope series are given in the depth domain. The age scale to the left of each record has been derived using linear interpolation and extrapolation of sedimentation rates between and beyond selected magnetic reversals, with ATNTS2004 ages of the selected reversals indicated next to the magnetostratigraphy. Isotope events are labeled following Flower and Kennett (1993) and Miller *et al.* (1996).

moment, it is therefore premature to connect the isotope excursion at *ca* 14.2 Ma (Mi3a) to the distinct minimum in the EOA curve of the same age. Independent astronomical age control on different records around the world is needed to substantiate this potential linkage.

The next 1.2-Myr minimum in obliquity amplitudes starts at *ca* 12.83 Ma, *i.e.*, from bed VI.12 upward. However, identical minimal values in the EOA curve as during the middle Miocene global cooling are only reached around 12.6 to 12.5 Ma, so that an isotope enrichment event is expected to occur just above the RIP section of our study (see Fig. 6.9). However, a recently published high-resolution and astronomical tuned isotope record from the SE Atlantic reveals a marked excursion to heavier values around 13.2 Ma, which is not recorded on Malta or in other published records of this interval (Westerhold *et al.*, 2005). Again, this clearly indicates that additional high-resolution and well-tuned benthic isotope records are required to depict Antarctic and Arctic ice growth events.

Finally, the Ras il Pellegrin section is an excellent candidate to define the Serravallian GSSP. The critical interval is continuous, is well exposed, and yields a good magnetic signal, a well-preserved record of microfossils, and bulk sediment stable isotope records framed within an astronomical calibrated age model. The level most suitable for defining the Serravallian GSSP is the middle Miocene global cooling step (Mi-3b). Indeed, this level corresponds with the lithological transition from the Globigerina Limestone to the Blue Clay Formations but field and biostratigraphical data indicate that the succession is continuous across this boundary. This proposed level is only slightly older than the *Sphenolithus heteromorphus* LCO, that at present serves as a guiding criterion for the Langhian-Serravallian boundary (Lourens *et al.*, 2004), but that is demonstrably diachronous between the Mediterranean (at 13.654 Ma; this study) and the equatorial Atlantic (at 13.523 Ma; Backman and Raffi, 1997).

6.10 Conclusions

The major step in middle Miocene climate cooling, characterized by a global shift to heavier $\delta^{18}O$ and $\delta^{13}C$ values (Mi3b and CM6, respectively), occurred at 13.82 ± 0.03 Ma and coincides with the beginning of a period of minimum amplitude variations in obliquity related to the 1.2-Myr and 172-kyr cycles, and with prominent minima in the 100- and 400-kyr eccentricity cycles. This peculiar orbital configuration is similar to that found for other prominent cooling events in the Oligocene and Miocene and is particularly evident in a new astronomical target curve (EOA) that combines the amplitude modulators of precession and obliquity. In particular, the coincidence of minima in the amplitude modulation of precession and obliquity seems imperative to punctuate global climate on a million year timescale or even to invoke irreversible global climate changes.

In the middle Miocene this remarkable orbital configuration may thus have triggered the climate cooling step by crossing a certain threshold and/or determined the exact moment of the cooling step that occurred superimposed on a longer-term cooling trend. The compilation and comparison of high-resolution, astronomically tuned proxy records over the middle Miocene climate transition is necessary to further unravel the causes and consequences of this major cooling step.

In addition to a better understanding of the middle Miocene cooling, the Ras il Pellegrin section on Malta has proven to be of importance for two other aspects as well. The first aspect is the good magnetic signal by which the Astronomical Polarity Time Scale (APTS) is extended down to the top of the C5ACn chron, showing discrepancies of less than 120 kyr with existing CK95 and ATNTS2004 timescales. The second aspect is that the Ras il Pellegrin section is suitable for defining the Serravallian GSSP, linking this stage boundary to a well-defined and globally synchronous oxygen and carbon isotope event.

6.11 Ackowledgements

The authors wish to thank G. Debono of the Maltese Oil Exploration Department and G. Maempel Zammit of the Ghar Dalom Cave and Museum for the working permissions. G. Maempel Zammit is also thanked for bringing the excellent Ras il Pellegrin section to our attention. A. Pace of the Superintendence of Cultural Heritage is thanked for understanding the need of research in order to show the value of a certain area. We hope that our work will contribute to the cultural heritage of the Maltese archipelago by demonstrating the suitability of the Ras il Pellegrin section for formally defining the Serravallian-Tortonian boundary at the base of the Blue Clay Formation. Silvia Iaccarino, Fabrizio Lirer, and Wanda Link are acknowledged for their help in the field, and Jiovanna Jiannelli, Gerrit van 't Veld, and Geert Ittman are acknowledged for biostratigraphical sample preparation. We would like to thank L. J. Lourens for helpful comments and two anonymous reviewers for their critical review and good suggestions, that improved the manuscript.

CHAPTER 7

Obliquity-dominated glacio-eustatic sea level change in the early Oligocene: evidence from the shallow marine siliciclastic Rupelian stratotype (Boom Formation, Belgium)

Hemmo A. Abels, Stefaan Van Simaeys, Frederik J. Hilgen, Ellen De Man, Noël Vandenberghe

Based on:
H.A. Abels, S. Van Simaeys, F.J. Hilgen, E. De Man, and N. Vandenberghe, 2007. Obliquity-dominated glacio-eustatic sea level change in the early Oligocene: evidence from the shallow marine siliciclastic Rupelian stratotype (Boom Formation, Belgium). *Terra Nova* 19, 65-73, doi. 10.1111/j.1365-3121.2006.00716.x.

7.1 Abstract

Our results prove that glacio-eustatic sea level oscillations in the early Oligocene were dominantly obliquity controlled with additional influence of the *ca* 100- and 405-kyr eccentricity cycles. This was derived from spectral analysis of resistivity records from an extended downhole section of the Boom Clay succession in Belgium, that reveals a prevailing obliquity control on the laterally persistent metre-scale alternations of shallow marine silt- and claystones in the Rupelian historical stratotype succession. These direct measurements of sea level variations in a shallow marine setting corroborate that variations with similar frequencies in benthonic oxygen isotope records from the open ocean indeed reflect, at least partly, ice volume change. A very tentative astronomical tuning has been established for the Boom Clay succession which awaits future confirmation with the addition of more accurate age calibration points.

7.2 Introduction

The transition from the Eocene greenhouse world to the Oligocene glaciated state is one of the more dramatic shifts in Cenozoic climate evolution. During the early Oligocene global cooling resulted in the development of a significant Antarctic cryosphere (*e.g.*, Lear *et al.*, 2000) and the onset of marked cyclicity in ice volume. Evidence for high-frequency glacial cycles comes from benthic $\delta^{18}O$ records in the open ocean that point to a control by the 41-kyr obliquity cycle, and 110- and 405-kyr eccentricity cycles (Wade and Pälike, 2004). However, these records reflect both deep water temperatures and ice volume, besides other possible factors such as changes in ocean circulation. Independent estimates of bottom water temperature using Mg/Ca ratios were made in order to deduce the ice volume part in oxygen isotope records (Lear *et al.*, 2000). Alternatively,

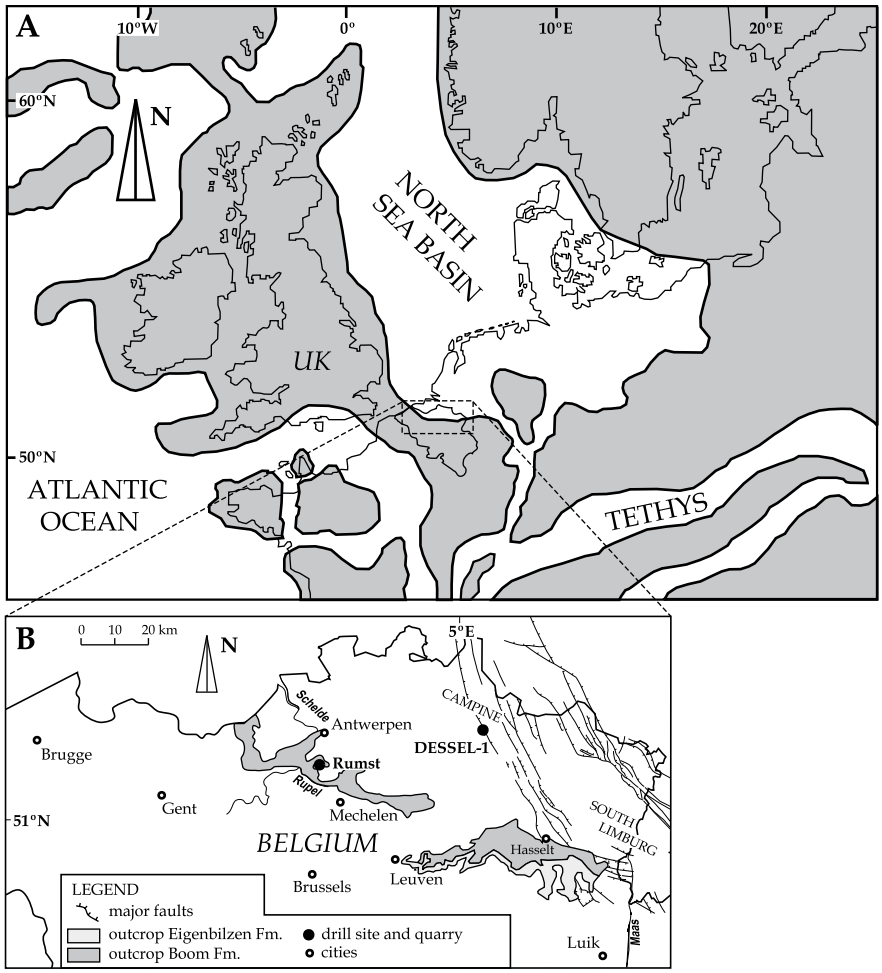

Figure 7.1 (A) Paleogeographical reconstruction of the North Sea Basin during early Oligocene times. (B) Locality map of the Dessel borehole site, the Swenden quarry in Rumst and outcrop area of the Boom Formation.

shallow marine settings can be studied to unravel the imprint of glacio-eustatic sea level variability, avoiding the indirect calibration of the ice volume variations (Pekar *et al.*, 2002).

A suitable shallow marine location to study high-frequency early Oligocene glacial cyclicity is the siliciclastic Boom Formation in Belgium. The Boom Clay is characterized by laterally persistent lithological alternations between silt and clay. These metre-scale sequences have been ascribed to sea level fluctuations that control the amount of sorting on the sea floor by varying the wave base (Vandenberghe, 1978; Van Echelpoel and Weedon, 1990; Vandenberghe *et al.*, 1997, 2001). Statistical analysis of lithology proxies in the outcrop area pointed at an astronomical control on the regular basic silt – clay sequence, which was attributed to the 100-kyr eccentricity cycle (Van Echelpoel and Weedon, 1990; Vandenberghe *et al.*, 2001). Recent drilling of the Lower Oligocene stratotype succession substantially lengthened the known stratigraphic record of the Boom Formation (Van Simaeys *et al.*, 2004) and produced high-quality proxy records for lithology,

providing an excellent opportunity to re-examine the astronomical origin of the sedimentary cyclicity and glacio-eustatic sea level fluctuations during the early Oligocene.

7.2.1 Geological setting and stratigraphic framework

The studied lower Oligocene Boom Formation was deposited in the southern part of the North Sea Basin, a slowly subsiding epi-continental basin bordered by the Fenno-Scandian Shield to the northeast, Central Europe to the south, and the British Isles to the west (Ziegler, 1990; Fig. 7.1). The siliciclastic deposits predominantly consist of shallow marine, coastal to outer shelf sediments and their outcrop area constitutes the main body of the Rupelian historical stratotype (Fig. 7.2; Luterbacher *et al.*, 2004; Van Simaeys *et al.*, 2004). The overall Boom Formation has a thickness of 150 m in the subsurface of the Campine blocks, of which only the lower 43 m are exposed in the Rupel area (Fig. 7.3).

Accurate age calibration of the Rupelian deposits to the Geologic Time Scale (GTS04; Gradstein *et al.*, 2004) remains a moot point because of the near absence of age-indicative planktonic calcareous microfossils, and uncertainties around paleomagnetic results (Lagrou *et al.*, 2004). The last occurrence (LO) of nannoplankton species *Reticulofenestra umbilica* positions the NP22/NP23 boundary just below the base of the Boom Formation (Steurbaut, 1992); this event has an age of *ca* 32.4 Ma in GTS04 (Luterbacher *et al.*, 2004). Towards the middle of the succession two distinct dinocyst events nearly coincide: the first occurrence (FO) of *Saturnodinium pansum* and the LO of common *Enneadocysta pectiniformis* (Van Simaeys *et al.*, 2005a), both dated at 29.18 Ma according to Luterbacher *et al.* (2004). The FO of *Distatodinium biffii* calibrated at 28.43 (Luterbacher *et al.*, 2004) is found higher up in the succession (Van Simaeys *et al.*, 2005a). Dinocyst calibration between the North Sea Basin and the central Italian sections shows that the Rupelian/Chattian unconformity in the stratotype area marks a hiatus covering the interval from around 27.5 to 27.0 Ma according to Van Simaeys *et al.* (2005b). Sedimentation of Chattian sediments is thought to start at around 26.8 Ma (Van Simaeys *et al.*, 2005b). New strontium isotope ages indicated in Figure 7.2 are briefly explained in the Methods section.

7.2.2 Lithology

The Boom Formation is characterized by a rhythmic alternation of silt and clay layers. A sinusoidal variation in grain size is present with the largest proportion of coarse grain sizes in the middle of the silt bed. The amount of organic matter, mainly of terrestrial origin (Vandenberghe, 1978; Vandenberghe *et al.*, 1997; Laenen, 1998), increases abruptly at the base of the Putte Member (Fig. 7.2). Individual organic-rich layers occur after a silt bed in the basal parts of a clay bed. Clay mineral analysis revealed that the illite, chlorite and smectite content varies in harmony with grain size, while the kaolinite content shows an opposite distribution. This aims at a more basinal origin of the clay minerals during the deposition of the clay beds, and a more coastal origin during the deposition of the silts (Laenen, 1998). The stratigraphic position of carbonate-rich layers, that evolved into septaria horizons, does not show any relationship with grain size, clay mineral distribution and organic matter, suggesting a sedimentary rather than a diagenetic origin (Vandenberghe *et al.*, 1997; Fig. 7.2).

7.2.3 Sedimentological interpretation

The lateral persistence of the individual silt-clay sequences (Vandenberghe *et al.*, 2001) requires a forcing mechanism that exerts a simultaneous influence over the entire basin at the same time. Sea

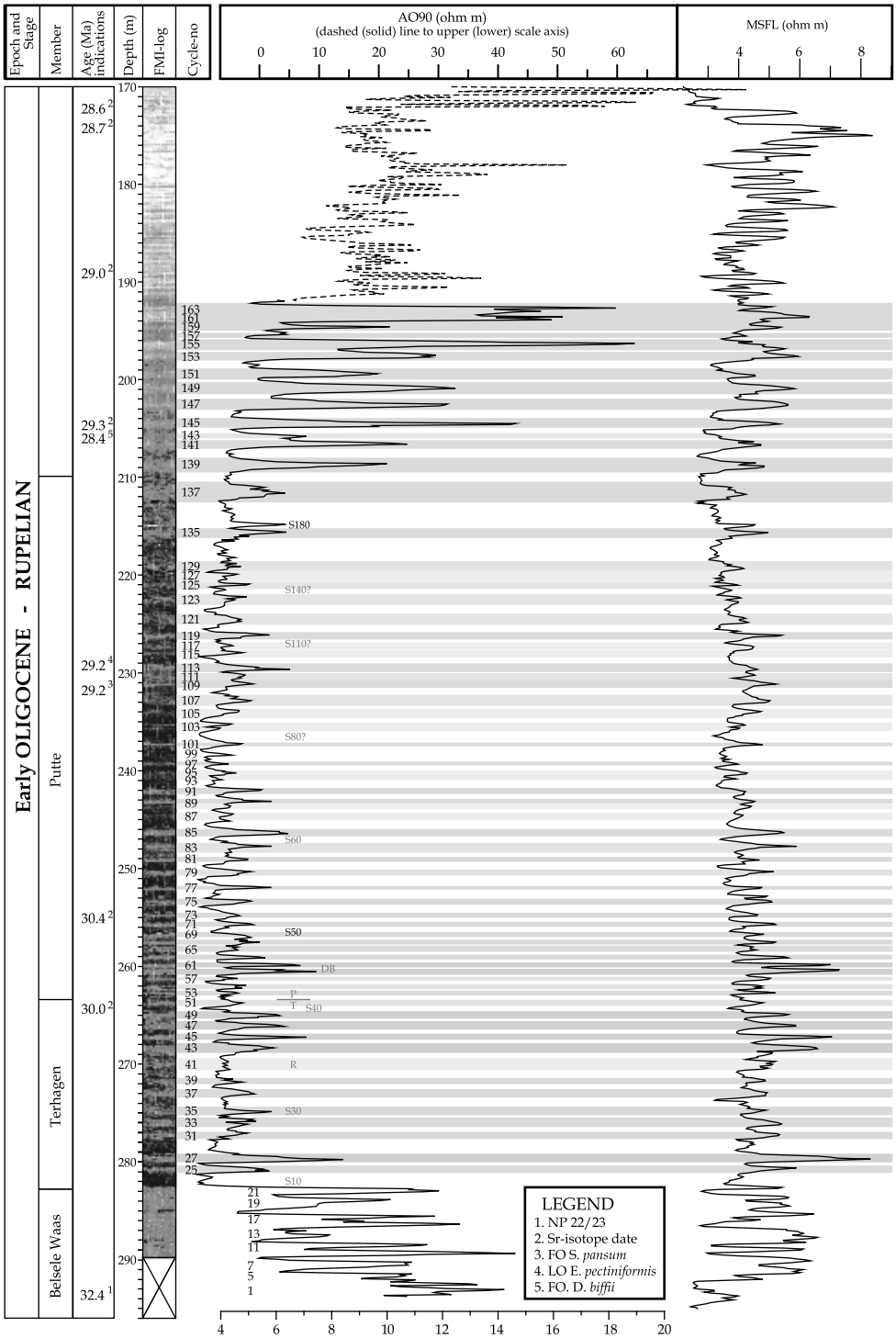
Epoch and Stage
Member
Age (Ma) indications
Depth (m)
FMI-log
Cycle-no
AO90 (ohm m)
(dashed (solid) line to upper (lower) scale axis)
0 10 20 30 40 50 60
MSFL (ohm m)
4 6 8
Early OLIGOCENE - RUPELIAN
Putte
Terhagen
Belsele Waas
28.6 2
28.7 2
29.0 2
29.3 2
28.4 5
29.2 4
29.2 3
30.4 2
30.0 2
32.4 1
170 180 190 200 210 220 230 240 250 260 270 280 290
163 161 159 157 155 153 151 149 147 145 143 141 139 137 135 129 127 125 123 121 119 117 115 113 111 109 107 105 103 101 99 97 95 93 91 89 87 85 83 81 79 77 75 73 71 69 65 61 57 53 51 49 47 45 43 41 39 37 35 33 31 27 25 21 19 17 13 11 7 5 1
S180
S140?
S110?
S80?
S60
S50
DB
P
T
S40
R
S30
S10
LEGEND
1. NP 22/23
2. Sr-isotope date
3. FO S. pansum
4. LO E. pectiniformis
5. FO. D. biffii
4 6 8 10 12 14 16 18 20

← *Figure 7.2* The FMI, AO90 and MSFL resistivity records of the Dessel-1 borehole covering the Rupelian stage. Important bio-stratigraphical events are shown with their inferred age. Successive highs (lows) in the AO90 record are labelled with an odd (even) number. In black the name of septaria horizons that were recognized in the borehole data and in grey other septaria horizons known from the Boom Clay. The latter were pinpointed in the Dessel stratigraphy by bed-to-bed correlation with other borehole and outcrop data of the same interval (see also Vandenberghe *et al.*, 2001). Ages are from Luterbacher *et al.* (2004; age 1, 3, 4 and 5). Strontium isotope dates are explained in Methods section (ages 2).

level variation influencing the amount of sorting by varying the wave base is the most plausible process that can account for this (Vandenberghe *et al.*, 1997, 1998). The more basinal origin of the clay minerals deposited in the clay beds during supposed sea level high-stands corroborates this mechanism. Accordingly, the terrestrial organic matter is then deposited during the transgressive part of the sequence (in the basal part of the clay beds) as a result of reworking of the vegetation cover of the flooded land, while the clay mineral assemblage indeed points to a more coastal origin during deposition of the silt beds during times of sea level low-stands. The supposed mechanism of sea level variations triggering the lithological variations fits all observations. A more regional mechanism as changes in run-off or in sediment load would produce local differences in the Boom succession that are not present. The origin of the marly beds however remains poorly understood.

The Boom Clay succession can thus be seen as an archive of early Oligocene glacio-eustatic sea level fluctuations, also because high-frequency sea level variability is not expected to be of (local) tectonic origin (Miller *et al.*, 2005).

7.3 Methods

Statistical analysis was performed on the AO90 and MSFL resistivity records of the Dessel-1 borehole (for location see Fig. 7.1). This borehole was selected for its higher resolution compared to other investigated boreholes and the presence of a Fullbore Formation Micro-Imager (FMI) log (Fig. 7.2). The Micro-Spherically Focused Log (MSFL) has a depth of investigation/analysis from between 2.5 to 15 cm, while the high-resolution deep laterolog measurement (AO90) has a depth of investigation of 300-400 cm.

The resistivity records are an accurate proxy for the silt-clay alternations in the Boom Formation, exhibiting higher values in the silt beds (Vandenberghe *et al.*, 2001). Carbonate contents in the clay did not influence the periodicity analysis. As a minor background component, calcite is present only in the short interval between the septaria levels S10 and S30. In the other parts of the section only septaria horizons are present of which the stratigraphic positions are well known. Of these only S180 (Fig. 7.2) exhibits a signal in the used resistivity records. The presence of some carbonate will possibly only slightly increase the noise in the spectral analysis.

The two resistivity logs show a distinct offset for the coarse-grained sediments in the lower Belsele-Waas Member and the upper sandier unit, which is the reflection of higher permeability in the coarser sediments. For the statistical analysis the interval between 212 and 282 m in the Dessel-1 borehole has therefore been selected because above and below distortion by increasing amounts of sand occurs. The lack of conspicuous intervals that could point to erosional levels and the extreme lateral continuity indicate that the succession within the selected interval is continuous, at least until the level of the basic silt-clay sequences.

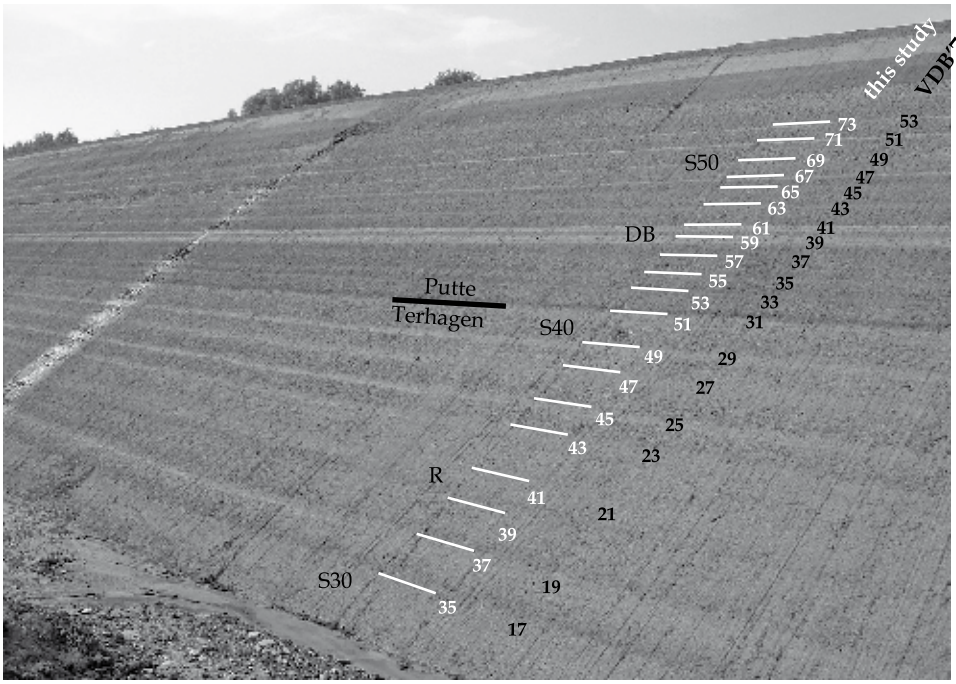

Figure 7.3 Photograph of a Boom Clay outcrop section in the Swenden quarry in Rumst, Belgium, which is located 45 km to the WSW of Dessel (Fig. 7.1). Light (dark) horizons represent silt (clay) beds. White lines indicate successive upper limits of a clay-silt couplet. The white numbers represent successive clay-silt alternations as numbered in the Dessel borehole (Fig. 7.2). The black cycle numbers indicate the numbering of Vandenberghe (1978). Septaria horizons recognized in the quarry are indicated, as well as the so-called double band (DB) and red layer (R). The Terhagen to Putte member transition is based on the rapid increase in preserved organic matter and can be recognized over large distances (Vandenberghe *et al.*, 2001).

The statistical analysis was carried out with the Analyseries program version 1.1.1 of Paillard *et al.* (1996) with compromise settings on the number of lags and percentage of the series. Subsequently, the Blackman-Tuckey power spectral analysis was applied using a Barlett window.

Age assessment by means of strontium isotope stratigraphy was performed by measuring the 87Sr/86Sr ratio of benthic foraminifera from nine horizons and evaluating it to the secular variation curve for Oligocene marine waters using the procedure of McArthur *et al.* (2001; ages derived from Look-Up Table, Version 4).

7.4 Results

7.4.1 Statistical analysis

The spectral analysis performed on the selected interval of the AO90 and MSFL depth records reveals spectral power in both resistivity records at periods around 1.13 and 1.45 m (Fig. 7.4A, B). Bandpass filtering of these periods shows that they are related to the basic silt-clay sequences (Fig. 7.5). In addition, a 3.65-m peak is present in both resistivity records and a 14-m peak in the

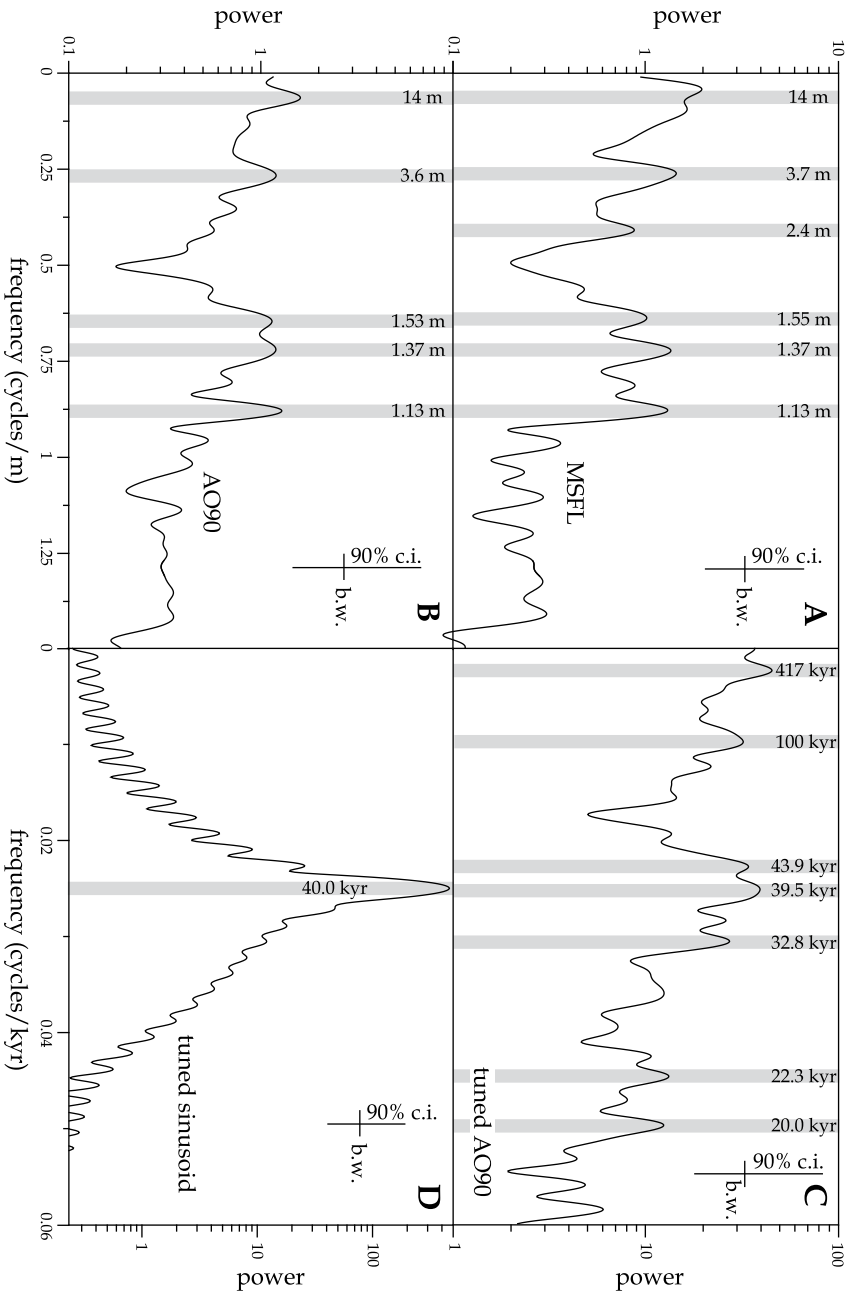

Figure 7.4 Blackman-Tuckey (BT) power spectra of the (a) MSFL and (b) AO90 resistivity records between 212 and 282 m in the Dessel borehole, and (c) of the tuned AO90 record in the time domain. Grey shades indicate distinct spectral peaks. (d) Power spectrum of a sinusoid tuned to the same interval of the obliquity target curve by using the identical tie-points as for the AO90 tuning. 90% confidence intervals (c.i.) and bandwidth (b.w.) are indicated with vertical and horizontal lines respectively.

power spectrum of AO90. Filtering these peaks shows that the 3.65 m peak reflects bundles of two or three basic sequences and the 14 m peak in AO90 reflects intervals of more and less silty beds (Fig. 7.5).

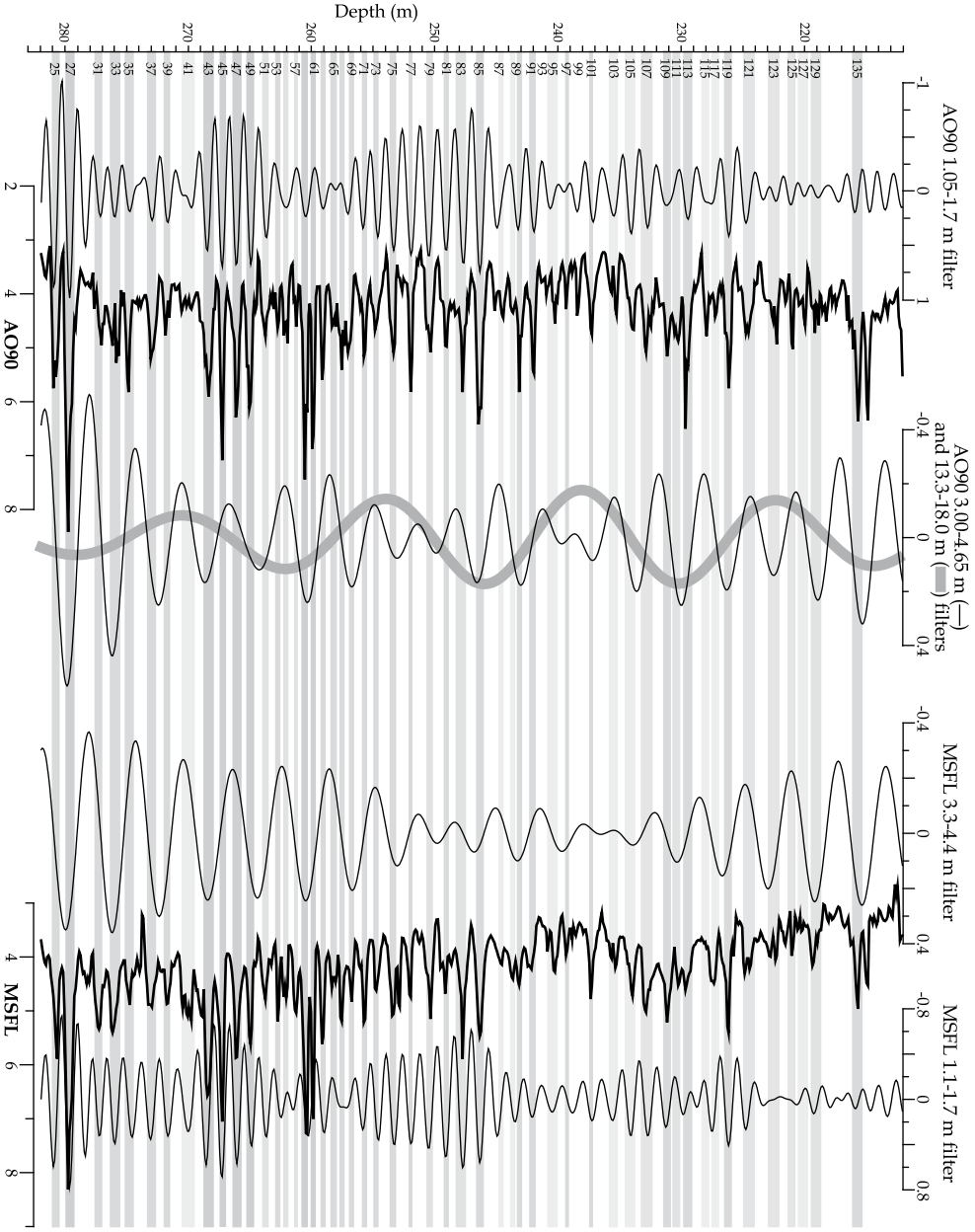

Figure 7.5 AO90 and MSFL resistivity records and their high- and low-frequency bandpass filters. Filtered intervals relate to distinct spectral peaks in the spectral analysis of the depth proxy series. To the left small-scale cycle numbers are indicated. Higher amplitudes in filters indicate periods of dominance of that period.

7.4.2 Astronomical forcing

Spectral analysis of depth series results in power spectra that may be distorted by diagenetic processes and bioturbation and by changes in sedimentation rate related to long-term trends and amplification of the astronomical forcing (Fischer *et al.*, 1991; Herbert, 1994; Van der Laan *et al.*, 2005). Power spectra of depth series that contain distinct peaks reveal important information about cyclic forcing mechanisms, even if age control is limited, by comparing spectral peaks with astronomical frequency ratios. In case of the Boom Clay succession, bandpass filtering of the distinct spectral peaks reveals that these three major periodicities are present throughout the studied interval (Fig. 7.5). Therefore a relatively constant sedimentation rate can be expected, while the separation of for example the 1.45 m peak into a 1.13, 1.37 and 1.54-m peak may be caused by small variations in sedimentation rate. The consistent regular cyclicity in a long interval is an argument for astronomical forcing of the sedimentary alternations (Van Echelpoel and Weedon, 1990). Moreover, there is a close resemblance of the ratio of 1: 2.8: 9.7 between the distinct spectral peak periods and the ratio of 1: 2.65: 9.9 for the astronomical frequencies of obliquity (41-kyr) and short- (95- and 123-kyr) and long-term (405-kyr) eccentricity, which provides the final convincing argument for astronomical forcing of the Boom Clay lithological cyclicity.

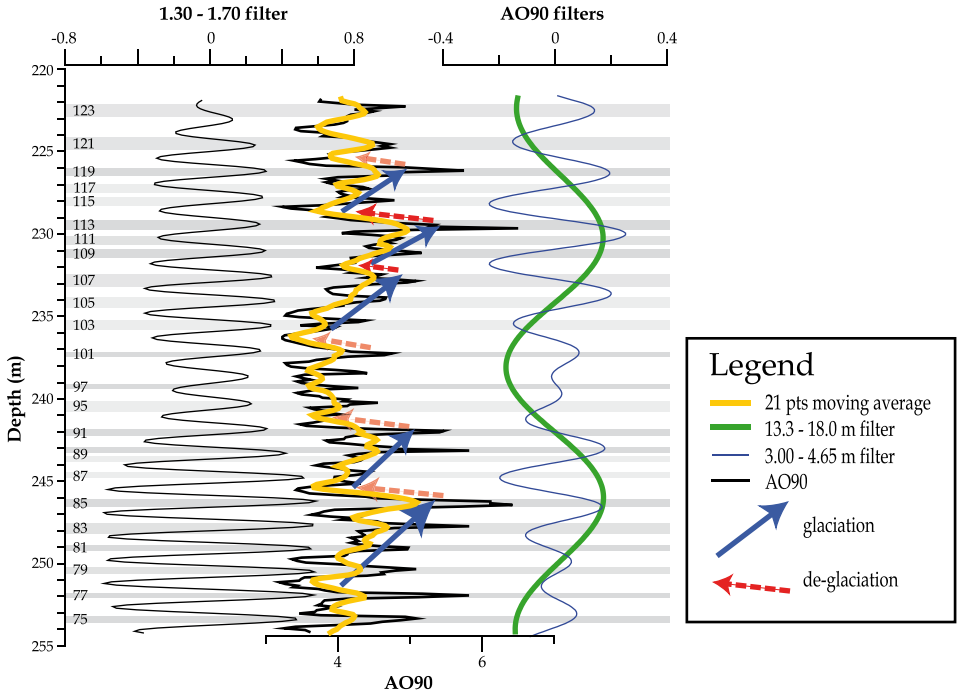

Figure 7.6 Detail of the Dessel stratigraphy showing the AO90 resistivity record, its 21-point moving average, and the 1.30-1.70, 3.00-4.65 and 13.3-18.0 m filters of the record. Blue (dashed red) arrows indicate gradual increasing (decreasing) grain size. A pattern of gradual increasing ice volume and fast deglaciations can be recognized, due to the interplay of obliquity with *ca* 100- and 405-kyr eccentricity. To the left small-scale cycle numbers are shown.

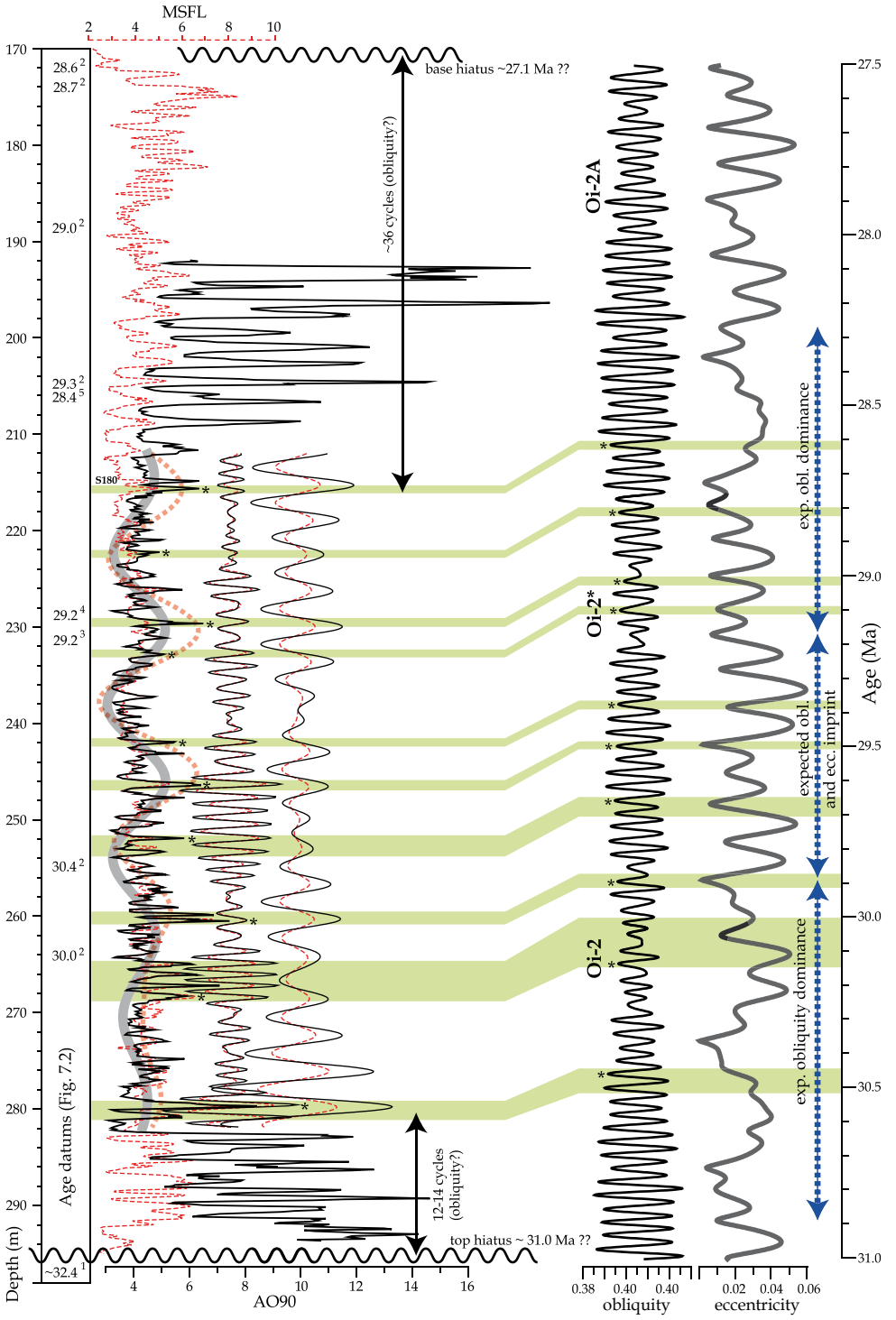
MSFL
2
4
6
8
10
base hiatus ~27.1 Ma ??
~36 cycles (obliquity?)
Oi-2A
Oi-2*
Oi-2
exp. obl. dominance
expected obl. and ecc. imprint
exp. obliquity dominance
Age (Ma)
27.5
28.0
28.5
29.0
29.5
30.0
30.5
31.0
Depth (m)
170
180
190
200
210
220
230
240
250
260
270
280
290
28.6 2
28.7 2
29.0 2
29.3 2
28.4 5
δ18O
29.2 4
29.2 3
30.4 2
30.0 2
~32.4 1
Age datums (Fig. 7.2)
12-14 cycles (obliquity?)
top hiatus ~ 31.0 Ma ??
4
6
8
10
12
14
16
AO90
0.38
0.40
0.40
obliquity
0.02
0.04
0.06
eccentricity

← *Figure 7.7* Tuning of the AO90 and MSFL (dashed record and filters) resistivity record of the Dessel borehole to the Laskar *et al.* (2004) obliquity target curve (grey lines) using available age datums (superscript refers to identical legends in Fig. 7.2). Dashed arrows show intervals where the astronomical target curves suggest periods of forcing dominance of obliquity or obliquity and eccentricity. Ages of the top of the lower hiatus and base of the upper hiatus were calculated by counting small-scale cycles that however may not continue to be obliquity cycles in those intervals. For the top interval, the cycle pattern of nearby well-logs is also used. Asterisks indicate used age tie-points for the time-series analysis. Indicated Oi-events are from Wade and Pälike (2004).

7.4.3 Obliquity control

Obliquity control (41-kyr) of the approximately 50 silt-clay sequences in the studied part of the Boom Clay succession (Fig. 7.5) results in a time span of 2050 kyr for the studied interval, which is in agreement with the known age constraints (Fig. 7.2). If precession would be designated to the basic sequence, only 1050 kyr would be present in the interval. This duration fits within the limits of the age constraints although it would be short and hiatuses that bound the succession remarkably long. However, the ratio of the spectral peaks does not at all resemble astronomical forcing (Fig. 7.4). Designation of eccentricity would account for a duration of 5 Myr, which is impossible for the studied interval considering the available age constraints (Fig. 7.2). The lithological cyclicity is thus dominantly controlled by obliquity forcing on sea-level fluctuations with additional imprint of the *ca* 100- and 405-kyr eccentricity cycles. Our interpretation of the astronomical forcing in the Boom Clay differs from previous studies that attributed the basic sequence to short-term eccentricity instead of obliquity (Van Echelpoel and Weedon, 1990).

7.5 Discussion

7.5.1 Early Oligocene glacial cyclicity

Our results confirm that the high-frequency variations in the benthic oxygen isotope record in the equatorial Pacific (Wade and Pälike, 2004) indeed partially reflect ice volume changes of the incipient Antarctic ice sheet and that these variations are controlled by obliquity and *ca* 100- and 405-kyr eccentricity orbital cycles. Unfortunately, no quantitative estimates of absolute sea level variations can be derived from the Boom Clay deposits.

The lower part of the Boom Formation is characterized by a more dominant obliquity signal, while towards the upper part the imprint of eccentricity becomes more prominent (Fig. 7.5). In Figure 7.6 a detail of the upper part is shown to visually depict the interplay between obliquity and *ca* 100- and 405-kyr eccentricity in the Early Oligocene eustatic sea-level variation. Gradual increases in grain size (blue arrows in Fig. 7.6) end rather abruptly with sudden decreases (red arrows). This strongly suggests a gradual increase in ice volume and hence a slow sea level lowering followed by rapid deglaciation and sea level rise, which show remarkable similarities with the late Pleistocene glacial history.

At around 240 m (Fig. 7.6) twice as many silt-clay alternations are present as expected from the normal obliquity forced cyclicity, as can be seen in the 1.30-1.70 m filter. We tentatively interpret these alternations as being related to precession forcing, although spectral analysis in the depth domain does not reveal a distinct peak that can be related to the precession band (Fig. 7.4A, B). However, Van Echelpoel and Weedon (1990) did find a cycle with half the length of the basic silt-clay sequence in the Boom Clay that probably reflects this kind of precession related alternations.

The presence of precession related cycles is to be expected in this particular interval because it coincides with a 400-kyr eccentricity maximum.

7.5.2 Astronomical tuning

Ideally the Boom Clay succession would be tuned to astronomical target curves, providing astronomical age control that ties the Rupelian historical stratotype to the geological time scale. For a tuning, characteristic patterns in the target curves and proxy records and at least one highly reliable age calibration point have to be present. However, the age calibration points for the Rupelian succession lack precision. The present age data serve as a starting point for a very tentative tuning that correlates the prolonged sea level low-stand from bed numbers 43 to 61 to the 405-kyr eccentricity and 1.2-Myr obliquity minima at 30.0 Ma (Fig. 7.7), following the results of other authors regarding the phase-relation of sea level low-stands to 41-kyr and 1.2-Myr obliquity minima and *ca* 100- and 405-kyr eccentricity minima (Wade and Pälike, 2004; Abels *et al.*, 2005) For the tuning subsequently every next silt bed (sea level low-stand) was correlated with the next obliquity minimum.

The whole tuning may have to be shifted one, or maybe even two, 405-kyr eccentricity cycles older or younger if more precise age calibration points become available, even though available age tie-points fit well with this provisional tuning. Note that the tuning reveals a consistent relation of coarser intervals (sea level low-stands) with *ca* 100- and 405-kyr eccentricity minima, although the used tuning procedure only correlated individual small-scale cycles with obliquity. The AO90 depth series is transformed to a time series by using a limited number of age tie-points (* in Fig. 7.7). The power spectrum of this time series shows peaks that correspond to 41.7, 100 and 417 kyr periods (Fig. 7.4C), while some power is also present at precession frequencies. In addition, we tuned a simple sinusoid to the same interval of the obliquity curve using the same tie-points to check the amount of spectral power we introduced to the AO90 depth series by tuning it to an astronomical target curve and so constructing the time series. When the power spectra of the two time series are compared (Fig. 7.4C, D) the *ca* 100- and 405-kyr peaks in the Boom Clay spectrum stand out very clearly, again indicating the presence of these periodicities in the early Oligocene sea level archive of the Boom succession.

7.6 Conclusions

Spectral analysis of borehole resistivity records indicates that shallow marine lithological sequences in the early Oligocene Boom Clay succession reflect glacio-eustatic sea-level variations that are primarily driven by the 41-kyr obliquity cycle. In addition, a secondary imprint of *ca* 100- and 405-kyr eccentricity has been identified. These cycles reflect changes in Antarctic ice volume and demonstrate that high-frequency variations recognized in open ocean benthic $\delta^{18}O$ records indeed partly reflect ice volume. Furthermore, it could be shown that glaciations tended to grow slowly, and ended rather abruptly. A provisional astronomical tuning is provided using present age calibration points and correlation of subsequent sea level low-stands with obliquity minima. This tuning clearly shows the presence of *ca* 100- and 405-kyr eccentricity cyclicity in the glacio-eustatic sea level archive of the Boom Clay, and the presence of some precession-related variations.

7.7 Ackowledgements

Henk Brinkhuis is thanked for critical reading of an earlier version of the manuscript and for helpful discussions. NIRAS is greatly acknowledged for providing the resistivity data of different boreholes. E.D.M. acknowledges the support of the Belgian Science Policy (Grant WI/36/C03). Strontium isotope analyses were performed at the Royal Holloway University (UK), under supervision of M. Thirlwall and S. Duggen. Two anonymous reviewers are thanked for their constructive comments.

CHAPTER 8

Synopsis

8.1 Synthesis

The results presented in this thesis substantiated that long-period obliquity climate forcing played a major role in the timing of the middle Miocene global cooling as recorded in marine sediments on Malta. Our results of the Madrid in Spain reject the imprint of this long-period obliquity forcing on the Miocene infill. Nevertheless, the formation-scale genetic red bed – limestone sequences in this continental basin might be related to low frequency eccentricity cyclicity. The data from the Late Miocene infill of the continental Teruel Basin reveal a similar orbital configuration for the transition from red bed to limestone sediments as in the Madrid Basin. However, enhanced sediment supply related to the entrance of an axial fluvial system time-equivalent at the other basin margin would rather suggest a local tectonic or geomorphic origin of the transition rather than climate change. The record of the shallow marine succession of the Boom Clay Formation is too short and poorly dated to investigate the presence of low frequency astronomically forced variability, although high frequency orbital cyclicity are clearly present. In the following, a synthesis of these two continental and two marine case studies will be presented in light of the long-period orbital control hypothesis.

8.1.1 Teruel Basin

The southern Teruel Basin (Fig. 4.1) exhibits excellent outcrops that are shown to be ideal for investigating the interplay between the different allogenic and autogenic forcing mechanisms that exist in continental, endorheic basins (Chapters 2 to 4). In this segment of the basin, at least five genetic sequences of middle to late Miocene age have been recognised (Anadón *et al.*, 1997; Ortí *et al.*, 2003). Here, we focussed on one sequence only of Late Miocene age, because detailed and time consuming stratigraphic and sedimentologic studies were required (Chapter 2 and 3) to analyse the geologic history and origin of this large-scale sequence (Chapter 4). Moreover, magnetostratigraphic studies to a succession upwards near Villastar (Fig. 3.1; H. Abdul Aziz, personal communication, 2006) and the Fuente Curria section stratigraphically downwards near Cascante del Rio (Fig. 8.2; unpublished results) did partly not produce a reliable paleomagnetic signal and partly not produce a characteristic polarity reversal pattern to accurately date these sediments. The Fuente Curria section, located just south of the Cascante composite section (Fig. 4.1), contains three subsequent genetic sequences, the uppermost of which is similar to that studied in the Cascante section (Fig. 8.1). The two older sequences contain respectively the Bolage limestone and the Libros gypsum unit (Ortí *et al.*, 2003). Further south, the Ademuz section is another suitable candidate section that contains two genetic sequences. This section is not studied at all due to lack time (Fig. 8.2).

In Chapter 4, we explicitly discuss the forcing mechanism behind the Cascante limestone sequence. Two detailed sedimentologic and magneto- and cyclostratigraphic studies in the Cascante (Chapter 2) and Prado (Chapter 3) areas allow to place the sediment records in a

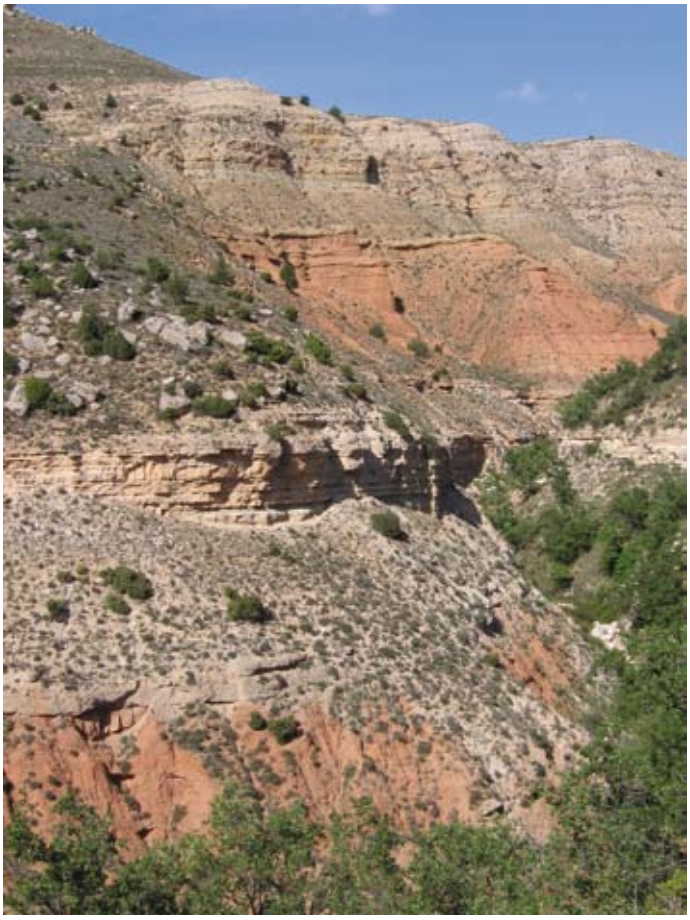

Figure 8.1 The Fuente Curria section, located just south of Cascante del Rio (Fig. 2.1), with the Bolage limestone unit at the base and the Libros gypsum unit in the middle. Just above the picture in the upper left, the stratigraphic interval covered by the Cascante section studied in Chapter 2 and 4 is present.

magneto-astrochronological framework and, in addition, to resolve the depositional setting. High-resolution correlation between the two sections indicate synchrony of reverse groundwater and lake-level changes in both areas (Chapter 4). Climate remains a potential driver behind the time-equivalent shifts. A shift to wetter conditions might have resulted in increased runoff and clastic supply, thereby filling up the Prado area and inundating the Cascante area. The paleoenvironmental changes in both sections coincide with a long-period eccentricity minimum. This is a similar phase relation to that found in the Madrid Basin (Chapter 5). Van Dam *et al.* (2006) suggested that long-period eccentricity minima would result in prolonged cooler and wetter periods, which would indeed be in accordance to the observed orbital configuration. No changes in global climate records are observed over the interval, indicating that the system was reacting to regional climate change, if climate was the cause (Chapter 4). In that case, the lack of short eccentricity related variability in the Prado section and short and long eccentricity in the upper part of the Cascante section is remarkable. Local tectonic or geomorphic changes resulting in a drainage area increase would

Figure 8.2 The outcrops near Ademuz in the south of the southern Teruel Basin, covering two genetic sedimentary sequences of supposedly middle to late Miocene age.

therefore equally explain the observed the lithofacies shifts. To further elaborate the cause behind this shift, additional integrated stratigraphic studies are need on lateral and intermediate sections across the time interval in the southern Teruel Basin. Also, the character of the axial fluvial system, its stratigraphic significance and origin are to be investigated.

8.1.2 Madrid Basin

In the Valdearenas-Muduex section (VDA-MX) in the northeastern part of the Madrid Basin, two large-scale sedimentary sequences have been accurately dated by means of magnetostratigraphy. The age model has important implications. Firstly, the sedimentary sequences recognised basin-wide and mostly referred to as tectono-sedimentary units (*cf* Pardo *et al.*, 1988) are shown to be not of the same age through the basin. This implies that either the units are strongly diachronous, and have different durations as well, or the different segments of the basin were physically or hydrologically separated, in line with the distinct lithofacies associations. Secondly, and more importantly here, both accurately dated transitions from red beds to limestones occur at times of minimum eccentricity related to the 2.4-Myr cycle. This orbital configuration is identical to that found for a similar transition in the Teruel Basin (see 8.1.1), clearly suggesting a link between the sedimentary sequences and long-period orbital forcing. Unlike in the Teruel Basin, in the Madrid Basin, the influence of long eccentricity forcing, possibly enhanced by the 0.97-Myr cycle, has been resolved, although the imprint is relatively weak. No influence of low frequency obliquity forcing is found in the VDA-MX section.

Figure 8.3 The Ciruelas section that is 11 km to the south of the VDA-MX section (Fig. 5.1). The section is thought to cover the similar stratigraphic interval as the VDA-MX section, with the Mixta 1 limestone interval in the middle and the Mixta 2 limestone interval at the top.

To substantiate the long-period eccentricity forcing in the Madrid Basin, the limestone interval in the top of the Lower unit should be accurately dated and also the time-equivalence of the sequences in the studied segment of the basin investigated. Preliminary data from the Ciruelas section (Fig. 8.3), located 11 km to the south, suggest both limestone intervals to be diachronous (Mixta 1 and 2; Chapter 5, Fig. 5.2 and 5.3), although rock magnetic analyses are needed to investigate the origin of the magnetic signal. In addition, the magnetostratigraphic pattern needs to be extended before a solid correlation to the polarity time scale can be made. Magnetostratigraphic dating of the partly overlapping Alarilla section, also located in the north-eastern sector of the basin and presently investigated by a Spanish research group, might provide additional constraints on the age of the end of the first genetic sequence of the Intermediate unit (Mixta 1) and hopefully also of the top of the Lower unit (Miguel Garcés, personal communication, 2008).

8.1.3 Malta

In Chapter 5, the integrated stratigraphy of the Blue Clay formation on Malta is presented. The accurate dating of the middle Miocene climate transition indicates that it is coincident with a 405-kyr eccentricity minimum and a 1.2-Myr obliquity amplitude node. This orbital configuration is similar to that found for increases in ice volume during the Oligocene and Miocene, indicating the potential power of low frequency obliquity forcing on ice volume and global climate (e.g. Lourens and Hilgen, 1997). However, we did not trace the impact of long-period obliquity in the Spanish basins (see 8.1.2), as was suggested by Van Dam *et al.* (2006) on the basis of faunal evidence. The Miocene stratigraphy of Malta is additionally characterised by the imprint of local

and regional processes. On the long turn, the closure of the Tethyan seaway to the Indian ocean played a major role during the early to middle Miocene (Koufos *et al.*, 2005). Locally, relative vertical movements of Malta and Gozo resulted from the northward movement of the Apulian Platform due to the convergence of Africa and Eurasia. Nevertheless, global climate change was recorded as a major sedimentary change from limestones to clays and marls across the transition (see also John *et al.*, 2003). Further studies are needed to resolve this remarkable interplay between local, regional, and global factors. High-resolution carbon and isotope records will help to quantify the effect of global climate change relative to other processes and benthic foraminifera assemblage studies will help to determine the timing and impact of the closure of the eastern connection (work in progress by Anja Mourik). Also, the origin of the glauconite sands in the upper part of the Blue Clay is being explored by an upward extension of the integrated stratigraphy with the aim to date the sandstone layer and unravel the potential connection with global eustasy and climate (and again long-period orbital forcing?), local vertical motions, and/or paleoceanographic changes due to regional or local tectonics.

8.1.4 Boom Clay

The shallow marine Boom Clay Formation in Belgium displays a long record of sea-level variations during the Early Oligocene. We show that obliquity forcing was the dominant factor in controlling repetitive sea-level oscillations. The additional impact of short and long eccentricity is recognised and some intervals reveal a saw-tooth pattern of glacial/interglacial cyclicity, very similar to the late Pleistocene. The part of the Boom Formation that is studied in detail has a length of approximately two million years, which is too short for recognition of multiple long-period orbital cycles. Analysis of long-period astronomical forcing in this interval of the succession would thus only be possible if independent absolute age control allows accurate comparison with orbital target curves. Unfortunately, at present, this is not possible as available age control is not detailed enough, because different dating methods display variable problems. Planktonic foraminiferal biostratigraphy is hampered by lack of sufficient plankton in much of the upper Rupelian and by temperature barriers delimiting the distribution of taxa such that events are diachronous or substitute species are to be used (De Man, 2006). Dinoflagellate cyst biostratigraphy is partly hampered by not sufficient age calibration of integrated stratigraphic frameworks and also the time-stratigraphic value of individual bio-events is not yet sufficiently resolved, despite a high-resolution dinocyst biostratigraphic zonation scheme built for the southern North Sea Basins in recent years (De Man, 2006; Van Simaeys *et al.*, 2004; Van Simaeys *et al.*, 2005). The error bars of Strontium isotope ages are too large for detailed correlation to orbital target curves, despite that the $^{87}Sr/^{86}Sr$ ratios are thought to represent a primary marine signal consistent with open ocean Sr-isotopic composition during the Oligocene and the ages to be reliable (De Man, 2006). In addition, paleomagnetic analysis did only reveal a weak signal that is possibly reliable in the base of the studied part of the Boom Clay (Lagrou *et al.*, 2004; M. Dekkers, personal communication, 2007). It is however not certain to which chron boundary the recognised reversal should be correlated. In summary, the dating methods applied and available are not yet accurate enough for the kind of correlation we want to establish.

In the studied interval, the Double Band, that are two glauconite-rich sandy layers, is interpreted as the NS-Ru2 to NS-Ru3 sequence boundary and correlated to the TA4.4/TA4.5 sequence boundary in the global eustatic curve of Haq *et al.* 1987 (De Man, 2006). This level seems to be the most likely candidate for the expression of long-period orbital forcing. In case of the early Oligocene glacio-eustatic sea-level history this low-stand would then occur during a minima of

the 1.2-Myr obliquity cycle in conjunction with the 405-kyr eccentricity cycle (Pälike *et al.*, 2006; Wade and Pälike, 2004). In the provisional tuning presented in Chapter 7, this configuration is used as starting point, thereby not proving long-period orbital forcing of sea level and ice volume but assuming it (Fig. 7.7). The studied record could not be extended up and downwards with the resistivity records that are used as proxy records here, because these display rapidly increasing values just below and above this interval (Fig. 7.2). This is because the underlying Belsele-Waas interval and the overlying 'transitional layers' towards the Rupelian – Chattian boundary are coarser and thus display higher resistivity (De Man, 2006). Examination of long-period orbital forcing by making use of other proxies for sea level was beyond the scope of this thesis.

8.2 The bright future

It has been mentioned innumerable times throughout this thesis, but once again; time control in sediment records is one of the keys to allow advance in untangling forcing mechanisms in continental and marine depositional settings. Accurate age control allows comparison with other climate or tectonic records, intra-basinal correlations, and investigation of the presence of orbital climate forcing. By doing this, many uncertain factors are directly filled in, leaving less space for discussion and bringing the study closer to a definite answer.

8.2.1 Short-period orbital forcing

Of the four continental studies presented, two comprise detailed sedimentologic and integrated stratigraphic work carried out on relatively small scales, before large-scale sedimentary sequences could be analysed in a basin-wide perspective. These two studies of the Upper Miocene stratigraphic infill of the southern Teruel Basin, both display short-period orbital forcing in different palaeoenvironmental settings. Our results indicate that earlier studies by Abdul Aziz (2001), Steenbrink (2001), and Van Vugt (2000) do not present exceptional cases, but reproducible and robust cyclostratigraphic methods. In this thesis, two different depositional environments are added to the list of continental settings in which magnetostratigraphic age constraints indicate orbital forcing of the net water budget on precession, obliquity, and short and/or long eccentricity scales (Abdul Aziz *et al.*, 2000; Krijgsman *et al.*, 1994; Kruiver *et al.*, 2002; Van Vugt *et al.*, 2001; Van Vugt *et al.*, 1998).

In the Madrid Basin, short-period orbital climate forcing was only shown related to the long eccentricity cycle, suggesting that higher frequency variability was overprinted by other processes as autocyclic behaviour of fluvial channels and flooding events. In the Teruel Basin, the Prado section revealed much more irregular cycle patterns than Cascante, indicating coincident imprint of other processes than orbital climate forcing. In fact, a gradual increase of other processes first starting to interfere with and later overprinting the orbital climate signal is seen from the Cascante to Prado sections in the Teruel Basin, and finally to the Valdearenas-Muduex section in the Madrid Basin. These findings thus not only show the importance of the application of integrated stratigraphic methods in continental sediment records. They also pave way for detailed studies of the climate and subsequent palaeoenvironmental response to orbital forcing, but especially of the interplay between these responses and other autogenic and allogenic processes and mechanisms.

8.2.2 Climate modelling

Additional climate modelling of precession extremes is needed in more detail and with higher complexity models than presented in Chapter 2. The role of surface hydrology and groundwater reservoirs should be included in more detail in these models. However, probably more urgent on the short term are transient runs to investigate the effect of short and long eccentricity on continental climate and paleoenvironments. In many continental basins, eccentricity is found to force sedimentary sequences in a linear way without revealing a clear precession signal (Dupont-Nivet *et al.*, 2007; Krijgsman *et al.*, 1994; Van Vugt *et al.*, 2001). Prolonged high- and low-stands of groundwater and lake level occur due to eccentricity cyclicity. However, eccentricity only has a very small direct effect on global annual received insolation and should thus only be able to exert its imprint through its amplitude modulation of precession. Memory effects are therefore needed in continental basins to explain the apparent linear response to eccentricity. Additional numerical modelling is thus needed to solve these questions.

8.2.3 Basin modelling

The intriguing interplay of different allogenic and autogenic forcing mechanisms in continental basin fills also asks for detailed numerical modelling of sedimentary basins. In fact, the reduced imprint of orbital climate forcing as observed from the Cascante to the Prado section could be an excellent case study for such a modelling exercise. Superposed orbitally induced climate change should let the system switch from well-drained floodplain environments to poorly drained paleosol, pond, and lacustrine environments on a precession scale. The dynamic interaction of vegetation, clastic supply, basin margin source rocks, runoff, precipitation/evaporation, hydrogeology, and sedimentary processes will be difficult to resolve, though hopefully valuable.

References

Abdul Aziz, H., 2001. Astronomical forcing in continental sediments. PhD-thesis, Utrecht University, Utrecht, the Netherlands. *Geological Ultraiectina*, **207**, pp. 191.

Abdul Aziz, H., F.J. Hilgen, W. Krijgsman, E. Sanz, and J.P. Calvo, 2000. Astronomical forcing of sedimentary cycles in the middle to late Miocene continental Calatayud Basin (NE Spain). *Earth and Planetary Science Letters*, 177, p. 9-22.

Abdul Aziz, H., F.J. Hilgen, G.M. Van Luijk, A. Sluijs, M.J. Kraus, J.M. Pares, and P.D. Gingerich, 2008. Astronomical climate control on paleosol stacking patterns in the upper Paleocene – lower Eocene Willwood Formation (Bighorn Basin, Wyoming). *Geology*, 36, p. 531-534.

Abdul Aziz, H., W. Krijgsman, F.J. Hilgen, D.S. Wilson, and J.P. Calvo, 2003a. An astronomical polarity timescale for the late Middle Miocene based on cyclic continental sequences. *Journal of Geophysical Research*, 108, doi. 10.1029/2002JB001818.

Abdul Aziz, H., E. Sanz-Rubio, J.P. Calvo, F.J. Hilgen, and W. Krijgsman, 2003b. Palaeoenvironmental reconstruction of a middle Miocene alluvial fan to cyclic shallow lacustrine depositional system in the Calatayud Basin (NE Spain). *Sedimentology*, 50, p. 211-236.

Abdul Aziz, H., J. Van Dam, F.J. Hilgen, and W. Krijgsman, 2004. Astronomical forcing in Upper Miocene continental sequences: implications for the Geomagnetic Polarity Time Scale. *Earth and Planetary Science Letters*, 222, p. 243-258.

Abels, H.A., H. Abdul Aziz, J.P. Calvo, and E. Tuenter, 2008. Shallow lacustrine microfacies document orbitally paced lake-level history in the Miocene Teruel Basin (NE Spain). *Sedimentology*, in the press.

Abels, H.A., H. Abdul Aziz, D. Ventra, and F.J. Hilgen, in review. Orbital climate forcing in mudflat to marginal lacustrine deposits in the Miocene Teruel Basin (NE Spain). *Journal of Sedimentary Research*.

Abels, H.A., F.J. Hilgen, W. Krijgsman, R.W. Kruk, I. Raffi, E. Turco, and W.J. Zachariasse, 2005. Long-period orbital control on middle Miocene global cooling: Integrated stratigraphy and astronomical tuning of the Blue Clay Formation on Malta. *Paleoceanography*, 20, doi. 10.1029/2004PA001129.

Abels, H.A., S. Van Simaeys, F.J. Hilgen, E. De Man, and N. Vandenberghe, 2007. Obliquity-dominated glacio-eustatic sea level change in the early Oligocene: evidence from the shallow marine siliciclastic Rupelian stratotype (Boom Formation, Belgium), *Terra Nova*, 19, 65-73.

Adhémar, J., 1842, Révolutions de la mer. Privately published, Paris.

Agustí, J., L. Cabrera, M. Garcés, W. Krijgsman, O. Oms, J.M. Parés, 2001. A calibrated mammal scale for the Neogene of Western Europe. State of the art. *Earth-Science Reviews*, 52, p. 247-260.

Albesa, J., J.P. Calvo, L. Alcalá, and A.M. Alonso Zarza, 1997. Interpretación paleoambiental del yacimiento de La Gloria 4 (Plioceno, Fosa de Teruel) a partir del análisis de facies y de asociaciones de gasterópodos y de mamíferos. *Cuadernos de Geología Ibérica*, 22, p. 239-264.

Alonso Zarza, A.M., 1990. Estudio petrologico y sedimentologico de las facies de abanicos aluviales del Neogeno en el sector NE de la Cuenca de Madrid y su relacion con las facies mas centrales, Provincia de Guadalajara. PhD-thesis, Universidad Complutense de Madrid, Madrid, Spain, 473 pp.

Alonso Zarza, A.M., 2003. Palaeoenvironmental significance of palustrine carbonates and calcretes in the geological record. *Earth-Science Reviews*, 60, p. 261-298.

Alonso Zarza, A.M., and J.P. Calvo, 2000. Palustrine sedimentation in an episodically subsiding basin: the Miocene of the northern Teruel Graben (Spain). *Palaeogeography, Palaeoclimatology, Palaeoecology*, 160, p. 1-21.

Alonso Zarza, A.M., and J.P. Calvo, 2002. Tajo Basin, *in* Gibbons, W., and Moreno, T., eds., The Geology of Spain: London, The Geological Society, p. 315-320.

Alonso Zarza, A.M., J.P. Calvo, and M.A. García del Cura, 1990. Litoestratigrafia y evolución paleogeografica del Mioceno del borde NE de la cuenca de Madrid (Prov. Guadalajara). *Estudios Geologicos*, 46, p. 415-432.

Alonso Zarza, A.M., J.P. Calvo and M.A. García del Cura, 1992. Palustrine sedimentation and associated features – grainification and pseudo-microkarst – in the Middle Miocene (Intermediate unit) of the Madrid basin, Spain. *Sedimentary Geology*, 76, p. 43-61.

Alonso Zarza, A.M., V.P. Wright, J.P. Calvo, and M.A. García del Cura, 1992. Soil-landscape and climatic relationships in the middle Miocene of the Madrid Basin. *Sedimentology*, 39, p. 17-35.

Anadón, P., and E. Moissenet, 1996. Neogene basins in the eastern Iberian range, *in* Friend, P.F., and Dabrio, C.J., eds., Tertiary basins of Spain. *World and Regional Geology Series,* 6, p. 68-71.

Anadón, P., F. Ortí, and L. Rosell, 1997. Unidades evaporíticas de la zona de Libros-Cascante (Mioceno, Cuenca de Teruel): Características estratigráficas y sedimentológicas. *Cuadernos de Geología Ibérica*, 22, p. 283-304.

Anadón, P., L. Rosell, and M.R. Talbot, 1992. Carbonate replacement of lacustrine gypsum deposits in two Neogene continental basins, eastern Spain. *Sedimentary Geology*, 78, p. 201-216.

Arlegui, L.E., J.L. Simón, R.J. Lisle, and T. Orife, 2005. Late Pliocene-Pleistocene stress field in the Teruel and Jiloca grabens (eastern Spain): contribution of a new method of stress inversion. *Journal of Structural Geology*, 27, p. 693-705.

Ashley, G.M., 2007. Orbital rhythms, monsoons, and playa lake response, Olduvai Basin, equatorial East Africa (ca. 1.85-1.74 Ma). *Geology*, 35, p. 1091-1094.

Astin, T.R., 1990. The Devonian lacustrine sediments of Orkney, Scotland; implications for climate cyclicity, basin structure and maturation history. *Journal of the Geological Society*, 147, p. 141-151.

Backman, J., and I. Raffi, 1997. Calibration of Miocene nannofossil events to orbitally tuned cyclostratigraphies from Ceara Rise. *Proc. of the ocean drilling program, Scientific results*, 154, p. 83-99.

Bailey, R.J., and D.G. Smith, 2008. Quantitative tests for stratigraphic cyclicity. *Geological Journal*, 10.1002/gj.1115.

Barberà, X., L. Cabrera, M. Marzo, and M. Ripepe, 1996. Sedimentación lacustre y ciclicidad: las sucesiones fluvio-lacustres del Oligoceno superior del sector SE de la cuenca del Ebro. *Geogaceta*, 20, p. 1072-1073.

Beaufort, L., 1994. Climatic importance of the modulation of the 100 kyr cycle inferred from 16 m.y. long Miocene records. *Paleoceanography*, 9, p. 821-834.

Bellanca, A., F. Sgarrella, R. Neri, B. Russo, M. Sprovieri, G. Bonaduce and D. Rocca, 2002. Evolution of the Mediterranean basin during late Langhian – early Serravallian: an integrated paleoceanographic approach, *Revista Italiana di Paleontologia e Stratigrafia,* 108.2, 223-239.

Berger, A.L., 1978. Long-term variations of daily insolation and Quaternary climatic changes. *Journal of Atmospheric Sciences*, 35, p. 2362-2367.

Berggren, W.A., D.V. Kent, C.C. Swisher, and M.-P. Aubry, 1995. A revised Cenozoic geochronology and chronostratigraphy, *in* Berggren, W.A., ed., Geochronology, time scales, and global stratigraphic correlation. SEPM Special Publication, Tulsa, p. 129-212.

Billups, K., H. Pälike, J.E.T. Channell, J.C. Zachos, and N.J. Shackleton, 2004. Astronomic calibration of the late Oligocene through early Miocene geomagnetic polarity time scale. *Earth and Planetary Science Letters*, 224, p. 33-44.

Bintanja, R., R.S.W. van der Wal, and J. Oerlemans, 2005. Modelled atmospheric temperatures and global sea levels over the past million years. *Nature*, 437, p. 125-128.

Bonaduce, G. and D. Barra, 2002. The ostracods in the paleoenvironmental interpretation of the late Langhian – early Serravallian Ras il-Pellegrin section (Malta), *Revista Italiana di Paleontologia e Stratigrafia,* 108.2, p. 211-222.

Bradley, W.H., 1929. The varves and climate of the Green River epoch. *U.S. Geol. Surv. Prof. Pap.*, 158E, p. 87-110.

Broekman, J.A., 1983. Environments of deposition, sequences and history of Tertiary continental sedimentation in the Basin of Teruel-Ademuz (Spain). *Proceedings of the KNAW, Series B*, 86, p. 25-37.

Broekman, J.A., R.E. Besems, P. van Daalen, and K. Steensma, 1983. Lithostratigraphy of Tertiary continental deposits in the Basin of Teruel-Ademuz (Spain). *Proceedings of the KNAW, Series B*, 86, p. 1-16.

Bromley, R.G., 1990. Trace fossils: biology and taphonomy, *Special topics in paleontology*, 3. Unwin, Hyman, London, 280 pp.

Buurman, P., 1980. Paleosols in the Reading Beds (Paleocene) of Alum Bay, Isle of Wight, U.K. *Sedimentology*, 27, p. 593-606.

Calvo, J.P., A.M. Alonso-Zarza and M.A. García del Cura, 1989. Models of Miocene marginal lacustrine sedimentation in response to varied depositional regimes and source areas in the Madrid basin (central Spain). *Palaeogeography, Palaeoclimatology, Palaeoecology*, 70, p. 199-214.

Calvo, J.P., A.M. Alonso Zarza, M.A. García del Cura, S. Ordóñez, J.P. Rodriquez-Aranda, and M.E. Sanz Montero, 1996. Sedimentary evolution of lake systems through the Miocene of the Madrid Basin: paleoclimatic and paleohydrological constraints, *in* Friend, P.F., and Dabrio, C.J., eds., Tertiary basins of Spain. *World and Regional Geology*, 6, Cambridge, Cambridge University Press, p. 272-277.

Calvo, J.P., S. Ordóñez, M.A. García del Cura, M. Hoyos, A.M. Alonso Zarza, E. Sanz, and J.P. Rodriquez-Aranda, 1989. Sedimentología de los complejos lacustres miocenos de la cuenca de Madrid. *Acta Geologica Hispanica*, 24, p. 281-298.

Cañaveras, J.C., J.P. Calvo, M. Hoyos, and S. Ordóñez, 1996. Paleomorphologic features of an intra-Vallesian paleokarst, Tertiary Madrid Basin: significance of paleokarstic surfaces in continental basin analysis, *in* Friend, P.F., and Dabrio, C.J., eds., Tertiary basins of Spain: the stratigraphic record of crustal kinematics. *World and Regional Geology*, 6, Cambridge, Cambridge University Press, p. 279-284.

Cande, S.C., and D.V. Kent, 1995. Revised calibration of the geomagnetic polarity timescale for the Late Cretaceous and Cenozoic. *Journal of Geophysical Research*, 100, p. 6093-6095.

Caroll, A.R., and K.M. Bohacs, 1999. Stratigraphic classification of ancient lakes: balancing tectonic and climatic controls. *Geology*, 27, p. 99-102.
Casanovas-Vilar, I., and J. Agustí, 2007. Ecogeographical stability and climate forcing in the Late Miocene (Vallesian) rodent record of Spain. *Palaeogeography, Palaeoclimatology, Palaeoecology*, 248, p. 169-189.
Cleaveland, L., J. Jensen, S. Goese, D. M. Bice and A. Montanari, 2002. Cyclostratigraphic analysis of pelagic carbonates at Monte dei Corvi (Ancona, Italy) and astronomical calibration of the Serravallian – Tortonian boundary: Geology, 30, p. 931-934.
Cohen, A.S., and C. Thouin, 1987. Nearshore carboonate deposits in Lake Tangayika. *Geology*, 15, p. 414-418.
Cojan, I., M.-G. Moreau, and L.E. Stott, 2000. Stable carbon isotope stratigraphy of the Paleogene pedogenic series of southern France as a basis for continental-marine correlation. *Geology*, 28, p. 259-262.
Coxall, H.K., P.A. Wilson, H. Pälike, C.H. Lear, and J. Backman, 2005. Rapid stepwise onset of Antarctic glaciation and deeper calcite compensation in the Pacific Ocean. *Nature*, 433, p. 53-57.
Croll, J., 1864. On the physical cause of the change of climate during geological epochs. *Philosophical Magazine*, 28, p. 121-137.
Currey, D.R., 1990. Quarternary palaeolakes in the evolution of semidesert basins, with special emphasis on Lake Bonneville and the Great Basin, USA. *Palaeogeography, Palaeoclimatology, Palaeoecology*, 76, p. 189-214.
Daams, R., A.J. van der Meulen, M.A.A. Sierra, P. Peláez-Campomanes, and W. Krijgsman, 1999. Aragonian stratigraphy reconsidered, and re-evaluation of the middle Miocene mammal biochronology in Europe. *Earth and Planetary Science Letters*, 165, p. 287-294.
Dart, C.J., D.W.J. Bosence, and K.R. McClay, 1993. Stratigraphy and structure of the Maltese graben system. *Journal of the Geological Society of London*, 150, p. 1153-1166.
De Boer, P.L., 1983, Aspects of middle Cretaceous pelagic sedimentation in southern Europe – production and storage of organic matter, stable isotopes, and astronomical influences. PhD-thesis, Utrecht University, Utrecht, the Netherlands. *Geologica Ultraiectina*, 31, 112 pp.
De Boer, P.L., and A. Smith, 1994. Orbital forcing and cyclic sequences. Oxford, Blackwell Scientific Publications, 559 pp.
De Man, E., 2006. Benthic foraminiferal biofacies analysis and stable isotopes of the middle Eocene to Oligocene successions of the southern North Sea Basin. PhD-Thesis, Katholieke Universiteit Leuven, Leuven, Belgium, 375 pp.
DeCelles, P.G., B. Carrapa, and G.E. Gehrels, 2007. Detrital zircon U-Pb ages provide provenance and chronostratigraphic information from Eocene synorogenic deposits in northwestern Argentina. *Geology*, 35, p. 323-326.
DeConto, R.M., and D. Pollard, 2003. Rapid Cenozoic glaciation of Antarctica induced by declining atmospheric CO2. *Nature*, 421, p. 245-249.
De Visser, J.P., 1991. Clay mineral stratigraphy of Miocene to recent marine sediments in the central Mediterranean. PhD-thesis, Utrecht University, Utrecht, the Netherlands, *Geologica Ultraiectina*, 75, 244 pp.
Dinarès-Turell, J., J.I. Baceta, V. Pujalte, X. Orue-Extebarria, G. Bernaola, and S. Lorito, 2003. Untangling the Paleocene climatic rhythms: an astronimically calibrated Early Palaeocene magnetostratigraphy and biostratigraphy at Zumaia (Basque basin, northern Spain). *Earth and Planetary Science Letters*, 216, p. 483-500.

Dunham, R.J., 1962. Classification of carbonates according to their depositional texture, *in* W.E. Ham, ed., Classification of carbonate Rocks. *AAPG Memoir*, 1, p.108-121.
Dupont-Nivet, G., W. Krijgsman, C.G. Langereis, H.A. Abels, S. Dai, and X. Fang, 2007. Tibetan plateau aridification linked to global cooling at the Eocene-Oligocene transition. *Nature*, 445, p. 635-638.
Eardley, A.J., R.T. Shuey, V. Gvosdetsky, W.P. Nash, M.D. Picard, D.C. Grey, and G.J. Kukla, 1973. Lake cycles in the Bonneville Basin, Utah. *Geological Society of America Bulletin*, 84, p. 211-216.
Echelpoel, E.van, 1994. Identification of regular sedimentary cycles using Wlash spectral analysis with results from the Boom Clay Formation, Belgium. *Spec. Publis.Int.Ass.Sediment.*, 19, p. 63-76.
Echelpoel, E. van, and G.P. Weedon, 1990. Milankovitch cyclicity and the Boom Clay Formation: an Oligocene siliclastic shelf sequence in Belgium. *Geological Magazine*, 127, p. 599-604.
Einsele, G., W. Ricken, and A. Seilacher, 1991. Cycles and events in stratigraphy. Berlin, Springer-Verlag, 995 pp.
Emiliani, C., 1955. Pleistocene temperatures. *Journal of Geology*, 63, p. 538-578.
Evans, H.F., T. Westerhold, H. Paulsen, and J.E.T. Channell, 2007. Astronomical ages for Miocene polarity chrons C4Ar-C5r (9.3-11.2 Ma), and for three excursion chrons within C5n.2n. *Earth and Planetary Science Letters*, 256, p. 455-465.
Felix, R., 1973. Oligo-Miocene stratigraphy of Malta and Gozo. *Mededelingen van de Landbouwhogeschool Wageningen*, 73-20.
Fischer, A.G., 1991. Orbital cyclicity in Mesozoic strata, *in* Einsele, G., Ricken, W., and Seilacher, A., eds., Cycles and events in stratigraphy. Berlin, Springer-Verlag, p. 48-62.
Fischer, A.G., T.D. Herbert, G. Napoleone, I. Premoli Silva, and M. Ripepe, 1991. Albian pelagic rhythms (Piobbico Core). *Journal of Sedimentary Petrology*, 61, p. 1164-1172.
Fischer, A.G., and L.T. Roberts, 1991. Cyclicity in the Green River Formation (lacustrine Eocene) of Wyoming. *Journal of Sedimentary Research*, 61, p. 1146-1154.
Fleming, J.R., 1998. Charles Lyell and climatic change: speculation and certainty, *in* Blundell, D.J., and Scott, A.C., eds., Lyell: the past is the key to the present. Geological Society of London, London, UK, *Special Publication*, 143, p. 161-169.
Flower, B.P., and J.P. Kennet, 1993. Middle Miocene ocean-climate transition: high-resolution oxygen and carbon isotopic records from deep sea drilling project site 588A, southwest pacific. *Paleoceanography*, 8, p. 811-843.
Flower, B.P., and J.P. Kennet, 1994. The middle miocene climatic transition: East Antarctic ice sheet development, deep ocean circulation and global carbon cycling. *Palaeogeography, Palaeoclimatology, Palaeoecology*, 108, p. 537-555.
Folk, R.L., 1959. Practical petrographic classification of limestones. *AAPG Bull.*, 43, p. 1-38.
Foresi, L.M., S. Bonomo, A. Caruso, E. di Stefano, G. Salvatorini and R. Sprovieri, 2002. Calcareous plankton high resolution biostratigraphy (foraminifera and nannofossils) of the uppermost Langhian – lower Serravallian Ras Il-Pellegrin section (Malta), *Revista Italiana di Paleontologia e Stratigrafia*, 108.2, p.195-210.
Foucault, A., and F. Mélières, 2000. Palaeoclimatic cyclicity in central Mediterranean Pliocene sediments: the mineralogical signal. *Palaeogeography, Palaeoclimatology, Palaeoecology*, 158, p. 311-323.

Freytet, P., and E.P. Verrecchia, 2002. Lacustrine and palustrine carbonate petrography: an overview. *Journal of Paleolimnology*, 27, p. 221-237.
Garcés, M., J. Agustí, L. Cabrera, and J.M. Parés, 1996. Magnetostratigraphy of the Vallesian (late Miocene) in the Vallès-Penedès Basin (northeast Spain). *Earth and Planetary Science Letters*, 142, p. 381-396.
Garcés, M., W. Krijgsman, J. van Dam, J.P. Calvo, L. Alcala, and A.M. Alonso-Zarza, 1997. Late Miocene alluvial sediments from the Teruel area: Magnetostratigraphy, magnetic susceptibility, and facies organization. *Acta Geologica Hispanica*, 32, p. 171-184.
Garcia, A., 1994. Charophyta: their use in paleolimnology. *Journal of Paleolimnology*, 10, p. 43-52.
Gawthorpe, R.L., and M.R. Leeder, 2000. Tectono-sedimentary evolution of active extensional basins. *Basin Research*, 12, p. 195-218.
Gilbert, G.K., 1894. Sedimentary measurement of Cretaceous time. *Journal of Geology*, 3, p. 121-127.
Gradstein, F.M., J.G. Ogg, A.G. Sith, W. Bleeker, and L.J. Lourens, 2004. A new Geologic Time Scale, with special reference to Precambrian and Neogene. *Episodes*, 27, p. 83-100.
Hazeleger, W., Molteni, F., Severijns, C., Haarsma, R., Bracco, A. and Kucharski, F., 2003. SPEEDO: A flexible coupled model for climate studies. *Exchanges*, 28, p.1-3.
Hays, J.D., J. Imbrie, and N.J. Shackleton, 1976. Variations in the Earth's orbit: Pacemaker of the Ice Ages. *Science*, 194, p. 1121-1132.
Heller, P.L., C.L. Angevine, N.S. Winslow, C. Paola, 1988. Two-phase stratigraphic model of foreland-basin sequences. *Geology*, 16, p. 501-504.
Herbert, T.D., 1994. Reading orbital signals distorted by sedimentation: models and examples. *Spec. Public. Int. Ass. Sediment.*, 19, p. 483-507.
Heslop, D., and M.J. Dekkers, 2002. Spectral analysis of unevenly spaced climatic time series using CLEAN: signal recovery and derivation of significance levels using a Monte Carlo simulation. *Physics of the Earth and Planetary Interiors*, 130, p. 103-116.
Hilgen, F.J., 1991. Astronomical calibration of Gauss to Matuyama sapropels in the Mediterranean and implication for the Geomagnetic Polarity Time Scale. *Earth and Planetary Science Letters*, 104, p. 226-244.
Hilgen, F.J., H. Abdul Aziz, H.A. Abels, J. Becker, K.F. Kuiper, L.J. Lourens, P.Th. Meijer, J. Steenbrink, E., Tuenter, E. van der Laan, and N. Weber, 2005. Mediterranean Neogene cyclostratigraphy and astrochronology: Recent progress and new developments, *in* A. Berger, M. Ercegovac, & F. Mesinger, *eds.*, Milutin Milankovitch 125th Anniversary Symposium: Paleoclimate and the Earth Climate System. *Proceedings of the Serbian Academy of Sciences and Arts, Belgrade, Serbia.*
Hilgen, F.J., H. Abdul Aziz, W. Krijgsman, C.G. Langereis, L.J. Lourens, J.E. Meulenkamp, I. Raffi, J. Steenbrink, E. Turco, N. Van Vugt, J.R. Wijbrans, and W.J. Zachariasse, 1999. Present status of the astronomical (polarity) time-scale for the Mediterranean Late Neogene. *Phil. Trans. R. Soc. Lond. A*, 357, p. 1931-1947.
Hilgen, F.J., H. Abdul Aziz, W. Krijgsman, I. Raffi, and E. Turco, 2003. Integrated stratigraphy and astronomical tuning of the Serravallian and lower Tortonian at Monte dei Corvi (Middle-Upper Miocene, northern Italy). *Palaeogeography, Palaeoclimatology, Palaeoecology*, 199, p. 229-264.
Hilgen, F.J., H.A. Abels, S. Iaccarino, W. Krijgsman, I. Raffi, R. Sprovieri, E. Turco, and W.J. Zachariasse, 2008. The global stratotype section and point (GSSP) of the Serravallian Stage (middle Miocene). *Episodes*, in the press.

Hilgen, F.J., W. Krijgsman, I. Raffi, E. Turco, and W.J. Zachariasse, 2000. Integrated stratigraphy and astronomical calibration of the Serravallian/Tortonian boundary section at Monte Gibliscemi (Sicily, Italy). *Marine Micropaleontology*, 38, p. 181-211.

Hinnov, L.A., 2000. New perspectives on orbitally forced stratigraphy. *Annual Reviews of Earth and Planetary Sciences*, 28, p. 419-475.

Holbourn, A., W. Kuhnt, and M. Schulz, 2004. Orbitally paced climate variability during the middle Miocene: high resolution benthic foraminiferal stable-isotope records from the tropical western Pacific, *in* Clift, P.D., W. Kuhnt, Pinxian, W., Hayes D., eds., Continent-ocean interactions within East-Asian marginal seas. *Geophysical Monograph Series*, 149, American Geophysical Union, 337 pp.

Holbourn, A., W. Kuhnt, M. Schulz, and H. Erlenkeuser, 2005. Impacts of orbital forcing and atmospheric carbon dioxide on Miocene ice-sheet expansion. *Nature*, 438, p. 483-487.

Holbourn, A., W. Kuhnt, M. Schulz, J.A. Flores, and N. Andersen, 2007. Orbitally-paced climate evolution during the middle Miocene "Monterey" carbon-isotope excursion. *Earth and Planetary Science Letters*, 261, p. 534-550.

Horton, B.K., K.N. Constenius, and P.G. DeCelles, 2004. Tectonic control on coarse-grained foreland-basin sequences: An example from the Cordilleran foreland basin, Utah. *Geology*, 32, p. 637-640.

Hüsing, S.K., F.J. Hilgen, H. Abdul Aziz, and W. Krijgsman, 2007. Completing the Neogene geological time scale between 8.5 and 12.5 Ma. *Earth and Planetary Science Letters*, 253, p. 340-358.

Huybers, P., and C. Wunsch, 2005. Obliquity pacing of the late Pleistocene glacial terminations. *Nature*, 434, p. 491-494.

Imbrie, J., J.D. Hays, D.G. Martinson, A. McIntyre, A.C. Mix, J.J. Morley, N.G. Pisias, W.L. Prell, and N.J. Shackleton, 1984. The orbital theory of Pleistocene climate: support from a revised chronology of the marine d18O record, *in* Berger, A.L., Imbrie, J., Hays, J.D., Kukla, G.J., and Saltzman, B., eds., Milankovitch and climate, Volume NATO Ser C126 (I), p. 269-305.

Jacobs, E., H. Weissert, G. Shields, and P. Stille, 1996. The monterey event in the Mediterranean: a record from shelf sediments of Malta. *Paleoceanography*, 11, p. 717-728.

John, C.M., M. Mutti, and T. Adatte, 2003. Mixed carbonate-siliciclastic record on the North African margin (Malta) – coupling of weathering processes and mid Miocene climate. *GSA Bulletin*, 115, p. 217-229.

Kemp, D.B., and A.L. Coe, 2007. A nonmarine record of eccentricity forcing through the Upper Triassic of southwest England and its correlation with the Newark Basin astronomically calibrated geomagnetic polarity time scale from North America. *Geology*, 35, p. 991-994.

Kent, D.V., and P.E. Olsen, 1999. Astronomically tuned geomagnetic polarity timescale for the Late Triassic. *Journal of Geophysical Research*, 104, p. 12831-12841.

Kiefer, E., 1988. Facies development of a lacustrine tecto-sedimentary cycle in the Neogene Teruel-Ademuz Graben (NE Spain). *Neues Jahrbuch für Geologie und Paläontologie*, 6, p. 327-360.

Kirschvink, J.L., 1980. The least-squares line and plane and the analysis of paleomagnetic data. *Geophys. J. R. Astr. Soc.*, 62, p. 699-718.

Koufos, G.D., D.S. Kostopoulos, and T.D. Vlachou, 2005. Neogene/Quarternary mammalian migrations in Eastern Mediterranean. *Belgian Journal of Zoology*, 135, p. 181-190.

Kraus, M.J., 2002. Basin-scale changes in floodplain paleosols: implications for interpreting alluvial architecture. *Journal of Sedimentary Research*, 72, p. 500-509.

Krijgsman, W., A.R. Fortuin, F.J. Hilgen, and F.J. Sierro, 2001. Astrochronology for the Messinian Sorbas basin (SE Spain) and orbital (precessional) forcing for evaporite cyclicity. *Sedimentary Geology*, 140, p. 43-60.

Krijgsman, W., F.J. Hilgen, C.G. Langereis, A. Santarelli, and W.J. Zachariasse, 1995. Late Miocene magnetostratigraphy, biostratigraphy and cyclostratigraphy in the Mediterranean. *Earth and Planetary Science Letters*, 136, p. 475-494.

Krijgsman, W., C.G. Langereis, R. Daams, and A.J. van der Meulen, 1994. Magnetostratigraphic dating of the middel Miocene climate change in the continental deposits of the Aragonian type area in the Calatayud – Teruel basin (Central Spain). *Earth and Planetary Science Letters*, 128, p. 513-526.

Kruiver, P.P., W. Krijgsman, C.G. Langereis, and M.J. Dekkers, 2002. Cyclostratigraphy and rock-magnetic investigation of the NRM signal in late Miocene palustrine-alluvial deposits of the Librilla section (SE Spain). *Journal of Geophysical Research*, 107, doi. 1029/2001JB000945.

Kruiver, P.P., C.G. Langereis, M.J. Dekkers, and W. Krijgsman, 2003. Rock-magnetic properties of multicomponent natural remanent magnetization in alluvial red beds (NE Spain). *Geophys. J. Int.*, 153, p. 317-332.

Kuiper, K.F., A. Deino, F.J. Hilgen, W. Krijgsman, P.R. Renne, and J.R. Wijbrans, 2008. Synchronizing rock clocks of earth history. *Science*, 320, p. 500-504.

Kuiper, K.F., F.J. Hilgen, J. Steenbrink, and J.R. Wijbrands, 2004. 40Ar/39Ar ages of tephras intercalated in astronomically tuned Neogene sedimentary sequences in the eastern Mediterranean. *Earth and Planetary Science Letters*, 222, p. 583-597.

Laenen, B., 1998. The geochemical signature of relative sea-level cycles recognised in the Boom Clay. *Aardkundige Mededelingen*, 9, p. 61-82.

Lagrou, D., N. Vandenberghe, S. Van Simaeys, and J. Hus, 2004. Magnetostratigraphy and rock magnetism of the Boom Clay (Rupelian stratotype) in Belgium. *Netherlands Journal of Geosciences*, 83, p. 209-226.

Laskar, J., 1999. The limits of Earth orbital calculations for geological time-scale use. *Royal Society of London, Philosophical Transactions, series A*, 357, p. 1735-1759.

Laskar, J., P. Robutel, F. Joutel, M. Gastineau, A.C.M. Correia, and B. Levrard, 2004. A long term numerical solution for the insolation quantities of the Earth. *Astronomy and Astrophysics* 428, p. 261-285.

Lear, C.H., H. Elderfield, and P.A. Wilson, 2000. Cenozoic deep-sea temperatures and global ice volumes from Mg/Ca in benthic foraminiferal calcite. *Science*, 287, p. 269-272.

Leeder, M.R., and R.L. Gawthorpe, 1987. Sedimentary models for extensional tilt-block/half-graben basins., *in* Coward, M.P., Dewey, J.F., and Hancock, P.L., eds., Continental extensional tectonics. London, *Geological Society Special Publication*, 28, p. 139-152.

Lindholm, R.C., and R.B. Finkelman, 1972. Calcite staining: semi-quantitative determination of ferrous iron. *Journal of Sedimentary Petrology*, 42, p. 239-242.

Lourens, L.J., 2004. Revised tuning of Ocean Drilling Program Site 964 and KC01B (Mediterranean) and implications for the $\delta^{18}O$, tephra, calcareous nannofossil, and geomagnetic reversal chronologies of the past 1.1 Myr. *Paleoceanography*, 19, doi. 10.1029/2003PA000997.

Lourens, L.J., and F.J. Hilgen, 1997. Long-periodic variations in the earth's obliquity and their relation to third-order eustatic cycles and late Neogene glaciations. *Quarternary International*, 40, p. 43-52.

Lourens, L.J., F.J. Hilgen, N.J. Shackleton, J. Laskar, and D.S. Wilson, 2004. The Neogene Period, *in* Gradstein, F.M., Ogg, J.G., and Smith, A., eds., A Geolologic Time Scale 2004. Cambridge, Cambridge University Press, p. 405-440.

Lourens, L.J., A. Sluijs, D. Kroon, J.C. Zachos, E. Thomas, U. Röhl, J. Bowles, and I. Raffi, 2005. Astronomical pacing of late Palaeocene to early Eocene global warming events. *Nature*, 435, p. 1083-1087.

Lourens, L.J., R. Wehausen, and H.-J. Brumsack, 2001. Geological constraints on tidal dissipation and dynamical ellipticity of the Earth over the past three million years. *Nature*, 409, p. 1029-1033.

Luterbacher, H.P., J.R. Ali, H. Brinkhuis, F.M. Gradstein, J.J. Hooker, S. Monechi, J.G. Ogg, J. Powell, U. Röhl, A. Sanfilippo, and B. Schmitz, 2004. The Paleogene Period, i*n* Gradstein F.M *et al.*, eds., A Geological Timescale 2004. Cambridge University Press, Cambridge, United Kingdom, 589 pp.

Luzón, A., A. González, A. Muñoz, and B. Sánchez-Valverde, 2002. Upper Oligocene-Lower Miocene shallowing-upward lacustrine sequences controlled by periodic and non-periodic processes (Ebro Basin, northeastern Spain). *Journal of Paleolimnology*, 28, p. 441-456.

Machette, M.N., 1985. Calcic soils of the southwestern United States. *Geological Society of America Special Paper*, 203, p. 1-21.

Machlus, M.L., P.E. Olsen, N. Christie-Bick, and S.R. Hemming, 2008. Spectral analysis of the Lower Eocene Wilkins Peak Member, Green River Formation, Wyoming: Support for Milankovitch cyclicity. *Earth and Planetary Science Letters*, 268, p. 64-75.

Magri, D., and P.C. Tzedakis, 2000. Orbital signatures and long-term vegetation patterns in the Mediterranean. *Quarternary International*, 73/74, p. 69-78.

McArthur, J.M., R.J. Howarth, T.R. Bailey, 2001. Strontium Isotope Stratigraphy: LOWESS Version 3: Best fit to the marine Sr-isotope curve for 0-509 Ma and accompanying Look-up Table for deriving numerical age. *The Journal of Geology*, 109, p. 155-170.

McFadden, L.D., and J.C. Tinsley, 1985. Rate and depth of pedogenic-carbonate accumulation in soils: Formulation and testing of a compartment model. *Geological Society of America Special Paper*, 203, p. 23-41.

McPhee, J., 1980, Basin and Range. Farra, Strauss, & Giroux, New York, p.127.

Megias, A.G., S. Ordóñez, and J.P. Calvo, 1981. Tertiary clastic gypsum deposits in the Madrid Basin. *Regional Meeting Internation Association of Sedimentologists*, p. 109-112.

Meyers, S.R., 2008. Resolving Milankovitchian controversies: The Triassic Latemar Limestone and the Eocene Green River Formation. *Geology*, 36, p. 319-322.

Meyers, S.R., and B.B. Sageman, 2007. Quantification of deep-time orbital forcing by average spectral misfit. *American Journal of Science*, 307, p. 773-792.

Meyers, S.R., B.B. Sageman, and L.A. Hinnov, 2001. Integrated quantitative stratigraphy of the Cenomanian-Turonian Bridhe Creek Limestone Member using evolutive harmonic analysis and stratigraphic modeling. *Journal of Sedimentary Research*, 71, p. 628-644.

Miller, K.G., J.D. Wright, and R.G. Fairbanks, 1991. Unlocking the ice house: Oligocene-Miocene oxygen isotops, eustasy, and margin erosion. *Journal of Geophysical Research*, 96, p. 6829-6848.

Miller, K.G., M.A. Kominz, M.A. Browning, J.D. Wright, G.S. Mountain, M.E. Katz, P.J. Sugarman, B.S. Cramer, N. Christie-Blick, and S.F. Pekar, 2005. The Phanerozoic record of global sea-level change. *Science*, 310, p. 1293-1298.

Miller, K.G., G.S. Mountain, and others., 1996. Drilling and dating New Jersey Oligocene-Miocene sequences: ice volume, global sea level, and exxon records. *Science*, 271, p. 1092-1095.

Molteni, F., 2003. Atmospheric simulations using a GCM with simplified physical parametrizations; Model climatology and variability in multi-decadal experiments. *Climate Dynamics*, 20, 175-191.

Montes, M., B. Beamud, M. Garcés, and J.P. Calvo, 2006. Magnetoestratigrafía de las unidades inferior e intermedia del mioceno de la cuenca de Madrid. *Revista Soc. Geol. España*, 19, p. 281-298.

Munsell, 1999. Munsell Soil Color Charts, *in* Company, M.C., ed., Maryland, Macbeth Division of Kollmorgen.

Nichols, G.J., and F. Watchorn, 1998. Climatic and geomorphic controls on rift sedimentation: Oligo-Miocene syn-rift facies in the Gulf of Aden, Yemen. *Marine and Petroleum Geology*, 15, p. 505-518.

Nijman, W., 1998. Cyclicity and basin axis shift in a piggyback basin: towards modelling of the Eocene Tremp-Ager Basin, South Pyrenees, Spain, *in* Mascle, A., Puigdefábregas, C., Luterbacher, H.P., and Fernandez, M., eds., Cenozoic foreland basins of western Europe. London, *Geological Society of London Special Publication*, 134, p. 135-162.

Normati, M., and J. Salomon, 1989. Reconstruction of a Berriasian lacustrine paleoenvironment in the Cameros basin (Spain). *Palaeogeography, Palaeoclimatology, Palaeoecology*, 70, p. 215-223.

Olsen, P.E., 1986. A 40-Million-Year lake record of early Mesozoic orbital climate forcing. *Science*, 234, p. 842-848.

Olsen, P.E., and D.V. Kent, 1996. Milankovitch climate forcing in the tropics of Pangaea during the Late Triassic. *Palaeogeography, Palaeoclimatology, Palaeoecology*, 122, p. 1-26.

Olsen, P.E., and D.V. Kent, 1999. Long-Period Milankovitch Cycles from the Late Triassic and Early Jurassic of Eastern North America and Their Implications for the Calibration of the Early Mesozoic Time-Scale and the Long-Term Behaviour of the Planets. *Philosophical Transactions: Mathematical, Physical and Engineering Sciences*, 357, p. 1761-1786.

Ortí, F., L. Rosell, and P. Anadón, 2003. Deep to shallow lacustrine evaporites in the Libros Gypsum (southern Teruel Basin, Miocene, NE Spain): an occurence of pelletal gypsum rhythmites. *Sedimentology*, 50, p. 361-386.

Pagani, M., M.A. Arthur, and K.H. Freeman, 1999. Miocene evolution of atmospheric carbon dioxide. *Paleoceanography*, 14, p. 273-292.

Paillard, D.L., L. Labeyrie, and P. Yiou, 1996. Macintosh program performs time-series analysis. *EOS transactions AGU*, 77, p. 379.

Pälike, H., J. Frazier, and J.C. Zachos, 2006a. Extended orbitally forced palaeoclimatic records from the equatorial Atlantic Ceara Rise. *Quarternary Science Reviews*, 25, p. 3138-3149.

Pälike, H., J. Laskar, and N.J. Shackleton, 2004. Geologic constraints on the chaotic diffusion of the solar system. *Geology*, 32, p. 929-932.

Pälike, H., R.D. Norris, J.O. Herrle, P.A. Wilson, H.K. Coxall, C.H. Lear, N.J. Shackleton, A.K. Tripati, and B.S. Wade, 2006b. The heartbeat of the Oligocene climate system. *Science*, 314, p. 1894-1898.

Pardo, G., J. Villena, and A. González, 1988. Contribución a los conceptos y a la aplicación del análisis tectosedimentario. Rupturas y unidades tectosedimentarias como fundamento de correlaciones estratigráficas. *Revista Soc. Geol. España*, 2, p. 199-221.

Pearson, P.N., and M.R. Palmer, 2000. Atmospheric carbon dioxide concentrations over the past 60 million years. *Nature*, 406, p. 695-699.

Pekar, S.F., N. Christie-Bick, M.A. Kominz, and K.G. Miller, 2002. Calibration between eustatic estimates from backstripping and oxygen isotopic records for the Oligocene. *Geology*, 30, p. 903-906.

Pelaez-Campomanes, P., B. Azanza, J.P. Calvo, R. Daams, E. Herráez, J. Morales, M. Nieto, and D. Soria, 2000. Bioestratigrafía de las faunas de mamíferos del Mioceno de Madrid: datación de las unidades estratigráficas, *in* Morales, J., ed., Patrimonio paleontológico de la Comunidad de Madrid: Madrid, Serie de la Consejería de Educación, Comunidad de Madrid, p. 103-129.

Pérez, A., A. Luzón, A.C. Roc, A.R. Soria, M.J. Mayayo, and J.A. Sánchez, 2002. Sedimentary facies distribution and genesis of a recent carbonate-rich saline lake: Gallocanta Lake, Iberian Chain, NE Spain. *Sedimentary Geology*, 148, p. 185-202.

Picard, M.D., and L.R. High, 1981. Physical stratigraphy of ancient lacustrine deposits. *SEPM Special Publication*, 31, p. 233-259.

Pietras, J.T., and A.R. Carroll, 2006. High-resolution stratigraphy of an underfilled lake basin: Wilkins Peak Member Eocene Green River Formation, Wyoming, U.S.A. *Journal of Sedimentary Research*, 76, p. 1197-1214.

Platt, N.H., 1989. Continental sedimentation in an evolving rift basin: the lower Cretaceous of the western Cameros Basin (northern Spain). *Sedimentary Geology*, 64, p. 91-109.

Platt, N.H., and V.P. Wright, 1991. Lacustrine carbonates: facies models, facies distributions and hydrocarbon aspects. *Spec. Publis.Int.Ass.Sediment.*, 13, p. 57-74.

Raffi, I., J. Backman, E. Fornaciari, H. Pälike, D. Rio, L.J. Lourens, and F.J. Hilgen, 2006. A review of calcareous nannofossil astrobiochronology encompassing the past 25 million years. *Quarternary Science Reviews*, 25, p. 3113-3137.

Raymo, M.E. and W.F. Ruddiman, 1992. Tectonic forcing of late Cenozoic climate. *Nature*, 359, p. 117-122.

Reinhardt, L., and W. Ricken, 2000. The stratigraphic and geochemical record of Playa Cycles: monitoring a Pangaean monsoon-like system (Triassic, middle Keuper, S. Germany). *Palaeogeography, Palaeoclimatology, Palaeoecology*, 161, p. 205-227.

Retallack, G.J., 2001. Soils of the past – an introduction to paleopedology. Oxford, Blackwell Science Ltd., 404 pp.

Retallack, G.J., 2005. Pedogenic carbonate proxies for amount and seasonality of precipitation in paleosols. *Geology*, 33, p. 333-336.

Rosen, M.R., 1994. The importance of groundwater in playas: a review of playa classifications and the sedimentology and hydrology of playas, *in* Rosen, M.R., ed., Paleoclimate and basin evolution of playa systems. Boulder, Colorado, *Geological Society of America Special Paper*, 289, p. 1-18.

Rossignol-Strick, M., 1983. African monsoons, an immediate climate response to orbital insolation. *Nature*, 304, p. 46-49.

Royer, D.L., 1999. Depth to pedogenic carbonate horizon as a paleoprecipitation indicator? *Geology*, 27, p. 1123-1126.

Royer, D.L., S.L. Wing, D.J. Beerling, D.W. Jolley, P.L. Koch, L.J. Hickey, and R.A. Berner, 2001. Paleobotanical evidence for near present-day levels of atmospheric CO2 during part of the Tertiary. *Science*, 292, p. 2310-2313.

Ruddiman, W.F., 2006. Orbital changes and climate. *Quarternary Science Reviews*, 26, p. 3092-3112.

Sagri, M., E. Abbate, and P. Bruni, 1989. Deposits of ephemeral and perennial lakes in the Tertiary Daban basin (Northern Somalia). *Palaeogeography, Palaeoclimatology, Palaeoecology*, 70, p. 225-233.

Sanz, M.E., A.M. Alonso Zarza, and J.P. Calvo, 1995. Carbonate pond deposits related to semi-arid alluvial systems: examples from the Tertiary Madrid basin, Spain. *Sedimentology*, 42, p. 437-452.

Schwarzacher, W., 1947. Über die sedimentäre Rhythmik des Dachsteinkalkes bei Lofer. *Verh. Geol.Bundersanst. Wien*, 10-12, p. 176-188.

Sesé, C., A.M. Alonso Zarza, and J.P. Calvo, 1990. Nuevas faunas de micromammiferos del terciario continental del NE de la cuenca de Madrid (Prov. de Guadalajara, España). *Estudios Geologicos*, 46, p. 433-451.

Shackleton, N.J., A.L. Berger, and W.R. Peltier, 1990. An alternative astronomical calibration of the Lower Pleistocene timescale based on ODP Site 677. *Transactions of the Royal Society of Edinburgh: Earth Sciences*, 81, p. 251-261.

Shackleton, N.J., S.J. Crowhurst, G.P. Weedon, and J. Laskar, 1999. Astronomical calibration of Oligocene – Miocene time. *Phil. Trans. R. Soc. Lond. A*, 357, p. 1907-1929.

Shackleton, N.J., and M.A. Hall, 1997. The Late Miocene stable isotope record, Site 926, *in* Shackleton, N.J., Curry, W.B., Richter, C., and Bralower, T.J., eds., Proceedings of the Ocean Drilling Program, Scientific Results, Volume 154.

Shackleton, N.J., and N.D. Opdijke, 1973. Oxygen isotope and paleomagnetic stratigraphy of equatorial Pacific core V28-238: oxygen isotope temperatures and ice volume on a 105 and 106 year scale. *Quat. Res.*, 3, p. 39-55.

Shevenell, A.E., and J.P. Kennett, 2004. Paleoceanographic change during the middle Miocene climate revolution: an Antarctic stable isotope perspective, *in* Exon, N.F., Kennett, J.P., and Malone, M.J., eds., The Cenozoic southern Ocean: Tectonics, sedimentation, and climate change between Australia and Antarctica. *Geophysical Monograph Series* 154, American Geophysical Union, p. 235-251.

Shevenell, A.E., J.P. Kennett, and D.W. Lea, 2004. Middle Miocene southern ocean cooling and Antarctic cyrosphere expansion. *Science*, 305, p. 1766-1770.

Sierro, F.J., J.A. Flores, I. Zamarreño, A. Vázquez, R. Utrilla, G. Francés, F.J. Hilgen, and W. Krijgsman, 1999. Messinian pre-evaporite sapropels and precession-induced oscillations in western Mediterranean climate. *Marine Geology*, 153, p. 137-146.

Sierro, F.J., F.J. Hilgen, W. Krijgsman, and J.A. Flores, 2001. The Abad composite (SE Spain): a Messinian reference section for the Mediterranean and the APTS. *Palaeogeography, Palaeoclimatology, Palaeoecology*, 168, p. 141-169.

Sierro, F.J., S. Ledesma, J.-A. Flores, S. Torrescusa, and W. Martínez del Olmo, 2000. Sonic and gamma-ray astrochronology: cycle to cycle calibration of Atlantic climatic records to Mediterranean sapropels and astronomical oscillations. *Geology*, 28, p. 695-698.

Sprovieri, M., A. Caruso, L.M. Foresi, A. Bellanca, R. Neri, S. Mazzola, and R. Sprovieri, 2002. Astronomical calibration of the upper Langhian/lower Serravalian record of Ras Il-Pellegrin

section (Malta island, central Mediterranean). *Rivista Italiana di Paleontologia e Stratigrafia*, 108, p. 183-193.
Sprovieri, M., R. Coccioni, F. Lirer, N. Pelosi, and F. Lozar, 2006. Orbital tuning of a lower Cretaceous composite record (Maiolica Formation, central Italy). *Paleoceanography*, 21, p. 1-19.
Steenbrink, J., 2001. Orbital signatures in lacustrine sediments. PhD-thesis, Utrecht University, Utrecht, the Netherlands. *Geologica Ultraiectina,* 205, 167 pp.
Steenbrink, J., N. Van Vugt, F.J. Hilgen, J.R. Wijbrands, and J.E. Meulenkamp, 1999. Sedimentary cycles and volcanic ash beds in the Lower Pliocene lacustrine succession of Ptolemais (NW Greece): discrepancy between 49Ar/39Ar and astronomic ages. *Palaeogeography, Palaeoclimatology, Palaeoecology*, 152, p. 283-303.
Steurbaut, E., 1992. Integrated stratigraphic analysis of Lower Rupelian deposits (Oligocene) in the Belgian Basin. *Annales Société Geologique Belgique*, 115, p. 287-306.
Tuenter, E., S.L. Weber, F.J. Hilgen and L.J. Lourens, 2003. The response of the African summer monsoon to remote and local forcing due to precession and obliquity. *Global and Planetary Change*, 36, p. 219-235.
Turco, E., F.J. Hilgen, L.J. Lourens, N.J. Shackleton, and W.J. Zachariasse, 2001. Punctuated evolution of global climate cooling during the late Middel to early late Miocene: High-resolution planktonic foraminiferal and oxygen isotope records from the Mediterranean. *Paleoceanography*, 16, p. 405-423.
Turco, E., L.M. Foresi, S.M. Iaccarino, F. Lirer, G. Salvatorini, M. Sprovieri, 2003. Langhian planktonic foraminiferal record from the Mediterranean; paleoecological and paleoceanographical implications, *Geoitalia 4th forum FISTE*, Bellaria, Italy, 16-18 sep.
Türkmen, I., and I.E. Kerey, 2000. Alluvial and lacustrine facies of the Yeniçubuk formation (lower-middle Miocene), Upper Kizilirmak basin, Türkiye (Turkey), *in* Gierlowski-Kordesch, E.H., and Kelts, K., eds., Lake basins through space and time. AAPG studies in geology, p. 449-464.
Van Dam, J.A., H. Abdul Aziz, M. de los Angeles Alvarez Sierra, F.J. Hilgen, L.W. van den Hoek Ostende, L.J. Lourens, P. Mein, A.J. van der Meulen, and P. Pelaez-Campomanes, 2006. Long-period astronomical forcing of mammal turnover. *Nature*, 443, p. 687-691.
Van Dam, J.A., 2006. Geographic and temporal patterns in the late Neogene (12-3 Ma) aridification of Europe: The use of small mammals as paleoprecipitation proxies. *Palaeogeography, Palaeoclimatology, Palaeoecology*, 238, p. 190-218.
Van Dam, J.A., and G.J. Weltje, 1999. Reconstruction of the Late Miocene climate of Spain using rodent palaeocommunity successions: an application of end-member modeling. *Palaeogeography, Palaeoclimatology, Palaeoecology*, 151, p. 267-305.
Van der Laan, E., S. Gaboardi, F.J. Hilgen, and L.J. Lourens, 2005. Regional climate and glacial control on high-resolution oxygen isotope records from Ain el Beida (latest Miocene, northwest Morocco): a cyclostratigraphic analysis in the depth and time domain. *Paleoceanography*, 20, doi. 10.1029/2003PA000995.
Van der Meulen, A.J., P. Pelaez-Campomanes, and S.A. Levin, 2005. Age structure, residents, and transients of Miocene rodent communities. *American Naturalist*, 165, p. E108-E125.
Van Houten, F.B., 1964. Cyclic lacustrine sedimentation, Upper Triassic Lockatong Formation, Central New Yersey and adjacent Pennsylvania. *Kansas Geol. Survey Bull.*, 169, p. 497-531.
Van Simaeys, S., H. Brinkhuis, J. Pross, G.L. Williams, and J.C. Zachos, 2005a. Arctic dinoflagellate migrations mark the strongest Oligocene glaciations. *Geology*, 33, p. 709-712.

Van Simaeys, S., E. De Man, N. Vandenberghe, H. Brinkhuis, and E. Steurbaut, 2004. Stratigraphic and palaeoenvironmental analysis of the Rupelian-Chattian transition in the type region: evidence from dinoflagellate cysts, foraminifera and calcareous nannofossils. *Palaeogeography, Palaeoclimatology, Palaeoecology*, 208, p. 31-58.

Van Simaeys, S., D. Munsterman, and H. Brinkhuis, 2005b. Oligocene dinoflagellate cyst biostratigraphy of the southern North Sea Basin. *Review of Paleobotany and Palynology*, 134, p. 105-128.

Van Vugt, N., 2000. Orbital forcing in late Neogene lacustrine basins from the Mediterranean. PhD-thesis, Utrecht University, Utrecht, the Netherlands. *Geologica Ultraiectina,* 189, 167 pp.

Van Vugt, N., C.G. Langereis, and F.J. Hilgen, 2001. Orbital forcing in Pliocene-Pleistocene Mediterranean lacustrine deposits: dominant expression of eccentricity versus precession. *Palaeogeography, Palaeoclimatology, Palaeoecology*, 172, p. 193-205.

Van Vugt, N., J. Steenbrink, C.G. Langereis, F.J. Hilgen, and J.E. Meulenkamp, 1998. Magnetostratigraphy-based astronomical tuning of the early Pliocene lacustrine sediments of Ptolemais (NW Greece) and bed-to-bed correlation with the marine record. *Earth and Planetary Science Letters*, 164, p. 535-551.

Vandenberghe, N., 1978. Sedimentology of the Boom Clay Formation, Belgium. *Bulletin van de Belgische Vereniging voor Geologie*, 102, p. 5-77.

Vandenberghe, N., B. Laenen, E. Van Echelpoel, and D. Lagrou, 1997. Cyclostratigraphy and climatic eustasy. Example of the Rupelian stratotype. *C.R.Acad.Sci.Paris, Sciences de la terre et des planètes*, 325, p. 305-315.

Vandenberghe, N., P. Laga, E. Steurbaut, J. Hardenbol, and P. Vail, 1998. Tertiary sequence stratigraphy at the southern border of the North Sea basin in Belgium, *in* De Graciansky, P, J. Hardenbol, T. Jacquin, and P. Vail, eds., Mesozoic and Cenozoic sequence stratigraphy of European basins. *SEPM Spec.Publ.*, 60, p. 119-154.

Vandenberghe, N., H. Hager, M. Van den Bosch, A. Verstraelen, S. Leroi, E. Steurbaut, J. Prüfert, and P. Laga, 2001. Stratigraphic correlation by calibrated well logs in the Rupel Group between North Belgium, the Lower Rhine area in Germany and Southern Limburg, and the Achterhoek in the Netherlands, *in* Vandenberghe, N., ed., Contributions to the Paleogene and Neogene Stratigraphy of the North Sea Basin. *Aardkundige Mededelingen*, 11, Leuven University Press, p. 69-84.

Varadi, F., B. Runnegar, and M. Ghil, 2003. Successive refinements in long-term integrations of planetary orbits. *The Astrophysical Journal*, 592, p. 620-630.

Vázquez, A., R. Utrilla, I. Zamarreño, F.J. Sierro, J.A. Flores, G. Francés, and M.A. Bárcena, 2000. Precession-related sapropelites of the Messinian Sorbas Basin (South Spain): paleoenvironmental significance. *Palaeogeography, Palaeoclimatology, Palaeoecology*, 158, p. 353-370.

Vincent, E., and W.H. Berger, 1985. Carbon dioxide and polar cooling in the Miocene: the Monterey hypothesis. *Geophysical Monograpgh*, 32, p. 455-468.

Wade, B.S., and H. Pälike, 2004. Oligocene climate dynamics. *Paleoceanography*, 19, doi. 10.1029/2004PA001042.

Warren, J., 1999. Evaporites; their evolution and economics: Oxford, Blackwell Science Ltd., 438 pp.

Weedon, G.P., 2003. Time-series analysis and cyclostratigraphy – examining stratigraphic records of environmental cycles. Cambridge, Cambridge University Press, 259 pp.

Westerhold, T., T. Bickert, and U. Röhl, 2005. Middle to Late Miocene oxygen isotope stratigraphy of ODP Site 1085 – SE Atlantic. *Palaeogeography, Palaeoclimatology, Palaeoecology*, 217, p. 205-222.

Westerhold, T., U. Röhl, J. Laskar, I. Raffi, J. Bowles, L.J. Lourens, and J.C. Zachos, 2007. On the duration of magnetochrons C24r and C25n and the timing of early Eocene global warming events: implications from the Ocean Drilling Program Leg 208 Walvis Ridge depth transect. *Paleoceanography*, 22, doi. 10.1029/2006PA001322.

Westerhold, T., U. Röhl, I. Raffi, E. Fornaciari, S. Monechi, V. Reale, J. Bowles, and H.F. Evans, 2008. Astronomical calibration of the Paleocene time. *Palaeogeography, Palaeoclimatology, Palaeoecology*, 257, p. 377-403.

Wilkinson, B.H., G.K. Merrill, and S.J. Kivett, 2003. Stratal order in Pennsylvanian cyclothems. *GSA Bulletin*, 115, p. 1068-1087.

Woodruff, F., and S.M. Savin, 1991. Mid-Miocene isotope stratigraphy in the deep sea: high-resolution correlations, paleoclimatic cycles, and sediment preservation. *Paleoceanography*, 6, p. 755-806.

Wright, J.D., and K.G. Miller, 1992. Miocene stable isotope stratigraphy, site 747, Kerguelen Plateau. *Proc. of the ocean drilling program, Scientific results*, 120, p. 855-866.

Wright, P.V., and S.B. Marriott, 2007. The dangers of taking mud for granted: Lessons from Lower Old Red Sandstone dryland river systems of South Wales. *Sedimentary Geology*, 195, p. 91-100.

Wright, V.P., and M.E. Tucker, 1991. Calcretes: an introduction, *in* Wright, V.P., and Tucker, M.E., eds., Calcretes. *Reprint Series of the International Association of Sedimentologists* 2: Oxford, Blackwell Scientific Publications, p. 1-22.

Zachos, J.C., M. Pagani, L. Sloan, E. Thomas, and K. Billups, 2001a. Trends, rhtyms, and aberrations in global climate 65 Ma to present. *Science*, 292, p. 686-693.

Zachos, J.C., G.R. Dickens, and R.E. Zeebe, 2008. An early Cenozoic perspective on greenhouse warming and carbon-cycle dynamics. *Nature*, 451, p. 279-283.

Zachos, J.C., N.J. Shackleton, J.S. Revenaugh, H. Pälike, and B.P. Flower, 2001b. Climate response to orbital forcing across the Oligocene – Miocene boundary. *Science*, 292, p. 274-278.

Ziegler, P.A., 1990. Geological atlas of western and central Europe. Shell Internationale Petroleum Maatschappij B.V. (Den Haag), 239 pp.

Zijderveld, J.D.A., 1967. Demagnetisation of rock: analysis of results, *in* Collison, D.W., Creer, K.M., and Runcorn, S.K., eds., Methods in paleomagnetism. Elsevier Publishing Company, Amsterdam, p. 254-386.

Samenvatting in het Nederlands (Summary in Dutch)

Lang-periodieke orbitaal forcering van het klimaat

Cyclostratigrafische studies van Cenozoïsche continentale en mariene successies in Europa

Regelmatige variaties treden op in de baan van de aarde rond de zon en de stand van de aardas ten opzicht van de zon. Deze vinden hun oorsprong in de gravitatieve interactie met de andere massa's in ons zonnestelsel. De meest alledaagse van deze orbitaal variaties is de dagelijkse rotatie van onze aarde om zijn as. Op de langere termijn variëren de stand (precessie) en de hoek (obliquiteit) van de aardas en de ellipticiteit (excentriciteit) van de baan om de zon. De dominante duur van deze quasi-periodische cycli zijn 19 en 23 duizend jaar voor precessie, 41 duizend jaar voor obliquiteit, en circa 100 en 405 duizend jaar voor excentriciteit. Astronomen zijn nu in staat de positie, stand, en beweging van de aarde terug te rekenen nu voor bijna het gehele Cenozoïcum, dat wil zeggen de laatste 66 miljoen jaar.

De mogelijke invloed van deze orbitaal cycli op het aardse klimaat is reeds gesuggereerd en bediscusseerd in de negentiende eeuw door onder andere Joseph Adhémar en James Croll. Deze theorie werd in de daaropvolgende eeuw aangepast en uitgebreid door de Servische wetenschapper Milutin Milankovitch, terwijl de definitieve bewijsvoering vanuit de archieven van het paleoklimaat werd gebracht door Jim Hays, John Imbrie en Nick Shackleton in 1976. Steeds nauwkeurigere dateringsmethoden en de uitbreiding van geïntegreerd stratigrafisch onderzoek in de loop van de 80-er en 90-er jaren van vorige eeuw leidden ertoe dat orbitaal sturing van het klimaat bewezen kon worden in oudere mariene en ook continentale sediment opeenvolgingen. Beaufort (1994) en Lourens en Hilgen (1997) veronderstelden dat aanwezige cycli van excentriciteit en obliquiteit met een veel langere duur dan de typische cycli wel eens belangrijke veranderingen zouden kunnen veroorzaken in ijsvolume en het globale klimaat gedurende het Neogeen en mogelijk eerder. Reeds eerder waren al cycli met een duur van miljoenen jaren aangetroffen in een aantal mariene sediment opeenvolgingen, bijvoorbeeld in het Krijt (De Boer, 1983). Ook continentale sedimenten uit het Trias tijdperk (vroeg Mesozoïcum) in Noord-Amerika bevatten een lang-periodieke afwisseling, welke zeer waarschijnlijk samenhangt met een lange cyclus in excentriciteit, hoewel dit niet rechtstreeks bewezen kon worden (Olsen en Kent, 1986 en 1999).

In 2004 was de tijd dus rijp om een onafhankelijk onderzoek uit te voeren naar veel jongere continentale sedimenten uit een tijdperk waarvoor betrouwbare astronomische curves beschikbaar zijn. De uitbreiding van astronomisch gecalibreerde tijdschalen naar de Eoceen – Oligoceen grens (34 miljoen jaar geleden) bood tevens de mogelijkheid om de ouderdom van belangrijke klimaatsveranderingen direct te vergelijken met de astronomische curves om een mogelijk verband aan te tonen.

In dit proefschrift worden een zestal studies uit de doeken gedaan, allen gericht op het opsporen van lang-periodieke orbitaal sturing van het klimaat en daarmee samenhangende veranderingen in het afzettings milieu. Vier studies zijn afkomstig uit de continentale bekkens van Teruel en Madrid in Spanje. Daarnaast zijn mariene sedimenten bestudeerd uit de Middellandse Zee (Malta) en uit

de Noordzee (België). Hieronder zullen al deze studies kort worden samengevat alsmede hun belangrijkste conclusies gegeven.

Het bekken van Teruel

In het Teruel bekken zijn een drietal studies uitgevoerd. In **hoofdstuk 2** wordt de Cascante sectie bestudeerd. In deze sectie is een sediment opeenvolging van Laat Miocene ouderdom ontsloten waarin regelmatige afwisselingen van rode en groene siltige klei en lacustriene kalk te zien zijn (Figuur 2.2). De klei en silt zijn afgezet op een doorgaans droogvallende vlakte, terwijl de kalk is afgezet in een ondiep meer. Eerder hebben Abdul Aziz en co-auteurs (2001; 2004) aangetoond dat de regelmatige afwisselingen op meter-schaal worden veroorzaakt door klimaatsverandering die samenhangen met precessie (21.000 jaar). Echter, deze auteurs vonden geen duidelijke aanwijzingen voor orbitaal gestuurde veranderingen gerelateerd aan andere orbitaal cycli en dan met name aan excentriciteit. Dit zou opmerkelijk zijn omdat excentriciteit de amplitude van de precessie cyclus bepaald. Om hier meer duidelijkheid in te krijgen hebben we de kalken aan een meer gedetailleerd sedimentologisch onderzoek onderworpen om hun afzettingsdiepte, biologische elementen, en andere karakteristieken te achterhalen. Dit onderzoek geeft aan dat er ook fluctuaties op langere termijn hebben plaatsgevonden in de diepte en stabiliteit van de meren waarin de individuele kalken zijn afgezet. Deze variaties kunnen tevens gekoppeld worden aan de korte en lange cyclus van excentriciteit, met een duur van 100 en 405 duizend jaar (Figuur 2.7). Ook is er bovenin de sectie een verdiepings trend dat het meer dat zich periodiek ontwikkeld diepter wordt gevonden, als voorbode van een dikke lacustriene kalk pakket bovenop de Cascante sectie. Dit dieper worden kan niet verklaard worden aan de hand van de boven genoemde orbitaal cycli en moet dus een andere oorzaak hebben. In dit hoofdstuk suggereren wij dat deze omslag zou kunnen samenhangen met een zeer lange excentriciteits cyclus met een periode van 2.4 miljoen jaar, mede omdat de trend samenvalt met een minimum van deze cyclus. Deze veronderstelling vereist nadere invulling, waarmee een begin wordt gemaakt in hoofdstuk 3.

In **hoofdstuk 3** wordt de Prado sediment opeenvolging bestudeerd die een gelijke ouderdom heeft als de Cascante sectie uit hoofdstuk 2. Deze opeenvolging, die zeven kilometer verwijderd ligt van Cascante, laat deels gelijke sediment karakteristieken zien, met rode kleien en lacustriene kalken, maar ook duidelijke verschillen. De sedimenten zijn minder vaak op droge, geoxideerde vlaktes afgezet, maar juist op nattere vlaktes waar de grondwaterspiegel hoger staat. Er worden ook relicten van kalk-bodems gevonden en tevens zijn de sedimentaire cycli veel minder regelmatig dan in Cascante. Wel zijn er net als in Cascante veranderingen op langere termijn te vinden. De sectie begint met relatief droge afzettingsmilieus aan de basis, verandert naar nattere milieus in het midden en weer drogere milieus aan de top. In Hoofdstuk 3 is een stratigrafisch en sedimentologisch onderzoek naar de Prado sectie uitgevoerd om de Prado sectie in een nauwkeurig in de tijd met Cascante te kunnen vergelijken en om de mogelijke orbitaal forcering in de Prado sectie te onderzoeken. Tijdscontrole met behulp van magnetostratigrafie laat wederom zien dat de sedimentaire cycli op meter-schaal geforceerd zijn door precessie. Echter, in tegenstelling tot in Cascante, kunnen niet alle details verklaard worden door orbitaal sturing van het klimaat op de precessie tijdschaal. Dit zou kunnen betekenen dat andere processen dan orbitaal forcering ook een (dominante) rol spelen in de Prado sectie. Op langere tijdschalen wordt ook de invloed van de 41 duizend jaar obliquiteits cyclus en de 405 duizend jaar excentriciteits cyclus gevonden, wat de orbitaal forcering hypothese van het milieu in het Prado gebied versterkt. Echter, de opvallende

afwezigheid van de 100 duizend jaar excentriciteits cyclus zou opnieuw kunnen aangeven dat andere processen ook een belangrijke rol spelen.

In **hoofdstuk 4** wordt de daadwerkelijke correlatie van Cascante naar Prado tot stand gebracht. Hiervoor wordt eerst de Cascante sectie naar boven uitgebreid vanaf de reeds bestudeerde sectie in Hoofdstuk 2. Vervolgens kunnen beide secties in detail met elkaar gecorreleerd worden met een onzekerheid van ten hoogste één sedimentaire cyclus (gemiddeld drie meter). Uit deze vergelijking blijkt dat belangrijke grootschalige sedimentaire veranderingen in beide secties op hetzelfde moment plaatsvinden. Echter, de sedimentaire karakteristieken van deze veranderingen blijken tegengesteld te zijn. Het begin van de stabiel(ere) meer-afzettingen in het Cascante gebied valt samen met een verlaging van de grondwaterspiegel in het Prado gebied. Dit is hoogst opmerkelijk en geeft aan hoe belangrijk een nauwkeurige tijdscontrole is bij dit soort geologisch onderzoek. Een aantal mogelijke oorzaken van deze tegengestelde verandering reactie wordt in het verdere hoofdstuk uiteengezet, waarbij op dit moment nog geen uitsluitsel gegeven kan worden.

Het bekken van Madrid

In **hoofdstuk 5** wordt een vergelijkbaar onderzoek in het bekken van Madrid gedaan. De Valdearenas-Muduex sectie gelegden in het noordoostelijk deel van het bekken bestrijkt een groot deel van het midden en laat Mioceen. In de sectie zijn twee grootschalige afwisselingen te zien van rode fluviatiele silt afzettingen en witte kalkbodems en ondiep lacustriene kalken. Op kleinere schaal vinden dergelijke afwisselingen ook plaats. Het onderzoek richtte zich op de vraag of de grootschalige afwisselingen zouden kunnen samenhangen met de lang periodieke orbitaal cycli. Met behulp van de verkregen magnetostratigrafische tijdscontrole kunnen de kalk-intervallen vergelijken met de tijdseries van de lang periodieke cycli in excentriciteit en obliquiteit. Hieruit blijkt dat, net als in Teruel, de basis van de kalkpakketten samenvallen met een minimum in de 2.4 miljoen jaar excentriciteits cyclus. Obliquiteit lijkt geen invloed te hebben uitgeoefend, wat aangeeft dat de afzettings-milieus vooral lokaal werden bepaald. Een kleuren data set met hoog oplossend vermogen werd opgesteld omde aanwezigheid van cyclische veranderingen statistisch te kunnen onderbouwen. Deze statistische analyse in het tijdsbereik laat zien dat ook de 405 en 970 duizend jaar excentriciteits cycli een rol speelden bij veranderingen in het afzettingsmilieu in het noordoostelijk deel van het bekken van Madrid. Al deze cycli laten een vertraagde reactie van ongeveer een kwart cyclus zien, wat zou kunnen aangeven dat er sprake is van een geheugen effect waardoor bepaalde factoren pas later hun invloed doen gelden. Dit kunnen bijvoorbeeld grondwater reservoirs zijn die slechts langzaam gevuld worden. Echter, de reactie op de 405 duizend jaar excentriciteits cyclus is in fase, terwijl de 0.97 en 2.4 miljoen jaar cycli uit fase reageren; wat vooralsnog onverklaard blijft. Om de controle van de lang-periodieke orbitaal cycli op de grootschalige afwisselingen in het bekken van Madrid verder te onderbouwen, moet bewezen worden dat de sequenties dezelfde ouderdom hebben binnen dat deel van het bekken dat hydrologisch verbonden was tijdens afzetting.

Malta

Op Malta is een mariene sediment opeenvolging bestudeerd met als doel de belangrijkste klimaatsverandering uit het midden Mioceen te traceren en te dateren, en te vergelijken met curves

van orbitaal cycli om een mogelijk verband te kunnen leggen. De opeenvolging op Malta wordt gekenmerkt door kleinschalige en grootschalige afwisselingen van mergelige klei en klei, terwijl onder de basis van de bestudeerde opeenvolging een veel kalkiger pakket aanwezig is (Figuur 6.2). Aan de hand van zuurstof en koolstof isotopen metingen wordt aangetoond dat deze kalk naar klei overgang samenvalt met de gezochte klimaatsverandering in het midden Mioceen, waarbij een permanente vergletsjering van grote delen van Antarctica plaatsvond en het klimaat op aarde netto afkoelde. Chemische element analyse is uitgevoerd om de lithologische variaties te kwantificeren en mogelijke orbitaal forcering te onderzoeken. De gecombineerde magneto- en biostratigrafie leveren een goede eerste order tijdscontrole. Deze controle laat zien dat de waargenomen cycli samenhangen met precessie en 100 en 400 duizend jaar excentriciteit. Deze cyclische afwisselingen zijn vervolgens naar de precessie en excentriciteits curves gecorreleerd wat een bijzonder goede en gedetailleerde tijdscontrole geeft, bijvoorbeeld ook over de klimaatsverandering heen. De tijdscontrole geeft aan dat de klimaatsverandering 13.82 miljoen jaar geleden plaatsvond en tijdens een bijzondere astronomische configuratie met een minimum in zowel de 405 duizend jaar excentriciteits en 1.2 miljoen obliquiteits cycli. Dezelfde configuratie is ook gevonden voor andere belangrijke en minder belangrijke klimaatsveranderingen in het jongere deel van het Cenozoïcum. Deze veranderingen zijn gerelateerd aan piekvoorkomens van ijs op Antarctica. De reden hiervoor zou het uitblijven van warme zomers door lage obliquiteit en excentriciteit kunnen zijn, waardoor beginnende ijskappen niet afsmelten en zichzelf in stand kunnen houden.

Boomse Klei

In het Oligoceen was het Noordzee bekken een grote binnenzee die zich uitstrekte ten noorden van het huidige België (Figuur 7.1). Hierin werden zeer karakteristieke silt en klei sedimenten afgezet die een opmerkelijke horizontale en lateraal consistente gelaagdheid laten zien (Figuur 7.2). In **hoofdstuk 7** wordt gebruik gemaakt van lange kwantitatieve data series van de Boomse Klei formatie van vroeg Oligocene ouderdom uit België. Deze data sets zijn verkregen uit boringen die geplaatst zijn om onderzoek te doen naar de mogelijke opslag van radioactief materiaal in de Belgische ondergrond. In de Boomse Klei formatie zijn regelmatige afwisselingen van silt en klei op meter schaal te zien. Deze afwisselingen worden gekoppeld aan schommelingen van de zeespiegel, waarbij tijdens relatief lage zeespiegels het fijnste materiaal niet wordt afgezet door de hogere energie op de zeebodem. Andere mogelijke verklaringen kunnen geen van allen de lateraal zeer consistente gelaagdheid verklaren. De zeespiegelvariaties worden op hun beurt gerelateerd aan variabele ijsvolumes op Antarctica. In de Boomse Klei kan dus indirect bepaald worden hoe het (globale) ijsvolume in het vroeg Oligoceen varieerde. Ook kan de rol van (lang-periodieke) orbitaal forcering hierbij bestudeerd worden. Statistische analyse geeft aan dat de zeespiegel vooral werd bepaald door de 41 duizend jaar obliquiteits cyclus. In sommige intervallen wordt ook de expressie van de 100 en 405 duizend jaar excentriciteits cycli gevonden. Het beeld dat hiermee verkregen wordt is sterk vergelijkbaar met dat voor de meer recentere geschiedenis van de ijstijden op onze aarde. Lang periodieke variaties konden helaas niet bestudeerd worden, omdat de tijdscontrole uiteindelijk niet accuraat genoeg was om de opeenvolging tot in detail met de astronomische curves te vergelijken. Daarnaast bleek de opeenvolging niet lang genoeg om meerdere van dit soort cycli te bevatten.

Acknowledgements

It is impossible to mention all of you here, although you all read this part, so in case you are or feel neglected, please accept my sincere gratitude to you, especially.

First of all, I want to thank my late grandmother Trijntje Abels – van der Velde, who started giving me rocks at an age of eight and took care for having some mineral and fossil books on my first bookshelf.

Then my thanks go to Jan-Willem Zachariasse, who picked me out of the 'soft-rock' students participating in the third year's fieldwork in 2001 as slave for the upcoming Malta fieldwork. Then my stratigraphy started. Jan-Willem, I really enjoyed our discussions on biostratigraphy, on geology in general, and on other (non-)fiction!

My sincere gratitude goes to Frits Hilgen for being my tutor ever since the Malta trip. Frits, thanks a lot for sharing your fascination for science and stratigraphy in these years including for the cycles that might always well be of orbital origin, if the realm is suitable enough of course!

Then, I would like to sincerely thank Hayfaa Abdul Aziz, who took me to Teruel in May 2002 for digging my first rabbit holes in continental sediments and afterwards continuously shared her experience in the Iberian basins and wines. Hayfaa, for me, it always has been an enormous pleasure to be with you in the lab and, especially also, the field!

I would like to thank Bert van der Zwaan for being my promotor and for the numerous scientific and political discussions we had. My special thanks go to my Dissertation Committee, to my magnificent paranymphs Kees Hordijk and Sander Smeets, and to the fourteen colleagues co-authoring this thesis.

Then, I thank all at Strat/Pal of course, including those who left, for sharing daily life, TFC's, thursday roles, and paleontological tea! I thank all at the Fort Hoofddijk for helping me with the machines at weird hours and for sharing their coffee, beers, and stokbrood. I thank the people from the Sedimentology, Palaeoecology, different Geochemistry and Geophysics groups, many of you made my time much more pleasant!

I want to thank the Master-students I guided, Sander Smeets, Wolter Bosch, Alex Klomp, and Marijke Lebbink, for having patience while this 2-meter guy was restlessly running around the building and other parts of the planet. I thank those who where around during my fieldcamps; José Pedro Calvo, Poppe de Boer, Lies(beth) Jasperse, Henk Kombrink, Marianne Lewis, Luis Mampel, Sander Smeets, Karel Steensma, Jan van Dam, Dario Ventra, and Anne van der Weerd in Spain, Anja Mourik, Marcus Badger, Rink Kruk, Wout Krijgsman, and Jan-Willem Zachariasse in Malta, and Silja Hüsing, Phil, and Allessandro Montanari in Italy, Guillaume Dupont-Nivet, Cor Langereis, Marijke Lebbink, Julia Straathof, Zhuqiang, and Wang Song in China, Douwe van

Hinsbergen, Wolter Bosch, Maartje Hamers, Floor Boekhout (DoMoWoMaFlo), Cor and Maud Meijers in Ukraine, and the team and students from Aliaga2005.

In particular also, I want to thank my foreign colleagues and friends from Spain, José Pedro Calvo, Luís Alcalá, Luís Luque, Luís Mampel (los Luíses!), and others at Dinopolis Teruel, Javier-Perez Rivares, Miguel Garcés, Elisenda Costa y Arnou, Bet Beamud, and others at the Universitat de Barcelona, and from Belgium, Noël Vandenberghe, Stefaan (Simi) Van Simaeys, and Ellen De Man for the pleasant collaborations and time!

I want to thank all of you that helped in the labs; Helen De Waard, Geert Ittman, Arnold van Dijk, Otto Stiekema, Jan Drenth, Tom van Hinte, and Tom Mullender, and also the building heroes Roy and Ronald. I thank the people at the PhD-platform, especially Chris Spiers, Reinoud Vissers, Aard-Peter van den Berg van Saparoea, Karin Visser, Thomas Geenen, and Cynthia Vilt, those at the faculty council, and those who participated the VMSG Alps-trip and Strat/Pal Sicily trip.

Almost finally, I thank Kees Hordijk for permitting me already seven years in his office consulting him too often on a wide array of subjects, for sharing the StratBucks coffee company, and for being the best roommate ever. Finally then, I thank my family and especially parents for being there, and Lies for sharing her life and love with me!

Curriculum Vitae

Hemmo Anne Abels was born on July 26, 1980, in Ter Wupping, that belongs to the local authority of Stadskanaal in the province of Groningen. Soon after, the family moved to Eexterzandvoort in the north of the province of Drenthe, where he grew up collecting stones, digging holes, and climbing trees. After graduating at the Praedinius Gymnasium in Groningen in 1998, he started the Geology curriculum at Utrecht University.

During his Master's research in Utrecht, he got interested in the integrated stratigraphy of marine and continental sediments, while working on Mediterranean land-based sections under supervision of dr. F.J. Hilgen, dr. H. Abdul Aziz, dr. W.J. Zachariasse, and dr. W. Krijgsman. This research team exposed the world of plankton and mammal biostratigraphy, cyclostratigraphy and astronomical forcing, and magnetostratigraphic analysis and dating. As an Erasmus student at the Petrología y Geoquímica department at Complutense University in Madrid in 2003 with Prof. dr. J.P. Calvo his interest enhanced by revealing the impact of additional detailed sedimentological research on cyclostratigraphic analysis of the, in this case, continental sediments.

His PhD-thesis project, under supervision of dr. F.J. Hilgen and dr. H. Abdul Aziz, allowed him to further develop expertise in integrated stratigraphic research, in which sedimentological analysis was increasingly used. At present, the interplay between sedimentology and integrated stratigraphy of Cenozoic continental sediments is his favourite playground aiming to unravel the wide range of forcing mechanisms acting simultaneously and with different proportions through space and time. During his PhD-project, he participated in a six-months stratigraphic and sedimentological

project on the reservoir characteristics of middle Carboniferous in the eastern Ukraine funded by Shell International. Further, he got involved in a project that intends to unravel Tibetan uplift, Paratethys retreat, and global cooling by analysing Paleogene continental sediments in the north-eastern Tibetan Plateau, China, led by dr. G. Dupont-Nivet and dr. W. Krijgsman.

In the next years, he will examine orbital forcing in the fluvial setting of the Paleogene Bighorn Basin, Wyoming, still at Utrecht University, while continuing his studies on Chinese and Mediterranean continental and marine successions. At present, it feels for him that real geology just started.

List of Publications

Abels, H.A., H. Abdul Aziz, D. Ventra, and F.J. Hilgen, in review. Orbital climate forcing in mudflat to marginal lacustrine deposits in the Miocene Teruel Basin (NE Spain). *Journal of Sedimentary Research*.

Abels, H.A., H. Abdul Aziz, J.P. Calvo, and E. Tuenter, 2008. Shallow lacustrine microfacies document orbitally paced lake-level history in the Miocene Teruel Basin (NE Spain). *Sedimentology*, in the press.

Hilgen, F.J., **H.A. Abels**, S. Iaccarino, W. Krijgsman, I. Raffi, R. Sprovieri, E. Turco, and W.J. Zachariasse, 2008. The global stratotype section and point (GSSP) of the Serravallian Stage (middle Miocene). *Episodes*, in the press.

Dupont-Nivet, G., W. Krijgsman, C.G. Langereis, **H.A. Abels**, S. Dai, and X. Fang, 2007. Tibetan Plateau Aridification linked to global cooling at the Eocene-Oligocene transition, *Nature*, 445, 635-638.

Abels, H.A., S. Van Simaeys, F.J. Hilgen, E. De Man, and N. Vandenberghe, 2007. Obliquity-dominated glacio-eustatic sea level change in the early Oligocene: evidence from the shallow marine siliciclastic Rupelian stratotype (Boom Formation, Belgium), *Terra Nova*, 19, 65-73.

Abels, H. A., F.J. Hilgen, W. Krijgsman, R.W. Kruk, I. Raffi, E. Turco, and W.J. Zachariasse, 2005. Long-period orbital control on middle Miocene global cooling: Integrated stratigraphy and astronomical tuning of the Blue Clay Formation on Malta, *Paleoceanography,* 20 (4), PA4012, doi. 10.1029/2004PA001129.

Hilgen, F.J., H. Abdul Aziz, **H.A. Abels**, J. Becker, K.F. Kuiper, L.J. Lourens, P.Th. Meijer, J. Steenbrink, E., Tuenter, E. van der Laan, and N. Weber, 2005. Mediterranean Neogene cyclostratigraphy and astrochronology: Recent progress and new developments, *in* A. Berger, M. Ercegovac, & F. Mesinger, e*ds.*, Milutin Milankovitch 125th Anniversary Symposium: Paleoclimate and the Earth Climate System. *Proceedings of the Serbian Academy of Sciences and Arts, Belgrade, Serbia.*